ENG 348-(EQC 2006/SP4)

Development of design guidelines for rocking structures

Trevor Kelly, Holmes Consulting Group

EQC PROJECT OPR4

STRUCTURAL AND CIVIL ENGINEERS

DEVELOPMENT OF DESIGN GUIDELINES FOR ROCKING STRUCTURES

HOLMES CONSULTING GROUP

FEBRUARY 2008

Report Prepared for the EQC Research Foundation

Development of Design Guidelines For Rocking Structures

EQC Project OPR4

February, 2008

Trevor E Kelly

Holmes Consulting Group
Level 1 39 Market Place
P O Box 90 745
Viaduct Basin
Auckland, New Zealand

Telephone +64 9 965 4789
Fax +64 9 965 4780
Email trevork@holmesgroup.com

ABSTRACT

Many new and existing buildings have insufficient weight to resist overturning loads due to earthquakes without uplift of part of their foundation. Uplift can be prevented by the use of tension piles, but these add significant costs and may cause larger loads on the structure above. Observations from past earthquakes suggest that local uplift and rocking will not be detrimental to seismic performance and may be even be beneficial in limiting forces transmitted into the structure. In some cases, rocking isolation systems have been implemented as a means of energy dissipation to improve earthquake performance.

The main impediment to permitting uplift is that the displacements, and the associated change in force patterns, cannot be quantified using conventional design techniques. Previous versions of the New Zealand structural design code allowed simplified procedures for the design of rocking structures provided that the ductility (upward displacement after uplift) was limited. The new loadings code, NZS 1170, removed this exemption and requires that a special study be performed whenever energy dissipation through rocking occurs.

Many of the buildings with the potential for rocking are relatively small buildings, and the design fees and programme cannot support the time and costs of a special study, which typically requires a high end computer analysis. Research is underway in academia to investigate aspects of rocking and uplift but these will address the theoretical aspects in much more detail than required for design office use and the delivery time will not meet the pressing need for published guidelines.

The objective of this project was to develop and publish guidelines to enable structural engineers to design and evaluate buildings which are subject to local uplift under earthquake actions. The guidelines were to be sufficiently robust to substitute for the special study currently required by NZS 1170.

This report presents these tentative guidelines, which enable designers to estimate the effects of rocking on structures without the time and expense involved in a computer study. The guidelines form a starting point for further development but in their present form are suitable for relatively simple and regular structures with moderate amounts of uplift.

TECHNICAL ABSTRACT

Many new and existing buildings have insufficient weight to resist overturning loads due to earthquakes without uplift. If uplift is allowed the deformations, and the associated redistribution of forces, cannot be quantified using conventional linear elastic analysis. Previous versions of the loadings code allowed simplified procedures for the design of rocking structures provided the ductility factor was limited to not more than 2. The new loadings code, NZS 1170, removed this exemption and requires that a special study be performed whenever energy dissipation through rocking occurs.

A special study in terms of NZS 1170 involves development of a computer model of the structure and an assessment of the time history of response of the building to a suite of probable earthquake motions. This type of analysis requires specialized software and a level of expertise which most design offices cannot provide.

Pioneering work in the development of design procedures of rocking structures was published in NZ in 1978 and this has been used as a basis for published guidelines such as FEMA 356. However, research since then has suggested that there are limitations in these procedures which prevent their widespread application.

In this project, series of time histories were frequency scaled to match the spectral shapes defined in NZS1170. These time histories were then used to evaluate the response of an extensive series of single wall rocking models. The single walls ranged from 3.600 m to 14.400 m in length and from one story to six stories in height. A range of subsoil conditions (clay, gravel, rock) was considered. Each wall configuration was evaluated for six sets of time histories (three soil conditions, both near fault and distant from a fault) each containing seven time histories, and for ten amplitudes of seismic load, a total of 420 time history analyses. The response was defined as the mean response from each set of seven time histories.

Results from these single wall models were used to develop a procedure to estimate maximum displacements as a function of earthquake amplitude. A method based on the spectral displacement at an effective period was found to be able to predict the analysis results very well when the effective period was defined as a function of ductility. The rocking mechanism was found to increase shear forces in the wall. This increase in shear was a strong function of both the number of stories and the wall ductility factor. Empirical equations were developed to estimate this dynamic amplification of inertia forces.

The example walls were extended to multiple planar walls and non-planar wall structures. The procedure was found to be able to satisfactorily estimate response for relatively regular structures but was less accurate where torsional effects were significant.

The procedures are simple enough for design office use and are suited for implementation using a spreadsheet format. The guidelines were developed using procedures which would typically be used for a "special study" but are not fully rigorous. They do not fully quantify impact effects; nonlinear soil properties; radiation damping etc. and so in this respect are tentative and will be subject to continued improvement.

SUMMARY OF TENTATIVE DESIGN PROCEDURE

Applicability

The design procedures presented here is intended for shear wall structures which rock under seismic loads. The development is based on the results of an extensive series of analysis on single walls and a more limited evaluation of multiple wall buildings and non-symmetrical buildings. The accuracy of the procedures will be best for:

1. Low rise walls, three stories or less.

2. Regular, symmetrical shear wall buildings.

3. Walls with relatively small ductility factors (DF), with a rocking strength (static restoring moment) of one-quarter or more of the elastic demand (DF less than 4).

The procedure is iterative in that the designer selects a foundation size either to meet serviceability requirements or to provide a rocking strength corresponding to a selected ductility factor. The performance is then assessed and the foundation size adjusted as required to achieve the design objectives.

Implementation

The procedures are suited for design office use and can be implemented using standard spreadsheet functions. The most complex step is the equation for effective period which is recursive, in that the calculation of T_e requires the calculation of R, which is itself a function of T_e. This can be solved using spreadsheet tools such as "Goal Seek".

Notation

a_{VN}	Coefficient for dynamic amplification factor
B	Foundation Width
$C(T_E)$	NZS1170 elastic coefficient at effective period.
$C_d(T_1)$	NZS1170 design coefficient at initial period.
C_0	Coefficient relating spectral displacement to roof displacement (1.0 for single story, 1.2-1.5 for multi-story).
C_M	Effective mass factor (1.0 for single story, 0.8-0.9 for multi-story).
C_Y	Yield coefficient for rocking wall
c	Length of compressive stress block at toe of wall
DF	Ductility factor
F_Y	Applied Lateral Load at Rocking
G	Soil shear modulus
g	Acceleration due to gravity
H	Wall Height
h_i	Height to floor i
k_i	Stiffness of soil spring i
K_R	Rocking Stiffness

Soils and gravels, G = 40,000 to 80,000 kN/m^2, υ = 0.3 to 0.4

Clays (undrained case), G = 2,000 to 20,000 kN/m^2, υ = 0.5

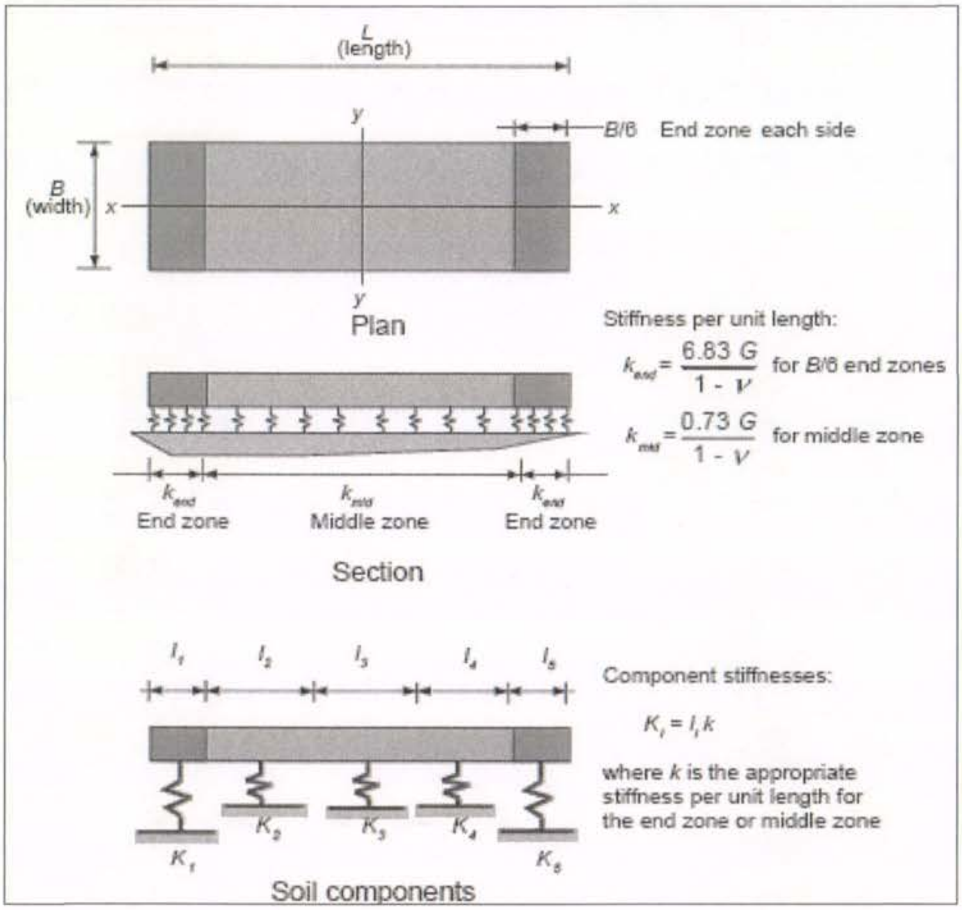

4. Wall Rocking Strength

Calculate the yield force $F_y = \dfrac{W(L-c)}{2\dfrac{H}{C_0}}$ and the yield coefficient $C_y = \dfrac{F_y}{Mg}$ where M is the seismic mass tributary to the wall. For non-planar walls, such as C shaped and L shaped sections, the moment capacity, $\dfrac{W(L-c)}{2}$ in the equation above, can be calculated by taking moments of the reaction forces at individual springs about the wall centroid. The coefficient C_0 relates spectral displacement to the roof displacement of multi-story walls. It has a value of 1.0 for single story buildings and increases with height to a range of between 1.2 and 1.5 for higher buildings. FEMA 356 provides tabulated values.

5. Estimate Period

Either extract the period from a linear elastic model of the wall or use the approximate formulas in Section 10.3. The soil spring stiffness can be calculated from FEMA 356 procedures, as above.

6. Seismic Displacements

The single degree of freedom displacement $\Delta = C(T_e)g\frac{T_e^2}{4\pi^2}$ from which the displacement at the top of the wall is calculated as $\Delta_{TOP} = \Delta C_0$.

The effective period is calculated from the elastic period as $T_e = T_i R_E$; R_E is the response reduction factor $R_E = \frac{C_m C(T_e)}{C_y}$; C_m is the effective mass factor obtained from a modal analysis or alternatively tabulated values from FEMA 356 (typically 1.0 for 1 or 2 story buildings, 0.8 or 0.9 for taller buildings). Note that the equation for effective period is recursive as R_E is a function of T_e which is the unknown variable.

7. Structural Ductility Factor

Structural ductility factor DF = C (T_i) / C_y

8. Dynamic Amplification Effects on Wall Shear

$V_U = F_Y \omega_V$

$\omega_V = 1 + a_{VN} DF \leq 0.5 + N$ for N > 1
$= 1.0$ for N = 1

N Number of Stories	Amplification Factor a_{VN}
1	0.00
2	0.10
3	0.15
4	0.40
5	0.60
6	0.90

9. Torsional Increase in Displacements

The number of 3D structures evaluated was insufficient to fully develop procedures to estimate increases in displacement due to torsion. The limited studies suggest the higher of two factors:

1. Increase the displacements by two times the calculated actual eccentricity. If the calculated eccentricity is 0.20B, allow for a 40% increase in displacements.

2. If the actual eccentricity is less than 5%, increase the displacements by the same factor as the accidental eccentricity. That is, allow a 10% increase in displacements due to 0.10B eccentricity.

10. Assess Performance

The performance of the wall, as defined by maximum displacements and dynamic amplification effects, is assessed to determine whether it achieves the project design objectives. If not, the foundation size is adjusted and the procedure repeated from Step 2 above. Increasing the foundation size decreases the ductility factor, which reduces both displacements and dynamic amplification effects.

TABLE OF CONTENTS

LIST OF FIGURES

LIST OF TABLES

1 INTRODUCTION

1.1 Uplift of Foundations

Many new and existing buildings have insufficient weight to resist overturning loads due to earthquakes without uplift of structural elements. Uplift can be prevented by the use of tension piles, but these add significant costs and may impose larger loads on the structure above. Observed and analytical evidence suggests that local uplift and rocking will not be detrimental to seismic performance and in fact may be beneficial in limiting forces transmitted into the structure. In fact, rocking isolation systems have been implemented as a means of energy dissipation.

Uplift is a nonlinear phenomenon in that the foundation changes state from full contact with the subsoil to partial contact. Because of this nonlinearity the structural deformations, and the associated redistribution of forces, cannot be quantified using conventional linear elastic analysis.

1.1.1 Code Requirements

For designs performed in New Zealand to the provisions of the loading code which applied through 2005, NZS4203:1992 [Reference 1], uplifting structures were governed by Clause 4.11.1.2 which stated that:

> *Where dissipation of energy is through rocking of foundations, the structure shall be subject to a special study, provided that this need not apply if the structural ductility factor is equal to or less than 2.0.*

In practice, this exclusion was interpreted as requiring no special design provisions provided that uplift occurred at a level of seismic load no less than 50% of the full elastic load. Many low-rise shear wall buildings met this restriction and so were designed to allow rocking for seismic loads which exceeded 50% of the load at which uplift occurred.

NZS1170.5:2004 [Reference 2], which replaces NZS4203, addresses rocking structures in Section 6.6 which requires that:

> *Where energy dissipation is through rocking of structures…, the actions on the structure shall be determined by a special study.*

A special study, in terms of NZS 1170, in most instances requires development of a computer model of the structure and an assessment of the time history of response of the building to a suite of probable earthquake motions. This type of analysis requires specialized software and a level of expertise which most design offices cannot provide.

Special studies are justified for large and important structures. However, the majority of structures where uplift may occur are of such scope that the cost of the special study is likely to exceed the design fee. For these buildings, anecdotal evidence suggests that many designers are allowing rocking to occur by default without quantifying the effects, solely due to the absence of guidelines to evaluate these effects within a design office environment.

The alternative, preventing rocking by the use of massive foundations or tension piles, leads to added expense and additional loads to the superstructure. This affects in particular the low-to-medium rise structures which form a significant proportion of commercial and residential projects in medium to high seismic loading zones.

For the retrofit of earthquake prone buildings, new foundations to resist uplift often form the major cost item and these costs are often such that the owner is discouraged from attempting a seismic upgrade. Guidelines for the design of new rocking elements to augment the strength of the existing building will result in more cost effective retrofits and encourage the continued safe usage of our building stock.

1.2 Objectives of This Project

Pioneering work in the field of the response of rocking structures was published in New Zealand in 1978 (Priestley et al [Reference 3]) and this has been used as a basis for published guidelines such as FEMA 356 [4]. However, research since then has suggested that there are limitations in these procedures which prevent their widespread application (References [5] and [6]). Development is required to further progress this work, aided by modern nonlinear analysis techniques which were not available in 1978.

The objective of this project is to complete research to enable the development and publishing of guidelines to enable structural engineers to design and evaluate buildings which are subject to local uplift under earthquake actions. The aim is to produce these guidelines in a form suited for design office use, utilizing standard design office tools (spreadsheets and linear elastic analysis programs) and sufficiently robust to substitute for the special study currently required by NZS 1170.

Output from the procedures should enable the designer to quantify uplift deformations and provide guidance as to methods to assess the effects of this uplift on force distributions within the structure and the effect of impact on the sub-soil.

1.3 Previous Research

The intention of this report is to develop design procedures for rocking structures and the theory relating to the dynamics of rocking blocks is not examined in detail here. It is described fully in references [3] to [10], discussed below. These references generally show that the response of rocking systems is best described by solving the second order ordinary differential equation based on the rotational moment of inertia of the block, with the dynamics of the system described by the block angular velocity. The energy loss of the system is replicated using an apparent coefficient of restitution approach first developed by Housner [7].

The pioneering work on rocking systems by Housner was later extended by a number of researchers, including Chopra [8], Ishiyama [9] and Psycharis [10], and also by researchers in New Zealand, as noted above [3]. Experimental work such as the uplifting frame studied by Huckelbridge [11] demonstrated the potential benefits of allowing partial uplift.

More recently, extensive experimental and analytical work at the University of Auckland has extended our knowledge of aspects of rocking and methods of evaluating rocking response (References [12] and [13]). This will result in a better understanding of the dynamics of rocking and the influence of factors such as the aspect ratio and interface material. In the medium to long term, this research will result in much more sophisticated tools to evaluate rocking structures.

Most rocking block studies assume a rigid block on a rigid foundation. For uplifting structures, soil interaction is important and the potential for soil yielding must be considered. This is a complex topic and work in this area is not yet developed sufficiently for design office use. Progress is being achieved, as shown in References [14], [15] and [16] for example. As this basic research is progressed it will be possibly to extend design office procedures to include these important effects.

On an ironic note, a Canadian study [17] evaluated the effect of foundation rocking on shear walls and recommended that footings need not be designed for ductility factors less than 2. The impetus for this study was the draft NZ code DR00902 which provided this provision, similar to that in the earlier NZS4203. This provision was omitted when the draft progressed into the final version, NZS1170, resulting in the need for these guidelines. The Canadian study related to walls much higher than those considered here (7 to 30 stories, versus up to 6 stories here) and also focused on the effects of uplift on drift but not on dynamic amplification of forces.

1.4 Rocking and Uplift

Although the title of this report refers to "rocking" structures, the content does not deal with classical rocking structures, the rigid blocks on rigid foundations which have been the subject of so much research. These blocks rock as the reaction switches from one corner of the block to the opposite corner and the restoring moment provided by the self weight changes sign each time the block rocks from one corner to the other.

The engineered structures which are the subject of this research rest on flexible foundations. As seismic excitation occurs the structure rocks such that part of the foundation separates from the supporting soil. As the load reverses, the uplifting portion of foundation reverts to contact with the subsoil and then the opposing end starts to separate. A structural model for this type of structure is an elastic foundation modelled by continuous elastic springs which cannot take tension, termed a Winkler model.

The models termed variously rocking or uplifting in this report are probably more accurately characterised as uplifting systems, as they have no tension attachment to the ground but do have more than two support points. Typically more than one support point is active at any point in the rocking cycle. Examples of uplifting structures would be shear walls where only a portion of the wall separates from the ground or a frame elevation with more than two columns where only the end column uplifts. This is the type of system which is the subject of this project. As the soil spring becomes stiffer (the foundation material moves from clays and gravels to rock), the wall response moves closer to that of a rigid uplifting block.

1.5 Procedures for Development of Guidelines

The procedure followed for this project was to perform a series of special studies on various wall configurations, with the characteristics of the special studies reflecting current design office practice, rather than research practice. The aim of the special studies was to develop methods to estimate the results of this type of study without doing a time history analysis of a specific structure. In particular, the goal was to develop procedures to estimate:

1. Maximum displacements at the top of the rocking structure.

2. The pressure on the sub-structure during rocking.

3. The distribution of forces in structure due to rocking if different from the non-rocking distributions.

The dynamic response of rocking blocks is complex behaviour, as the previous and current research referenced above demonstrates. It is likely that the ongoing research will provide a better understanding of the dynamics of rocking structures and ways to incorporate rocking into design.

This study is an interim attempt to quantity the response sufficient for design office use. The guidelines are developed using procedures which would typically be used for a "special study" but are not fully rigorous – they do not fully quantify impact effects, nonlinear soil properties, radiation damping etc.

2 METHODS FOR ESTIMATING NONLINEAR DISPLACEMENTS

A rocking structure separates from the foundation during seismic events and so is defined as a nonlinear system. For linear elastic systems the design parameters required are maximum forces or stresses. For nonlinear systems the forces and stresses are known, as they correspond to the defined strength of the system, and in this case the required design parameters are maximum deformations, such as nonlinear displacements or plastic rotations.

This section assesses methods used in codes and guidelines to assess the magnitude of nonlinear displacements for structures of a given strength level. These methods for the estimation of displacements form the starting point for the development of these guidelines for rocking structures.

New Zealand codes, in common with most other seismic design codes worldwide for new structures, specify a hierarchy of analysis procedures from equivalent static analysis, to linear response spectrum analysis and then linear or nonlinear time history analysis. Rocking is a nonlinear phenomenon and, of these methods, only the nonlinear time history can incorporate rocking. However, this type of analysis is currently not suitable as a design office procedure other than for special or important structures. Codes for new buildings generally require only linear elastic analysis and the designer then estimates nonlinear displacements using formulations of either the equal displacement or equal energy theories, discussed further below.

In the United States, FEMA 356 [(Reference [4]) guidelines for existing buildings specify a further procedure, the Nonlinear Static Procedure (NSP, sometimes called a Pushover Analysis). This is a nonlinear procedures so can be used to incorporate rocking and uplift, but it does not require the same resources as a time history analysis.

The following sections describe the code procedures and also the three methods which can be used with the FEMA 356 NSP procedure to assess rocking structures:

1. Equal displacement and equal energy concepts

2. A single wall rocking formulation.

3. The FEMA 356 [4] Nonlinear Static Procedure, based on the initial effective stiffness, which can be used for buildings which incorporate any type of nonlinearity.

4. The ATC-40 [18] Capacity Spectrum approach, which is an alternative method based on the secant stiffness which can be also incorporated within the FEMA NSP. This method is also suited for any type of nonlinearity.

Although only the second of these procedures specifically deals with rocking, the others are intended for general purpose nonlinearity and so are adaptable to rocking or uplifting structures. In the following sections the characteristics of each method are briefly described. Their suitability for attaining the objectives of this development is assessed in Chapter 6, using the results from a series of time history analyses on single wall models.

2.1 Equal Displacement and Equal Energy Concepts

Procedures such as those in the FEMA guidelines and in building codes such as NZS1170 reduce elastic forces to account for ductility based on one of two concepts, the first termed the equal displacement theory and the second the equal energy theory. These are assumed to apply for different period ranges. The formulations for these two concepts are developed referring to Figure 2-1, where a response modification factor, R, is used to relate the yield strength of the structure to the maximum force level in an equivalent elastic structure. The R factor may also be called the ductility factor (DF) or, in NZS1170, it is termed the inelastic spectrum scaling factor, k_μ.

Figure 2-1 Equal Displacement and Equal Energy Concepts

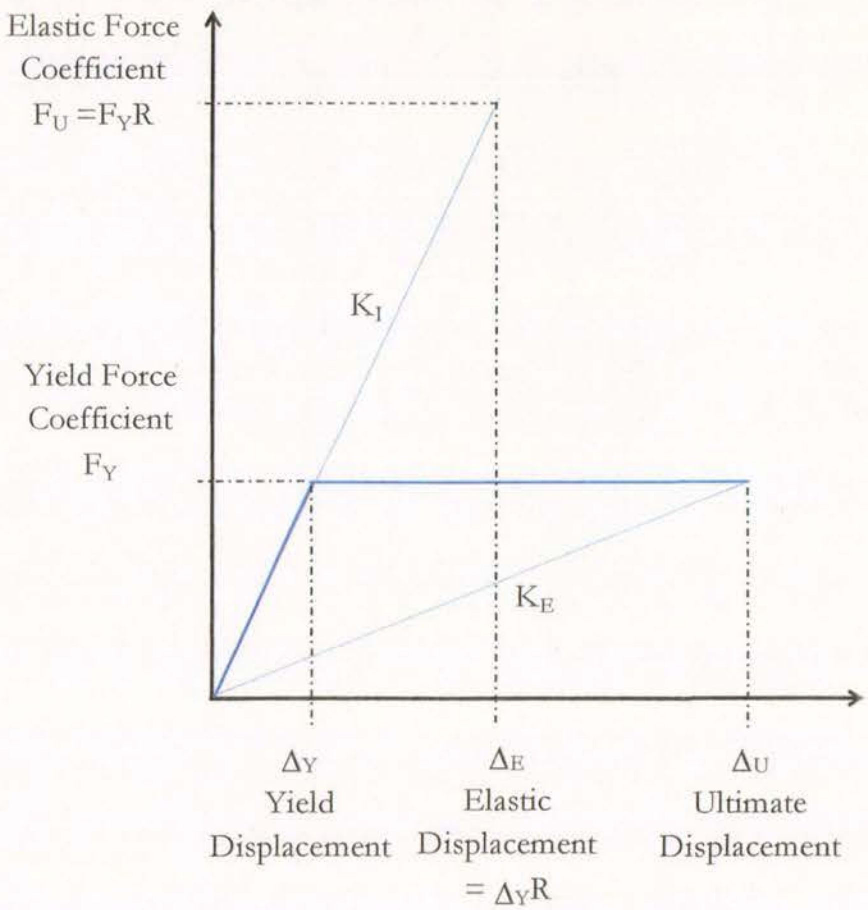

1. The equal displacement theory, usually applied for longer period structures, assumes that nonlinear displacements will be equal to the displacement for an elastic system of the same period (same initial stiffness). This implies that for the nonlinear system:

$$\Delta_U = \Delta_E \tag{2-1}$$

2. The equal energy theory assumes that the hysteretic energy of the nonlinear system will equal the elastic strain energy of the yielding system. The energy is measured by the area beneath the force-displacement curves in Figure 2-6:

Elastic Energy $$EL = \frac{(RF_Y)(\Delta_Y R)}{2} \qquad (2\text{-}2)$$

Elasto-Plastic Energy $$EP = \frac{\Delta_Y F_Y}{2} + F_y(\Delta_U - \Delta_Y) \qquad (2\text{-}3)$$

Equating EL and EP $$\frac{F_Y \Delta_Y R^2}{2} = F_Y(\Delta_U - \frac{\Delta_Y}{2}) \qquad (2\text{-}4)$$

Equation (2-4) can be formulated in terms of R as:

$$R^2 = \frac{2\Delta_U}{\Delta_Y} - 1 \qquad (2\text{-}5)$$

Using the definition of displacement ductility ratio $\mu = \frac{\Delta_U}{\Delta_Y}$ (2-6)

Substituting μ in to Equation (2-5) gives:

$$R = \sqrt{2\mu - 1} \qquad (2\text{-}7)$$

The formulation of R in terms of ductility, as expressed in Equation (2-7), is the form used in codes to reduce the elastic spectrum to obtain design forces. However, Equation (2-5) can also be formulated to calculate the maximum displacement when the strength ratio, R, is known:

$$\Delta_U = \frac{(R^2 + 1)}{2} \Delta_Y \qquad (2\text{-}8)$$

In NZS1170, the factor k_μ, equivalent to R, is defined (for all soil classes except E) as equal to μ for periods greater than 0.70 seconds and equal to $\frac{(\mu - 1)T_1}{0.7} + 1$ for periods less than 0.70 seconds. This is intended to present a transition from the equal energy concept at a period of 0.35 seconds ($k_\mu = \frac{\mu + 1}{2}$) to the equal displacement concept at a period of 0.70 seconds ($k_\mu = \mu$). The formulation for the equal energy concept implied by NZS1170 differs somewhat from equation (2-7) but, as shown in Figure 2-2, is a linear approximation to the power function.

For design to NZS1170, the elastic spectral coefficient is reduced by the factor k_μ and the displacements are then scaled by the ductility factor, μ to obtain the nonlinear displacements. This implies that for periods greater than 0.70 seconds, for Soil Types other than E, the nonlinear displacements will be equal to those for an elastic system of the same period. For shorter periods the nonlinear displacements will be greater than the elastic displacements by a factor which depends on the period and ductility.

Figure 2-2 Equal Energy Implementation in NZS1170

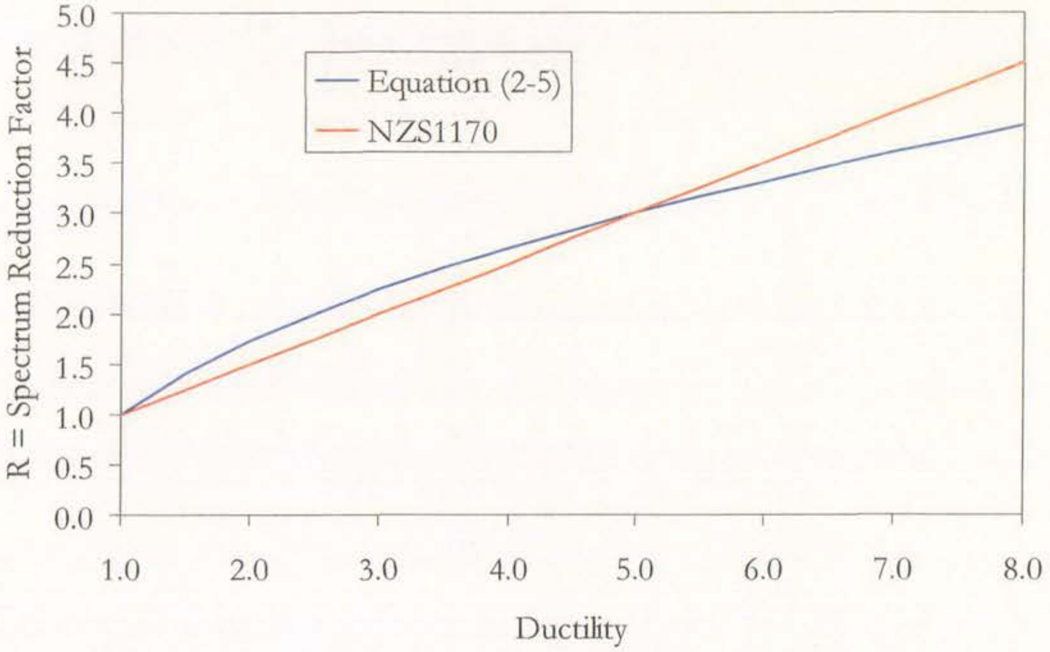

2.2 FEMA Wall Rocking Formulation

FEMA 356 provides a procedure for consideration of foundation rocking. The procedure is based on work from a variety of researchers, including Housner [7], Yim & Chopra [25], Makris & Roussos [24] and Priestley and Evison [3]. Figure 2-3 shows the rocking block formulation on which the procedure is based.

Figure 2-3 FEMA 356 Procedure for Rocking Behaviour

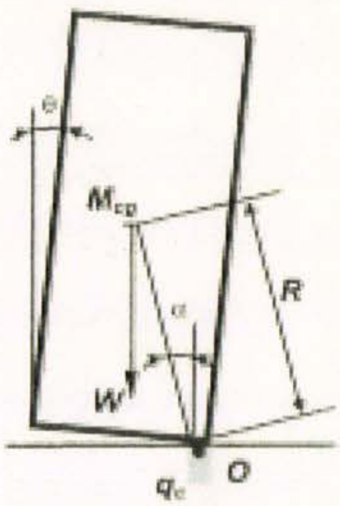

The calculations involved in implementing the procedure are listed below. Effective viscous damping is calculated as a function of the geometric and mass properties of the block. A function is derived for the effective period of response in terms of the amplitude of rocking, defined by the drift angle, θ. As the spectral displacement is a function of period, which is itself a function of displacement, the equation cannot be solved directly and so either iterative of graphical solutions are used.

1. Mass, weight, and centre of gravity

The mass, M, is the total seismic mass tributary to the wall. The weight, W, is the vertical gravity load reaction. For the purposes of these calculations, the vertical location of the centre of gravity is taken at the vertical centre of the seismic mass and the horizontal location of the centre of gravity is taken at the horizontal centre of the applied gravity loads.

2. Soil contact area and centre of contact

The soil contact area is taken as W/q_C. The wall rocks about point O located at the centre of the contact area.

3. Wall rocking potential

Determine whether the wall will rock by comparing the overturning moment to the restoring moment. For this calculation, S_a is based on the fundamental, elastic (no-rocking) period of the wall. The wall will rock if $S_a > (W/Mg)\tan\alpha$. If rocking is not indicated, discontinue these calculations.

4. Rocking calculations

Calculate I_o, the mass moment of inertia of the rocking system about point O. Calculate the effective viscous damping, β, of the rocking system as follows:

$$\beta = 0.4(1-\sqrt{r}) \; where \; r = \left[1 - \frac{MR^2}{I_O}(1-\cos(2\alpha))\right]^2 \tag{2-9}$$

Construct the design response spectrum at this level of effective damping using the damping factors listed in Table 2-1 (the factor B_s is applied to the constant acceleration region of the spectrum, factor B_l to longer periods).

By iteration or graphical methods, solve for the period and displacement that simultaneously satisfy the design response spectrum and the following rocking period equation:

$$T = \frac{4}{\sqrt{\frac{WR}{I_O}}}\cosh^{-1}\left(\frac{1}{1-\frac{\theta}{\alpha}}\right) \; where \; \theta = \frac{\delta_{rocking}}{R\cos\alpha} \tag{2-10}$$

Also recall that $S_d = S_a g \dfrac{T^2}{4\pi^2}$ (2-11)

At the desired solution, $\delta_{rocking} = S_d$ (2-12)

Table 2-1 FEMA 356 Damping Factors

Effective Viscous Damping	Coefficient B_s	Coefficient B_1
<2%	0.8	0.8
5%	1.0	1.0
10%	1.3	1.2
20%	1.8	1.5
30%	2.3	1.7
40%	2.7	1.9
>50%	3.0	2.0

2.3 FEMA Nonlinear Static Procedure

In addition to the rocking formulation, FEMA 356 also specifies a nonlinear static procedure which can be used to evaluate the seismic performance of all types of structures. The procedure is used to solve for displacement of a control node, typically located at roof level of the structure.

In the standard NSP method, the nonlinear force-displacement relationship between base shear and displacement of the control node is replaced with an idealized relationship to calculate the effective lateral stiffness, K_e, and effective yield strength, F_y, of the building as shown in Figure 2-4. This relationship is bilinear, with initial slope K_e and post-yield slope α.

Line segments on the idealized force-displacement curve are located using an iterative or graphical procedure that approximately balances the area above and below the curve. The effective lateral stiffness, K_e, is taken as the secant stiffness calculated at a base shear force equal to 60% of the effective yield strength of the structure. The post-yield slope, α, is determined by a line segment that passes through the actual curve at the calculated target displacement. The effective yield strength is not greater than the maximum base shear force at any point along the actual curve.

The effective fundamental period, T_e, is calculated as:

T_e Effective period. $= T_i \sqrt{\dfrac{K_i}{K_e}}$ (2-13)

T_i Elastic fundamental period (in seconds) in the direction under consideration, calculated by elastic dynamic analysis

K_i Elastic lateral stiffness of the building in the direction under consideration.

K_e Effective lateral stiffness of the building in the direction under consideration.

The target displacement, δ_t, is defined as

$$\delta_t = C_0 C_1 C_2 C_3 S_a \frac{T_e^2}{4\pi^2} g \tag{2-14}$$

Figure 2-4 Use of Capacity Curve For NSP

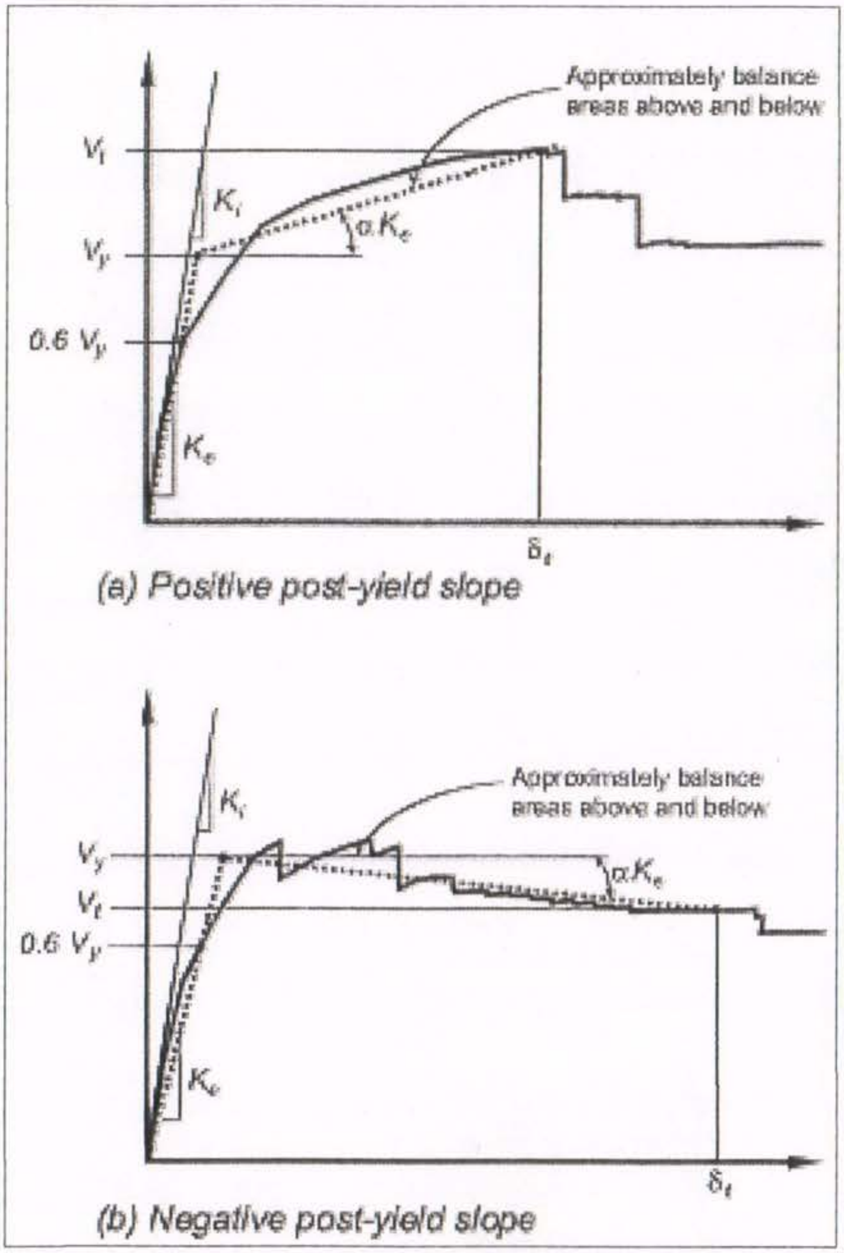

The variables in equation (2-14) are defined as:

C_0 Factor relating roof to spectral displacement. Equal to 1.0 for a single story structure, else extracted from tabulated values or calculated as the product of participation factor and mode shape amplitude.

C_1 Factor relating elastic to inelastic displacements, a function of R and T_e.

$= 1.0$ for $T_e \geq T_s$ (2-15)

$= [1.0 + (R - 1) T_s/T_e]/R$ for $T_e < T_s$ (2-16)

T_s is the transition period between constant acceleration and constant velocity on the design spectrum.

C_2 Factor for hysteresis shape. For a strength degrading structure, this is a function of performance level and period.

C_3 Set to 1.0 for buildings with a positive post-yield stiffness.

S_a Response spectrum acceleration for the appropriate period and damping.

The strength ratio, R, used to calculate the modification factor C_1 in Equation (2-16), is defined as:

$$R = \frac{S_a}{V_y / W} \cdot \frac{1}{C_0} \tag{2-17}$$

Equation (2-14) is a conversion from spectral acceleration to spectral displacement (see Equation (2-11)) with an adjustment by factors C_0, C_1, C_2 and C_3 which depend on the type of structure, structural characteristics and type of hysteresis. As a rocking structure produces elastic unloading, rather than hysteretic behaviour, the factors are unlikely to be able to be used directly for rocking response.

2.4 ATC-40 Capacity Spectrum Procedure

The method described by ATC-40, and permitted in FEMA 356 as an alternative NSP method, is termed the Capacity Spectrum Method. Details of this procedure are not specified in FEMA 356, but it is considered an acceptable alternative procedure and was described in FEMA 274, where it was termed Method 2.

In Method 1, discussed in the preceding section, the design displacement response is calculated using an initial effective stiffness. Method 2 determines the maximum response based on the displacement corresponding to the intersection of the load-displacement relation (also known as the capacity curve) for the building and the spectral demand curve used to characterize the design seismic hazard.

Method 2 uses both the initial effective stiffness and secant stiffness information to calculate the target displacement. Figure 2-4 illustrates the different stiffness used by the two methods. Ideally, the two methods should produce the same design displacement. This is achieved for most cases by using different damping values for the two methods. Method 1 uses the damping effective for response near the yield level, typically 5% of the critical value. Method 2 uses a higher damping value, determined based on the shape of the hysteresis and the maximum deformation level.

The procedure may require iterations as both damping and secant period are a function of displacement. The implementation is based on development of the capacity curve as described above for Method 1 but the procedure for deriving the target displacement is different:

1. A target displacement is estimated, based on either an initial assumption or information obtained from previous iterations in the procedure. Given this target displacement, an effective initial stiffness is determined. The secant stiffness is defined by the slope of a line from the origin to the nonlinear load-deformation relation at the point corresponding to the target displacement. The corresponding global displacement ductility is defined as $\mu = K_e/K_s$.

2. The equivalent viscous damping is determined as a function of the global displacement ductility and the expected shape of the hysteresis relation for response at that ductility level using either explicit calculation or tabulated data for different seismic framing systems.

3. Given the equivalent viscous damping determined as described above, a design response spectrum for that damping is constructed. This can be achieved by first constructing the general acceleration response spectrum for 5% damping, and then modifying it by the coefficients in Table 2-1 for different levels of damping. The acceleration response spectrum can be converted to a displacement response spectrum by multiplying the acceleration response spectrum ordinates by the factor. Figure 2-5 illustrates the effect of different damping levels on a typical acceleration and displacement response spectrum.

4. Compare the displacement response amplitude calculated for the assumed secant stiffness and damping with the displacement amplitude assumed in Step 1. If the values differ by more than about 10%, iterate the process beginning with Step 1. It is possible to plot both the spectral acceleration and the spectral displacement on a single graph. Figure 2-6 plots an example for a range of equivalent viscous damping. The radial lines correspond to lines of constant period. Using this format, the target displacement for the equivalent SDOF system is at the intersection of the load-deformation envelope with the response spectrum for the appropriate damping level. Note that the target displacement for the equivalent SDOF system in general is not the same as the target displacement at the roof level; to arrive at the roof level target displacement requires transformation back to the MDOF system.

Figure 2-5 Capacity Spectrum

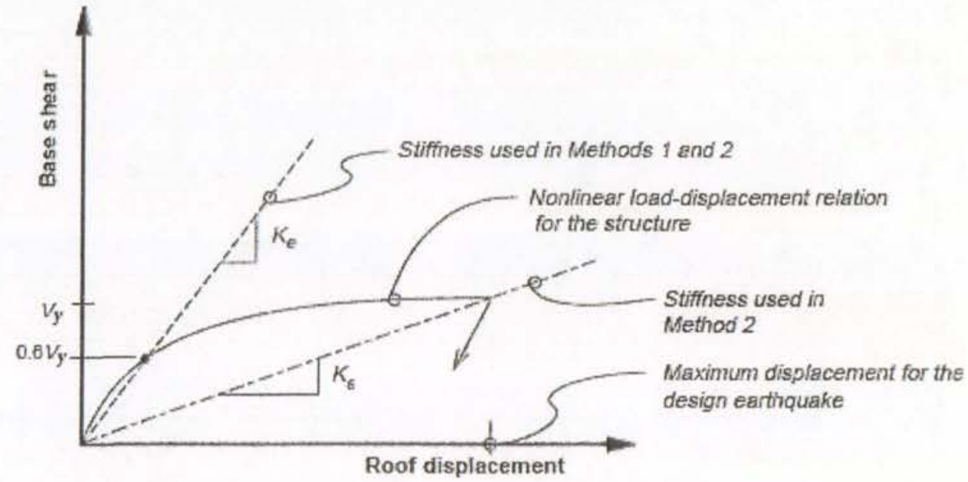

Figure 2-6 Capacity Spectrum Procedure

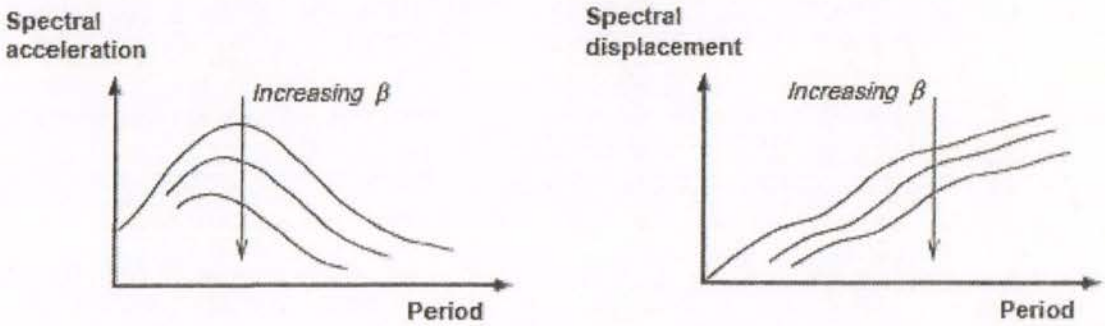

Figure 2-7 Spectral Demand Curves

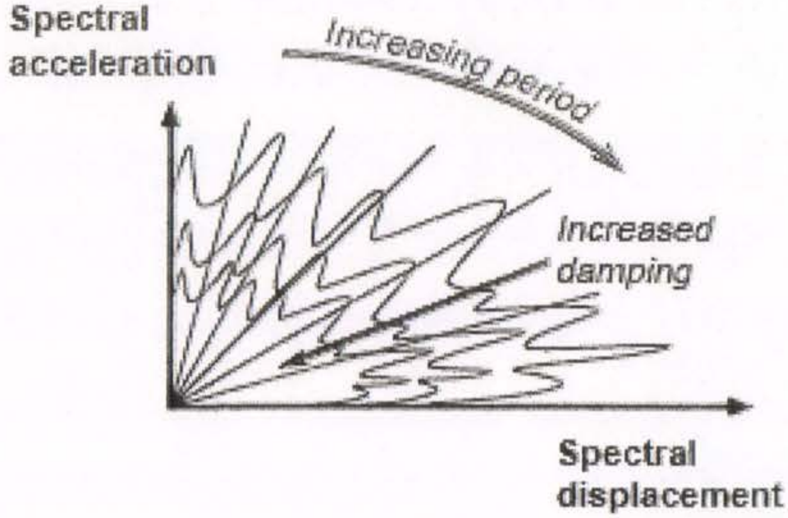

3 NONLINEAR ANALYSIS OF ROCKING SYSTEMS

3.1 Analysis of Rocking Blocks

As discussed in the introduction, research on the response of rocking systems has shown that the response is best described by solving the second order ordinary differential equation based on the rotational moment of inertia of the block, with the dynamics of the system described by the block angular velocity. The energy loss of the system is replicated using an apparent coefficient of restitution approach first developed by Housner [7].

This procedure has been shown to be the most appropriate for single rocking blocks. However, for buildings which have rocking or uplifting components the rocking elements are usually only a portion of the total structural system. The overall building system is described by the translational masses at floor levels and the lateral stiffness of the structural elements such as beams, columns and walls. The formulation based on rotational inertia and angular velocity cannot be extended to encompass a complete building system and so a more general nonlinear approach is required.

3.2 Analysis of Buildings

Nonlinear analysis of buildings is based on the displacement method, where the stiffness matrix of the total building is assembled from the stiffness of each component and the mass matrix assembled from component masses. For dynamic response, the displacements of the building are calculated under the actions of imposed translational base accelerations. Energy dissipation is modelled using the Rayleigh damping function, where a damping matrix is assembled as coefficients applied to the stiffness and mass matrices respectively.

Although general purpose analysis procedures are not ideal for rocking block analysis, any practical evaluation of buildings is constrained to use them. The main reservations relate to the form of the energy dissipation function, as Rayleigh damping is not well suited to model the coefficient of restitution approach to energy loss. In this section, experimental results on rocking block system are used to assess methods by which a general purpose analysis computer program can be used to model systems which have uplifting or rocking elements.

3.3 Analysis Procedure

The nonlinear analyses performed as part of this study were based on the ANSR-II computer program, a general purpose computer program developed at the University of California, Berkeley [19]. A modified version of this program has been in use for the evaluation of rocking systems for over a decade [20, 26] and has been shown to be able to accurately model nonlinear response [21].

The analysis models are developed based on engineering mechanics formulations to attempt to duplicate the physical behaviour and have been demonstrated to be able to match the resistance function of rocking and uplifting models very accurately, as evidenced by comparisons with static tests under applied displacements. However, it is much more difficult to accurately capture the dynamic characteristics of rocking and uplifting systems. The response of a structure subjected to input ground accelerations, a_g, is defined by the equation of motion:

$$[\mathbf{M}]\ddot{\Delta}+[\mathbf{C}]\dot{\Delta}+[\mathbf{K}]\Delta=-[\mathbf{M}]a_g \tag{3-1}$$

In this equation, [M], [C] and [K] are respectively the mass, damping and stiffness matrices of the structure. The response of the structure is described by the acceleration, $\ddot{\Delta}$, the velocity, $\dot{\Delta}$, and the displacement, Δ.

It is straightforward to define the mass properties of most structures and the stiffness properties can be defined by engineering mechanics and experimental results. However, the energy dissipation represented by the damping, C, is more difficult to define. Most nonlinear analysis programs use a "dissipation function" defined by Rayleigh in1877 [22], a function now commonly known as Rayleigh damping. In this procedure, a damping matrix is constructed as a function of both the mass and stiffness:

$$[\mathbf{C}]=\alpha[\mathbf{M}]+\beta[\mathbf{K}] \tag{3-2}$$

Mass proportional damping increases with increasing period whereas stiffness proportional damping decreases with increasing periods. The two damping coefficients, α and β, allow an equivalent viscous damping to be defined at two periods, as shown in the example in Figure 3-1, where the coefficients are selected to provide 5% damping at periods of 0.10 and 1.0 seconds. For periods between these two limits the damping will be less than 5% (with a minimum of 2.9% in this example) but will increase beyond 5% for periods outside this range. The increase is more rapid for periods shorter than the specified range.

Figure 3-1 Rayleigh Coefficients for 5% Damping at 0.10 and 1.0 Seconds

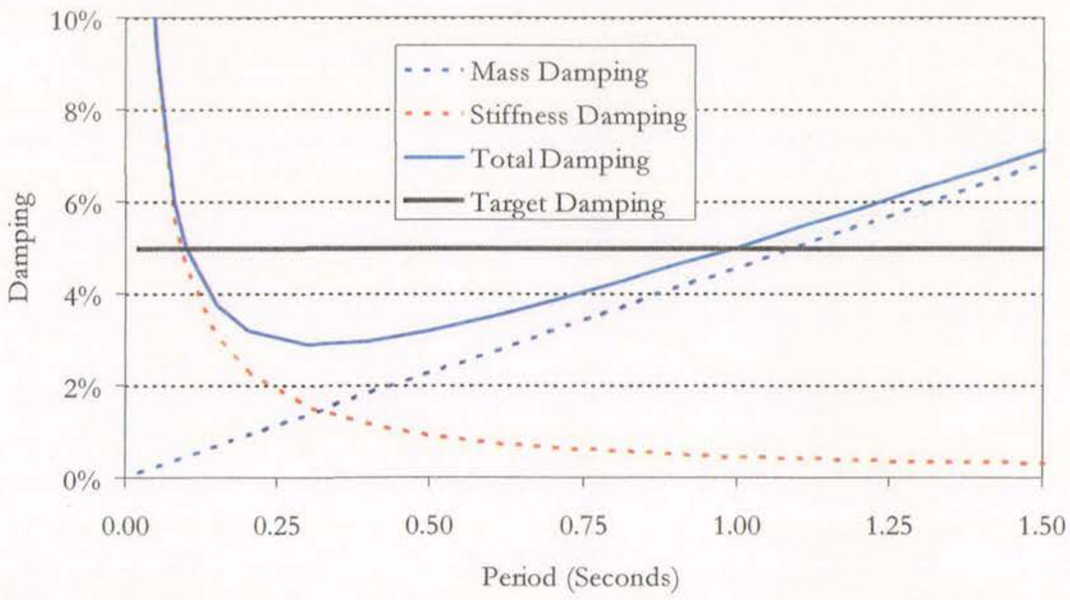

Nonlinear structures by definition do not have a constant period and so Rayleigh damping is at best an approximation of the actual energy loss mechanism. The aim of the correlations with test results in this section is intended to develop empirical procedures which can be used to specify damping coefficients which produce approximately the correct dynamic response.

3.4 Face Loaded Wall Test

Reference [23] details a free vibration test of a 3.000 m high specimen of 230 mm thick unreinforced brick. The wall was pre-cracked at the base and mid-height and loaded horizontally adjacent to the mid-height joint. The centre of the wall was displaced approximately 143 mm then released so that the wall's free damped response could be measured. The wall effectively formed two rocking blocks.

Figure 3-2 ANSR Face Load Model

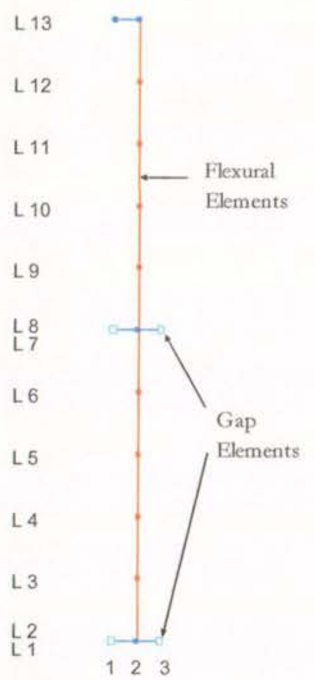

An ANSR-II model of the wall was developed as shown in Figure 3-2. This is similar in form to the Drain-2DX model reported in Reference [23]. The wall was modelled with flexural elements, with properties based on gross dimensions and default properties for brick masonry. The gap element stiffness was based on an elastic modulus of the masonry of E_M = 4,400,000 kPa and an area $A = A_G/4$ = 0.028175 m^2, where Ag is the gross area of wall. An element length of L = 0.250 m was assumed, such that $K = E_M A/L$ = 496,000 kN/m.

Figure 3-3 compares the force-displacement loading function from the test and as predicted by ANSR-II. The mechanism for static load resistance is well defined and, as expected, the analysis results match the experimental curve well.

Figure 3-3 Wall Static Test

(a) From Reference [23] **(b) ANSR Analysis**

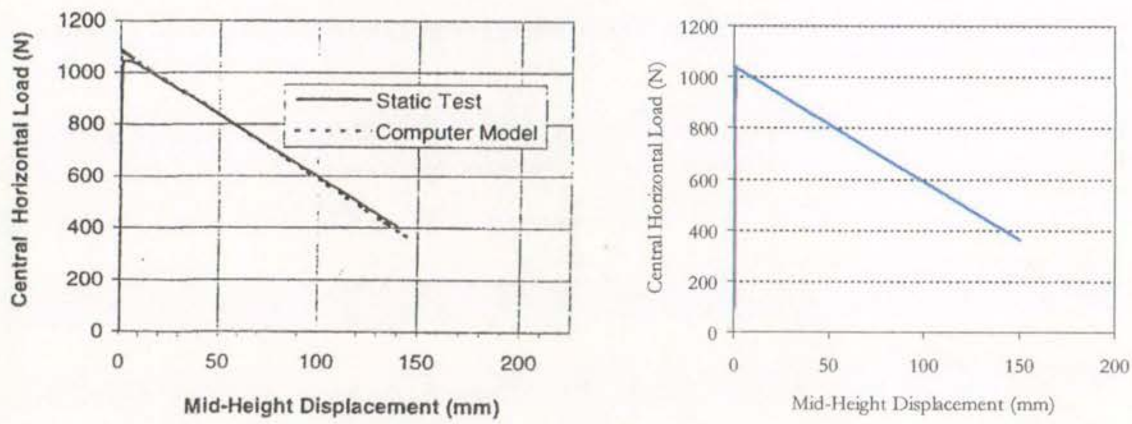

For the dynamic analysis for, the lower limit of the period range for damping was defined as the elastic period of the wall, 0.052 seconds, and the upper limit set at 1.0 seconds, the estimated maximum period of response. The damping fraction from which the Rayleigh coefficients α and β were calculated was modified to match the experimental decay. A value of 10% at each of the upper and lower periods was found to provide the best fit to the experimental results, as shown in Figure 3-4.

Figure 3-4 Wall Dynamic Test

From Reference [23] **ANSR Analysis**

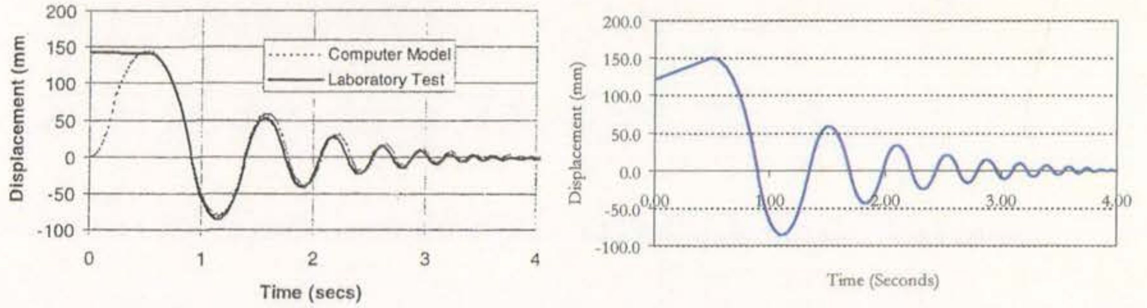

The specified fraction of 10% of viscous damping is not the actual damping for the analysis but rather defines the maximum value for any period between the upper and lower limits (see Figure 3-1). The actual damping provided is a minimum of 4.3% at a period of 0.23 seconds. The damping coefficients are not applied to the gap elements and so not all elements in the model are damped (that is, only part of the stiffness matrix, [K], is multiplied by β). Because of this, the minimum system damping will be some value less than 4.3%.

3.4.1 Fitted Damping Curve

An average effective damping can be estimated by fitting an exponential curve to the peaks of the calculated decay curve, as shown in Figure 3-5. The curve is not an exact match as rocking walls do not provide constant viscous damping. However, a decay curve calculated using the average period of 0.23 seconds and a damping fraction of 3% provides a good fit to the peaks. The test results suggest that the decay of the bare unreinforced wall provides the equivalent of 3% viscous damping.

Figure 3-5 Wall Test Fitted Damping Decay Curve

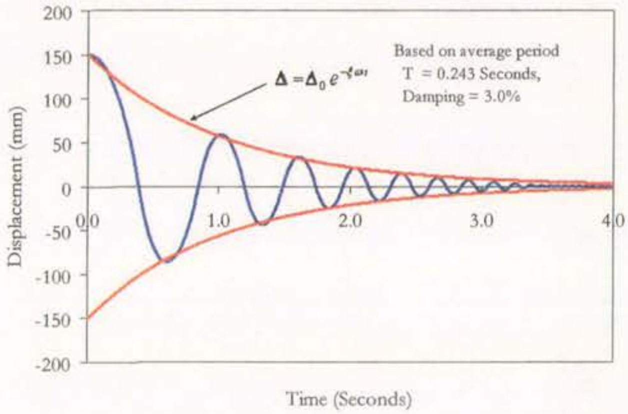

3.4.2 Sensitivity of Face Load Model

As discussed above, the stiffness of the gap elements modelling gap openings was based on material and geometric properties with an assumed effective length of 250 mm. This length is arbitrary in that there is no engineering mechanics basis for the selection of this value. However, the results tend not to be sensitive to this value provided it is not so short as to provide a very high stiffness and ill-conditioning of the stiffness matrix.

Figure 3-6 shows the effect on the analytical decay of decreasing the effective length from 250 mm to 15 mm, which increases the stiffness by a factor of 250/15 = 16.7. The difference is relatively small for the large amplitude cycles and the differences only become significant once decay has reduced to about 10% of the initial value.

Figure 3-6 Effect of Gap Stiffness

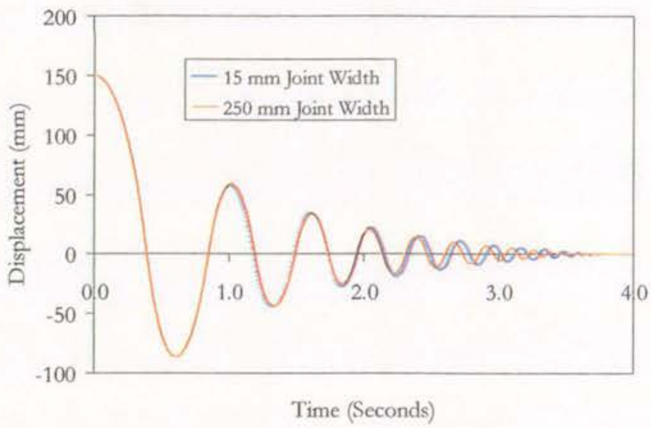

3.5 Free Rocking Block

Reference [13] reports the results of a number of tests for free rocking blocks. A number of aspect ratios for concrete masonry blocks were considered and this correlation used two of these, h/b = 3 and h/b = 5, where h is the block height and b the dimension in the direction of rocking.

An ANSR-II model was developed as shown in Figure 3-7. This is a combination of linear elastic panel elements to represent the block and gap elements to represent the separation and uplift at the base. The total mass of the block was lumped, one-half at mid-height and one-half at the top.

The lower limit period to defined damping was set at the elastic period of the walls, calculated as 0.006 seconds for h/b = 3 and 0.013 for h/b = 5. The upper period was set at 100 times this value, 0.60 and 1.30 seconds respectively. The upper limit was based on the estimate of the maximum period of response as indicated by the tests.

As for the face loaded wall, the fraction of viscous damping was adjusted so as to provide the best fit to experimental results. For these two blocks, the best fit was found to be when the damping fraction was defined as 15% of critical.

Figure 3-7 ANSR Free Rocking Model

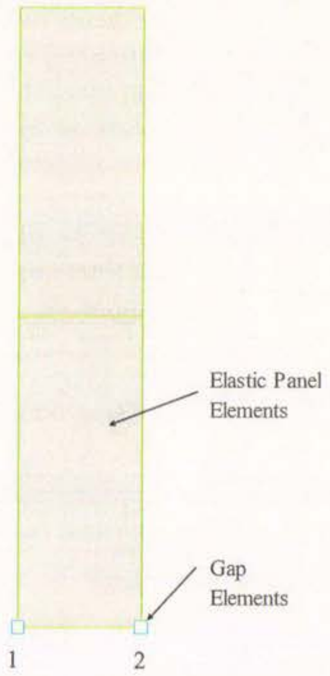

Figure 3-8 shows the time history of block rocking from release for both aspect ratios. The initial cycles from the analysis are generally similar to the experimental results but the low amplitude displacements continue for a longer time than the experimental results, indicating that the model provides less damping at low amplitudes than the test specimens.

Figure 3-8 Wall Rocking Decay

(a) From Reference [13] **(b) ANSR Analysis**

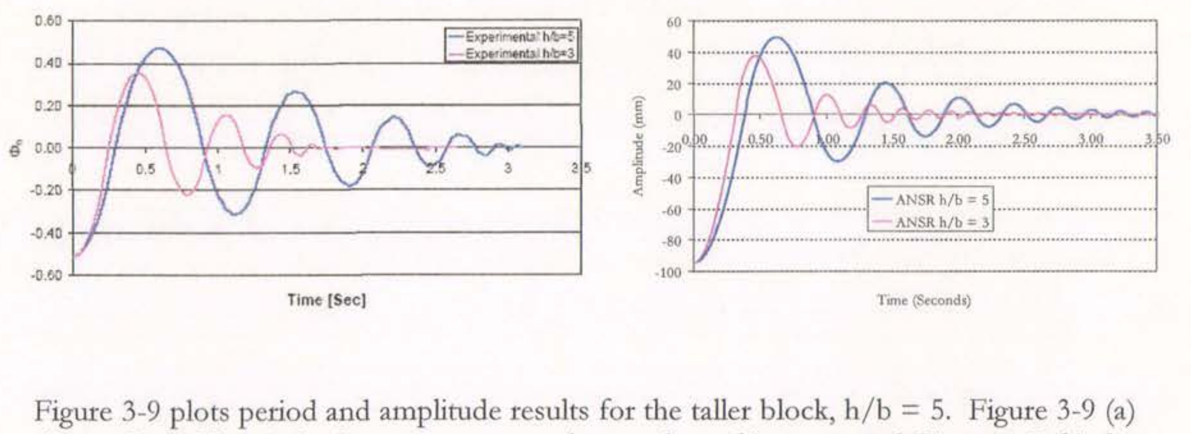

Figure 3-9 plots period and amplitude results for the taller block, h/b = 5. Figure 3-9 (a) shows the half period of response versus the number of impacts and Figure 3-9 (b) the amplitude versus the number of impacts. This latter plot defines the energy dissipation, or equivalent damping. The zigzag pattern of the experimental values was attributed to imperfections in the blocks. In general, the ANSR-II analyses modelled the change in period and amplitude well for the first 10 impacts, although as shown in Figure 3-8 the analysis rocking continued for more impacts than the test, indicating that the analysis under-damped low amplitude motions.

Figure 3-9 Period and Damping h/b = 5

(a) Variation in Period **(b) Variation in Amplitude**

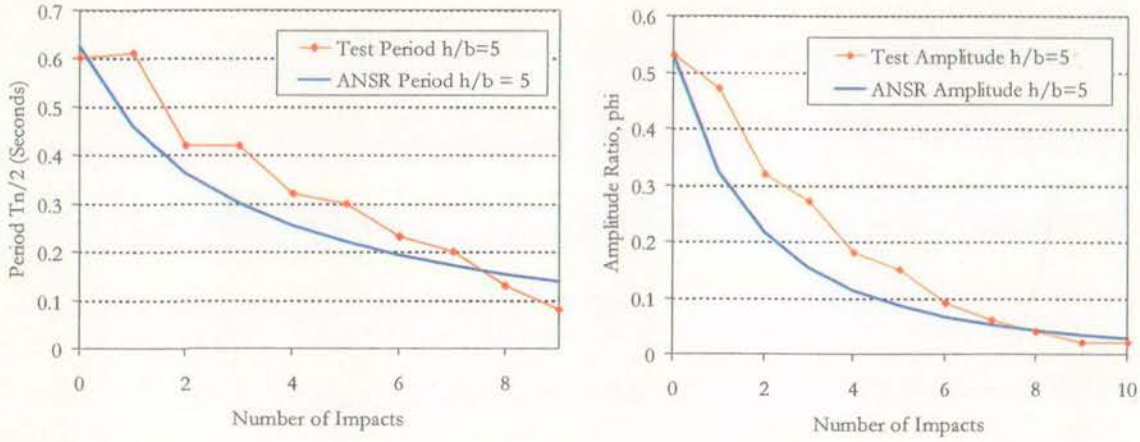

Figure 3-10 plots similar results for the shorter block, h/b = 3. Figure 3-10 (a) shows the half period of response versus the number of impacts and Figure 3-10 (b) the amplitude versus the number of impacts. In general, the ANSR-II analyses modelled the change in period and amplitude better for this wall than for the taller wall. However, as for the h/b = 5 wall, the damping did not bring the analysis block to rest but continued to rock at low amplitudes when the experimental block had returned to rest.

Figure 3-10 Period and Damping h/b = 3

(a) Variation in Period **(b) Variation in Amplitude**

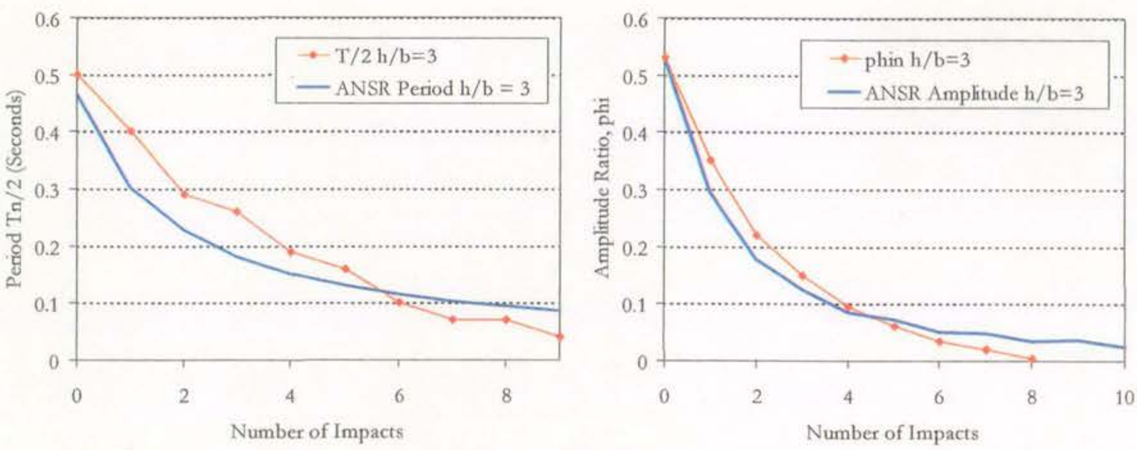

3.5.1 Fitted Damping Curve

As for the rocking wall, an average effective damping can be estimated by fitting an exponential curve to the peaks of the calculated decay curve, as shown in Figure 3-11.

Decay curves calculated using the average period of vibration over the rocking cycles (0.11 seconds and 0.19 seconds for h/b = 3 and 5 respectively) and a damping fraction of 3.5% of critical provides a reasonable fit to the peaks. Therefore, the energy dissipation of the block can be approximated with the equivalent of 3.5% viscous damping.

Figure 3-11 Free Rocking Fitted Damping Decay Curves
(a) h/b = 3 (b) h/b = 5

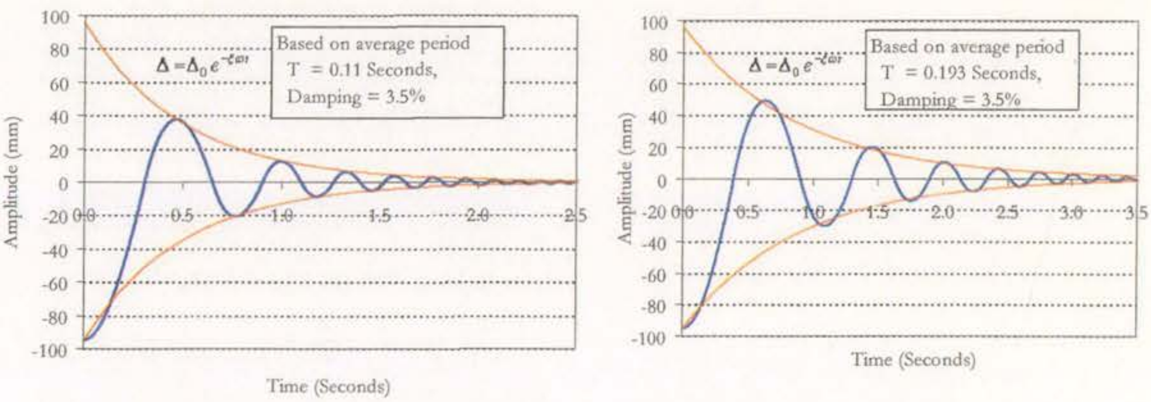

3.6 Evaluation Of Damping Factors

Table 3-1 summarizes the periods and damping fractions used for the analyses which provided the best fit to the experimental response for the test programs described in the preceding sections.

For these free rocking blocks the damping fraction used to calculate Rayleigh coefficients to provide a correlation with the tests ranged from 10% to 15%. This was much higher than the apparent equivalent viscous damping in the test program which was calculated as from 3% to 3½%.

Based on these results it appears that analysis models of structures with free rocking require higher damping coefficients than would be calculated from the apparent viscous damping. The likely reason for this is because the stiffness damping coefficients are not applied to the gap elements. When no elements with stiffness damping cross the rocking interface, as in uncontrolled rocking, a higher nominal damping fraction is required to provide the required effective damping.

Table 3-1 Summary of Model Damping Parameters

Project	Period T_1	Period T_2	Damping Fraction for Calculation	Actual Damping
1. Opus Face Load Test	1.00	0.052	10%	3.0%
2. UA Free Rocking Wall h/b = 3	0.60	0.006	15%	3.5%
3. UA Free Rocking Wall b/h = 5	1.30	0.013	15%	3.5%

3.7 Procedure For Nonlinear Analysis

Based on the correlation with test results, the following procedures are recommended for the incorporation of Rayleigh damping in the analysis of models with rocking and uplifting elements:

1. Set the first period as the expected maximum period of response. For most actual nonlinear buildings an estimate of approximately 1.5 times the elastic period will be conservative but in some cases preliminary analyses may be needed to estimate this value.

2. Set the second period as the period at which an effective mass ratio of at least 90% is achieved. For single degree of freedom systems, such as single rocking blocks, set the second period as the elastic (non-rocking) period of the block.

3. Set the damping fraction to calculate Rayleigh coefficients at both periods as the nominal viscous damping of the structure. This will be 5% for code type evaluations.

The correlations here have shown that this procedure may underestimate the energy dissipation in a freely rocking structure where the loss of energy is not well represented by Rayleigh damping. Therefore, results will tend to be conservative.

4 SELECTION AND SCALING OF EARTHQUAKE RECORDS

Time history analysis is the only method of accurately evaluating the seismic response of nonlinear systems such as rocking or uplifting structures. The usual input load function for this type of analysis is an acceleration time history at support level. This chapter discusses the selection and scaling of time history records to be used for the nonlinear analysis studies.

4.1 Code Requirements

4.1.1 New Zealand Practice

The NZ loading code, NZS1170 [2], requires that a minimum of three time history records be selected from actual records that have a seismological signature consistent with the signature of events which contributed to the target design spectrum. Where three appropriate time histories are not available, simulated ground motion records may be used to make up the family.

Once the records are selected, the code specifies a procedure by which scaling factors are applied to the three records such that the envelope of the three records exceeds the target spectrum at all periods within the range of 0.4 to 1.3 times the structure period. The evaluation of performance is then based on maximum response of the three records.

4.1.2 United States Practice

U.S guidelines such as those published by FEMA [4] are similar to NZ codes in that a minimum of 3 records are scaled so as to exceed the target spectrum and the response is then based on the maximum of the three records. The scaling procedure differs from NZ practice in that, rather than scaling the dominant component of the earthquake to envelope the target spectrum, FEMA requires that the record be scaled so that the SRSS of the two components envelopes 1.4 times the target spectrum. As the two components of recorded earthquakes tend not to be similar in magnitude, the FEMA procedure tends to produce higher scaling factors than NZS 1170.

FEMA provides an alternative method, whereby when seven or more time history records are employed, the average rather than maximum value of each response parameter shall be permitted to determine design acceptability. In practice, most evaluations using time history analysis in the U.S. are based on a minimum of seven time history records.

4.2 Frequency Scaling

In NZ, the usual practice is to apply a scalar factor to the input time history. In the US, seismologists often adjust the amplitudes of the record in the frequency domain so as to provide a closer match to the target spectrum. Typically this type of scaling is an empirical procedure based on the following steps:

1. A response spectrum of the actual recorded earthquake is generated.

2. Scale factors are calculated at each frequency point by dividing the ordinates of the target spectrum by the corresponding ordinate of the spectrum of the recorded time history.

3. The recorded time history is converted to the frequency domain using a Fast Fourier Transform (FFT).

4. The Fourier amplitudes are modified by multiplication by the calculated scale factors at each frequency point. The phase angles are left unchanged.

5. The modified Fourier transform is converted back to the time domain using an inverse FFT.

6. The response spectrum of the modified earthquake record is generated.

7. The error between the target spectrum and spectrum of the modified time history is calculated at each value. If the average error is less than a target value, usually 5%, the recorded record is accepted, otherwise return to Step 2 above.

This process does not have a theoretical basis other than that the response spectra of the target spectrum and that of the modified time history have similar amplitudes at each frequency point considered. However, in practice the average nonlinear response using a series of frequency scaled time histories does seem to provide a smooth response. This provides a procedure by which time history input can be equivalent to that of a code response spectrum in terms of the response not being sensitive to relatively small changes in period.

4.2.1 Effect on Time History

<u>El Centro 1940 Record</u>

The procedure described above was applied to the El Centro 1940 N-S (ELC-NS) component with the target spectrum based on NZS1170 Z = 0.44, Soil Type C. The scaling was performed for two conditions, (1) distant from the fault (FF-C) and (2) within 2 km of the fault (NF-C).

Figure 4-1 plots the spectra of the original record and also the record modified for the two fault conditions. As expected, the two scaled records provide almost identical spectral ordinates for periods less than T = 1.5 seconds, after which the near fault factor, N, increases the ordinates.

Figure 4-2 plots the three records used to generate the response spectrum in Figure 4-1. The latter two traces, the modified records, exhibit more high frequency content than the original record although they have a generally similar shape. The far fault and near fault records do not exhibit any obvious visual differences. This is because the frequency scaling procedure has incorporated near fault effects by adding low amplitude, low frequency waves to the original record rather than a single acceleration pulse as occurs in actual near fault records.

In Figure 4-3 a 5 second window, from 5 to 10 seconds, has been plotted for ELC-NS and FF-C. This shows more clearly the differences in the two traces. The modified record retains many of the characteristics of the original record but there is additional high frequency content superimposed on the record. This is because, as shown in Figure 4-1, the original record is deficient in spectral amplitude is the range of periods from 0 to 0.50 seconds compared to the target spectrum.

Figure 4-1 Frequency Scaled El Centro 1940-N-S 5% Damped Spectra

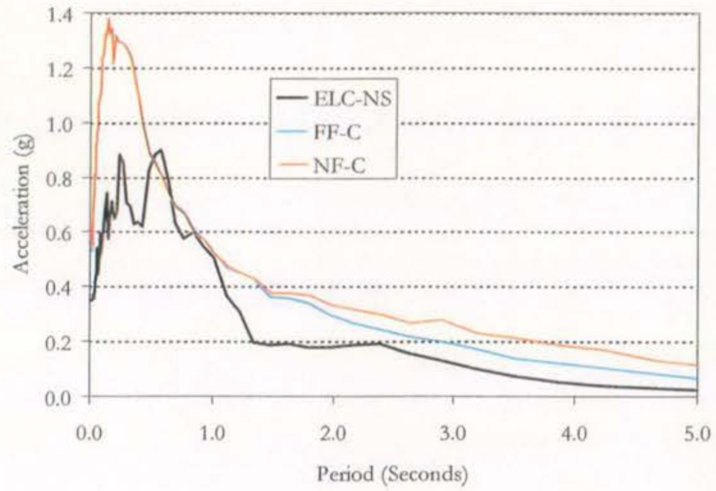

Figure 4-2 Frequency Scaled El Centro 1940-N-S 5% Time Histories

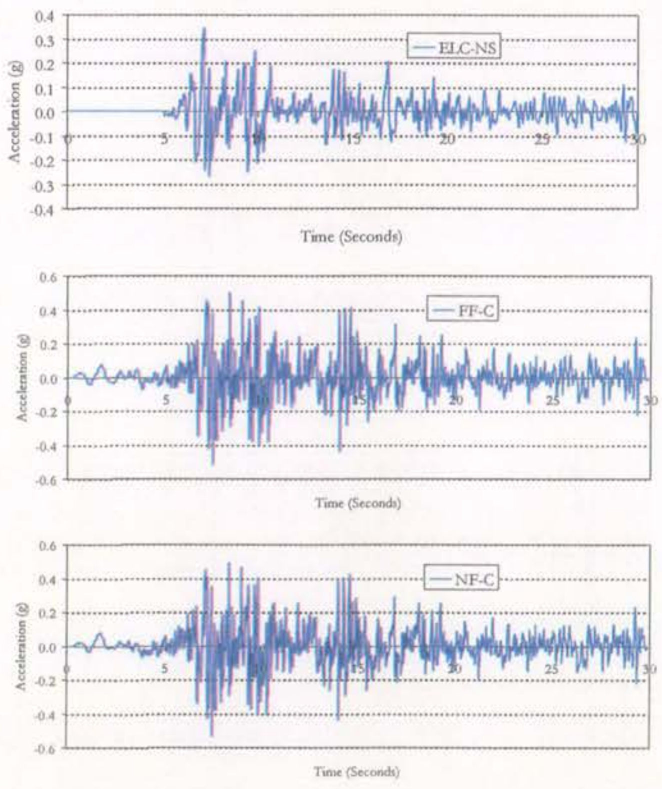

Figure 4-3 Detail of El Centro Time History

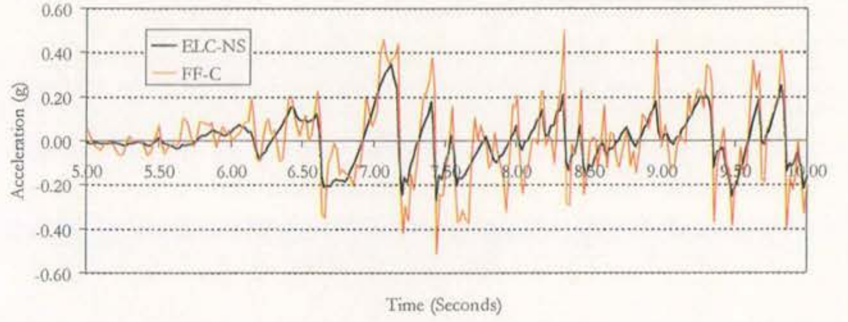

Kocaeli 1999 Duzce Record

Figure 4-4 provides details of the scaling of the Duzce Record from the 1999 Kocaeli, Turkey, earthquake, a record which exhibited near fault characteristics. This figure shows the original and modified records on the left, the 5% damped response spectra on the right and a detail of the portion of the record from 12 to 16 seconds, which exhibits large acceleration pulses, bottom right. The original record has been scaled by 1.25, which is the factor calculated for a 2 second period when the record is part of a suite for Z = 0.44, Soil D, the same as for the modified record.

The detail from 12 to 16 seconds shows that the modified record appears to retain the pulse characteristics of the original record. Superimposed on this are the shorter period motions, where the original record was deficient.

Figure 4-4 Kocaeli 1999 Duzce Record

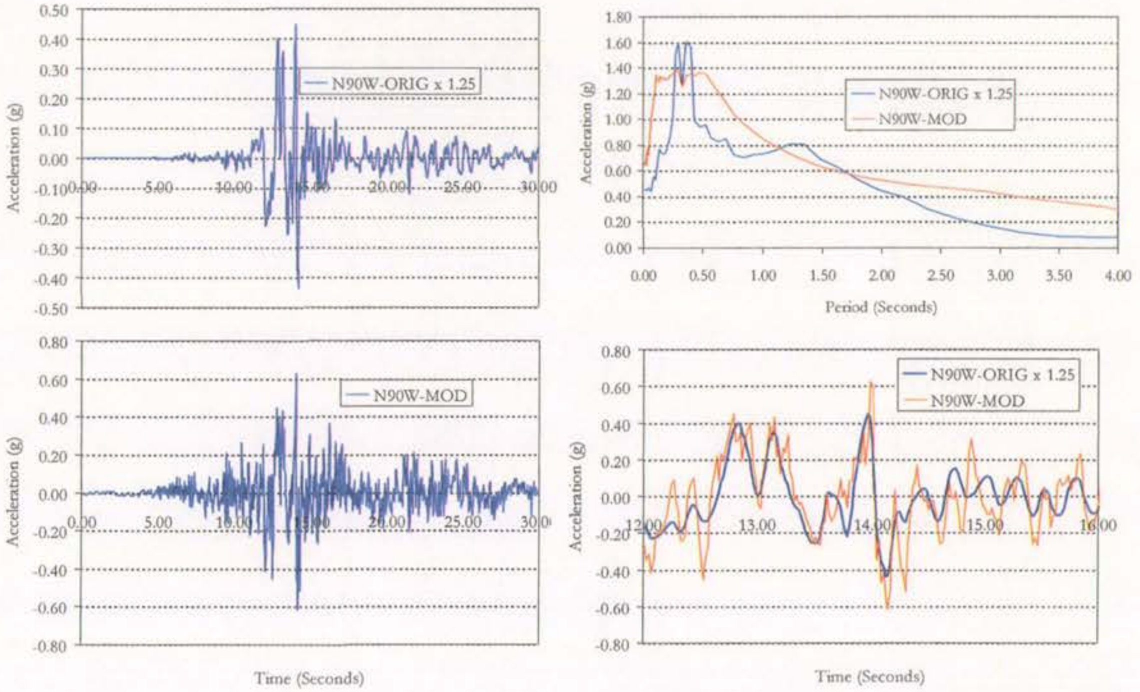

El Centro 1979 Array 6 Record

Figure 4-5 provides similar details of the scaling of the Array 6 Record from the 1979 El Centro earthquake, a record which also exhibits near fault characteristics. The original record has been scaled by 1.06, which is the factor calculated for a 2 second period when the record is part of a suite for Z = 0.44, Soil D, the same as for the modified record.

The detail from 5 to 10 seconds shows that the scaling effects are similar to that for Duzce. The modified record appears to retain the pulse characteristics of the original record and superimposed on this are the shorter period motions, where the original record was deficient.

Figure 4-5 El Centro 1979 Array 6 Record

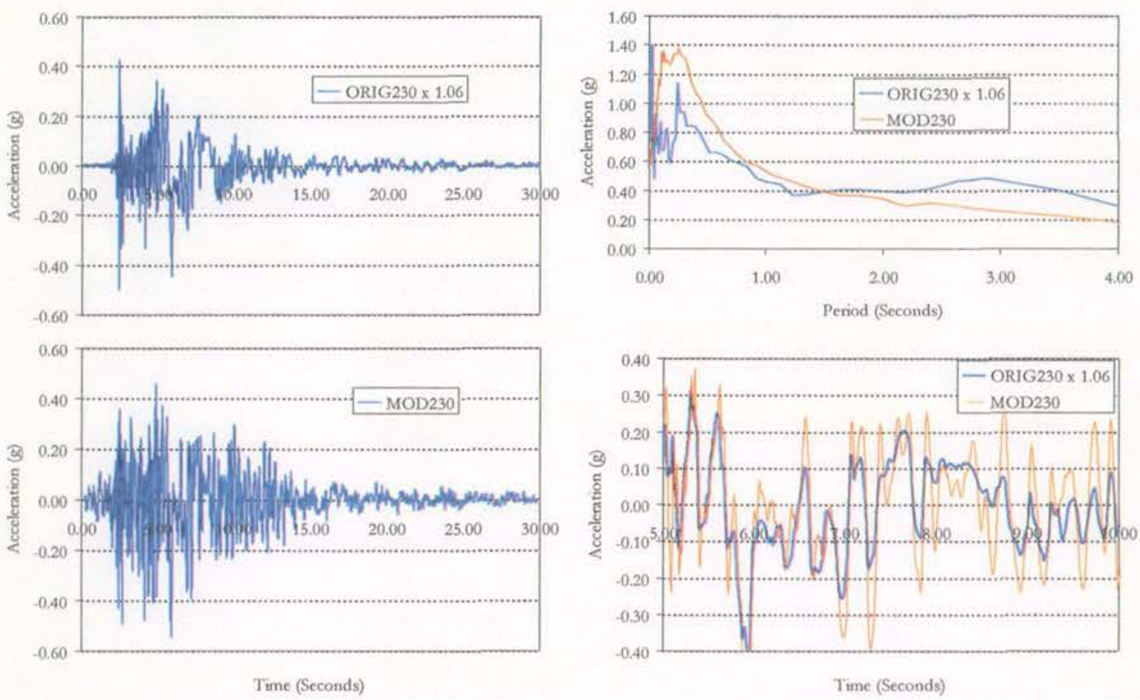

4.3 Suites of Records Selected For Scaling

4.3.1 Far Fault Records

For sites distant from faults (> 20 km) the set of 7 records listed in Table 4-1 was selected for frequency scaling. The records are from sites in NZ (1), USA (5) and Italy (1). Both components of each record were scaled.

Figure 4-6 compares the 5% damped acceleration and displacement response spectrum from each scaled record with the target values. (It is not intended that individual records be distinguished in Figure 4-6, rather that the dispersal be apparent). The spectra of all scaled records are generally close to the target.

Table 4-1 Acceleration Records Used for Distant from Fault

FILE	TITLE
MA1	Matahina Dam D (bottom centre) Edgecumbe 1987 N83E
LACC_NOR	Century City – LACC North
JOSHUA	Joshua Tree - Fire Station
GILROY#2	Gilroy #2 - Hwy 101/Bolsa Rd. Motel Chan 1: 90 deg Santa Clara
ELC1	USA El Centro Imperial Valley (USA) 1940 N90W
BO1	Italy Bovino Campano Lucano (Italy) 1980 N90E
WWASH	Olympia N04W Western Washington E Apr 13 1949

Figure 4-6 5% Damped Spectra Soil C Z = 0.44 Distant from Fault

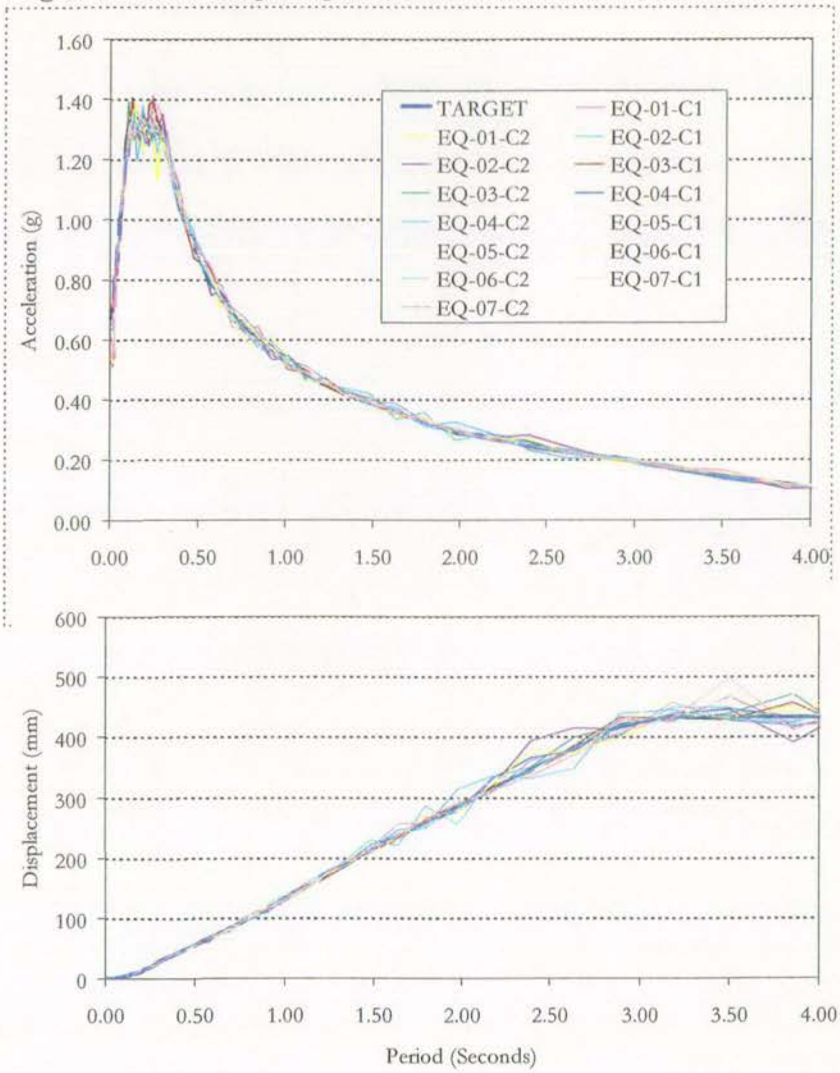

4.3.2 Near Fault Records

For sites close to faults (within 2 km) the set of 7 records listed in Table 4-2 was selected for frequency scaling. The records are from sites in the USA (4), Turkey (1), Mexico (1) and Iran (1). All these records with the exception of ELC1 were recorded close to the fault.

Figure 4-7 compares the 5% damped acceleration and displacement response spectrum from each scaled record with the target values. (As for Figure 4-6, it is not intended that individual records be distinguished, rather that the dispersal be apparent). As for the far fault records, the spectra of all scaled records are generally close to the target although the match was not so good for periods beyond about 3.50 seconds for some records.

Table 4-2 Acceleration Records Used for Near Fault

FILE	TITLE
SYLMARH	Northridge 1994 Sylmar-County Hosp Parking Lot Ch 1 90 Deg
NEWHALL	Northridge 1994 Newhall - LA County Fire Station 90 deg
ELC1	USA El Centro Imperial Valley (USA) 1940 N90W
ECARR6	1979 Imperial Valley CA El Centro Array #6 230
DUZ1	Duzce Meteoroloji Kocaeli (Turkey) 1999 N90W
CDC1	Caleta de Campos Michoacan (Mexico) 1985 S00E
TBP1	Tabas (Iran) 1978 N90E

Figure 4-7 5% Damped Spectra Soil C Z = 0.44 Within 2 km of Fault

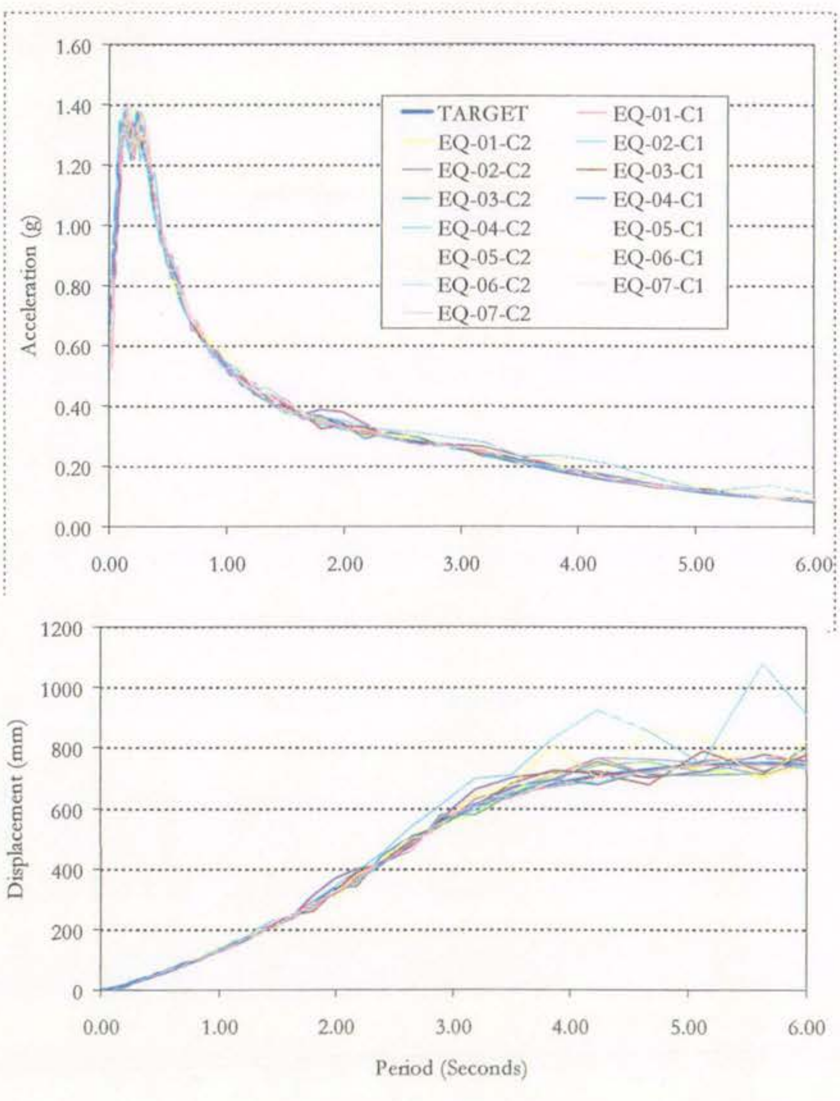

4.4 Response Of Nonlinear Systems to Scaled Records

The objective of this project is to develop guidelines for rocking systems, which are nonlinear structures. In this section, characteristics of the response of nonlinear systems to records scaled in the frequency domain are determined by examining the response of a series of single mass models.

4.4.1 Development of Nonlinear Spectra

Nonlinear response spectra are used with the effective stiffness method of analysis, particularly for base isolation systems. To develop nonlinear spectra, a single degree of freedom nonlinear system is defined as shown in Figure 4-8. This system is defined by the mass, M, and three parameters defining the stiffness properties of the system, the initial stiffness, K_u, the yielded stiffness, K_d, and the characteristic strength, Q_d. The characteristic strength is normalized to the mass, for example, $Q_d = 0.05$ indicates a strength of 0.05Mg.

Figure 4-8 Nonlinear Single Degree of Freedom Model

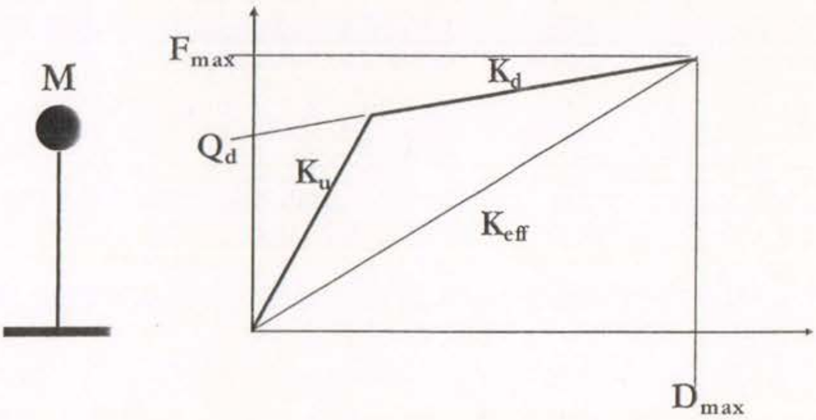

The procedure used to develop a nonlinear spectrum for a particular input acceleration time history is as follows:

1. Define the characteristic strength, Q_d, the strain hardening ratio, K_d/K_u and the viscous damping or which the spectrum is to be generated.

2. Set a starting elastic period, T, and an arbitrary initial stiffness, K_u.

3. Calculate the mass, M, required to provide the elastic period, T, as $M = \dfrac{T^2 K}{4\pi^2}$.

4. Calculate the mass proportional damping factor corresponding to the yielded stiffness as $\alpha = \dfrac{4\pi\lambda}{T_d}$ where λ is the target damping (5%) and T_d is the period associated with the yielded stiffness, K_d.

5. Using time history analysis, analyze the system for the input acceleration record and record the maximum force, F_{max}, and displacement, D_{max}.

6. Calculate the secant stiffness of the system at the point of maximum displacement, K_{eff}, and from this the effective period $T_{eff} = 2\pi\sqrt{\frac{M}{K_{eff}}}$.

7. Calculate the actual damping fraction provided at the effective period as $\lambda_0 = \frac{\alpha T_{eff}}{4\pi}$.
   If this differs by more than a specified tolerance (0.01) from the target damping, calculate a new alpha factor based on T_{eff} and return to step 5 until convergence is attained.

8. Increment the period, T, and return to step 3 until the period exceeds a predetermined limit.

Each analysis provides a point on the nonlinear spectrum. A complete set of results over all period points is plotted as maximum acceleration versus effective period and maximum displacement versus effective period to produce the nonlinear acceleration and displacement spectra respectively.

This method was applied to develop nonlinear spectra for NZS1170 design spectra based on Z = 0.44. Spectra were generated using the seven frequency scaled records developed as described above for Soil Types B, C and D and both distant from the fault and near fault conditions.

The spectra assumed that viscous damping was 5% and that the ratio of yielded stiffness to initial stiffness was 1/6.5, a median value for building structures. The curves were generated for characteristic strengths of Q_d = 0.05, 0.10, 0.15 and 5.0. The last value is a check point, set sufficiently high that yield will not occur and the nonlinear spectrum should replicate the elastic spectrum.

Once spectra have been generated for each series of seven time histories, mean spectra are generated by interpolating each of the seven individual spectra at a series of constant period increments.

4.4.2 Far Fault Nonlinear Spectra

Figure 4-9 plots the acceleration and displacement spectra for the case where the strength was set so high that yield would not occur (left hand plots, defined as the elastic spectrum) and for the configuration where the characteristic strength is 0.05 times the building weight (right hand plots). In each case, all seven earthquakes plus the average curve are plotted. It is not intended that individual records be distinguished in Figure 4-9, rather that the dispersal be apparent

The elastic spectrum in Figure 4-9 should correspond to the spectrum match shown in Figure 4-6 and in fact does show similar characteristics, with the response of all records close to the mean value.

The nonlinear spectra for Q_d = 0.05 in Figure 4-9 show much more dispersion than the elastic spectra. The nonlinear displacement spectra also differ from the elastic spectra in that they do not plateau at a 3.0 second period but rather continue to increase with increasing period.

Figure 4-9 Nonlinear Response for Distant from Fault Soil C

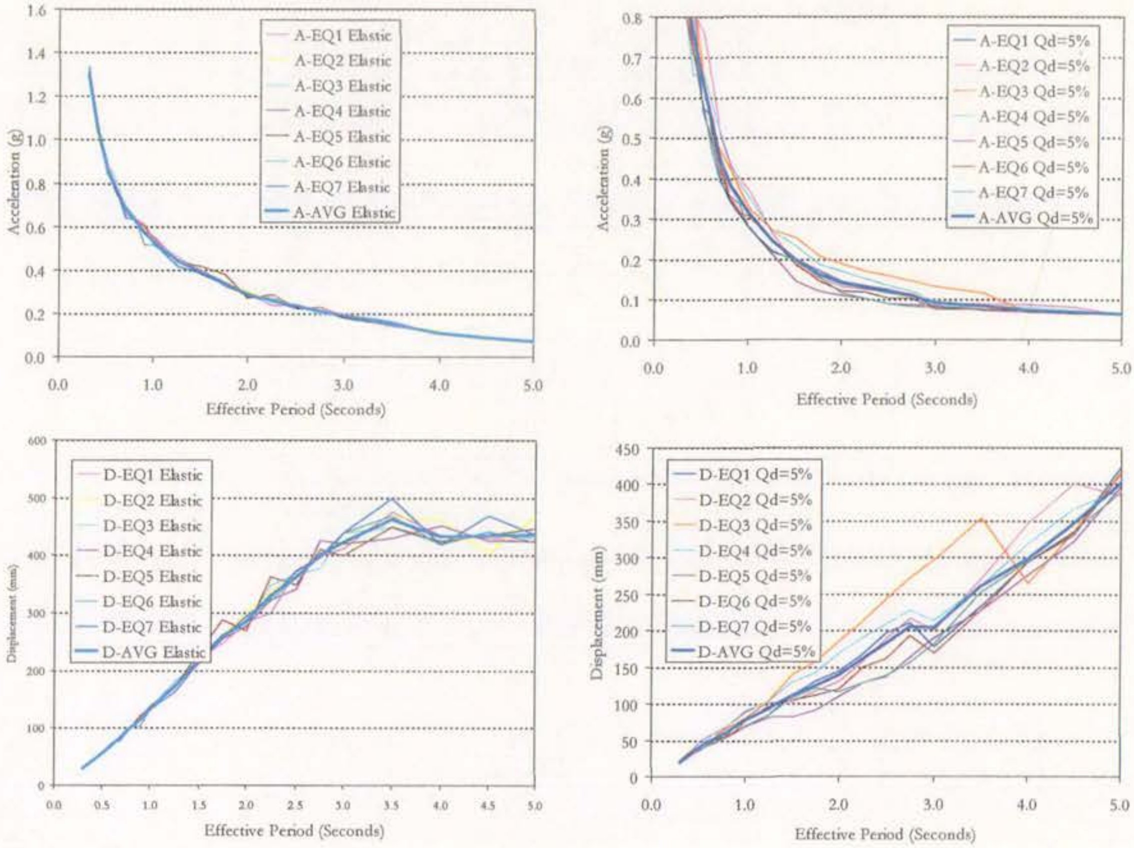

In Figure 4-10, the average acceleration and displacement response spectra are plotted for the elastic case and the three yielding cases, $Q_d = 0.05, 0.10$ and 0.15. The spectra for a specified yield level merge with the elastic spectra when the period reaches the point at which the acceleration ordinate on the elastic spectrum equals the yield level.

Figure 4-10 Average Nonlinear Response for Distant from Fault Soil C

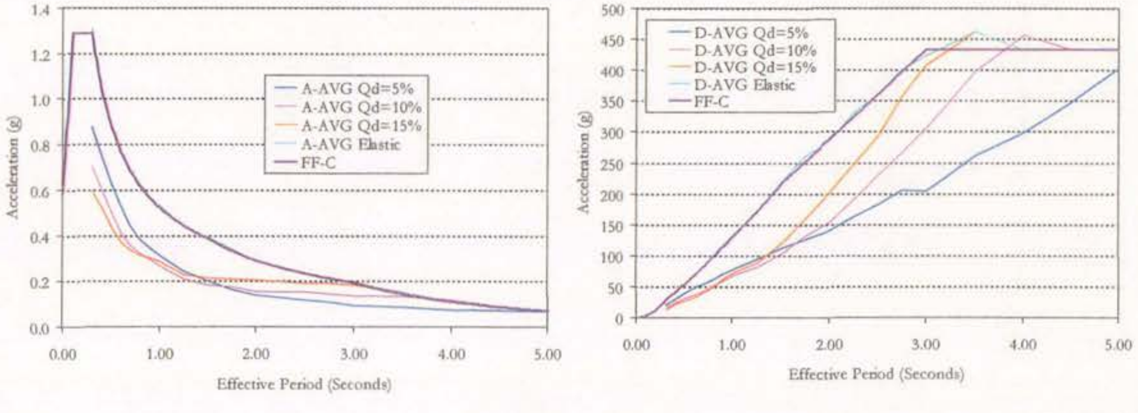

4.4.3 Near Fault Nonlinear Spectra

Figure 4-11 and 4-12 plot respectively the individual spectra and the average spectra, as for the fault distant configuration in Figures 4-9 and 4-10. These show similar features to the preceding plots in that the nonlinear spectra show much more dispersion than the elastic spectra. The elastic displacement spectrum does not plateau at a period of 3.0 seconds as the fault distant spectrum does. This is because of the effect of the near fault factor, N.

Figure 4-11 Nonlinear Response for Near Fault Soil C

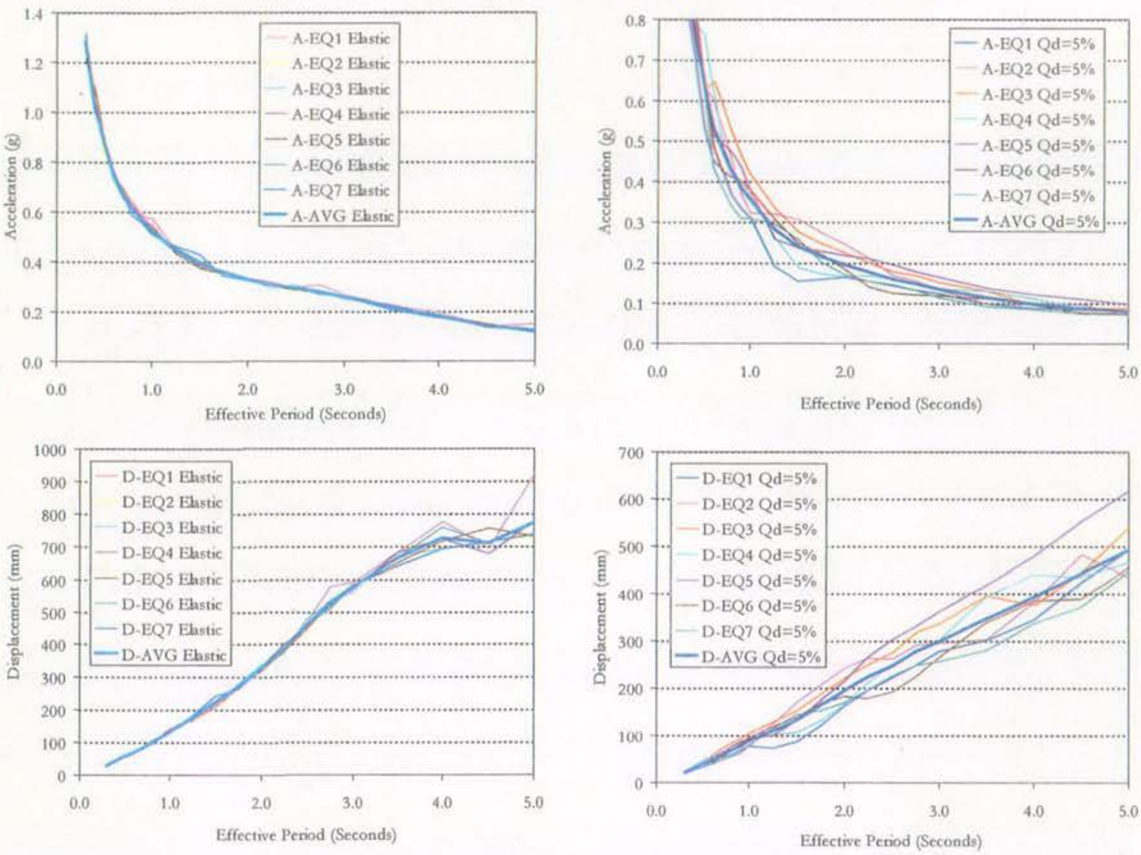

Figure 4-12 Average Nonlinear Response for Near Fault Soil C

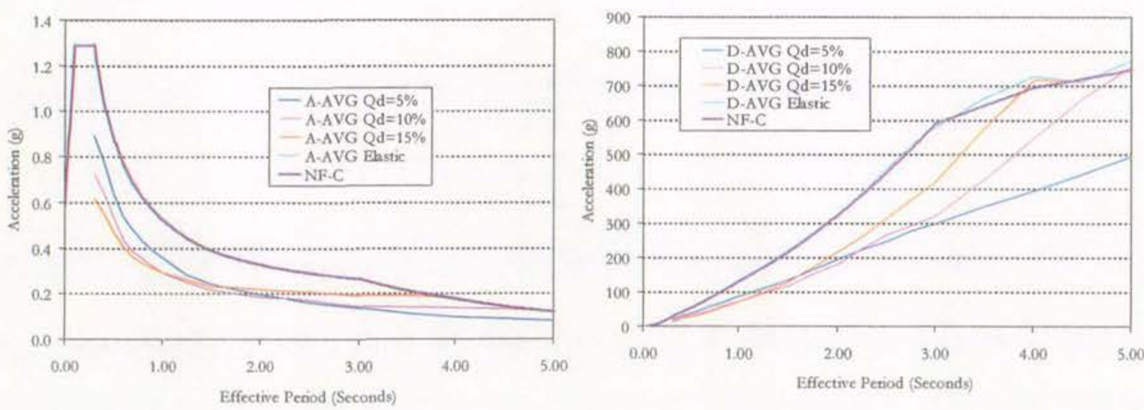

4.5 Target Response Spectra Used For This Study

The New Zealand code defines 5 different site subsoil classes, identified as A (strong rock) through E (very soft soil). Classes A (strong rock) and B (rock) have the same spectral equations and so are effectively the same for evaluation purposes. Soil Type E is very soft soil and is encountered less often than classes B, C and D. For this reason the evaluation was restricted to three subsoil classes:

1. Class B, defined as rock with a compressive strength above 1 MPa and an average shear wave velocity over the top 30 m greater than 360 m/s.

2. Class C, defined as shallow soil sites which have a low amplitude natural period not exceeding 0.60 seconds or which have depths of soil less than tabulated limits (maximum of 60 m for very stiff or dense materials of 100 m for gravels).

3. Class D, defined as deep of soft soil types which have a low amplitude natural period greater than 0.60 seconds or which have depths of soil greater than the tabulated limits for Soil C or are underlain by less than 10 m of soft soils.

Sites with more than 10 m of soft soils are defined as Class E, which was not included within the scope of this project.

NZS1170 defines a spectral shape for each soil type and then modifies the shape by a near fault factor, N(T,D) which is a function of the period, T, and the distance to the nearest of 11 listed major New Zealand faults. N has a value of unity for periods less than 1.50 seconds or fault distances greater than 20 km and increases to a maximum value of 1.72 for periods greater than 5 seconds at locations within 2 km of one of the major faults.

For this project, locations were defined as either "near fault" (within 2 km of major faults, maximum N factor) or "far fault" (over 20 km from a major fault, N equals unity). This combination of three site classes and two fault locations produced the six spectral shapes shown in Figure 4-13 (acceleration spectra) and Figure 4-14 (displacement spectra). The plots in these two figures are for the maximum value of ZR = 0.70.

As the subsoil stiffness reduces (from Class B to D) the peak spectral acceleration increases and the length of the plateau of maximum accelerations increases.

The near fault factor has no effect for periods less than 1.50 seconds but beyond that point increases spectral accelerations for all soil types. As shown on the displacement spectra in Figure 4-14, the spectra distant from the fault reach a constant displacement at periods of 3.0 seconds. The effect of the near fault factor is that spectral displacements continue to increase to periods of 5 seconds.

A set of 7 frequency scaled records was generated for each of the 6 shapes shown in Figure 4-13, using as seeds the sets of records listed in Tables 4-1 or 4-2 as appropriate. All evaluations were then based on mean results of response to the seven records.

Figure 4-13 Acceleration Response Spectra

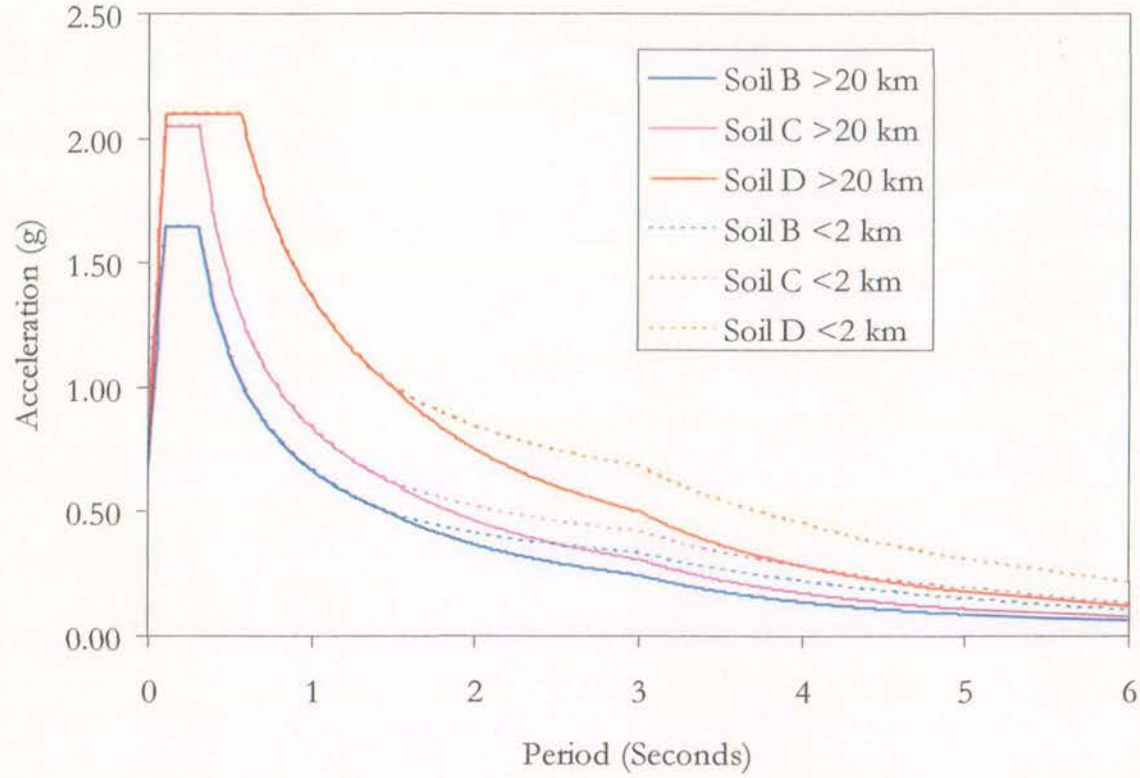

Figure 4-14 Displacement Response Spectra

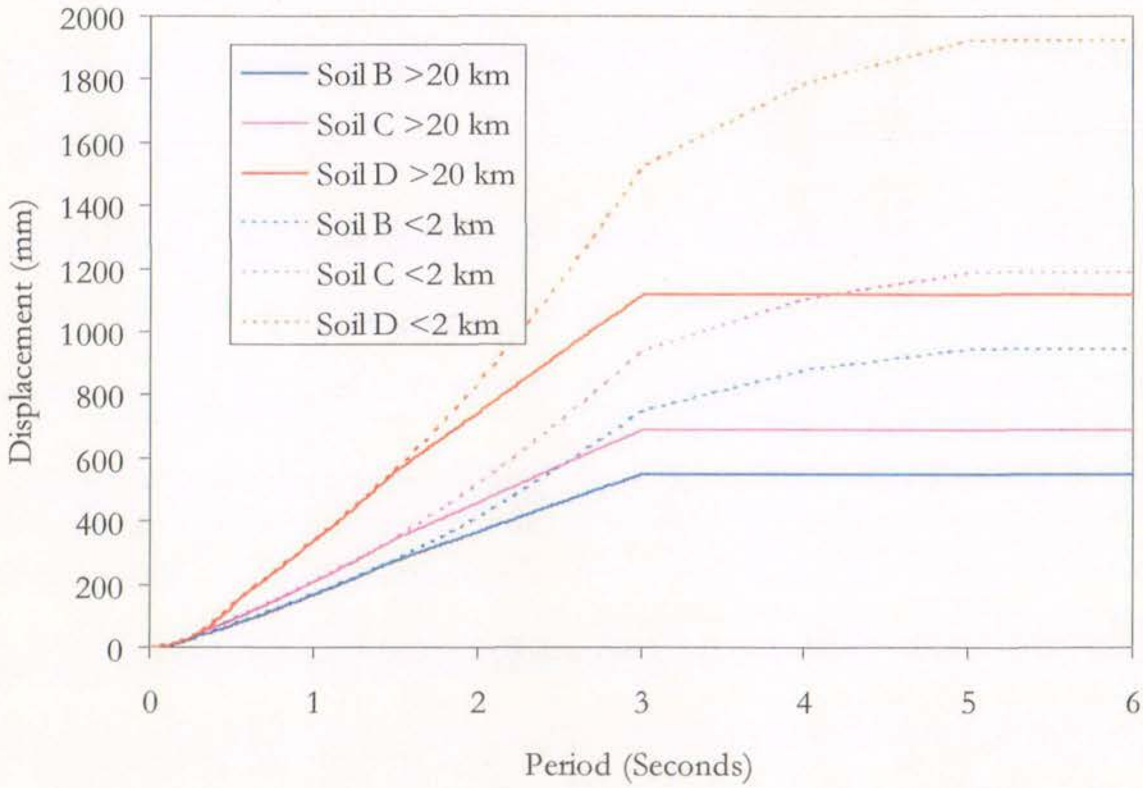

5 ANALYSIS OF SINGLE WALL ROCKING MODELS

The first stage of the development of these guidelines was to evaluate the seismic response of a series of single walls. The modelling and analysis methodology followed the procedures discussed in Chapter 3 and used the sets of seven frequency scaled time histories described in Chapter 4. The parametric studies of single walls used a series of different wall heights and aspect rations, foundation stiffness properties and earthquake amplitude.

5.1 Foundation Modelling

For the nonlinear analyses, the walls were assumed founded on shallow footings and the analysis procedure specified by FEMA 356 for this type of foundation was adopted, as shown in Figure 5-1. Using this procedure, a set of soil springs is defined by the soil shear modulus, G, and Poisson's ratio, ν. The springs are based on a calculated stiffness per unit length over the two end zones and a central portion, with the end zone stiffness higher than the central zone. The end zones are defined as extending a distance of B/6 from each end of the wall, where B is the foundation width.

Figure 5-1 Shallow Footing Model (From FEMA 356 Figure 4-5)

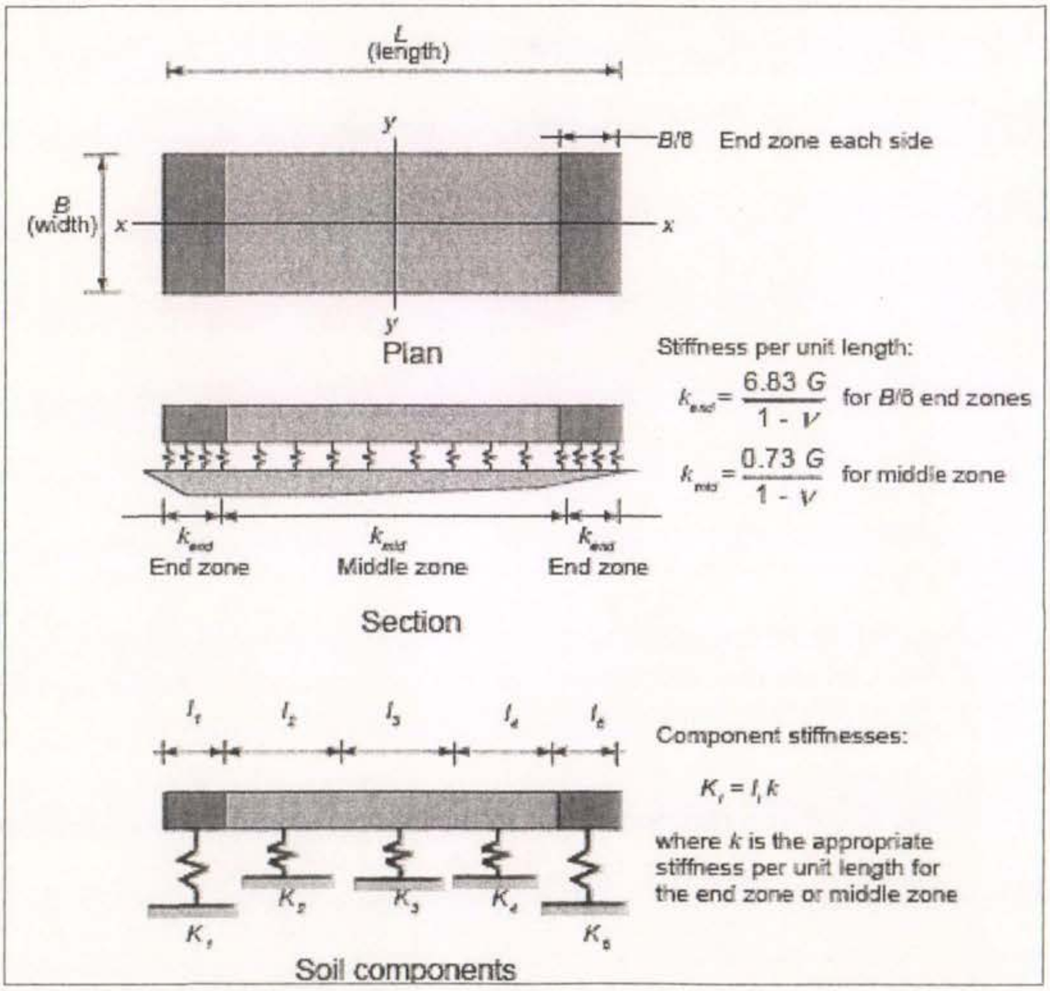

Foundation stiffness properties were based on a typical range of values of:

1. Soils and gravels, G = 40,000 to 80,000 kN/m^2, υ = 0.3 to 0.4

2. Clays (undrained case), G = 2,000 to 20,000 kN/m^2, υ = 0.5

For these analyses, the soil was assumed linear elastic. Strength properties are a function of many factors including soil strength; foundation shape; foundation size; load inclination; seismic effects plus others. For this reason, it is difficult to incorporate soil yielding into parametric studies. The effects of soil nonlinearity are discussed later in these guidelines.

For each wall configuration, the soil spring properties were calculated in the input spreadsheet, as shown in the example in Table 5-1. Properties were generated for up to seven variations in soil properties but for most wall configurations only three were evaluated (clay mean values, sand and gravel mean values and very high values, intended to represent walls founded on rock). A standard footing width of 1.000 m was used for most wall configurations, as discussed below.

Table 5-1 Calculation of Foundation Spring Properties

Footing Width	1.000	metre
Wall Length	3.600	metre
Wall Height	10.800	metre

		End I	Middle	End J			
Variation		0.167	0.653	0.167	G	mu	
A	1	4553	1908	4553	2000	0.50	Clay Lower Level
B	**2**	**22767**	**9539**	**22767**	**10000**	**0.50**	**Clay Mean Level**
C	3	45533	19077	45533	20000	0.50	Clay Upper Level
D	4	70051	29350	70051	40000	0.35	Sand & Gravel Lower Level
E	**5**	**105077**	**44025**	**105077**	**60000**	**0.35**	**Sand & Gravel Mean Level**
F	6	140103	58699	140103	80000	0.35	Sand & Gravel Upper Level
G	**7**	**1751282**	**733744**	**1751282**	**1000000**	**0.35**	**Rigid Case**

5.2 Wall Configurations

Three basic wall lengths were selected, with Type 1 having a length of 7.200 m, Type 2 one-half that value, 3.600 m, and Type 3 two times that value, 14.400 m. Each type was evaluated for one, two and three stories with the story height constant at 3.600 m. Each type was evaluated for foundation conditions B, E and G (Table 5-1), corresponding respectively to medium clay, medium gravel and rock.

These base dimensions and foundation stiffness values provided a total of 3 x 3 x 3 = 27 configurations. To extend the scope of the parameter studies, two extra variations were included:

1. The 3.600 m long wall was evaluated for 4, 5 and 6 stories for each of foundation conditions B, E and G, providing 9 additional configurations.

2. The 7.200 m wall 3 stories high was evaluated for foundation conditions A, C, D and F, providing 4 additional configurations.

The total number of wall variations was 27+9+4 = 40, as shown in the wall matrix in Table 5-2. To develop mass and weight properties, it was assumed that the walls were part of a square building 14.400 m on side (the maximum length of any wall) with a floor weight of 10 KPa so a total seismic weight of 2074 kN per floor. As there were two walls in each direction to resist seismic loads but four walls to support gravity, the seismic mass was based on (2074/2) kN per wall per floor and the gravity load based on (2074/4) kN per wall per floor.

Figure 5-2 Single Wall Configurations

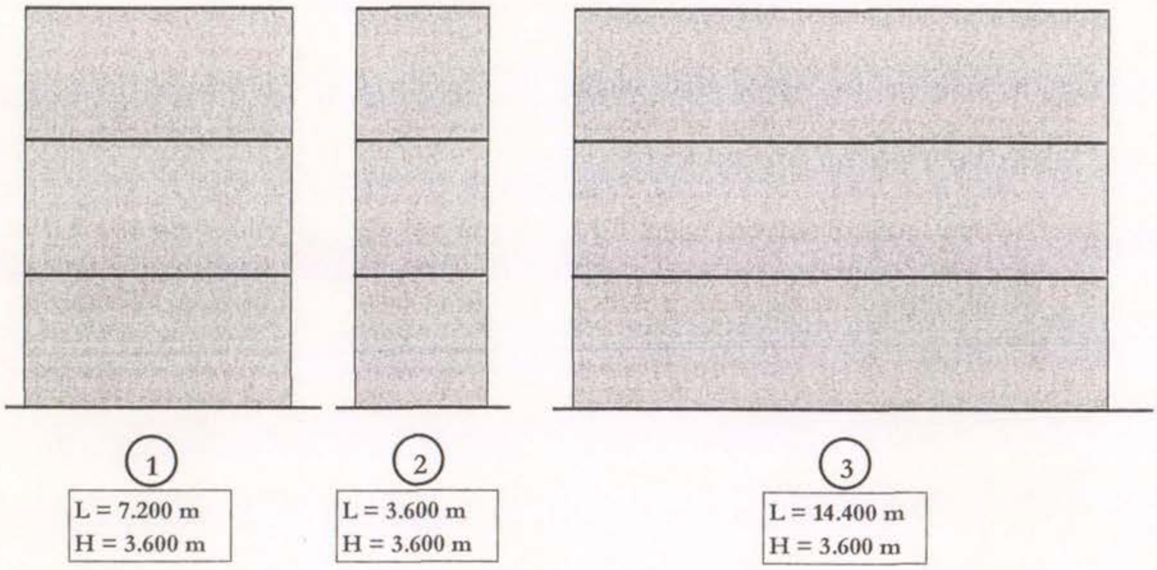

Table 5-2 Single Wall Matrix

Soil Spring Stiffness	7.200 m Wall Length Stories			3.600 m Wall Length Stories						14.400 m Wall Length Stories		
	1	2	3	1	2	3	4	5	6	1	2	3
Soft Clay K=2,000			1-3-A									
Clay K=10,000	1-1-B	1-2-B	1-3-B	2-1-B	2-2-B	2-3-B	2-4-B	2-5-B	2-6-B	3-1-B	3-2-B	3-3-B
Hard Clay K=40,000			1-3-C									
Soft Gravel K=40,000			1-3-D									
Sand/Gravel K=60,000	1-1-E	1-2-E	1-3-E	2-1-E	2-2-E	2-3-E	2-4-E	2-5-E	2-6-E	3-1-E	3-2-E	3-3-E
Hard Gravel K=80,000			1-3-F									
Rock K=1,000,000	1-1-G	1-2-G	1-3-G	2-1-G	2-2-G	2-3-G	2-4-G	2-5-G	2-6-G	3-1-G	3-2-G	3-3-G

To avoid excessive variations in model properties, a single foundation width of 1.0 m was used for all walls up to 3 stories high, even though in practice the soil strength, and so the required foundation width, would vary for the different soil types. The bearing pressure under gravity loads ranged from 36 KPa to 432 KPa for the foundation dimensions used for the analyses.

The lower pressure would be satisfactory for most soil types but the higher value would likely only be permissible on firm or rock sites. This leads to some inconsistencies in that all soil springs configurations were evaluated for all seismic subsoil classes. Also, seismic considerations would influence the required foundation size as discussed in Section 6.5.

The inconsistency between foundation pressures and soil spring properties were considered acceptable for two reasons:

1. The aim of the single wall studies was to develop a procedure to predict displacements, rather than to assemble empirical data, and so these analytical studies need not represent actual walls.

2. Use of a single foundation width for a range of soil stiffness values ensured that the walls analyzed had a wide range of periods. Varying foundation widths as a function of soil stiffness would tend to reduce the spread of periods between different soil springs.

In terms of vertical deformations, a 3 story wall on Type B springs deformed 10.4 mm under gravity loads. On Type E springs the vertical deflection was 2.2 mm and on the Type G springs the vertical deflection was 0.1 mm.

5.3 Evaluation Procedure

For each wall configuration an input spreadsheet was prepared. This workbook contained details of the analysis model and the foundation conditions. A macro in the workbook was used to prepare and write text input files for a series of ANSR analyses for the specific type of analysis (modal analysis, pushover analysis and time history analysis).

5.3.1 Development of Analysis Model

Each of the basic wall configurations was modelled using 7 x 7 gridlines, as shown in Figure 5-3 for the Type 1 three story wall. The spacing between grids was modified as a function of the different wall lengths and number of stories. The first and last gridlines were located at a distance of one-half the end zone from each end of the wall (see Figure 5-1). For most walls, the end zone was 0.167 m long and so the net wall length modelled was the gross length minus (0.167/2) m at each end.

Figure 5-4 is a rendered version of the finite element model in Figure 5-3. This shows the element types included in the analysis model:

- The walls were modelled using plane stress elements with properties based on a 200 mm thick concrete wall. The plane stress elements were set to remain linear elastic so that all nonlinearity would be restricted to uplift and rocking of the wall base.

- Rigid beam elements were included at each floor level to represent a rigid diaphragm. These beams were pinned at each grid intersection so as to function as truss elements to enforce equal translations at each wall node at floor levels.

- A 750 mm x 450 mm ground beam was included at the base of the wall. This was mainly to provide a visual check on the uplift status of the wall base. The stiffness of the beam was negligible compared to that of the concrete wall.

- A dummy foundation floor plate element was included. This had no effect on response but, as with the ground beam, provided for a visual check that separation was occurring.

- Gap elements were inserted at each grid intersection between the ground beam and the foundation. The gap elements had stiffness properties so as to represent the different soil types, calculated as shown in Table 5-1.

In addition to the structural elements in Figure 5-4, a dummy pin ended column element was used to provide second order (P-delta) effects as the plane element does not include second order effects. The seismic mass was applied at each floor level and the gravity load distributed over each nodal point. As detailed above, the total gravity load was one-half the seismic weight at it was assumed the gravity load was shared with two walls in the orthogonal direction.

Figure 5-3 Finite Element Grid for Type 1 Three Story Wall

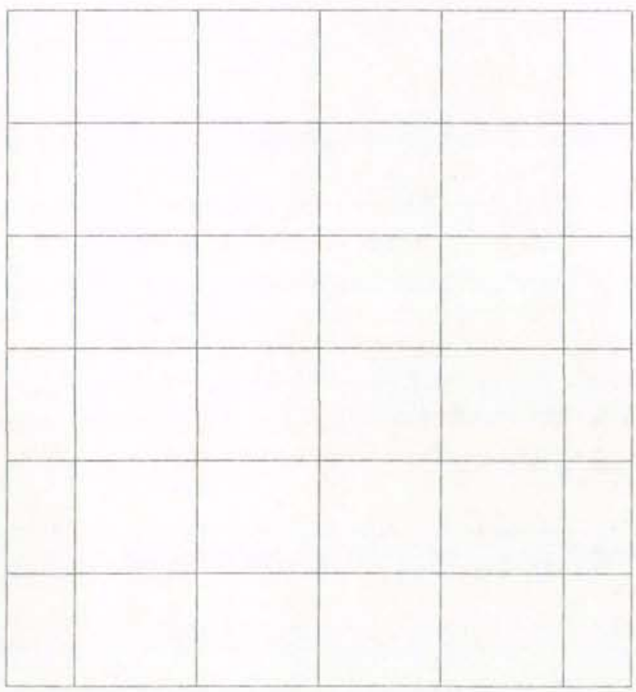

Figure 5-4 Rendered Analysis Model for Type 1 Three Story Wall

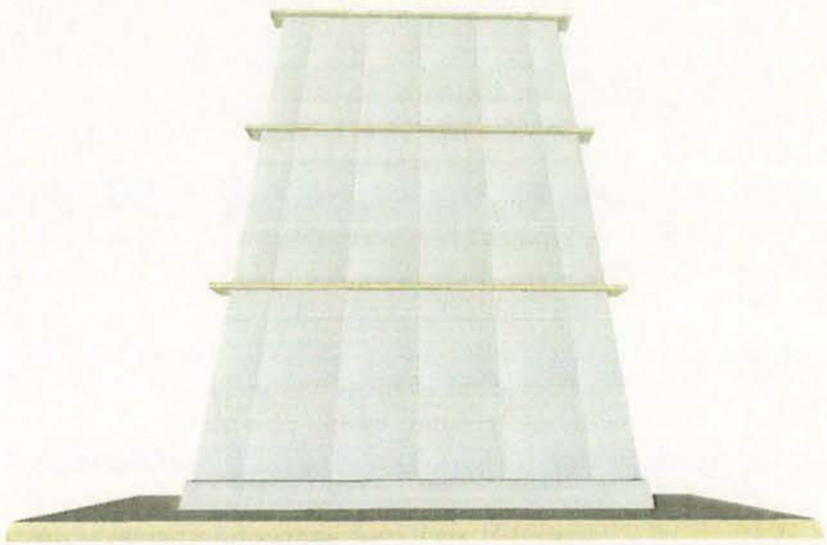

5.3.2 Modal Analysis

For each wall, a modal analysis was performed to extract periods, effective mass factors and participation factors. The periods were used to define damping coefficients. The other parameters are used later as part of the development of the design procedure to reduce the multi-degree-of-freedom systems to equivalent single degree-of-freedom systems.

Table 5-3 lists the fundamental period of each wall configuration evaluated. For reference, the period of each wall with a fixed base is also listed. The modal analysis is performed using a linear elastic procedure and so it is assumed that all gaps are closed.

The foundation condition listed as "rock" is used to define soil springs which are very stiff and the periods range from 1.07 to 1.25 times the fixed base period, with an average of 1.20 times the fixed base period. The periods for the gravel and clay foundations are influenced much more by the spring stiffness. For medium sand/gravel, the period is an average of 2.65 times the fixed base period and for medium clay, the period is twice as long, an average of 5.33 times the fixed base period.

As discussed above, the foundation width for most walls was defined as a standard 1.0 metres, even though the softer soils would likely require wider footings to keep bearing pressure within allowable limits. The standard width ensured that there was a wide spread of periods between the different soil spring types, as is displayed by the values in Table 5-3. However, because of this standardized footing width the ratio of periods to that of the fixed base wall will not accurately reflect the ratio for actual walls designed for seismic loads.

Table 5-3 Single Wall Periods (Seconds)

Soil Spring Stiffness (kN/m)	7.200 m Wall Length Stories			3.600 m Wall Length Stories						14.400 m Wall Length Stories		
	1	2	3	1	2	3	4	5	6	1	2	3
Soft Clay K=2,000			1.99									
Clay K=10,000	0.24	0.53	0.90	0.56	1.25	2.09	2.50	3.21	3.91	0.10	0.22	0.37
Hard Clay K=40,000			0.65									
Soft Gravel K=40,000			0.53									
Sand/Gravel K=60,000	0.12	0.26	0.44	0.27	0.61	1.03	1.29	1.72	2.10	0.05	0.11	0.18
Hard Gravel K=80,000			0.39									
Rock K=1,000,000	0.05	0.10	0.18	0.10	0.24	0.43	0.69	1.04	1.26	0.03	0.05	0.08
Fixed Base	0.04	0.08	0.14	0.08	0.19	0.36	0.62	0.96	1.18	0.02	0.04	0.07
Ratio Compared to Fixed Base Period												
Clay	6.15	6.54	6.34	7.27	6.51	5.87	4.01	3.34	3.31	4.17	5.00	5.44
Sand/Gravel	3.08	3.21	3.10	3.51	3.18	2.89	2.07	1.79	1.78	2.08	2.50	2.65
Rock	1.28	1.23	1.27	1.30	1.25	1.21	1.11	1.08	1.07	1.25	1.14	1.18

5.3.3 Wall Stability

For a wall with an applied lateral displacement, the wall will remain stable until displacements are such that the centroid of the weight is beyond the toe of the wall about which rocking occurs. This is shown schematically in Figure 5-5. For a wall with uniformly distributed weight the centroid is a mid-height and instability will occur when the top displacement exceeds the wall dimension.

Figure 5-6 plots the lateral force versus top displacement for the Type 2 (3.600 m long) wall 3 stories high. This example has the B foundation springs, medium clay. The plot shows that the applied force is positive until the displacements exceed 2.950 m. The model wall has a length of 3.433 m (between end springs) and so this is the theoretical displacement limit for instability. The 16% difference between the analysis value and the theoretical value is likely due to discretization effects of the finite element grid such that the weight is not exactly uniformly distributed.

The wall plotted in Figure 5-6 will remain stable for top displacements up to 2.950m, even though the stiffness is negative. If the load lateral load is removed at any displacement less than 2.950 m the wall will return to its original position. If the lateral load is removed at a displacement greater than 2.950 the wall will continue to tip and complete overturning will occur.

This characteristic of no overturning even though the incremental stiffness is negative is termed dynamic stability – a static load implies overturning once the lateral load is sufficient to initiate uplift. However, under dynamic loads a second condition must be satisfied, the displacements must be such that the wall exceeds the stability limit.

Figure 5-5 Theoretical Displacement Limit

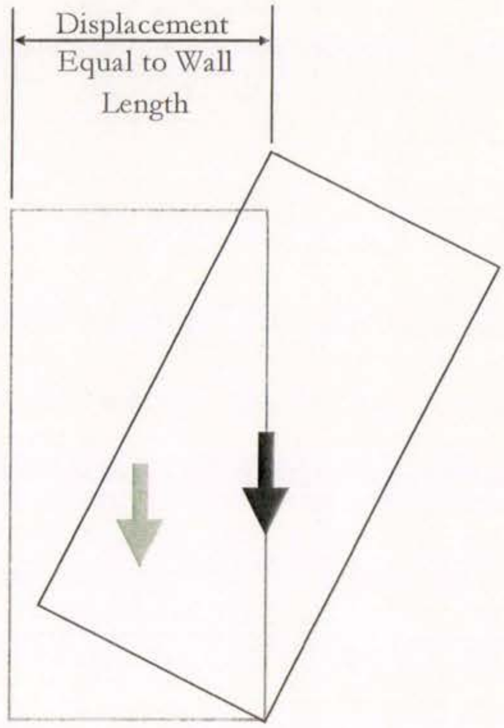

Figure 5-6 Wall 2-3-B Stability

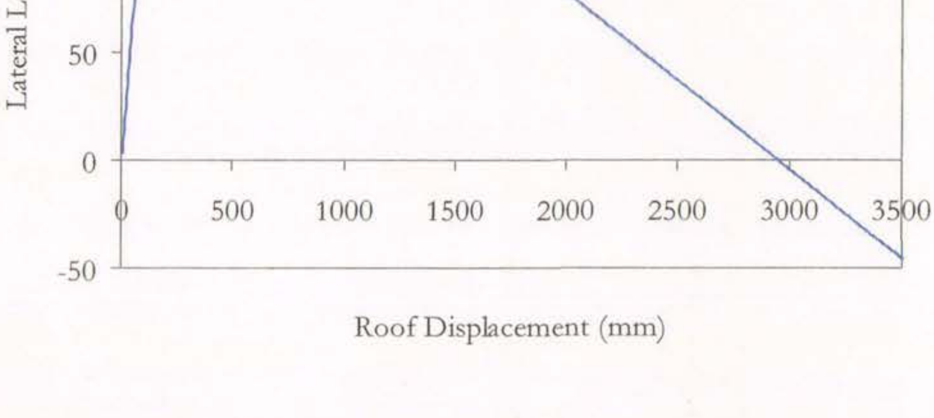

5.3.4 Wall Damping Decay

As discussed above, Wall 2-3-B will return to the original position if the lateral load is removed at any top displacement less than 2.950 m. Figure 5-7 demonstrates this, plotting the results of an analysis where a top displacement of 2.000 m is applied and is then removed suddenly. The wall is allowed to vibrate freely, with no applied loads or displacements. This provides a response of the form shown in Figure 5-7.

Figure 5-7 Wall 2-3-B Damping Decay

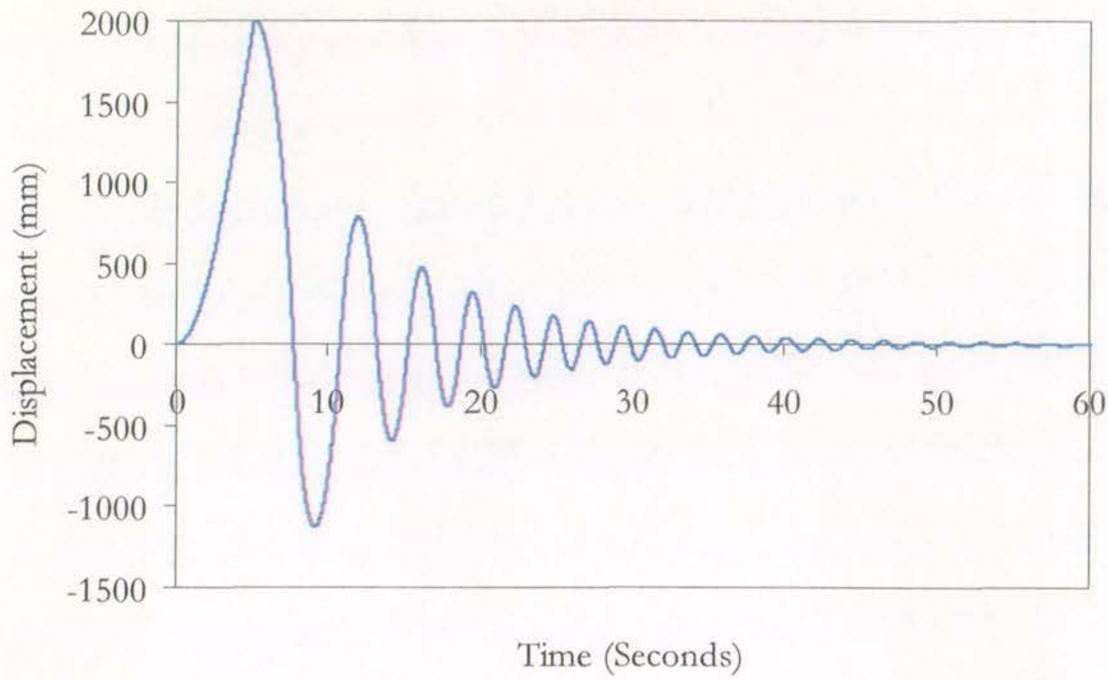

The displacement trace in Figure 5-7 may be used to calculate the periodicity and damping characteristics of a nonlinear model. This can supplement the information provided by the modal analysis reported earlier, which is based on linear elastic response.

For Wall 2-3-B the elastic period is 2.09 seconds. For nonlinear analysis, the damping coefficients are based on a period elongation by a factor of 1.5, and so 5% damping is provided at 3.14 seconds. With this coefficient, the theoretical damping at 2.09 seconds is about 3.7%.

Table 5-4 lists calculations of the period, based on the time increment between successive cycles, and the damping based on the logarithmic decrement method, also between successive cycles.

- The period in the first cycle is much greater than the elastic value, over 6 seconds, but reduces rapidly and by the 9th cycle has reduced to a constant period of 2.15 seconds. This is slightly longer than the 2.09 second period from the modal analysis because second order stiffness (P-Δ) is included in the pushover analysis.

- The damping in the initial cycle is over 10% but this also reduces rapidly and by the 9th cycle has converged to the final value of 3.1%, close to the estimated value of 3.7%. This confirms that the coefficients will tend to over-damp the system when the period exceeds 1.5 times the elastic period, or 3.14 seconds.

Table 5-4 Wall 2-3-B Damping and Period Calculations

	Positive Cycles				Negative Cycles			
Cycle	Time	Δ	Period	Damping	Time	Δ	Period	Damping
2	6.91	788	6.91	14.8%	9.15	-596	5.01	10.1%
3	11.09	472	4.18	8.1%	12.83	-385	3.68	7.0%
4	14.41	320	3.32	6.2%	15.87	-272	3.04	5.5%
5	17.23	234	2.82	5.0%	18.53	-203	2.66	4.7%
6	19.76	178	2.53	4.3%	20.94	-157	2.41	4.0%
7	22.08	140	2.32	3.8%	23.19	-126	2.25	3.6%
8	24.29	113	2.21	3.4%	25.37	-102	2.18	3.2%
9	26.44	93	2.15	3.2%	27.52	-84	2.15	3.1%
10	28.60	76	2.16	3.1%	29.68	-69	2.16	3.1%
11	30.75	63	2.15	3.1%	31.83	-57	2.15	3.1%
12	32.91	51	2.16	3.1%	33.99	-47	2.16	3.1%
13	35.06	42	2.15	3.1%	36.14	-38	2.15	3.1%
14	37.22	35	2.16	3.1%	38.3	-31	2.16	3.1%
15	39.37	28	2.15	3.1%	40.45	-26	2.15	3.1%
16	41.53	23	2.16	3.1%	42.61	-21	2.16	3.1%
17	43.68	19	2.15	3.1%	44.76	-17	2.15	3.1%
18	45.84	16	2.16	3.1%	46.92	-14	2.16	3.1%
19	47.99	13	2.15	3.1%	49.07	-12	2.15	3.1%
20	50.15	11	2.16	3.1%	51.23	-10	2.16	3.1%
21	52.3	9	2.15	3.1%	53.38	-8	2.15	3.1%
22	54.46	7	2.16	3.1%	55.54	-6	2.16	3.1%
23	56.61	6	2.15	3.1%	57.69	-5	2.15	3.1%
24	58.77	5	2.16	3.1%	59.85	-4	2.16	3.1%

5.3.5 Wall Pushover Analysis

The initial portion of the pushover curve, used above to assess stability and damping, can be used to examine the characteristics of a rocking wall. As the magnitude of the lateral displacement increases, successive gap elements separate. Figure 5-8 shows the configuration of the 7.200 m long wall at a top displacement of 1.000 m, at which point 6 of the 7 gap elements have opened.

When the force versus displacement function is plotted, as in Figure 5-9 (a), it is seen to be piecewise linear, a series of straight lines which change slope each time another gap element opens. Initially the positive stiffness provided by more than one gap in compression is greater than the negative P-Δ stiffness but once all gaps except one open the wall response is purely plastic (defined as no increase in resistance with increasing displacement). Once this occurs, the net stiffness is negative due to the P-Δ effects. Figure 5-9 (a) compares this with the force-displacement plot for linear soil springs, which are not permitted to separate under tensile loads. The linear system matches the rocking wall up to the point where the first gap opens.

Figure 5-8 Wall 1-3-B Configuration at 1.000 m Displacement

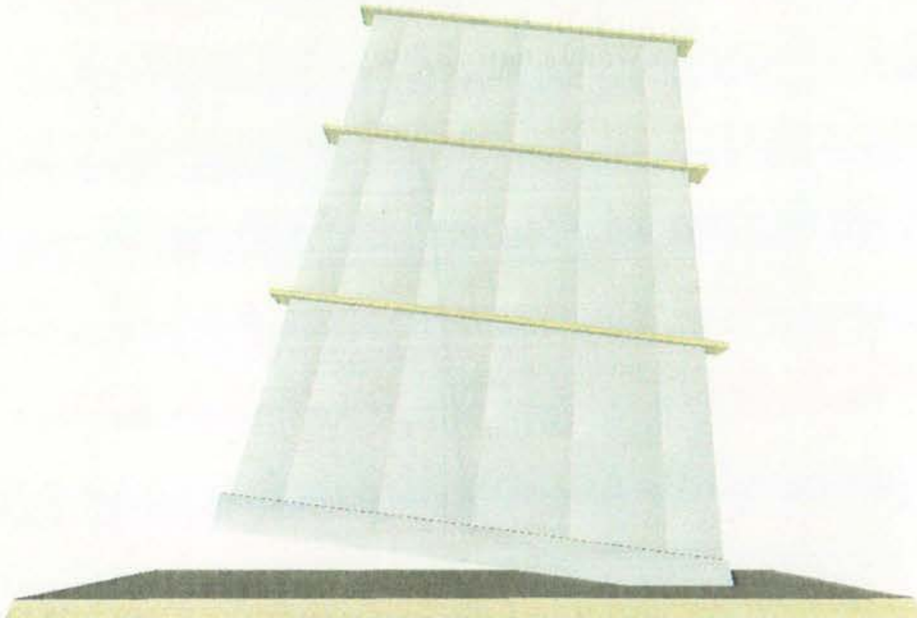

The loading curve shown in Figure 5-9 (a) is typical of yielding structural systems, defined by an initial elastic stiffness, a strain hardening segment and a reducing strength due to P-Δ effects. However, the cyclic curve which includes multiple loading and unloading cycles, shown in Figure 5-9 (b), is different from hysteretic systems. This is because unloading follows the loading curve, termed elastic unloading. This differs from a yielding system in that there is no hysteretic area generated and so no hysteretic energy absorption. The reason for this is that although the force-displacement curve is nonlinear there is no material yielding.

Figure 5-9 Example Pushover Curve
(a) Loading Curve

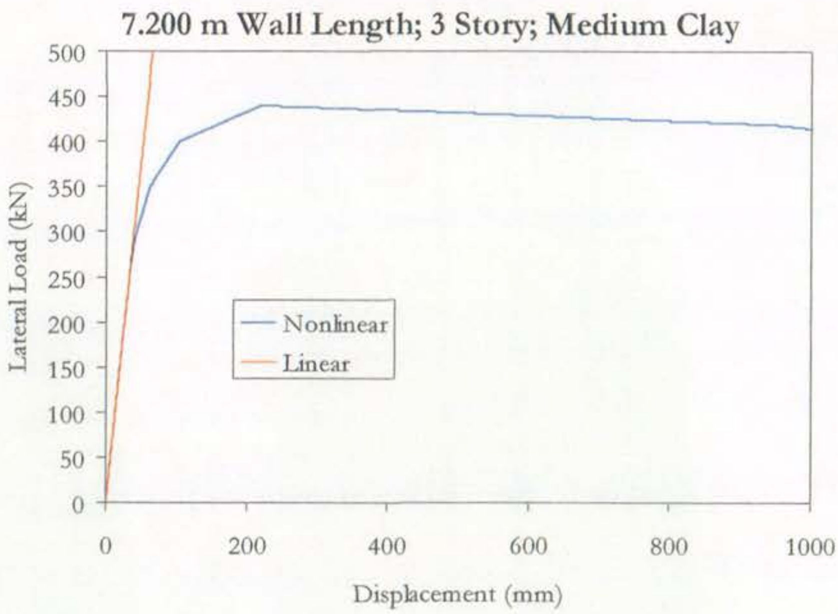

(b) Cyclic Response

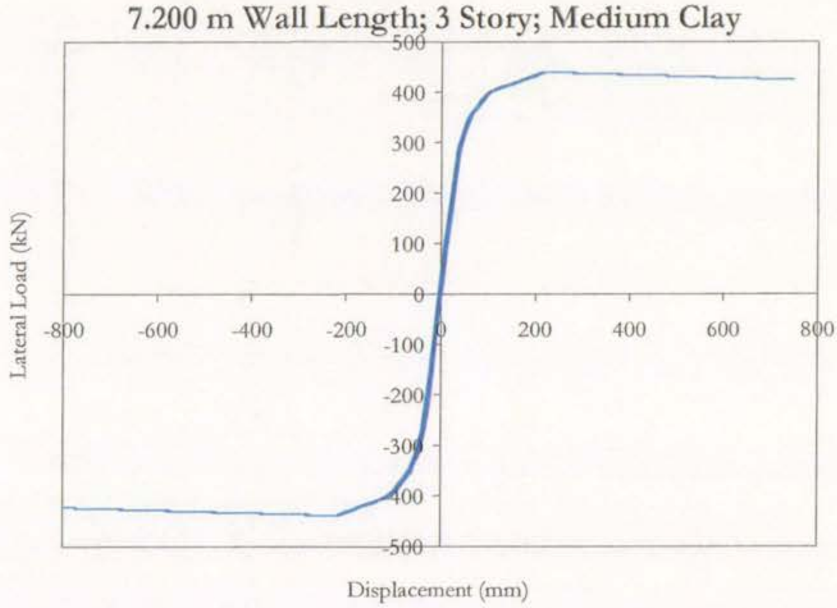

The stiffness of the soil springs has a marked effect on the shape of the pushover curve, as shown in Figure 5-10 which compares the response for the seven different foundation conditions considered, from soft clay to rock. As the stiffness of the soil springs is reduced, Figure 5-10 shows that there are two main effects:

1. The peak force which the wall can resist is reduced, and the displacement at which the peak occurs is higher. For rock the peak force of 500 kN occurs at a displacement of 25 mm. For soft clay, the peak force is reduced to 366 kN and this force occurs at a displacement of 513 mm.

2. The displacement to which the net stiffness remains positive increases as the soil spring stiffness reduces. This is because more of the springs remain in contact and so the resisting moment increment is greater than the negative P-Δ moment increment.

Figure 5-10 Effect of Soil Spring Stiffness on Pushover Curve (Stiffness kN/m)

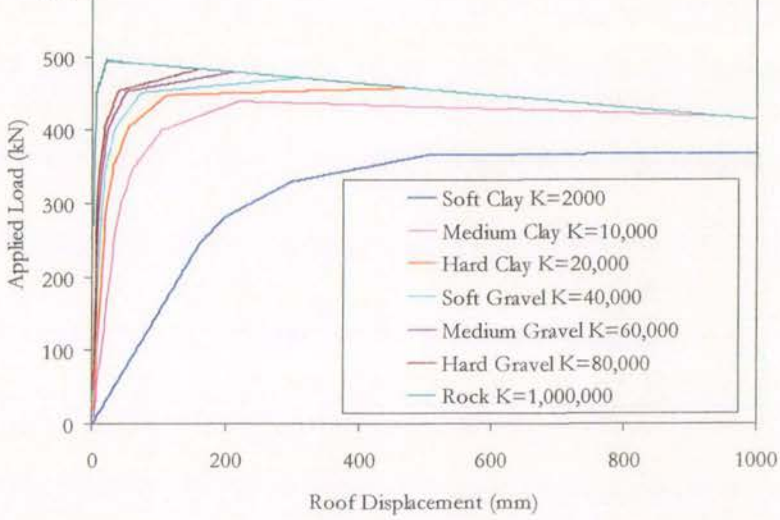

5.3.6 Time History Analysis

The seismic analyses were performed for a total of six sets of input motions. Each set contained seven time histories, each frequency scaled to match the site and fault distance conditions listed in Table 5-5, as discussed previously in Section 4.

Table 5-5 Soil and Near Fault Variations

1.	Site Subsoil Class A or B	Rock	Fault Distance < 2 km
2.	Site Subsoil Class C	Shallow Soil	Fault Distance < 2 km
3.	Site Subsoil Class D	Deep Soil	Fault Distance < 2 km
4.	Site Subsoil Class A or B	Rock	Fault Distance > 20 km
5.	Site Subsoil Class C	Shallow Soil	Fault Distance > 20 km
6	Site Subsoil Class D	Deep Soil	Fault Distance > 20 km

Subsoil Class E, very soft soil, was not included in this study as it is less common than the other types and many Class E sites have the potential for liquefaction and so should be the subject of more intense study than these generic guidelines can provide.

From NZS 1170, the elastic site hazard spectrum for horizontal loading, $C(T)$, for a given return period is:

$$C(T) = C_h(T)\, Z\, R\, N(T,D)$$

where

$C_h(T)$ = the spectral shape factor
Z = the hazard factor
R = the return period factor limited such that ZR does not exceed 0.7
$N(T,D)$ = the near-fault factor

The hazard factor, Z, ranges from 0.13 in the lowest seismic zones to a maximum of 0.60 in local areas of the Alpine Fault. The return period factor, R, ranges from 0.50 for to 1.8 depending on the Importance Level as listed in Table 5-6.

Table 5-6 R Factors for Importance Levels

Importance Level	R	Type
IL1	0.50	Structure presenting low degree of hazard to life and property
IL2	1.00	Normal structures & structures not in other importance levels
IL3	1.30	Structures containing people in crowds or contents of high value to the community.
IL4	1.80	Structures with special post-disaster functions

The theoretical maximum product of ZR would be 0.6 x 1.8 = 1.08 but, as noted above, the product need not exceed 0.70.

A scaling factor of ZR = 0.70 was applied to the earthquake records to define the maximum level evaluated. Each set of records was then evaluated for increments of this scaling factor from 0.10 to 1.0 at a step of 0.10, a total of 10 analyses for each of the 6 variations listed in Table 5-5. As there were 7 earthquakes for each of the 6 soil class variations, each data set comprised a total of 420 analyses for a particular wall configuration.

The approximate locations at which these earthquake factors would be appropriate are listed in Table 5-5. For example, an earthquake factor of 0.20 would approximately correspond to normal structures (IL2) in the lowest seismic zones such as Auckland or Dunedin. The maximum factor of 1.0 would correspond to essential facilities in high seismic zones such as in the Wellington region.

Table 5-7 Earthquake Factors

Earthquake Factor	ZR	Approximately Equal To
1.0	0.70	IL4 in Wellington region
0.9	0.63	IL2 in Otira / Arthurs Pass (normal structures)
0.8	0.56	IL2 in Hamner Springs
0.7	0.49	IL3 in Wellington region
0.6	0.42	IL2 in Wellington region (normal structures)
0.5	0.35	IL4 in Christchurch
0.4	0.28	IL3 in Christchurch IL4 in Auckland / Dunedin
0.3	0.21	IL2 in Christchurch (normal structures) IL3 in Auckland / Dunedin
0.2	0.14	IL2 in Auckland region (normal structures) IL2 in Dunedin region
0.1	0.07	IL1 in Auckland / Dunedin

The solution parameters were common to all time history analyses:

- Rayleigh damping coefficients were calculated to provide 5% viscous damping at 1.5 times the calculated elastic period and at a period one-tenth this value.
- All records were applied for a 50 second duration, which included the strong motion portion of all records.
- The integration time step was generally set at no longer than $1/200^{th}$ of the fundamental period. This is one-half the time step generally used for time history analysis but was set at the smaller value because impact forces in gap elements give rise to higher unbalanced loads. This resulted in very small time steps for some model. Wall 3-1-G, the 14.400 m long single story wall on rock, had a period of 0.027 seconds and so the time step was set at 0.0001 seconds. This required a total of 500,000 time steps per analysis for each of the 420 analyses performed.

5.4 Time History Numerical Stability Check

The single story wall time history results can be used to assess the numerical stability of the integration scheme by checking that each displacement / base shear point falls on the pushover curve. This check can only be performed for the single story models as the dynamic force vector differs from the static force vector for multi-degree-of-freedom models. Figure 5-11 plots the points from the 420 time history analyses on the pushover curve for Wall 1-1-B. This wall had a period of 0.241 seconds and the time step of 0.001 seconds represented $T_1/241$.

Figure 5-11 Wall 1-1-B Capacity Curve

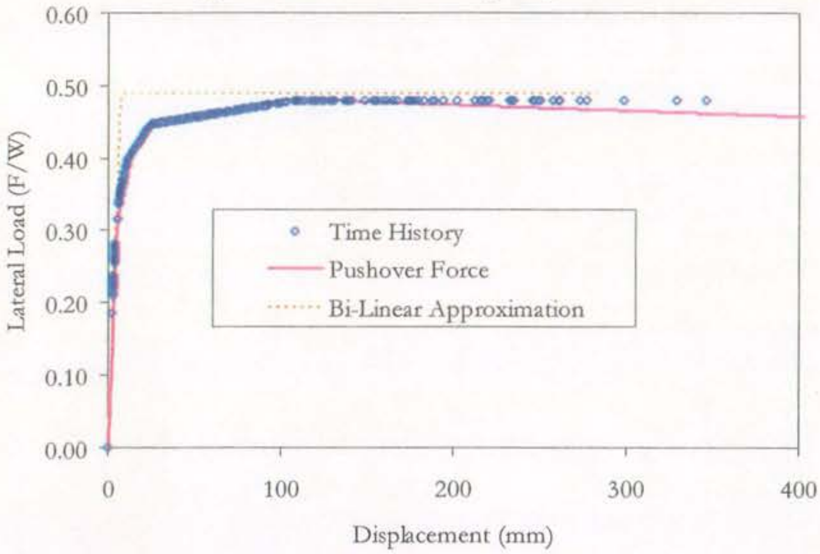

The time history shear force is calculated as the integration of the internal element forces in the seven plane elements across the base of the wall. As this is the resisting force, compared to applied force for the pushover, it does not include P-Δ effects and so the yielded stiffness is horizontal rather than falling. The time history points match the pushover force well, with a maximum error of less than 1%.

Figure 5-12 plots similar results for Wall 1-1-G, which has very stiff springs compared to wall 1-1-B. This reduced the period to 0.048 seconds and the time step of 0.0002 seconds represented $T_1/240$. The time history results match the pushover curve well for displacements up to about 35 mm but for higher displacements there is increasing discrepancy, with an error up to 22%

Figure 5-12 Wall 1-1-G Capacity Curve

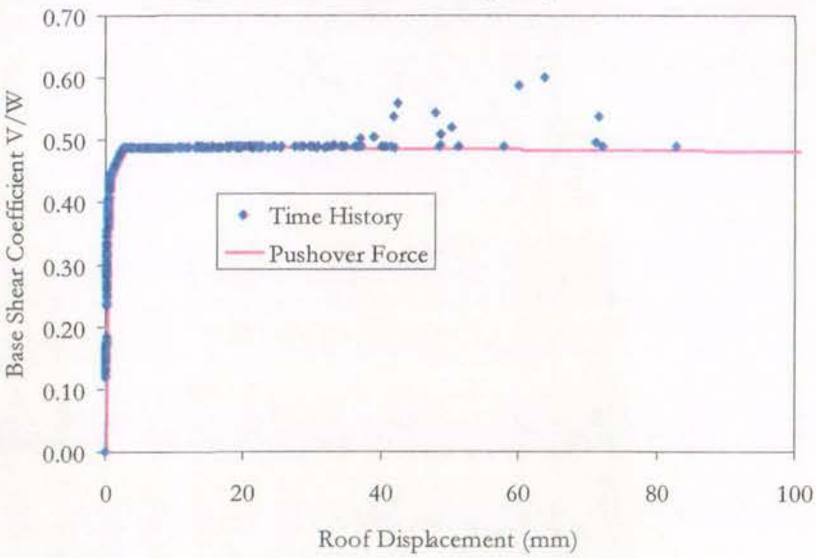

The error exhibited by the results in Figure 5-12 is less when the mean of seven time histories are compared with the pushover curve rather than the individual results. Figure 5-13 is for the same wall as Figure 5-12 but with 60 data points representing mean results rather than the 420 individual results in Figure 5-12. In this case, the error has reduced from 22% to 5%. This level of error is considered acceptable, given that variability between the different earthquakes is much more than this and that errors of this magnitude only occur for the stiffest springs.

Figure 5-13 Wall 1-1-G Capacity Curve with Mean Time History Results

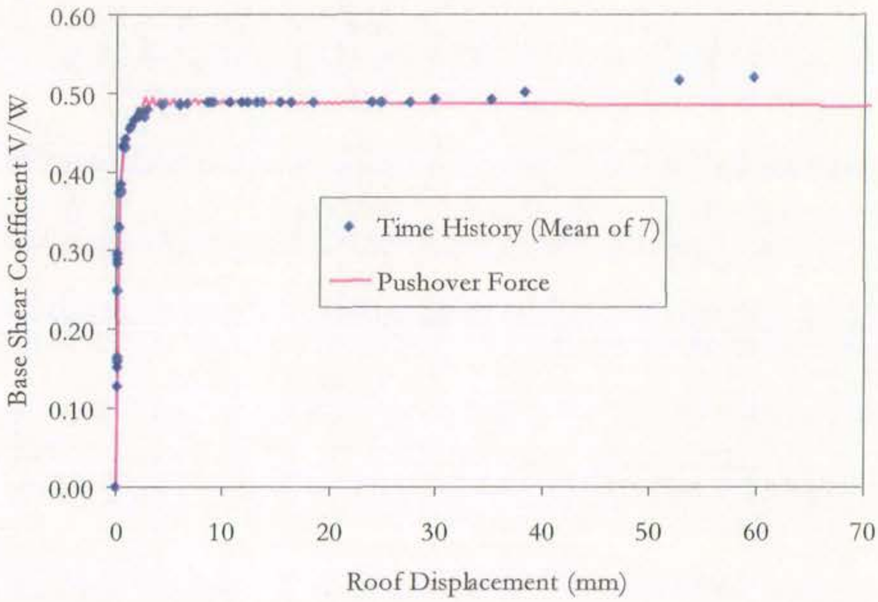

5.5 Results Processing

The majority of the nonlinear analysis input files were set to produce a simple envelope of results at the end of each analysis, rather than a detailed time history of response. This restriction was necessary to reduce the amount of data to be reduced to a manageable level, as there were 40 wall configurations with 420 analyses for each, producing a total of 16,800 nonlinear runs.

A processor program was used to read the output file for each analysis and import a summary of peak results to an output workbook. The data imported to the workbook is as shown in Table 5-8.

Table 5-8 Envelope Results for Time History Analyses

EQ	Scale Factor	Time	Displ.	Accel.	Shear	Gap Elements		
						Open	C	d
(1)	(2)	(3)	(4)	(5)	(6)	(7)	(8)	(9)
1	1.59	50.00	43.10	0.50	0.45	5	-367	67.76
1	1.43	50.00	62.66	0.54	0.46	5	-411	104.00
1	1.27	50.00	55.52	0.54	0.46	5	-395	90.79
1	1.11	50.00	38.49	0.52	0.45	5	-356	59.20
1	0.95	50.00	30.56	0.48	0.45	5	-338	44.50

EQ	Scale Factor	Time	Displ.	Accel.	Shear	Gap Elements		
						Open	C	d
(1)	(2)	(3)	(4)	(5)	(6)	(7)	(8)	(9)
1	0.80	50.00	26.84	0.47	0.45	5	-330	37.61
1	0.64	50.00	18.26	0.44	0.42	4	-289	22.66
1	0.48	50.00	9.80	0.39	0.38	3	-233	8.61
1	0.32	50.00	6.88	0.35	0.35	3	-205	4.18
1	0.16	50.00	3.09	0.21	0.21	0	-146	0.00
2	1.59	50.00	91.04	0.55	0.47	5	-476	156.60
2	1.43	50.00	69.49	0.55	0.46	5	-427	116.70
2	1.27	50.00	44.65	0.51	0.45	5	-370	70.62
2	1.11	50.00	35.69	0.50	0.45	5	-350	54.02
2	0.95	50.00	22.42	0.46	0.44	4	-313	29.71
2	0.80	50.00	20.57	0.45	0.43	4	-302	26.58
2	0.64	50.00	15.09	0.42	0.41	4	-271	17.29
2	0.48	50.00	7.93	0.36	0.36	3	-215	5.77
2	0.32	50.00	6.58	0.34	0.34	2	-201	3.76
2	0.16	50.00	3.43	0.24	0.24	0	-153	0.00

(1) The earthquake number, from 1 to 42, representing 7 for each of the six soil and fault distant conditions.

(2) The scale factor applied to the earthquake. The input records are scaled to ZR=0.44 and so the maximum scale factor of 1.59 produces ZR = 0.70.

(3) The envelope time recorded for the analysis, in seconds. Each analysis was defined for 50 seconds duration so an envelope time less than 50 seconds indicated a premature termination because convergence could not be achieved.

(4) The maximum displacement at roof level, in mm.

(5) The maximum acceleration at roof level, in g.

(6) The maximum base shear coefficient, which is the sum of the shear forces in the plane stress elements at the base of the wall divided by the seismic weight.

(7) The maximum number of gaps which opened simultaneously at any time step. There are typically 7 gaps and so a maximum of 6 can open simultaneously. A value of 0 indicates elastic response.

(8) The maximum compressive force in any gap elements, in kN.

(9) The maximum displacement in the gap, which is the gap opening in mm.

A macro in the output workbook was used to read the values from each analysis and assemble the mean values from each set of 7 time histories. The macro was set to include only analyses which terminated normally, that is, where the envelope time was 50 seconds. If 5 or more of a particular set terminated normally then the data point was accepted as valid, if less than 5 then the data point was discarded.

5.6 Results of Evaluation

The processed results described above were used to define displacement versus earthquake amplitude curves for each of the six soil class and fault conditions evaluated for each wall configuration. Figure 5-14 shows an example of the six curves generated for the 3.600 m single story wall on medium clay springs.

In addition to the nonlinear results, the plots in Figure 5-14 show the elastic response, which is generated by an analysis assuming that the soil springs act as elastic springs in both tension and compression rather than compression only. For most walls, the nonlinear results for the lowest earthquake amplitude did not open any gap elements and so the results were equivalent to those for the linear analysis.

For the elastic system the results by definition are directly proportional to earthquake amplitude and so the displacement versus earthquake amplitude plot forms a straight line for each condition.

If the inelastic displacements were equal to the elastic displacements (as assumed by the equal displacement theory discussed earlier) then the nonlinear analysis curves would also form a straight line. It is apparent from Figure 5-14 that this assumption is not warranted. The time history results vary from the elastic results and the variation increases as displacements increase. For example:

1. The Soil B Far Fault records produce the smallest response quantities. The time history displacement of 226 mm for ZR = 0.7 is 2.8 times the elastic displacement of 80 mm.

2. The Soil D Near Fault records produce the largest response quantities. In this case the time history displacement of 918 mm for ZR = 0.70 is 5.6 times the elastic displacement of 162 mm, a factor twice as high.

It is clear from this that the response of rocking walls is highly nonlinear and does not conform to an equal displacement theory. The response of these single wall models is examined in more detail in the following section to help develop guidelines to predict the displacements plotted in Figure 5-14.

Figure 5-14 Time History Displacements for Wall 2-1-B

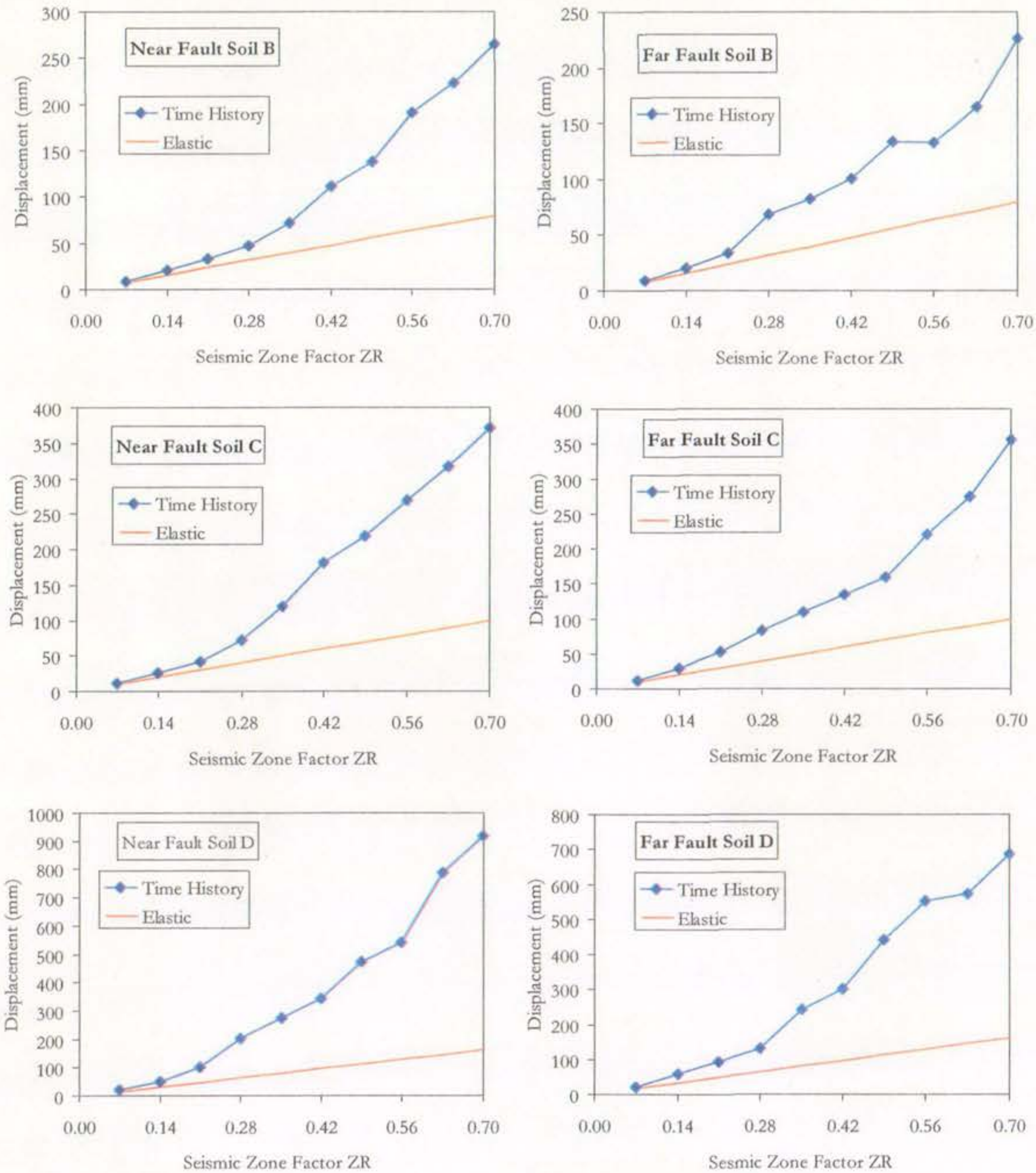

6 DETAILED RESPONSE OF SINGLE WALL MODELS

The preceding chapter section discussed the nonlinear analysis of a series of single wall models for varying soil conditions and earthquake input. In this chapter, the effect on response of earthquake amplitudes and wall parameters are considered. A further set of analyses is performed to evaluate the effect of varying the number of springs used to represent the foundation. From these results, the wall inertia force and reaction forces are examined in detail.

6.1 Response versus Earthquake Amplitude

The variation in response with increasing earthquake amplitude is examined in more detail for Wall 2-1-B (Figure 5-14), which is a 3.600 m single story wall on medium clay springs. Figure 6-1 plots the peak displacements for each earthquake for Soil C, Near Fault, with a scale factor of 1.0 (ZR = 0.7). The displacements range from 296 mm to 506 mm, which is a variation of -20% to +36% of the mean displacement of 371 mm. This is typical of the variation between the different records for nonlinear analysis. The response for the Newhall record, which produced the highest displacement, was selected to illustrate characteristics of response in the discussion below.

Figure 6-1 Maximum Displacements in Wall 2-1-B

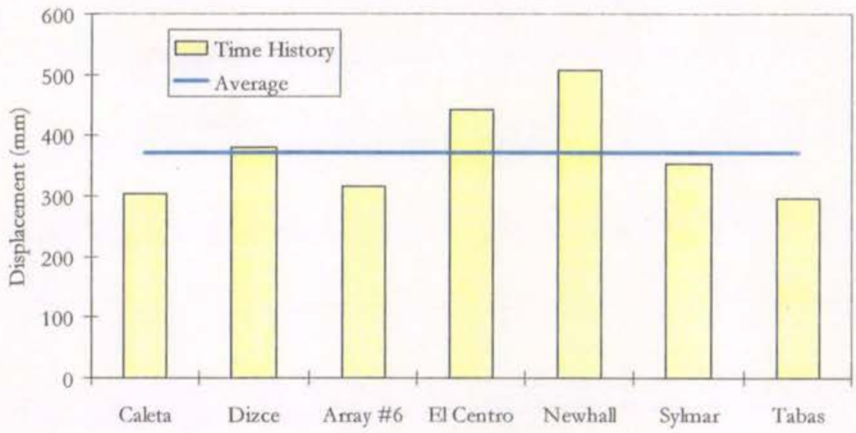

Table 6-1 summarizes the peak results for this wall for each earthquake scale factor for the Newhall record. This table lists top displacement and acceleration, base shear and gap conditions.

The values in Table 6-1 show that the top displacement and the gap opening both increase with increasing earthquake magnitude but the other parameters tend to reach a maximum value and then increase only slowly if at all. Figure 6-2 plots the top displacement and gap opening, which increase exponentially with earthquake magnitude, and compare this with maximum gap compression, which reaches a maximum value and then remains constant.

As shown in Table 6-1, the response is elastic for a zone factor of ZR=0.07, indicated by no open gaps. At a zone factor of ZR=0.42 there are six open gaps, which represents the maximum possible open gaps as there are seven gaps in total and at least one must be in compression to resist the wall reaction. Once 6 gaps are open the compression load represents the full gravity load on the wall and does not increase over this value. This limiting condition also sets a limit on the base shear, which remains constant as earthquake zone factors increase from 0.42 to 0.70. Similarly, top accelerations increase only slightly.

Table 6-1 Peak Response for Wall 2-1-B Soil Class C; Near Fault

Seismic Zone Factor ZR	Top Displacement (mm)	Top Acceleration. (g)	Base Shear V/W	Open Gaps (of 7)	Gap Compression (kN)	Gap Opening (mm)
0.70	506	0.337	0.223	6	509	461
0.63	472	0.333	0.223	6	509	428
0.56	425	0.309	0.223	6	509	383
0.49	351	0.299	0.222	6	509	313
0.42	255	0.286	0.223	6	508	221
0.35	68	0.235	0.221	5	410	47
0.28	70	0.234	0.221	5	411	48
0.21	49	0.224	0.215	4	378	29
0.14	31	0.209	0.205	3	340	15
0.07	12	0.151	0.151	0	248	0

Figure 6-2 Variation in Deformation and Gap Force

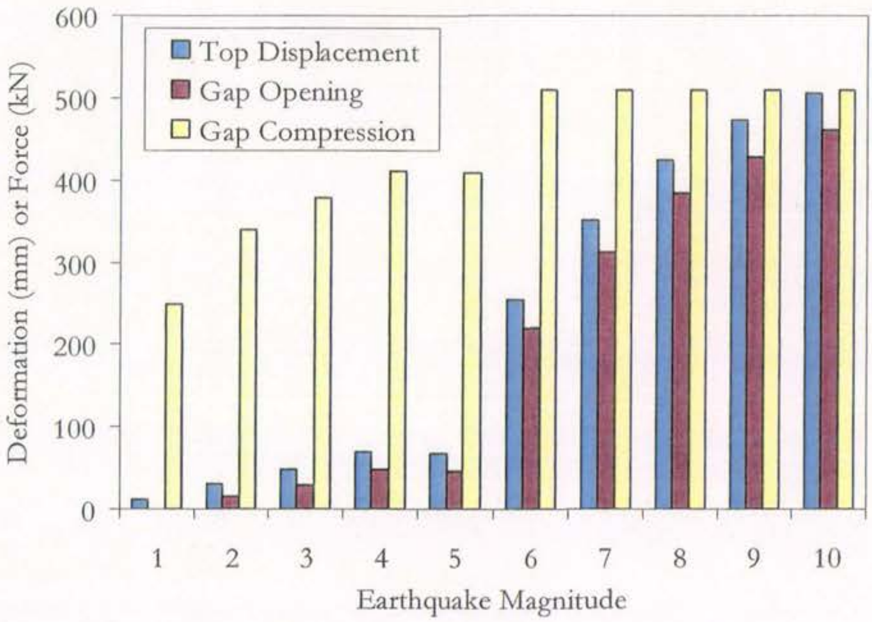

The time history of wall top displacements is plotted in Figure 6-3 for earthquake zone factors of ZR = 0.07, 0.42 and 0.70. This plot shows that there is not only a large increase in amplitude but the periodicity of response also increases by a large factor as the scale factor increases. At the zone factor of 0.07 the response is at approximately the elastic period of 0.56 seconds. At the zone factor of 0.42, the maximum displacement occurs in a cycle from 7.56 to 9.76 seconds, an effective period of 2.20 seconds. When the scale factor is increased to the maximum of ZR = 0.70, the maximum displacement occurs in a cycle from 7.73 to 10.45 seconds, an effective period of 2.72 seconds.

Figure 6-3 Displacement for Wall 2-1-B Soil Class C; Near Fault

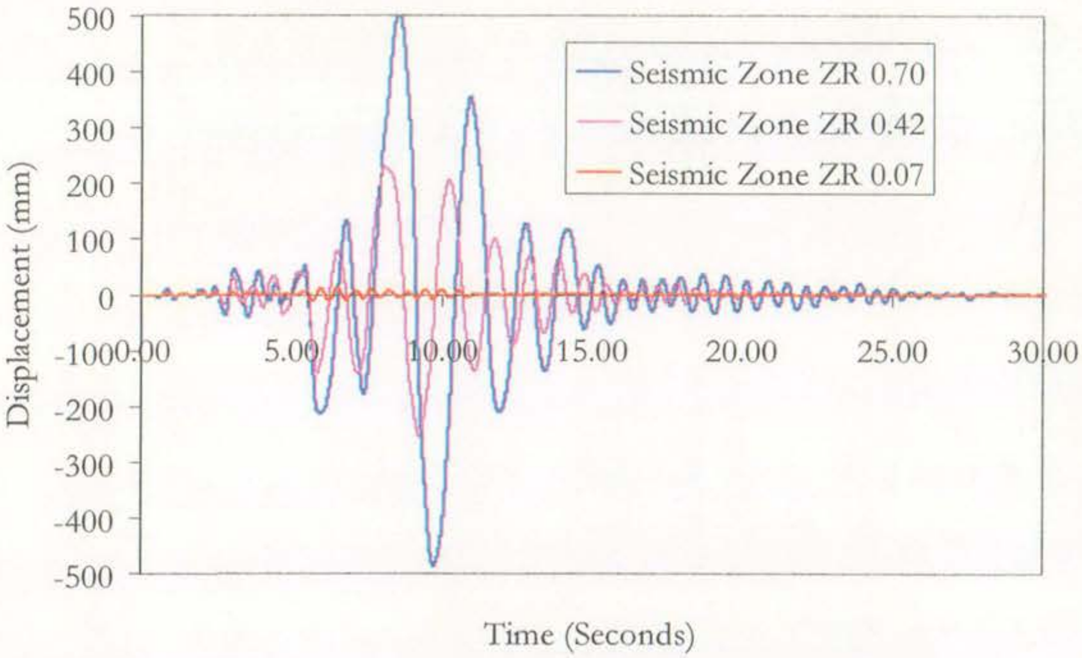

Figure 6-4 plots the base shear versus time for the same scale factors as in Figure 6-3 and Figure 6-5 the top acceleration versus time. These two plots show how the limit in base moment provided by the uplift mechanism acts as a fuse to reduce the maximum base shears and accelerations. As discussed later, this response is much more complex for multi-story walls.

Figure 6-4 Base Shear for Wall 2-1-B Soil Class C; Near Fault

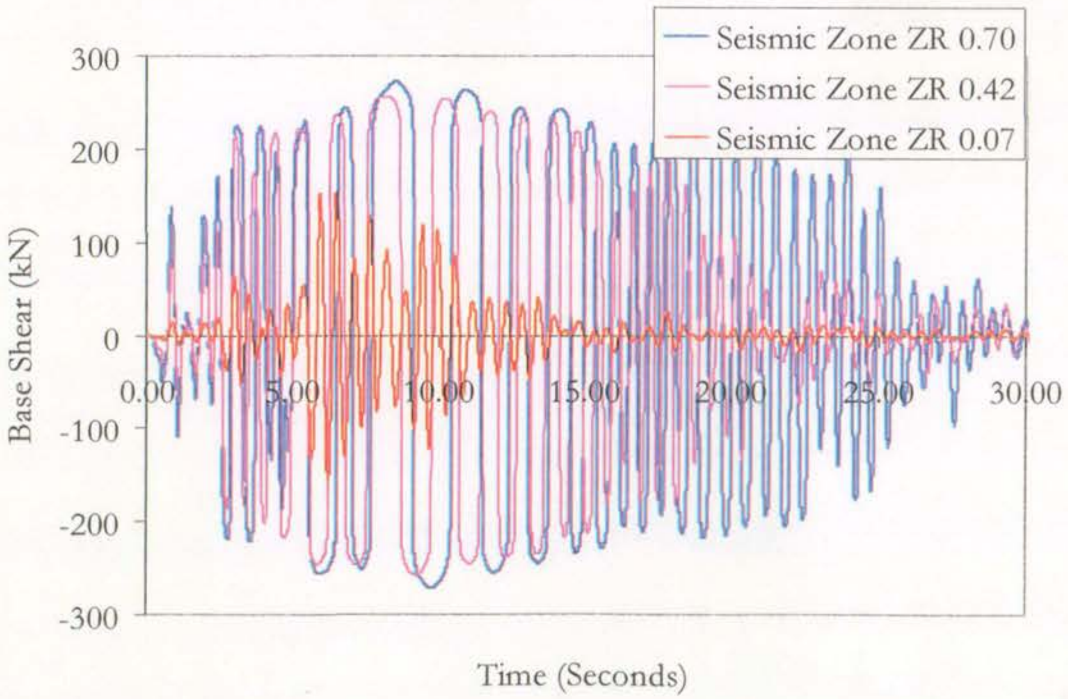

Figure 6-5 Accelerations for Wall 2-1-B Soil Class C; Near Fault

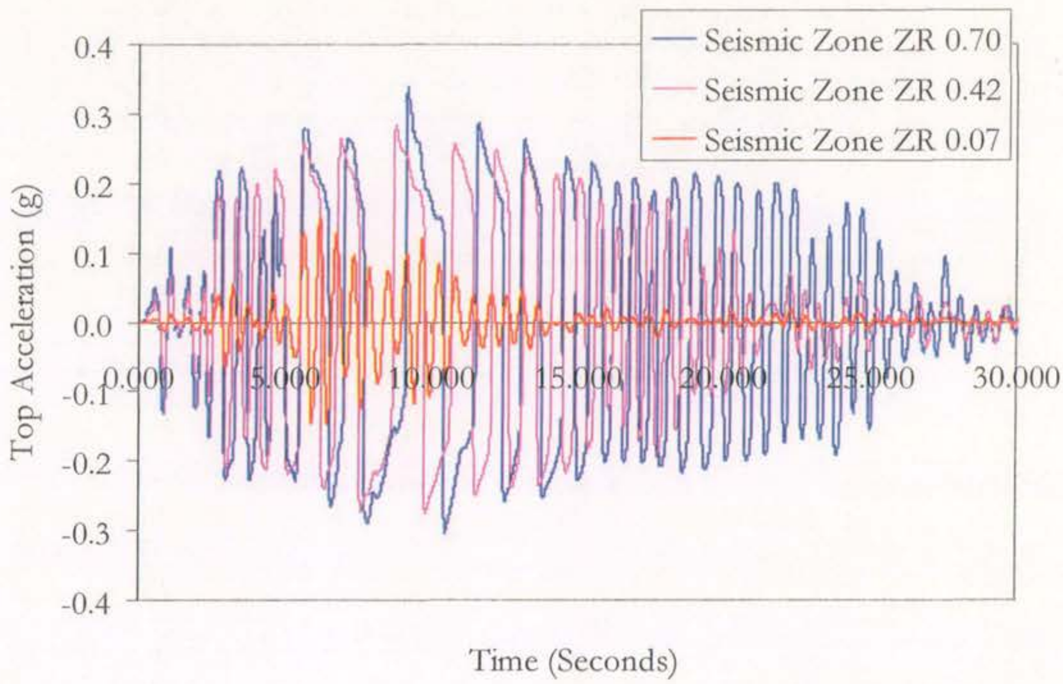

6.2 Effect of Wall Parameters on Maximum Displacement

6.2.1 Soil Spring Stiffness

The effect of different seismic and subsoil parameters is examined using the results of Wall 1, which is a 7.200 m long wall three stories high. Table 6-2 lists peak displacements in this wall for 7 different subsoil stiffness values, 3 seismic site soil conditions and both near fault and far fault locations. The values are all for the maximum seismic input, ZR = 0.70.

Note that for this discussion, the full matrix of soil springs and seismic conditions is examined, although some of these are inconsistent. For example, hard gravel or rock soil springs are unlikely for a Soil D seismic soil class.

Table 6-2 Peak Displacements: Wall 1-3 ZR=0.70

	Soft Clay	Medium Clay	Hard Clay	Soft Gravel	Medium Gravel	Hard Gravel	Rock
Near Fault							
Soil B	1060	459	375	323	288	250	98
Soil C	1356	728	539	456	377	357	204
Soil D	2438	1587	1218	1073	885	827	499
Far Fault							
Soil B	743	394	293	274	245	202	125
Soil C	945	676	482	412	357	325	160
Soil D	1512	1173	880	780	670	709	383

There is a consistent trend that the softer the soil springs, the larger the displacements. Figure 6-6 plots the peak displacements for a Near Fault Site on Subsoil D. A similar trend is noted for all seismic conditions.

Figure 6-6 Effect of Soil Spring Stiffness on Time History Response

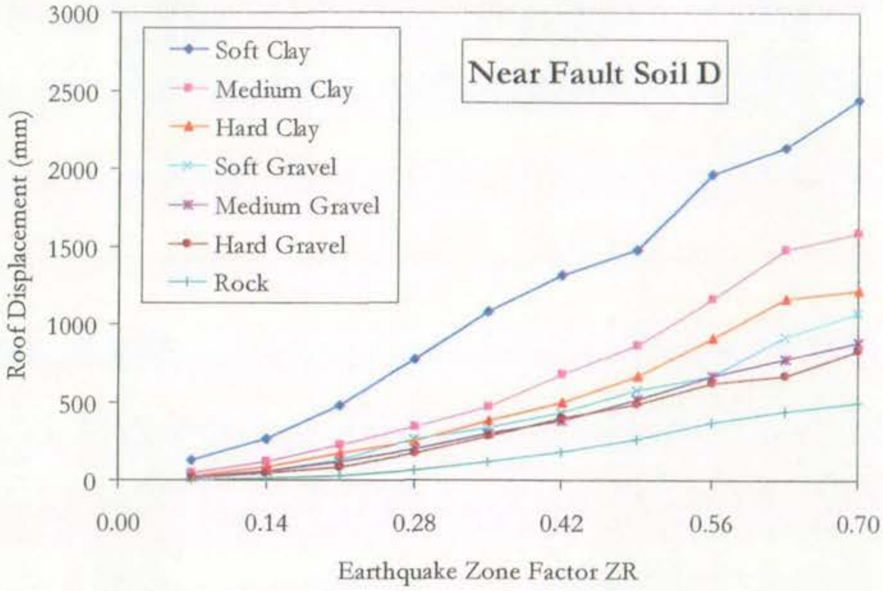

6.2.2 Site Soil Class

As for soil springs above, the softer the seismic soil category the higher the displacements. This is consistent over all soil spring values, as shown in Figure 6-7. As noted above, though, some results are inconsistent in that soft clay would not occur on Soil Class B and rock would not occur with a Soil Class D.

There is a very large difference between the softest and firmest site. Displacements on rock springs on Site Class B are 98 mm whereas those on soft clay springs on Site Class D are 2438 mm, higher by a factor of over 24 times.

Figure 6-7 Effect of Site Soil Class on Time History Response

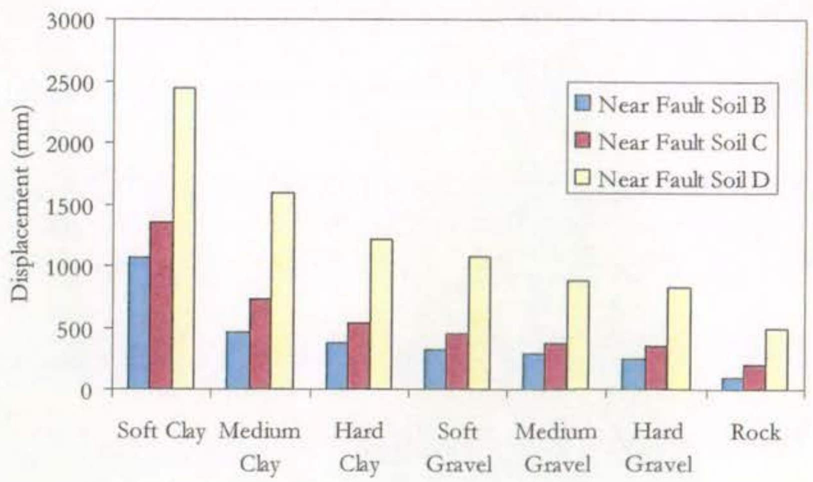

6.2.3 Near Fault Effects

The fault distance does not make a difference for periods less than 1.5 seconds as the near fault amplification factor N(T,D) has a value of 1.0 for periods up to 1.50 seconds. The period of response of rocking walls depends on three factors, (1) the wall stiffness, (2) the stiffness of the soil springs and (3) the earthquake amplitude. Therefore, the effects of the near fault factors increase as the wall height increases, the soil springs soften or the earthquake amplitude increases.

Figure 6-8 compares the near fault and far fault displacements for Wall 2-3, the 3.600 m long wall 3 stories high, located on Site Class B with three different soil conditions:

1. For a rock site there is essentially no difference between the near fault and far fault response, regardless of earthquake amplitude.

2. For a gravel site there is essentially no difference between the near fault and far fault response up to earthquake amplitudes of about ZR = 0.35 but for higher amplitudes the near fault gives progressively higher displacements until at ZR = 0.70 the near fault displacements are 26% higher.

3. For a clay site the near fault records cause higher displacements for almost all earthquake amplitudes. The difference increases with amplitude and at amplitude ZR = 0.70 the near fault displacements are 57% higher.

Table 5-3 lists the elastic periods for this wall as 0.43 seconds on rock, 1.03 seconds on gravel and 2.09 seconds on clay. As near fault effects occur for periods exceeding 1.50 seconds, this explains why the wall on clay is affected for all earthquake amplitudes. The wall on gravel is only affected when the rocking causes the period of response to increase by 50%. On rock, the period would need to increase by a factor of 3.5 before near fault effects would influence results.

Figure 6-8 Effect of Near Fault Factor on Time History Response Site Class B

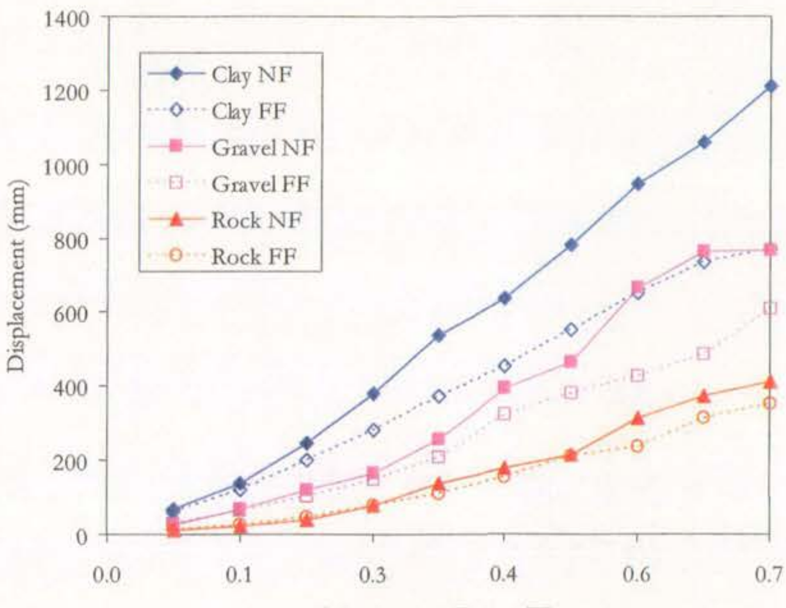

6.2.4 Wall Aspect Ratio

Table 6-3 and Figures 6-9 and 6-10 illustrate the effect of the wall aspect ratio, defined as the total wall height divided the by wall length, on maximum displacements. The results compared are for Soil Spring Set B, which is medium Clay, for seismic Soil Class D, with no near fault effects.

Table 6-3 Effect of Aspect Ratio on Displacements

Seismic Zone Factor ZR	Single Story Walls			Three Story Walls		
	H/B=1.0	H/B=0.5	H/B=0.25	H/B=1.0	H/B=0.5	H/B=0.25
Maximum Top Displacement (mm)						
0.07	5	1	0.1	66	17	3
0.14	21	2	0.2	150	54	7
0.21	67	5	0.3	313	104	18
0.28	98	11	0.5	428	155	31
0.35	121	20	0.6	614	245	76
0.42	168	36	1.0	790	336	122
0.49	208	64	1.3	911	454	156
0.56	289	98	1.9	950	606	198
0.63	372	135	4.0	1058	659	223
0.70	432	148	6.1	1185	670	274
Displacement Relative to H/B = 0.25						
0.07	48	8	1	23	6	1
0.14	100	10	1	23	8	1
0.21	206	15	1	18	6	1
0.28	216	24	1	14	5	1
0.35	192	31	1	8	3	1
0.42	173	37	1	6	3	1
0.49	158	49	1	6	3	1
0.56	152	52	1	5	3	1
0.63	94	34	1	5	3	1
0.70	71	24	1	4	2	1
Average	141	28	1	11	4	1

The response is extremely sensitive to the aspect ratio but the differences in relative displacements between the single story and the three story walls for the same range of aspect ratios indicates that response is not solely a function of aspect ratio but also a function of height. That is, absolute wall dimensions are important as well as the ratio between them.

1. For single story walls, there is over an order of magnitude increase in displacements when the aspect ratio increases from 0.25 to 0.50 and an increase by another order of magnitude as the aspect ratio increases further to 1.00. As the earthquake magnitude increases, the ratio tends to increase up to a certain amplitude and then decrease. The average ratios of displacements are 141:28:1 for aspect ratios 1:½:¼.

2. For the three story walls, the increase in displacements with increased aspect ratio is still substantial but less than for the single story walls. There is an increase in displacements by a factor of about 5 when the aspect ratio in increases from 0.25 to 0.50 and an increase by about 10 as the aspect ratio increases further to 1.00. The actual ratio is more sensitive to earthquake magnitude than the single story walls and tends to decrease proportionately as the earthquake magnitude increases. The average ratios of displacements are 11:4:1 for aspect ratios 1:½:¼, much less than the single story walls..

Figure 6-9 Effect of Aspect Ratio on Single Story Walls

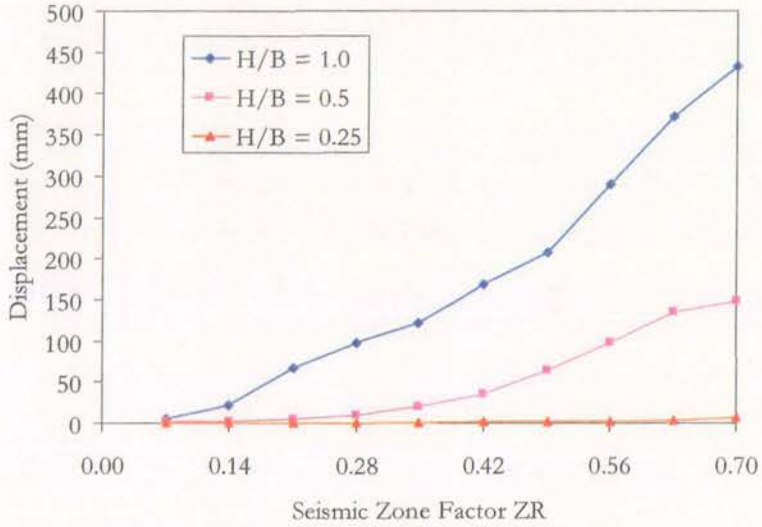

Figure 6-10 Effect of Aspect Ratio on Three Story Walls

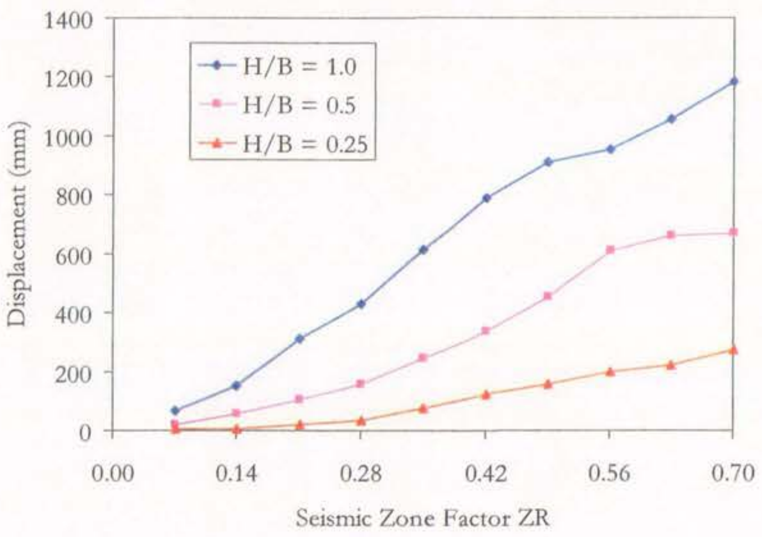

6.2.5 Wall Height

Wall 2, the 3.600 m long configuration, was evaluated for heights ranging from 1 to 6 stories. Table 6-4 lists the maximum displacements for each wall, normalized to the single story results, for the wall on springs corresponding to rock and for the same wall with springs corresponding to medium clay. These results are plotted in Figures 6-11 and 6-12 respectively. For both spring types, the displacements for low amplitude earthquakes tend to be higher by a larger ratio than the ratio of heights. For example, at ZR=0.07 the displacement of a 6 story wall on clay springs is 15 times as high as the displacement of a 1 story wall on the same springs. As the earthquake amplitude increases the ratio tends to decrease. For ZR=0.70 the 6 story wall on clay has displacements only 5 times as high as the single story wall. For all amplitudes, the stiff springs give a higher ratio than the soft springs.

Table 6-4 Displacements Normalized to Single Story Displacements

Seismic Zone Factor ZR	H = 1	H = 2	H = 3	H = 4	H = 5	H = 6
Wall 2 With Rock Springs Near Fault Class B						
0.07	1.0	7.9	18.9	31.2	55.5	70.5
0.14	1.0	8.4	13.3	31.2	50.4	59.7
0.21	1.0	3.8	7.5	18.8	25.1	36.3
0.28	1.0	3.2	7.8	14.7	23.3	33.6
0.35	1.0	2.4	7.1	11.2	20.6	23.0
0.42	1.0	2.9	7.3	12.3	20.3	22.3
0.49	1.0	2.9	6.0	12.1	15.6	21.5
0.56	1.0	3.4	7.7	12.7	18.5	21.8
0.63	1.0	3.8	6.7	12.0	15.5	17.3
0.70	1.0	3.6	5.8	9.9	14.5	15.1
Wall 2 With Clay Springs Near Fault Class C						
0.07	1.0	3.3	7.3	9.7	13.4	15.1
0.14	1.0	3.2	7.2	8.8	11.9	13.5
0.21	1.0	3.5	8.4	9.8	13.9	14.6
0.28	1.0	3.0	7.5	8.8	10.5	11.0
0.35	1.0	2.8	5.7	7.0	8.1	8.7
0.42	1.0	2.8	4.9	6.0	6.3	7.0
0.49	1.0	3.0	4.7	5.8	6.6	6.7
0.56	1.0	2.7	4.5	5.0	5.7	6.2
0.63	1.0	2.4	4.3	4.8	5.1	5.6
0.70	1.0	2.5	4.2	4.6	4.8	4.9

Figure 6-11 Effect of Wall Height on Rock Site

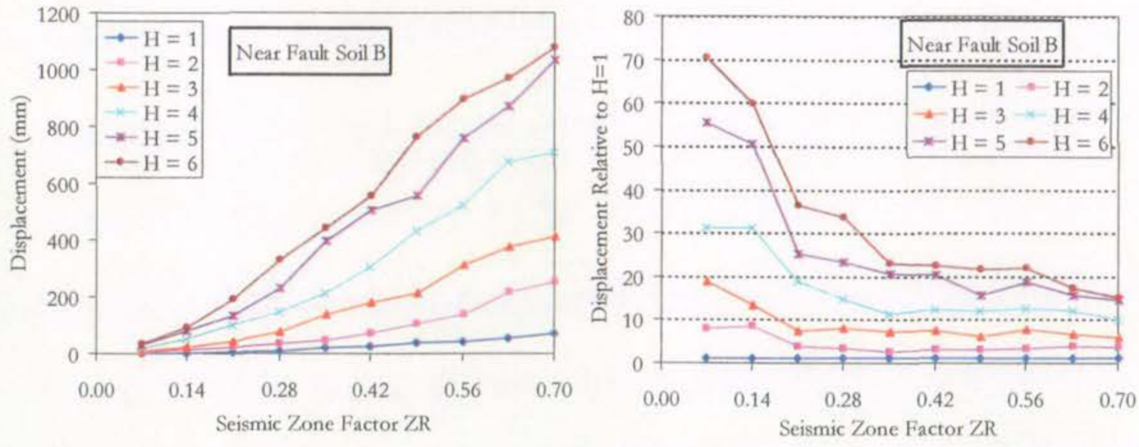

Figure 6-12 Effect of Wall Height on Clay Site

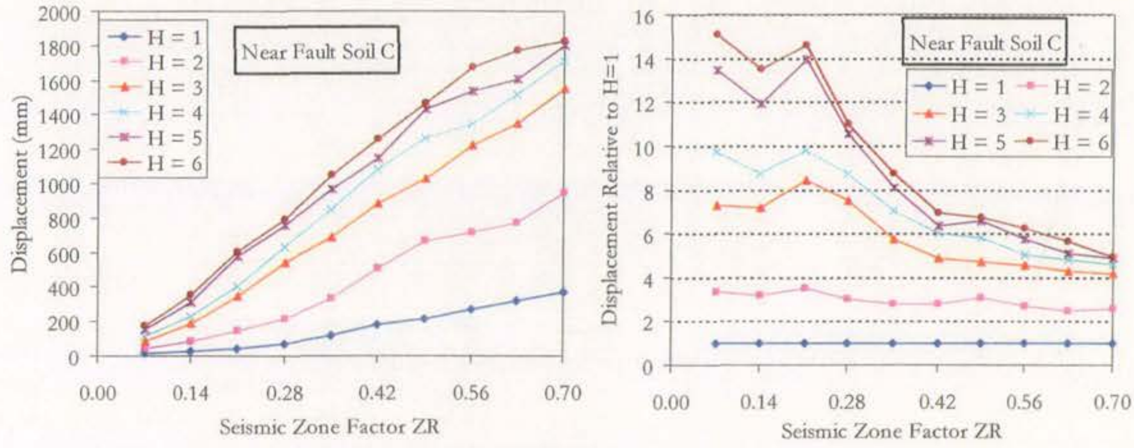

6.3 Effect of Soil Spring Discretization

The baseline single wall analysis studies used a wall sub-divided into 6 segments, with a soil spring at each grid line, providing a total of 7 springs across the base of the wall. The effect of this discretization of the soil properties was assessed by reducing the number of springs to 2, one at each end of the wall. This is the coarsest model possible for soil springs on a single wall, and represents a configuration often used in practice for the analysis of structures with a large number of walls.

To assess the effect of a single spring at each end of the wall, the three story model of Wall 1 was used, a 7.200 m long x 10.800 m high wall. The full series of analyses was repeated for each of soil types B (medium clay), E (medium gravels) and G (rock).

The procedure used was to replace the 7 springs with a single spring at each end. The spring constant at each end of the wall was set so as to provide the same second moment of inertia about the horizontal axis as the 7 spring model (same rocking stiffness).

A consequence of reducing the number of springs is that the wall is required to span horizontally between the end springs. As shown by the comparison of periods in Table 6-5, this effect becomes more marked as the soil stiffness increases. The period is almost the same for the medium clay (Soil Type B) but 9.1% higher for the rock support (Soil Type G). This is the expected pattern, as the stiffer springs provide a higher degree of internal support than the softer springs.

Table 6-5 Effect of Number of Springs on Period

Soil Type	Period (Seconds)		Effect of Reducing Spring Number
	7 Spring Model	2 Spring Model	
B Medium Clay	0.900	0.903	+0.3%
E Medium Gravel	0.438	0.444	+1.4%
G Rock	0.175	0.191	+9.1%

Figure 6-13 illustrates the effect of replacing the seven springs with two springs on the capacity curves for the wall for the soft and stiff soils respectively, Soil Type B (Medium Clay) and Soil Type G (Rock). This shows that the two models have the same stiffness for small deformations (the initial elastic stiffness) and large deformations (P-Delta stiffness) but differ in the transition zone between these two extremes. The 2 spring model provides a higher peak resisting force because the peak occurs at a lower displacement level than for the 7 spring model. At the lower displacement, the reduction on the peak force due to P-Δ effects is lower for the 2 spring mode.

This effect of the number of springs on peak force is inversely proportional to soil stiffness. For the softest springs considered, Soil Type B, the peak force for the 2 spring model is 12% higher than for the 7 spring model (492 kN compared to 439 kN respectively). For the hardest spring considered, Soil Type G, the peak force for the 2 spring model is only 0.4% higher than for the 7 spring model (497 kN compared to 495 kN respectively).

Figure 6-13 Effect of Number of Springs on Capacity Curve

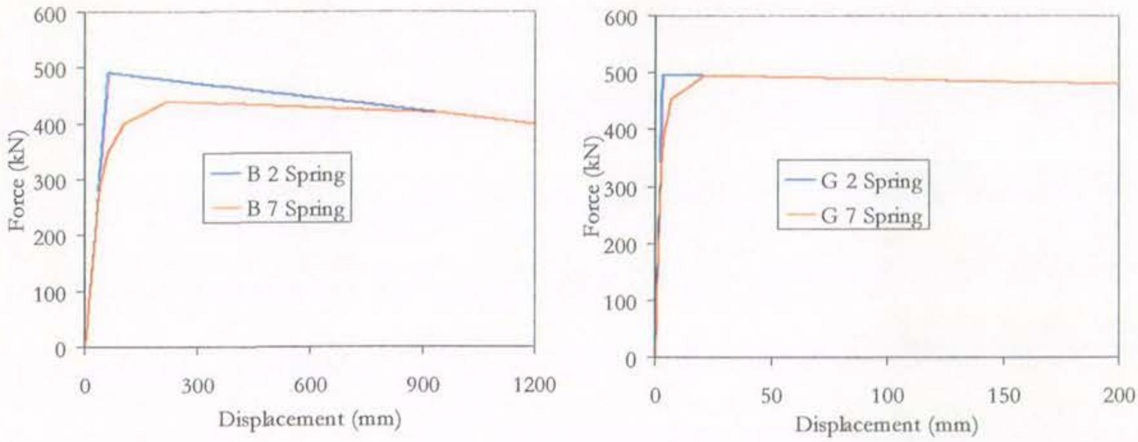

As for the original seven spring model, a total of 420 analyses were performed for each of the three soil types considered for six seismic conditions (Near and far fault for each of subsoil conditions B, C and D). As the trends were similar for each series of analyses only the two extreme soil types and two seismic conditions are discussed here.

Figure 6-14 compares the dynamic force-displacement curve and the wall displacement versus amplitude for Near Fault seismic input Soil B and Soil D for the medium clay soil springs (Type B). Figure 6-15 plots the same results for the Rock soil springs (Type G).

Figures 6-14 and 6-15 illustrate that reducing the number of springs from 7 to 2 has a significant effect on the maximum base shear force for a given displacement (the left hand plots) but little effect on the predicted maximum displacement for a given seismic amplitude (the right hand plots).

The 2 spring models produce a base shear coefficient which is consistently about 20% higher than recorded by the 7 spring models for all displacements sufficient to cause rocking. From the capacity curves in Figure 6-13, some increase in base shear would be expected but those static curves suggest that the increase would be small for stiff springs. However, the results for the rock springs in Figure 6-15 show a similar increase to those for the softer clay springs in Figure 6-14. This suggests that the increase in base shear for the 2 spring model is related to a dynamic rather than static phenomenon. This is likely because the 2 spring configuration produces a bi-linear model rather than the multi-linear model produced by the 7 spring configuration. The former makes resonance at a particular period more likely and the results appear to demonstrate this.

Although this parametric study on the number of springs was relatively limited in scope, the results for different soil springs and seismic input suggest that a reduced number of springs would be conservative for both forces and deformations:

- A 2 spring model would tend to over-estimate the maximum base shear for a given earthquake amplitude relative to the base shear from a 7 spring model.

- The 2 spring model would predict essentially the same peak displacements for a given earthquake amplitude as the 7 spring model. Differences between the two models are less than between different earthquakes for the same model.

Figure 6-14 Effect of Number of Springs for Medium Clay (Type B)

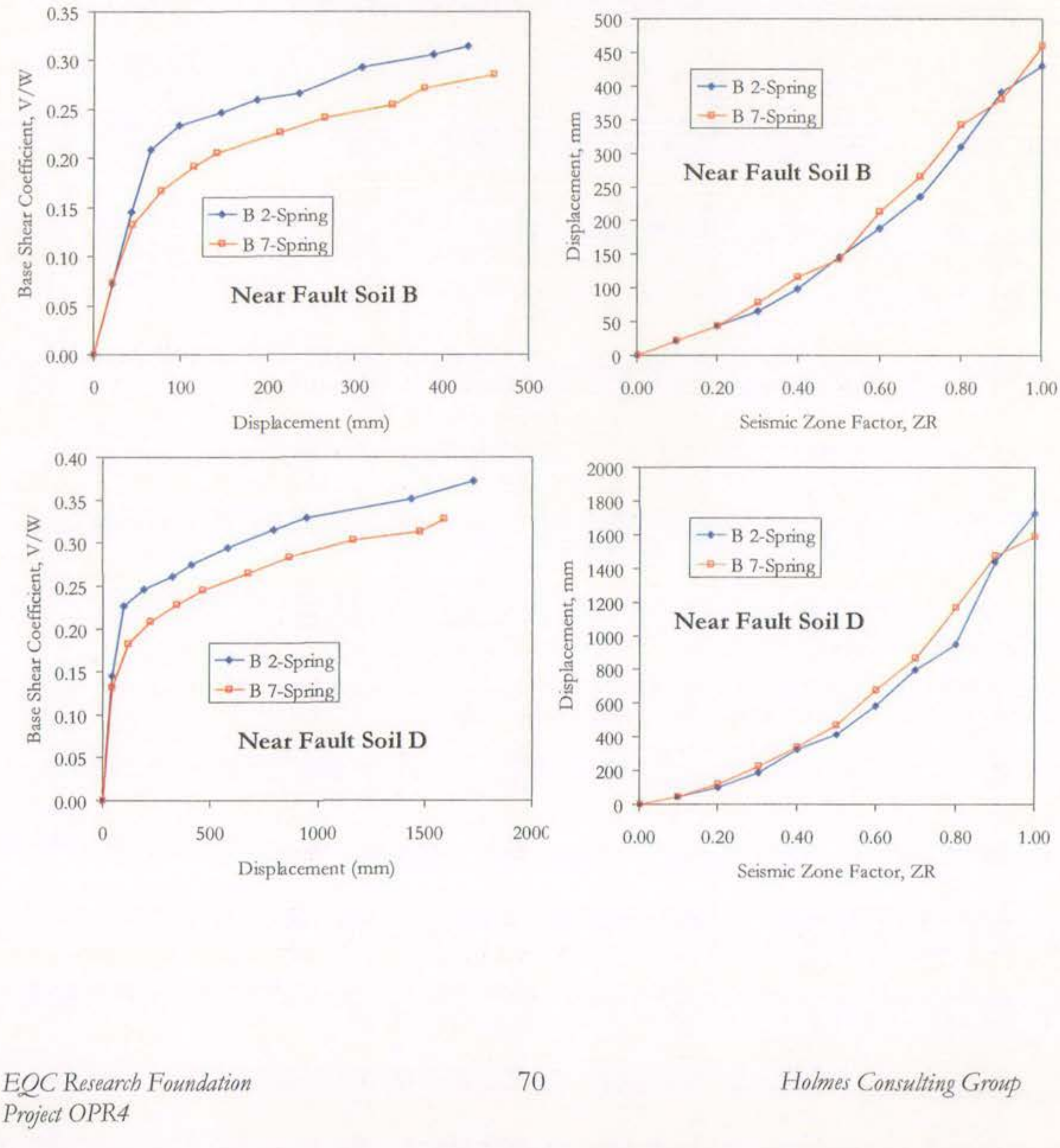

Figure 6-15 Effect of Number of Springs for Rock (Type G)

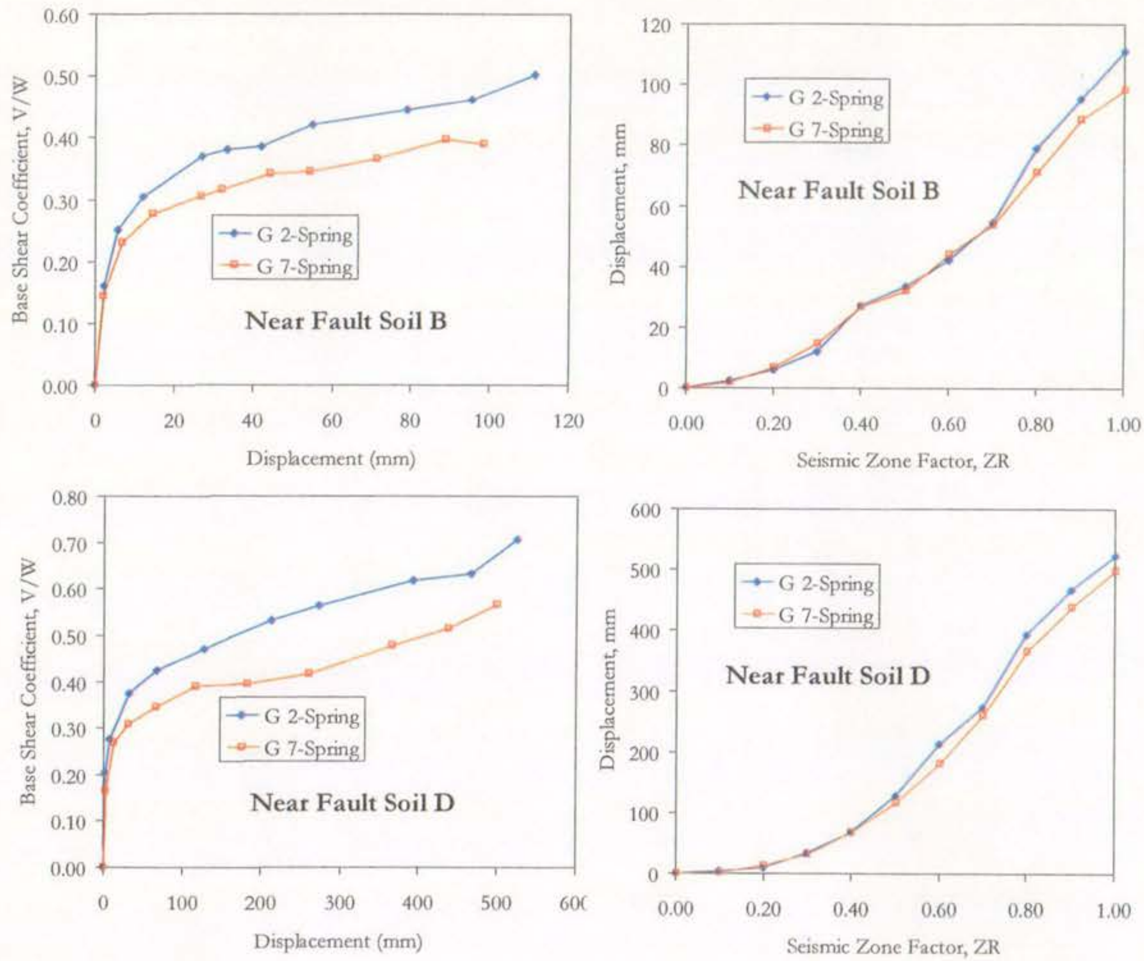

6.4 Inertia Force Distribution

As discussed in the preceding chapter (with reference to numerical stability, illustrated by Figures 5-11 and 5-12) the maximum inertia force for single story walls equals the elasto-plastic strength of the rocking system, within the limits of numerical accuracy of the integration procedure. This equality arises because a single wall has a single mass. The applied inertia force equals this mass times the acceleration and the overturning moment is the inertia force times the height to the mass. This overturning moment must equal the restoring moment for equilibrium. The base shear is equal to the overturning moment divided by the height to the mass.

For multi-story walls there are multiple masses and each mass may be acted on by a different acceleration and so have a different inertia force. The total overturning moment, which is the sum of the inertia forces times the height, must equal the restoring moment as for single story walls. However, the base shear force is equal to the moment divided by the effective height which is unknown.

Figure 6-16 plots the shear forces on the 3 story model of Wall 1, the multi-story equivalent of the plot in Figure 5-11. It is seen that the shear force corresponds to the pushover curve for low amplitude response, where the wall is not rocking. However, as the amplitude increases the time history shear force at a given displacement tends to exceed the shear force from the static pushover analysis. The difference tends to increase with increasing amplitude and for very large displacements the shear force may approach twice the static shear force. The increase of dynamic shear over static shear is termed "dynamic amplification", and has been recognised in NZ codes for over 20 years, resulting in the requirement for an ω (omega) factor to be applied to seismic shear forces to provide design shear forces in ductile frames and ductile shear walls.

Figure 6-16 Shear Force on Wall 1-3-B

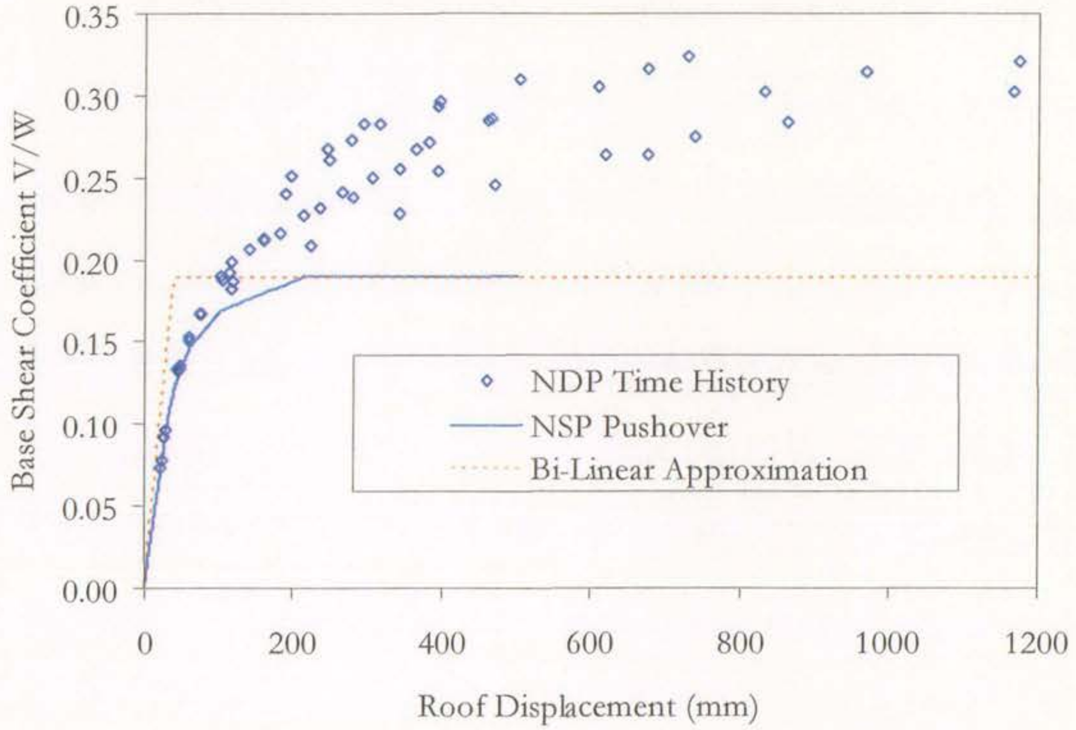

The dynamic amplification effects are illustrated by the time history of response for the three story model of Wall 2 (the 3.6 m long wall) on medium clay springs, as shown in Figures 6-17 and 6-18 for respectively overturning moment and shear force. For this wall, the wall length is 3.433 m and the weight is 1530 kN. This provides a theoretical resisting moment, for infinitely stiff springs, of 1530 x 3.433/2 = 2627 kN-mm.

Figure 6-17 plots the time history of overturning moment for this wall and the concurrent wall top displacement. The moment reaches a peak value of 2047 kN-m, about 20% less than the theoretical limit. The reduction compared to the theoretical limit is because the lever arm is reduced by the displacement. Because of second order effects, the moment reaches a peak value but then, as the displacement increases, the moment capacity reduces. This gives the characteristic "scalloped" shape exhibited in Figure 6-17. The maximum displacement in this wall is 1686 mm and so the theoretical reduced moment is 1530 x (3.433 – 1.686) / 2 = 1336 kN-m. It is seen from Figure 6-17 that this moment occurs at about 28 seconds, when the displacement is a maximum.

If it is assumed that seismic inertia forces follow a triangular pattern, based on accelerations increasing linearly with height, then the effective height of application of the inertia forces would be two-thirds the wall height. Therefore, the maximum moment of 2047 kN-m would imply a maximum shear force of (2047 / (0.67 x 10.8) = 284 kN.

Figure 6-17 Wall 2-3-B Time History of Overturning Moment EQ 1

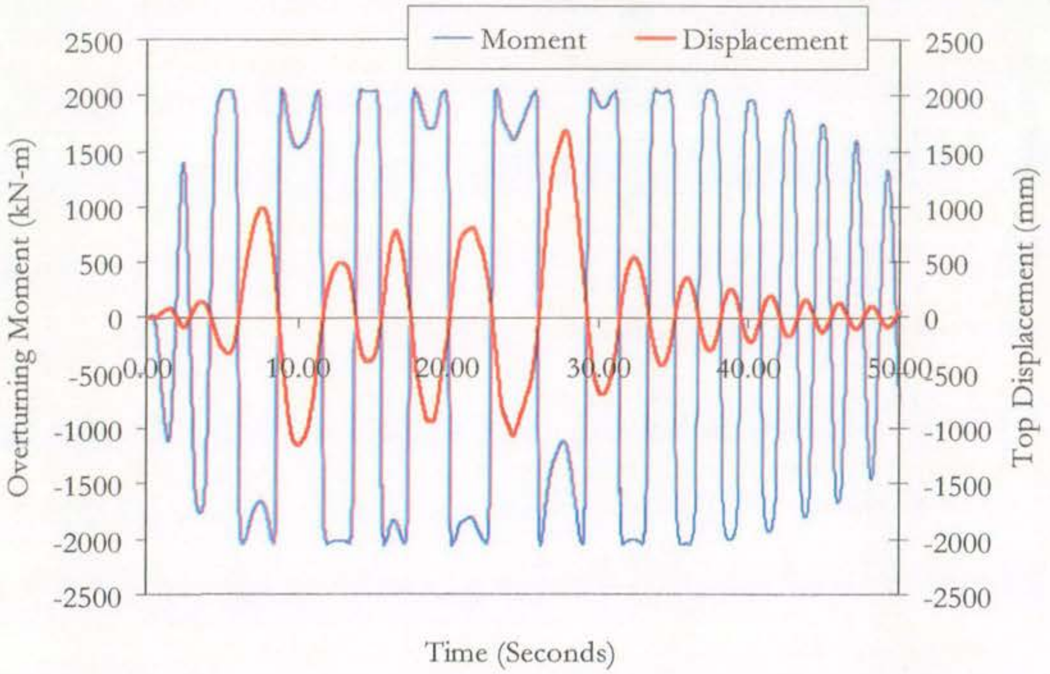

The concurrent base shear force time history, plotted in Figure 6-18, exhibits much less regularity than the base moment. For both the initial and final portions of the earthquake response the shear force follows a pattern similar to that of the moment. The maximum shear forces in these portions of record are about 250 kN, close to the theoretical value of 284 kN if the forces act at two-thirds the height.

Figure 6-18 Wall 2-3-B Time History of Shear Force EQ 1

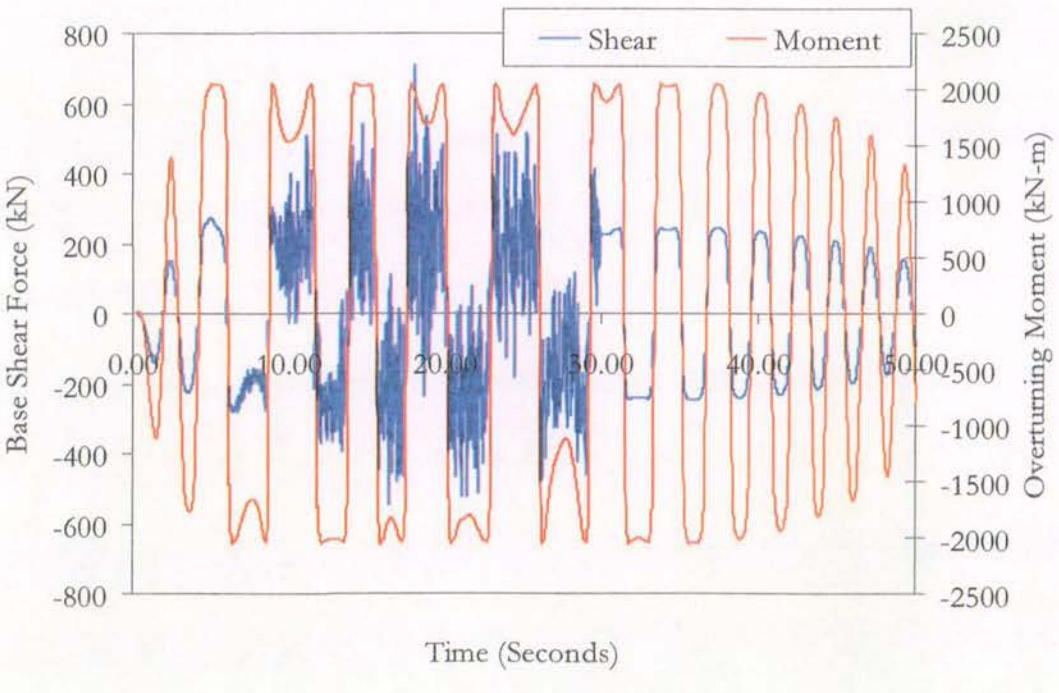

However, the strong motion portion of the record, from about 10 seconds to 20 seconds, causes an erratic pattern of shear forces due to an apparent high frequency motion superimposed on the fundamental rocking period of the wall. The shear forces in this strong motion portion of shaking are much higher than in the initial portion, with a peak shear force of 709 kN, 2.5 times the expected shear force of 284 kN.

The base moment time history is plotted with the shears on Figure 6-18 and this shows that the irregular pattern of shear forces occurs at the time the base moment is reducing due to second order effects, although peak shear forces do not occur at times of peak displacement.

Capacity design is based on an assumption that the formation of a mechanism acts as a "fuse" and inhibits increases in forces, other than those due to overstrength and strain hardening. Typically, overstrength and strain hardening add about 50% to the forces at the time of formation of the mechanism. For the wall results reported here, there is no overstrength or strain hardening and so the increase by 150% is due to dynamic effects. The manner is which these effects arise is illustrated by the calculations in Table 6-6, based on the distributions of inertia forces plotted in Figure 6-19.

For static analysis, the force distribution was based on the FEMA 356 formulation, where the inertia force at each floor is calculated as a fraction of the total based shear, V, as a function of the floor weight, w, and height, h, according to:

$$F_x = V \frac{w_x h_x^k}{\sum_{i=1}^{n} w_i h_i^k}$$

The power, k, has a value of 1.0 for periods less than 0.5 seconds and 2.0 for periods exceeding 2.50 seconds. Wall 2-3-B in Table 6-13 has a period of 2.09 seconds and so the static load is proportional to the height to the power of 1.73.

The dynamic inertia forces in Table 6-6 are those occurring at time T = 18.03 seconds, when the base shear force reached a peak value of 709 kN (see Figure 6-18). It is seen from Table 6-6, and Figure 6-19, that the dynamic inertia forces change sign, with a negative force at the top floor and positive force at the lower two floors. The effect of this is that even though the overturning moment is almost equal to the static overturning moment the shear force is over three times as high. The implies a dynamic amplification factor, ω, of over 3.0

Table 6-6 Wall 2-3-B Calculation of Overturning Moment

Elevation	Inertia Force (kN)		Shear Force (kN)		Overturning Moment (kN-m)	
(m)	Static	Dynamic	Static	Dynamic	Static	Dynamic
10.800	139	-268	139	-268	0	0
7.200	67	374	205	106	499	-966
3.600	19	603	225	709	1238	-585
0.000	0	0	225	709	2047	1967

Figure 6-19 Wall 2-3-B Static and Dynamic Force Distributions

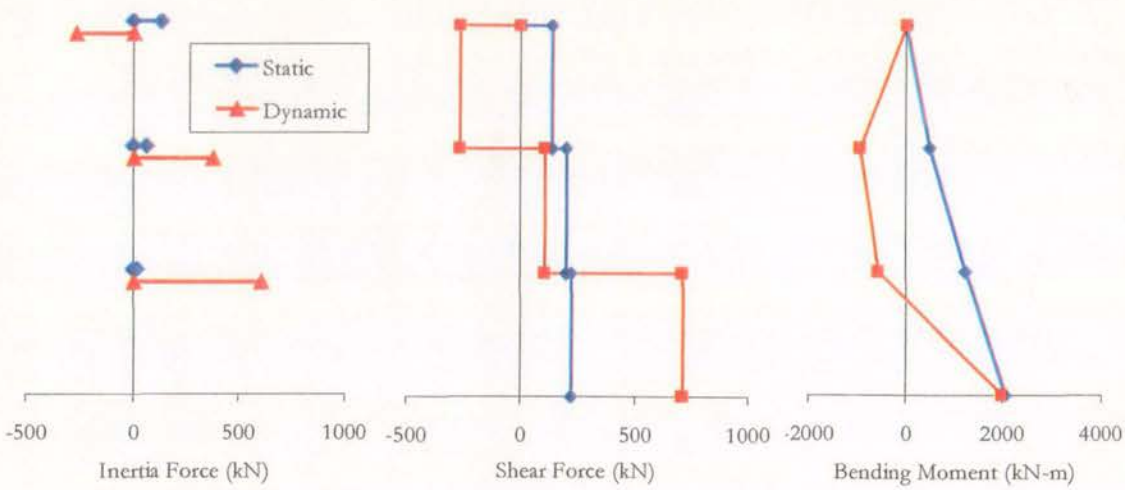

6.5 Reaction Force on Soil

6.5.1 FEMA Guidelines

FEMA-356 addresses the concentration of reaction forces under rocking foundations in C4.4.2.1.5, the relevant section of which is reproduced below:

> For rigid footings subject to moment and vertical load, contact stresses become concentrated at footing edges, particularly as uplift occurs. The ultimate moment capacity, M_c, is dependent upon the ratio of the vertical load stress, q, to the expected bearing capacity, q_c. Assuming that contact stresses are proportional to vertical displacement and remain elastic up to the expected bearing capacity, q_c, it can be shown that uplift will occur prior to plastic yielding of the soil when q/q_c is less than 0.5. If q/q_c is greater than 0.5 then the soil at the toe will yield prior to uplift. This is illustrated in Figure C4-3 (reproduced below as Figure 6-20).

Figure 6-20 Idealized Concentration of Stress at Edge of Rigid Footings (FEMA 356 Figure C4-3)

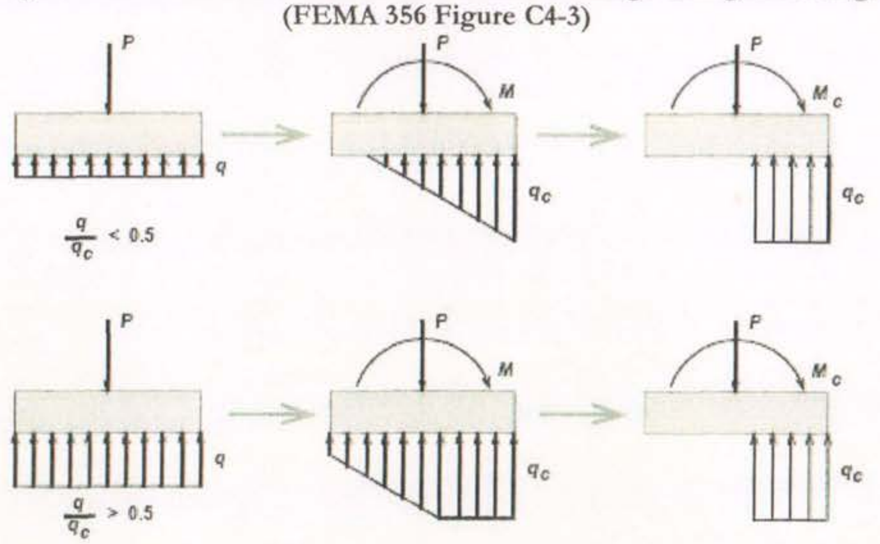

Typically, foundation design in seismic zones is such that the factor of safety between gravity stresses and ultimate bearing capacity is greater than 2 and so the condition shown in the lower portion of Figure 6-20 applies, where uplift occurs prior to plastic yielding of the soil.

6.5.2 Design Office Practice

For design office calculations, it is generally assumed that the overturning moment is resisted by a compression stress block, as shown in Figure 6-21. It is assumed that the stress block is centred at the location of the concentrated reaction, extends to the compression face of the foundation and is symmetric about the reaction point.

Figure 6-21 Assumed Soil Pressure Distribution

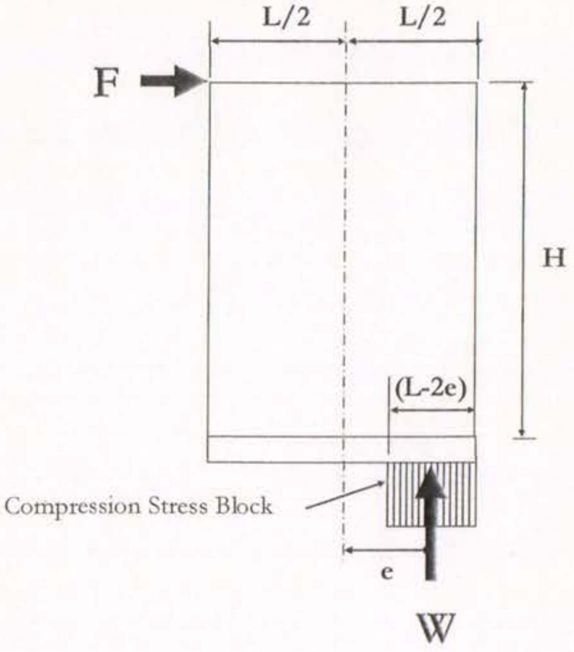

6.5.2.1 Design for No Uplift

For a given lateral load the stress block assumptions of Figure 6-21 can be used to derive an expression for the required width of the foundation, B, as a function of the ultimate bearing capacity, q_C:

1. The overturning moment, M, is calculated as the product of the inertia load, F, and the effective height, H. This is the moment required to cause uplift of the wall – see Section 7 in the report for more details.
2. The eccentricity of load, e, is calculated as $e = \frac{M}{W} = \frac{FH}{W}$
3. The length of the compression block is calculated as $c = L - 2e = (L - \frac{2FH}{W})$
4. The compression stress $q_c = \frac{W}{cB}$, which gives $c = \frac{W}{q_c B}$

5. From this, $c = \dfrac{W}{q_c B} = (L - \dfrac{2FH}{W})$

6. Reform in terms of the beam width $B = \dfrac{W}{q_c(L - \dfrac{2FH}{W})}$

For example, consider Wall 1-3-B, the three story wall 7.200 m long, with a period of 0.900 seconds. Elastic design for a seismic zone Z=0.14, Soil C, requires a lateral load of 0.18W = 560 kN. The required foundation width as a function of ultimate bearing capacity is shown in Figure 6-22. For this particular wall, the soil strength of 300 KPa requires a 4.260 m wide foundation, which would reduce to a width of 0.640 m if the strength were 2,000 KPa.

This assumes that the foundation length, L in the equations above, is the same length as the wall. For low soil strengths, the required width can be reduced by extending the foundation beyond the end of the wall and designing for flexure in the extended portion. For the wall example in Figure 6-22 the width of 4.260 m could be reduced to 1.610 m by extending the foundation by 1.0 m at each end of the wall, resulting in a 9.200 m long beam beneath the 7.200 m wall.

Figure 6-22 Required Foundation Beam Width for Given Rocking Strength

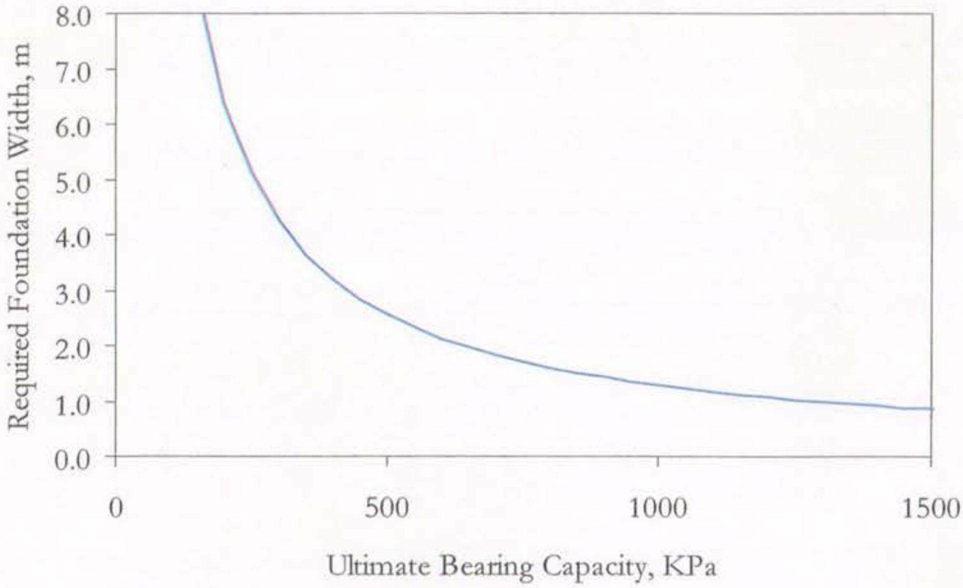

6.5.2.2 Walls Permitted to Uplift

If the foundation dimensions are less than that required for the elastic seismic load then uplift will occur. Figure 6-23 plots the rocking load capacities for various combinations of width and length for the same wall used in the example above. For increases in foundation widths above the minimum value the rocking load initially increases rapidly but then levels off as the stress block becomes smaller. Increases in foundation length beyond the length of the all itself give consistent increases in lateral load capacity.

Figure 6-23 Effect of Foundation Size on Rocking Strength

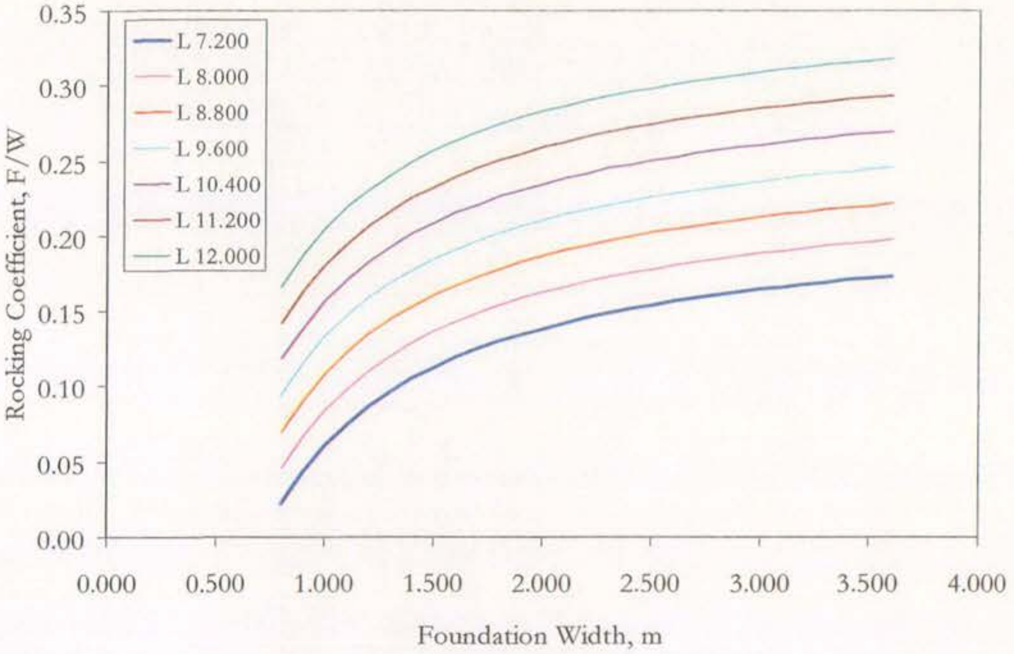

The calculations of rocking coefficient versus foundation size, as plotted in Figure 6-23, can be used to determine the required foundation size to limit the ductility factor to a specified value. To obtain the ductility plot shown in Figure 6-24, the elastic design coefficient, $C(T_1)$, is multiplied by the reciprocal of the rocking coefficient in Figure 6-23.

For example, for this wall Figure 6-24 shows that for a foundation beam the same length as the wall (L = 7.200 m) a width of 1.200 m with result in a ductility factor of 2 but a reduction in width to 0.900 m will double the ductility factor to 4.

Figure 6-24 Ductility Factor Versus Foundation Size

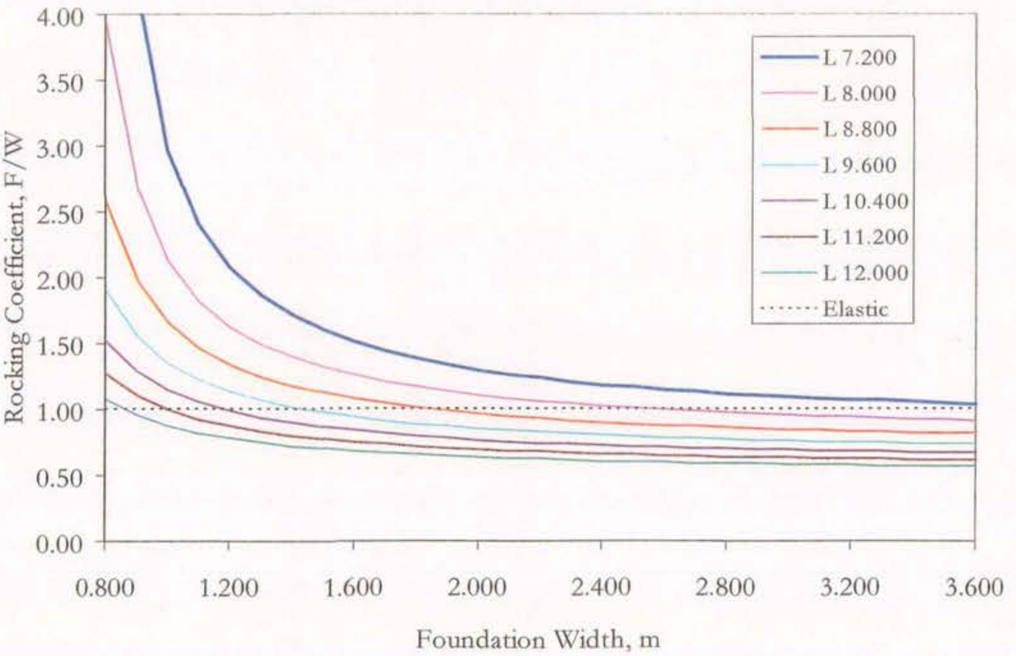

6.5.3 Comparison of Design Office Practice with Analysis Model

The design office procedure described above produces an effective stress block which differs in size from that assumed in the development of the analysis model, where the end spring size was based on the FEMA recommendation of one-sixth the foundation width, B/6, as discussed in Section 5.1 of this report. However, the calculated overturning moment is relatively insensitive to this, as listed in Table 6-7 for all the single walls evaluated.

Table 6-7 lists the calculated location of the edge of the stress block from the compression face, c, and the moment calculated assuming the resultant at the centroid this stress block, M_D using the design office definition of stress block and M_A using the FEMA definition used for the analysis. The values show that although the variation in c was large the effect of the moment was much less, with differences ranging from +1% to +14%.

Table 6-7 Calculation of Overturning Moment

Wall ID	N	Foundation L	Foundation B	Weight W	Design c	Design M_D	Analysis c	Analysis M_A	$\frac{M_A}{M_D}$
1	1	7.2	1.0	518	0.86	1643	0.167	1866	114%
1	2	7.2	1.0	1037	0.86	3285	0.167	3733	114%
1	3	7.2	1.0	1555	0.92	4885	0.167	5600	115%
2	1	3.6	1.0	518.	0.17	889	0.167	933	105%
2	2	3.6	1.0	1037	0.17	1779	0.167	1866	105%
2	3	3.6	1.0	1555	0.18	2662	0.167	2800	105%
2	4	3.6	2.0	2074	0.19	3540	0.333	3733	105%
2	5	3.6	2.5	2592	0.26	4333	0.417	4666	108%
2	6	3.6	3.0	3111	0.21	5280	0.500	5599	106%
3	1	14.4	1.0	518.	0.17	3688	0.167	3733	101%
3	2	14.4	1.0	1037	0.17	7379	0.167	7466	101%
3	3	14.4	1.0	1555	0.38	10907	0.167	11199	103%

6.5.4 Soil Reactions from Analyses

The maximum reaction force on the soil at the base of the single walls is evaluated by tabulating the maximum force in the gap elements at either end of the wall. An example of the variation with amplitude is given in Figure 6-25 for the 3 story configuration of Wall 1 (the 7.200 m long wall). The reaction forces are plotted for all earthquake amplitudes for each of the three soil conditions included in the evaluation.

Figure 6-25 shows that the variation in reaction force follows a pattern which is predictable based on the engineering mechanics of the rocking mechanism:

1. The reaction force increases with increasing earthquake amplitude. This is expected as the wall rocks and the reaction becomes concentrated onto a smaller compression block of soil.

2. The stiffer the soil springs the faster the increase in reaction force with earthquake amplitude. Again, this is expected because the softer soil springs have a larger gravity load deformation and it takes a larger seismic displacement to disengage the springs.

3. The reaction force converges to the total weight of the wall. At some displacement, all springs except that at the extreme compression end of the wall disengage. At this point, all the weight is supported on a single spring.

The condition where all weight is supported on the end spring is similar to the design office assumption, as illustrated in Figure 6-21, except that the area of the stress block is based on the spring tributary area rather than calculated from the load eccentricity.

Figure 6-25 Wall 1 (L = 7.200 m) 3 Story Reaction Forces

Near Fault Soil B **Near Fault Soil D**

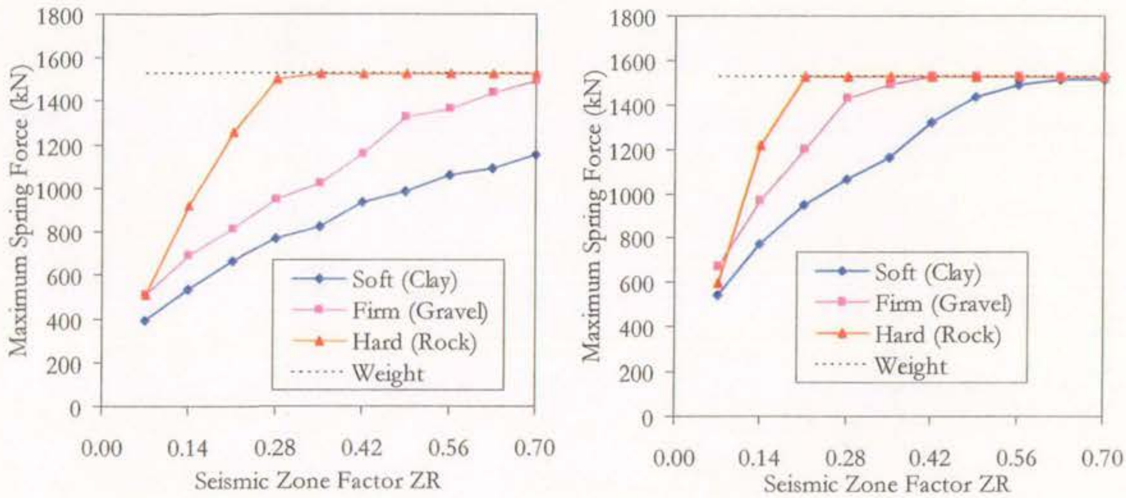

6.5.5 Effect of Vertical Mass on Reactions

The reaction forces described in the preceding section are the same as would be expected from a static analysis and do not exhibit any dynamic effects, even though some impact force would be expected as the gap elements close. The reason for this is that the analysis model included translational mass only, not vertical mass. This follows normal design office practice for structural analysis.

The effect of ignoring vertical mass on response was assessed by repeating some analyses with a vertical mass, corresponding in magnitude to the gravity load on the wall, lumped at the nodes. The wall selected for these analyses was the 3 story configuration of Wall 1 (7.200 m long) on Clay springs (Type B) and rock springs (Type G). The time history of forces and displacements in the gap elements was recorded.

Figure 6-26 shows the full 50 second time history of compression forces in the extreme gap elements for the analyses with and without vertical mass (Mv) for the model on soft soil springs. When vertical mass is ignored, the compression force follows a time history trace approximating the rocking period of the wall, with a period of about 3 seconds between successive peaks during the strong motion portion of record. The amplitude of the peak is limited by the vertical weight of the wall, 1526 kN. When vertical mass is added to the model there is an additional higher frequency motion superimposed on the long period motion.

This periodicity shows up more clearly in Figure 6-27, which is plotted for the time slice from 16.0 to 19.0 seconds. This figure shows that the period of the high frequency motion is about 0.38 seconds. The displacement trace in Figure 6-27 indicates that when the gap closes the wall "bounces" on the soil spring, causing the compression force to vary by about ±100% from the mean value, which is the value when vertical mass is not included in the model.

Figure 6-26 Wall 1-3-B Reaction Forces Full Time History

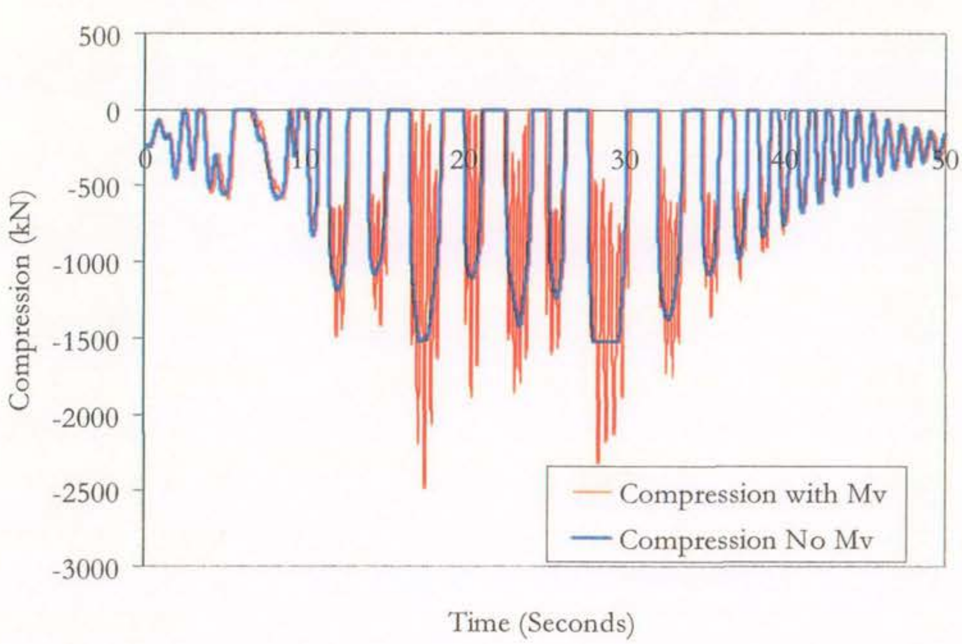

Figure 6-27 Wall 1-3-B Reaction Forces Partial Time History

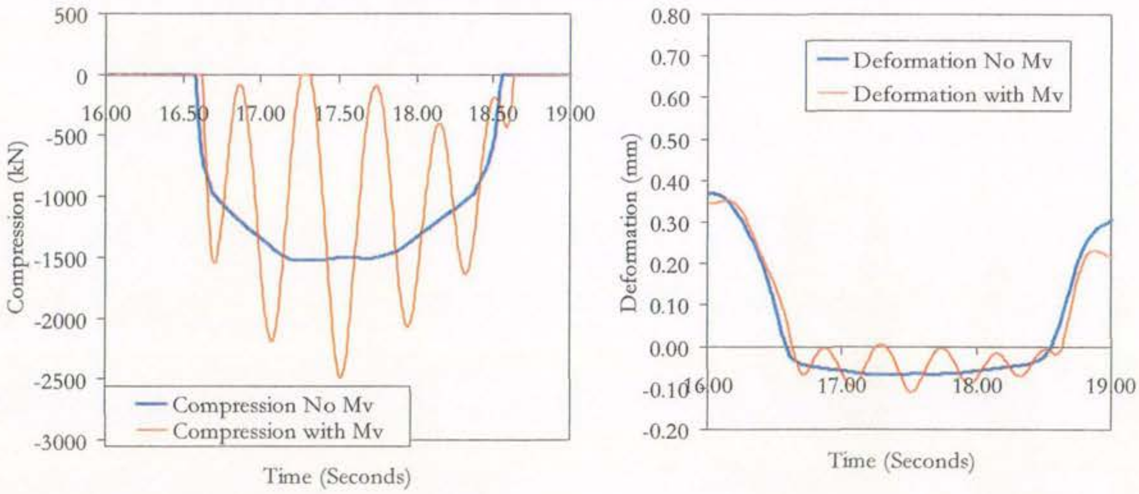

Figure 6-28 plots the gap forces and deformation from 26.5 to 28.5 seconds for the same wall as for Figure 6-27 except with the very stiff rock springs, rather than clay foundation springs. Similar behaviour is noted except that the "bouncing" is much more pronounced, with a period of only about 0.10 seconds and the amplitude varying by up to -100% and +300% of the values when vertical mass is excluded from the analysis. The negative variation is limited to -100% as at this point the gap re-opens and the force reverts to zero.

Figure 6-28 Wall 1-3-G Story Reaction Forces

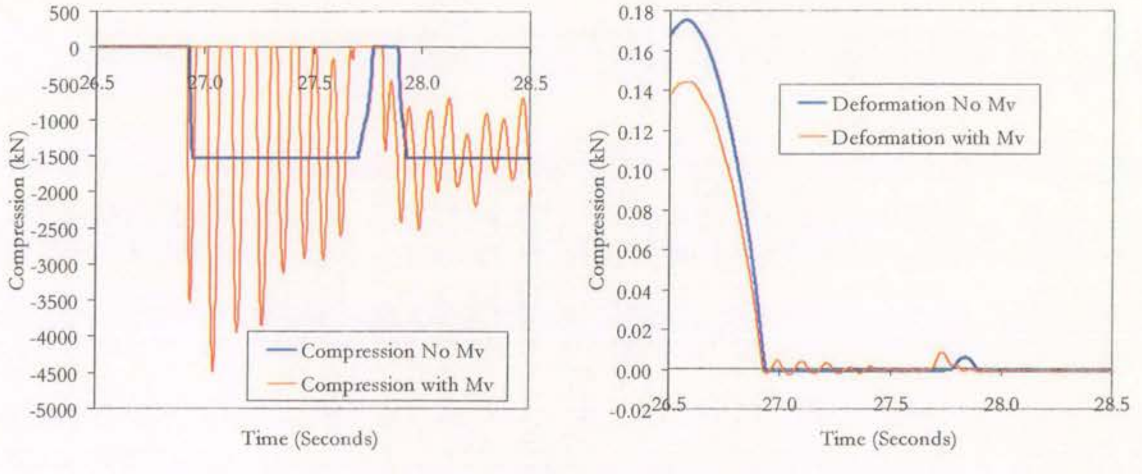

Figure 6-29 shows the effect the vertical mass has on recorded maximum wall reactions. This figure should be compared to Figure 6-25, which is the same wall but for the analysis without vertical mass included. Once vertical mass in included the reaction forces are no longer limited to the wall weight and can increase from 2 to 3 times this value, depending on the earthquake amplitude and soil spring stiffness.

Figure 6-29 Wall 1 (L = 7.200 m) 3 Story Reaction Forces with Vertical Mass
Near Fault Soil B **Near Fault Soil D**

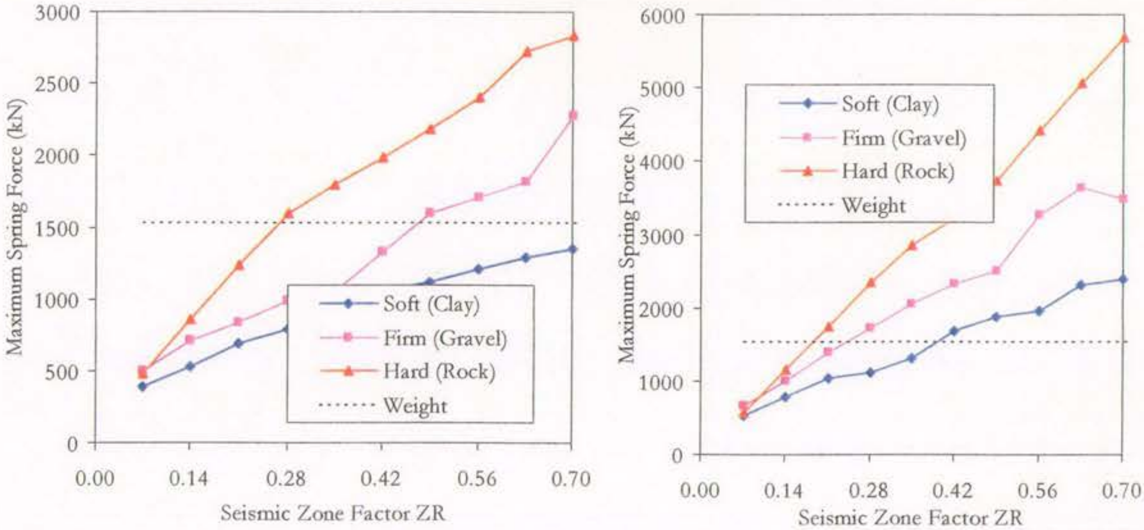

The actual behaviour of the soil is more complex than shown in Figures 6-25 to 6-29 because soil structure interaction is a complex process and includes other important effects, which as soil nonlinearity (the strain dependence of properties and local soil yielding) and radiation damping. These effects would tend to inhibit the type of resonance shown in Figures 6-26 to 6-29 and so the maximum amplification of reaction forces is likely to be much less than is obtained by including full vertical mass. This is discussed further later in this report when design procedures are developed.

6.6 Effect of Selection of Records Comprising Earthquake Suite

As discussed in Section 3, a different set of records was used to scale records for locations near to active faults than those used for sites distant from faults. In each case, the seven records selected were frequency scaled to match the target spectrum.

The target spectra for near and far fault locations differ only by the effect of the near fault factor N(T,D) which is unity for all periods up to 1.50 seconds and then increases to a maximum of 1.72 for periods of 5.0 seconds or longer. Therefore, the target spectra for both near fault and far fault locations are identical for periods up to 1.50 seconds after which they diverge.

This feature enables the results from the stiffer walls (which have a maximum period of response less than 1.50 seconds) to be used to assess the effect of the particular characteristics of the seven records selected for frequency scaling. If the effect is negligible then the average displacements from both the near fault and the far fault sets of records would be similar. To check this, three wall prototypes for which the maximum period of response did not exceed 1.50 seconds were selected and the maximum displacements are compared in Figures 6-30 to 6-32:

1. Figure 6-30 is the 1 story wall 3.600 m long, which was elastic for the ZR = 0.07 but yielded above this level for all three soil sites. The maximum period, under ZR = 0.70 Soil D, was 1.274 seconds.

2. Figure 6-31 is the 2 story wall 7.200 m long, which was elastic for the ZR = 0.07 but yielded above this level for all three soil sites, similar to the 3.00 m wall. For this wall the maximum period, under ZR = 0.70 Soil D, was 1.110 seconds.

3. Figure 6-32 is the 3 story wall 14.400 m long remained elastic to the ZR = 0.21 for Soil B but yielded above ZR = 0.07 for Sites C and D. For this wall the maximum period, under ZR = 0.70 Soil D, was 1.015 seconds.

All three walls shows a similar characteristic, in that displacements are almost identical for low amplitude input but the discrepancy increases as the seismic amplitude increases. There is no consistent pattern of the near fault records producing higher response than the far fault records, or vice versa, which suggests that the differences relate more to the natural scattering between records rather than the specific characteristics of the starting records.

The results in Figures 6-30 to 6-32 agree with the findings in Section 3, where it was found that nonlinear spectra generated from a set of 7 frequency scaled records showed much more dispersion than the equivalent case elastic spectra. In the figures below, the response at ZR = 0.07 represents elastic response as none of the walls uplifts at this amplitude. In all cases, the peak displacements under both the near fault and far fault records sets are almost equal.

As the amplitude increases the displacements are quite similar even at ZR = 0.28, a level of load at which all walls are uplifting for all soil types. Beyond that point the discrepancy tends to be more marked. It appears that the increased dispersion between elastic and inelastic response is a function of the degree of nonlinearity.

The differences exhibited by the response in Figures 6-30 to 6-32 set a limit to the accuracy of any method which may be developed to predict displacements for rocking walls. The time history method of analysis for nonlinear systems does not produce an "exact" response but rather as estimate of response. Therefore, any procedure to predict the displacements should aim to meet the characteristics of the nonlinear response but not necessarily exactly match the numerical values. Any method would be expected to exhibit at least as much dispersion from the analysis values as the near fault and far fault results in Figures 6-30 to 6-32 show.

The figures also show that more reliability could be placed on results for low to moderate ductilities than high ductility response in that the dispersion increases with increasing ductility. This suggests that any simplified procedures developed will be suited for low ductility structures and that where ductility is high a special study may be warranted if a reasonable degree of confidence in results is required.

Figure 6-30 Effect of Record Selection: 3.6 m Wall 1 Story High Spring Set E

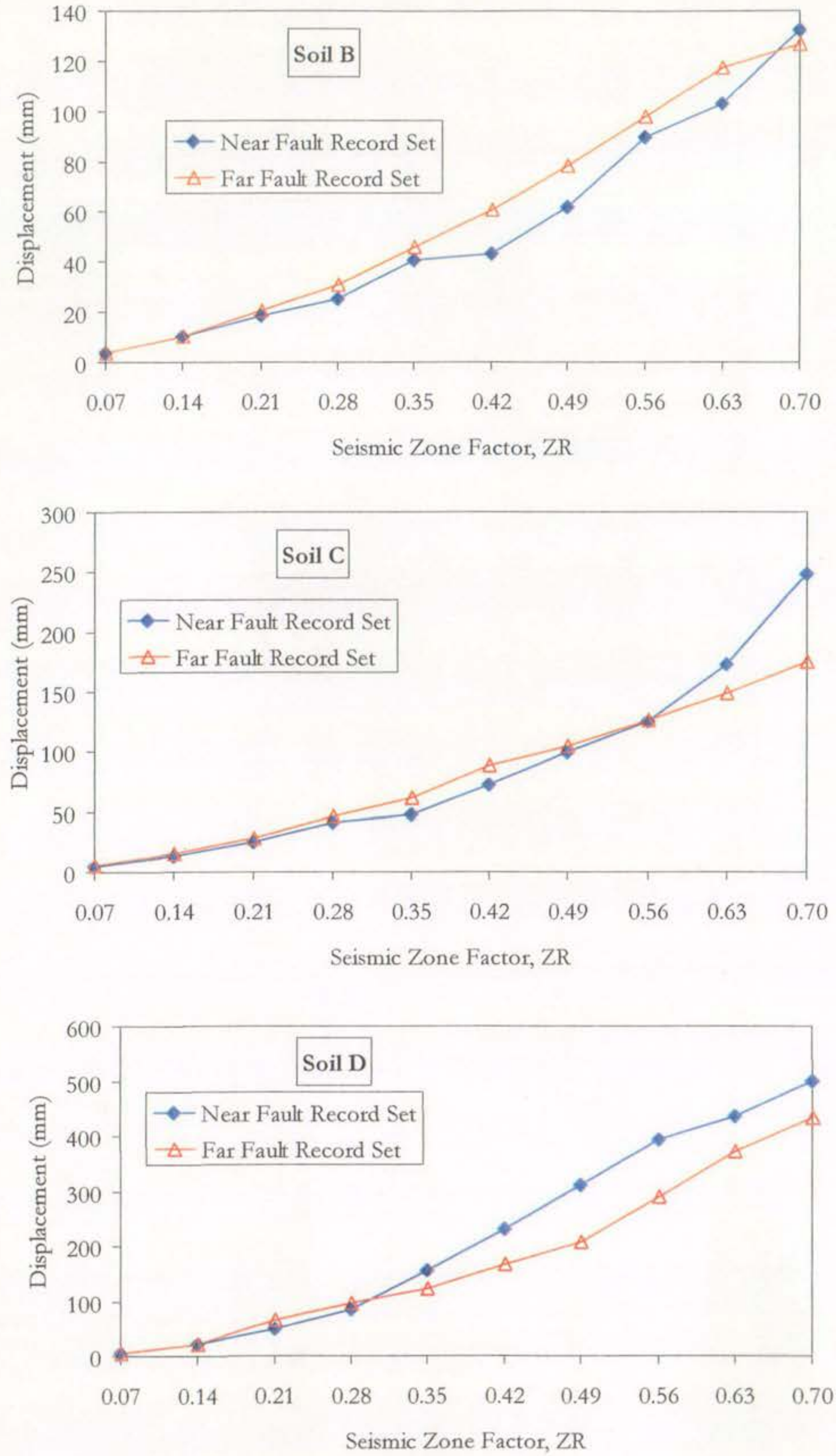

Figure 6-31 Effect of Record Selection: 7.2 m Wall 2 Stories High Spring Set E

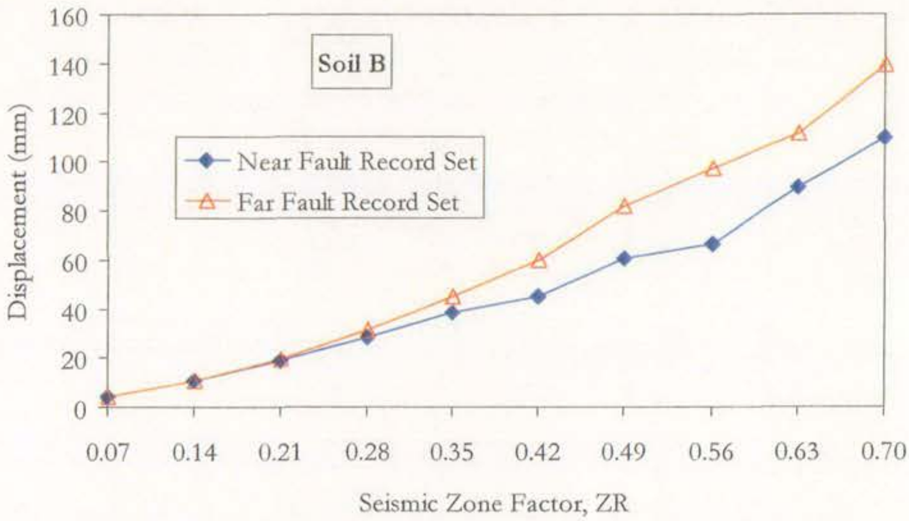

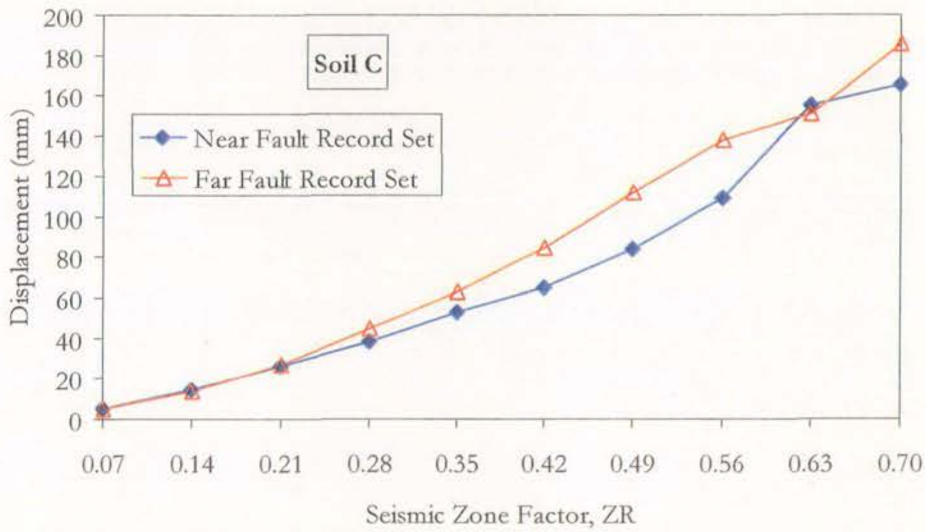

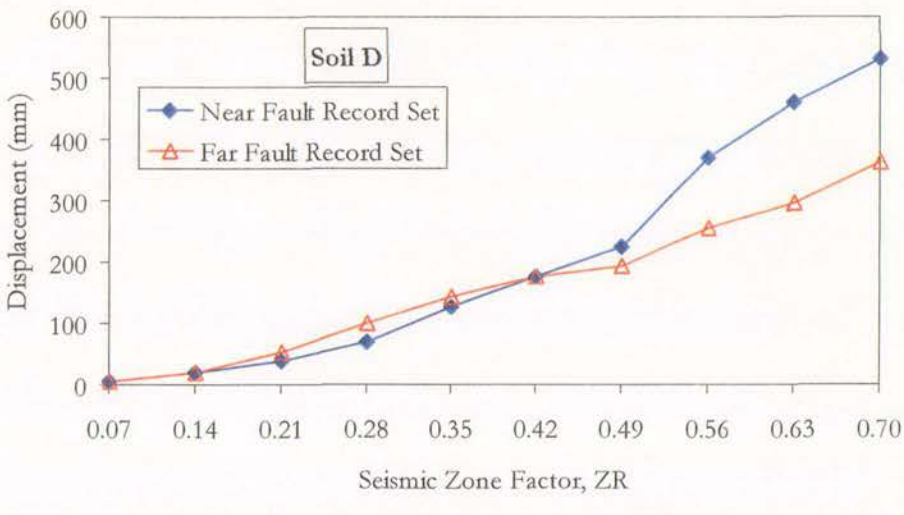

Figure 6-32 Effect of Record Selection: 14.4 m Wall 3 Stories High Spring Set B

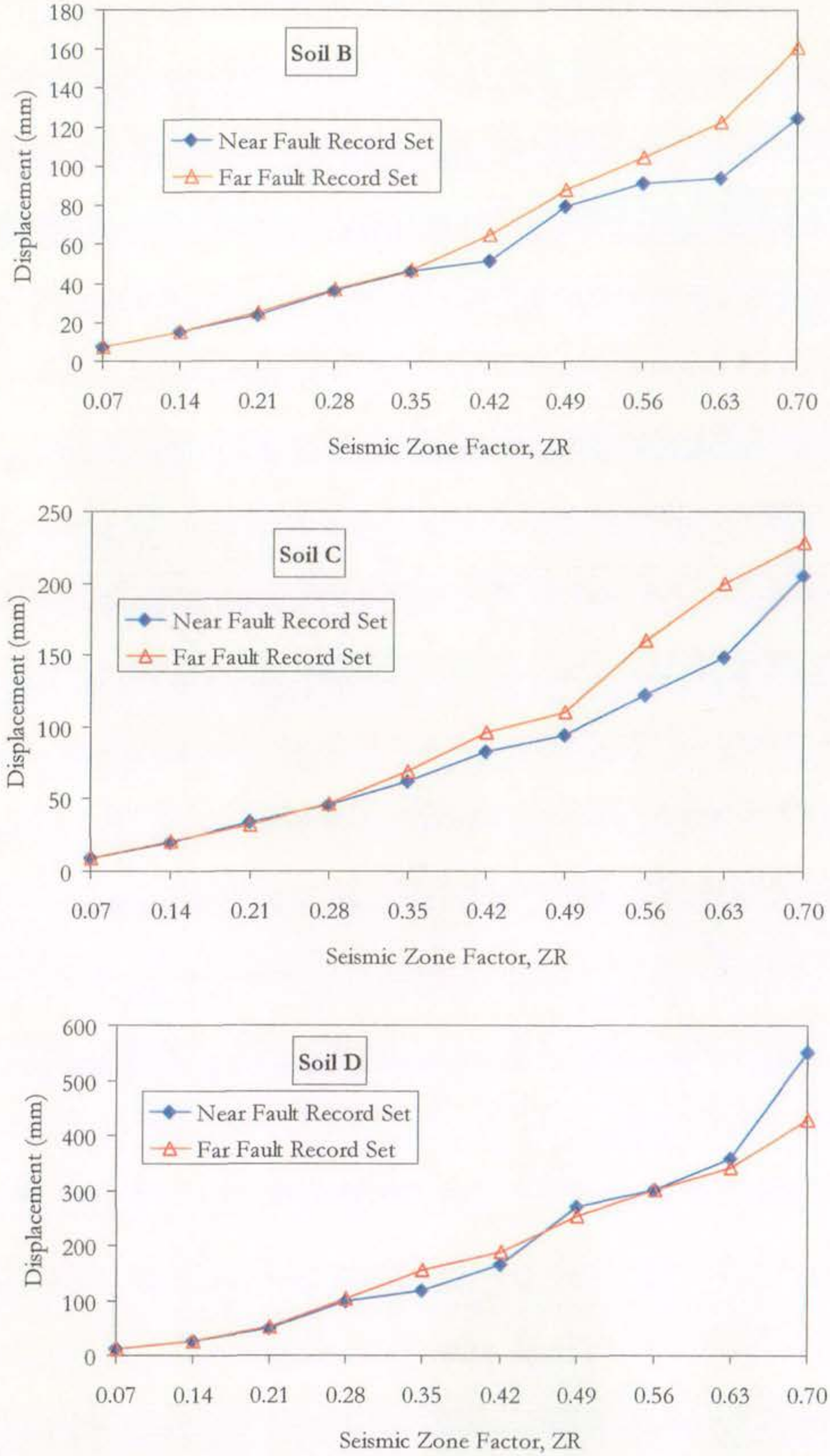

7 DESIGN ACTIONS ON SINGLE WALLS

7.1 Predicting Displacements

As described in the preceding sections, 40 wall configurations were each evaluated for 10 earthquake amplitudes for each of three soil site classes and two near fault conditions, providing a total of 2400 data points with which to assess procedures to predict displacement.

As discussed in Chapter 2, FEMA 356 provides three methods which can be used to predict displacements in nonlinear systems. One is based on a rocking wall formulation and the other two are the methods of implementing FEMA NSP procedure, the initial effective stiffness and the secant stiffness methods respectively. For new buildings, equal displacements and equal energy theories are used. Of these,

1. The rocking wall formulation is based on an assumption of a rigid block rocking on a rigid foundation. It is apparent from the results of the analyses that wall displacements are a function of foundation stiffness, and so a rigid foundation assumption will not be sufficient to develop a procedure to predict the displacements. Even if the procedure could be modified to incorporate soil springs, the calculations are based on the mass moment of inertia about the point of rocking. This inertia can be calculated relatively simply for a uniform block where the mass is in the block itself but it is much more complex to calculate for a building structure where the mass is distributed over the floor diaphragms. Therefore, there was no attempt to correlate this formulation with the analysis results.

2. The effective stiffness method is a general purpose procedure for nonlinear systems and so is not restricted to rigid foundation conditions. Also, it uses the translational mass of the building rather than mass moment of inertia and so does not have the disadvantages of the rocking method. As implemented in the FEMA NSP, the effective stiffness method uses a factor, C_1, to relate maximum expected inelastic displacements to displacements calculated for linear elastic response. This factor has a value of 1.0 for periods $Te > T_s$ where $T_s = 0.30$ for soils classes B and C and 0.56 seconds for soil class D. It was apparent from the time history results that the inelastic displacements of a rocking system were much higher than the elastic displacements regardless of period. However, the method appeared promising if a procedure to relate inelastic to elastic displacements could be developed for rocking systems.

3. The alternative FEMA NSP procedure, the secant stiffness method, can also incorporate flexible foundations and translational mass. It differs from the effective stiffness procedure in that the secant stiffness method uses hysteretic damping to account for the reduction in amplitude due to inelastic action. The reduction is based on the area of the hysteresis curve of the nonlinear system. However, as discussed earlier, the response of a rocking system is nonlinear but not hysteretic because the unloading curve follows the loading curve. Therefore, hysteretic damping would not be expected to be appropriate for this type of system.

4. The equal stiffness method is based on generally similar principles to the equal displacement and equal energy theories implicit in the NZS 1170 inelastic spectrum scaling factor, in that it assumes equal displacements for some period ranges and a variation of equal energy for short periods.

A number of formulations of the effective stiffness and secant stiffness methods were assessed but all were deficient, in that empirical adjustment factors were required to match the time history response and even then they did not match at all amplitudes. It became apparent that the secant stiffness method was fatally flawed because of the lack of a hysteresis loop area in rocking structures and so this method was abandoned and the development focussed on the effective stiffness method.

Eventually, a variation of the secant stiffness method was developed where the response was based on an effective period but hysteretic damping was ignored. This method, described below, provides an excellent correlation with the analysis results.

7.1.1 Single Story Walls

The procedure used to estimate displacements is based on the configuration of the wall and the seismic input. The stages of the procedure are to define the resistance characteristics of the wall, including the elastic period, and then solve for the demand, where demand is defined as maximum imposed displacement for the given seismic loads.

The development of the procedure is illustrated using the response of Wall 2-1-B, which is the single story wall 3.600 m long supported on medium clay.

7.1.1.1 Wall Period and Resistance Function

The effect of the rocking and uplift at the wall foundation is to modify the period of response and central to the procedure is the initial elastic stiffness of the wall on its foundation. The period can be extracted from a computer model which includes the soil springs, as described earlier in this report, or can be calculated approximately using spreadsheet calculations (see Section 10.3).

The resistance of the wall can be calculated from statics, using the free body approximation for a rocking wall shown in Figure 7-1. The yield force of the wall is calculated from the dimensions of the wall, H x L, and the gravity load reaction on the wall, W, as $F_Y = WL/2H$. The force can then be normalised to a yield coefficient by dividing by the seismic weight (mass times the gravitational constant), $C_Y = F_Y/Mg$ where M is the total seismic mass tributary to the wall and $g = 9.81$ m/sec^2. Because buildings usually have orthogonal walls, and sometimes also gravity columns, to support part of the gravity load the seismic weight, Mg, is generally higher than the gravity load on the wall, W, by a factor of at least 2.

Wall 2-1-B has a computed elastic period of 0.557 seconds. The prototype building is assumed to have a total weight of 1037 kN. There are 2 x 3.600 m long walls in each direction and the weight is equally distributed to each wall. Therefore, on each wall the gravity load is W = 1037 / 4 = 259 kN and the seismic weight, Mg = 1037 /2 = 518 kN.

The effective wall length is 3.433 m (distance between outermost springs) and the height is 3.600 m. The yield force is:

$$F_y = \frac{WL}{2H} = \frac{259x3.433}{2x3.600} = 123.5kN \tag{7-1}$$

From which the yield coefficient is calculated as:

$$C_y = \frac{F_y}{Mg} = \frac{123.5}{518} = 0.238 \tag{7-2}$$

Figure 7-1 Calculation of Yield Coefficient

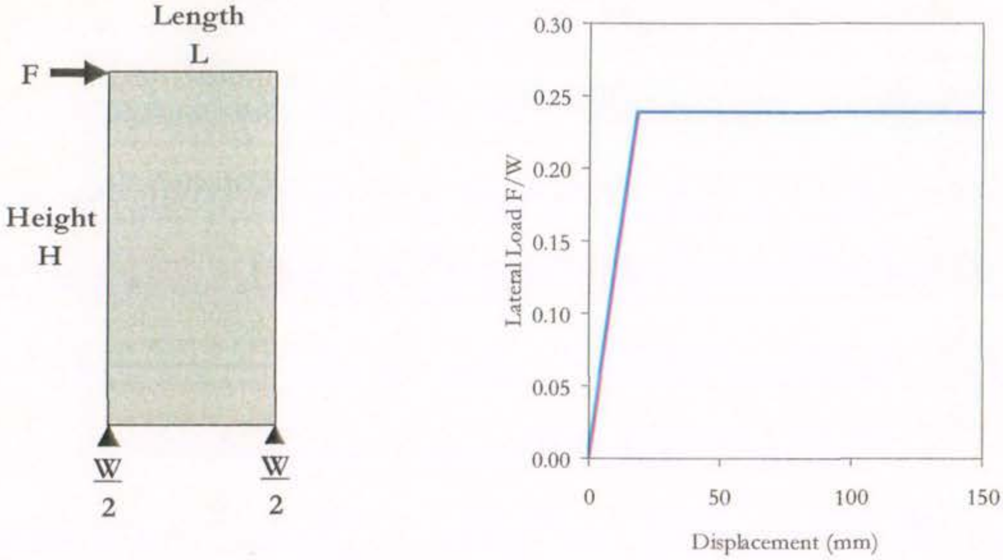

The yield displacement can be calculated from the mass, M, stiffness, K, and period, T, using the established dynamic relationship:

$$T = 2\pi\sqrt{\frac{M}{K}} \tag{7-3}$$

This can be re-arranged to define the stiffness, K, as:

$$K = \frac{4\pi^2 M}{T^2} \tag{7-4}$$

The yield displacement, Δ_y, is a function of the yield force and stiffness

$$\Delta_y = \frac{F_y}{K} \tag{7-5}$$

Substituting K from Equation (7-4) and $C_y = F_y/Mg$ from Equation (7-2) gives:

$$\Delta_y = \frac{F_y T^2}{4\pi^2 M} = \frac{C_y g T^2}{4\pi^2} = \frac{0.237x9810x0.557^2}{4\pi^2} = 18.27\,mm \tag{7-6}$$

The yield coefficient and yield displacement, calculated as listed above, define the bilinear approximation to the resistance function for the wall, as shown in Figure 7-1.

The extent to which this bilinear approximation is in fact an approximation is illustrated in Figure 7-2, which compares the bilinear curve with the capacity curve developed by applying a top displacement to the nonlinear analysis model. The yield moment capacity calculated as above tends to overestimate the actual capacity because it does not incorporate progressive softening as the wall starts to separate at one end and subsequent gaps lose contact as the displacement increases. At the stage all gaps have opened, the ultimate strength reached is less than that predicted by equation (7-1) because the deflections have reduced the effective lever arm.

Given that there are approximations involved in all seismic evaluations, this slight over-estimate of strength is acceptable. This over-estimate is greatest for relatively soft springs, as plotted in Figure 7-2, and will reduce for gravel or rock foundations.

Figure 7-2 Capacity Curve; Single Story 3.600 m Wall, Medium Clay

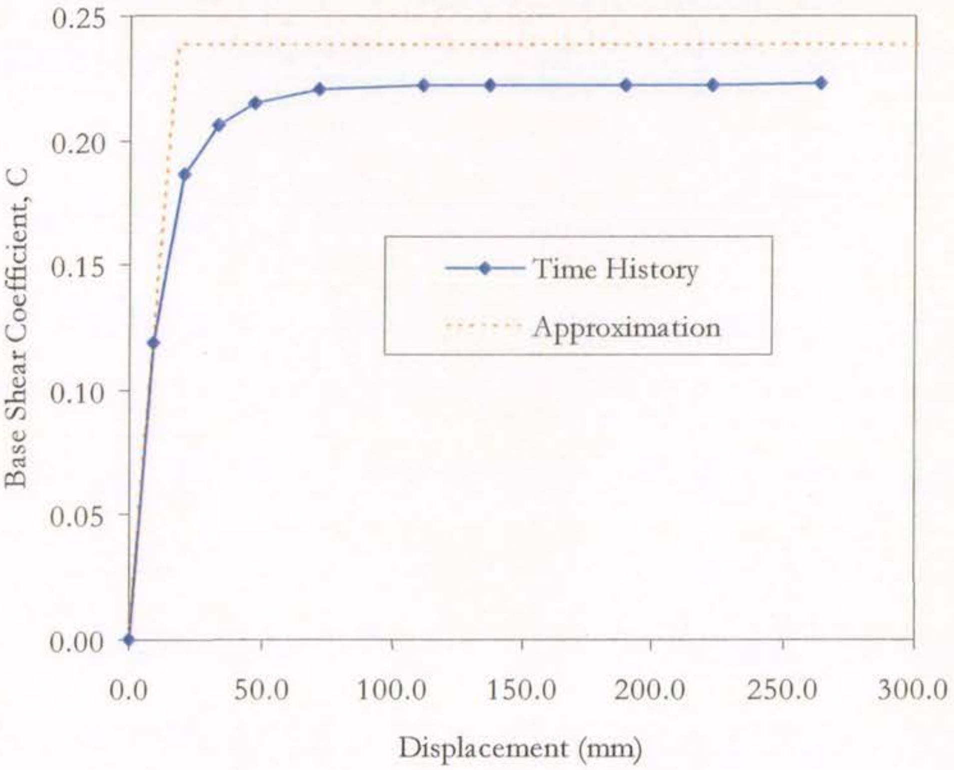

7.1.1.2 Solve for Displacement Demand

It was apparent that the factor relating elastic to inelastic displacement would be a function of the ductility in the system as the inelastic response tended to diverge from elastic response as the amplitude of motion increased. Development of a procedure therefore focussed on the response modification factor, R, which is the ratio of elastic force to inelastic force and so forms a measure of ductility demand.

From trial and error, and evaluation of different potential schemes, the best match to the nonlinear results found to be to solve for an effective period, T_e, such that

$$T_e = T_i R_E \tag{7-7}$$

Where R_E is the response reduction factor defined as:

$$R_E = \frac{C_m C(T_e)}{C_y} \tag{7-8}$$

Equation (7-7) is recursive as R_E is a function of the effective period T_e which is the unknown variable. This requires an iterative type of solution, using tools such as Goal Seek in Excel©. This is discussed below. In Equation (7-8) C_m is the effective mass in the fundamental mode, equal to 1.0 for single story walls.

Once T_e has been calculated, the displacement can be calculated from the spectral acceleration using the relationship between spectral acceleration and displacement:

$$\Delta = C(T_e) g \frac{T_e^2}{4\pi^2} \tag{7-9}$$

This is illustrated in Figure 7-3 for Wall 2-1-B.

Figure 7-3 Elastic and Effective Periods

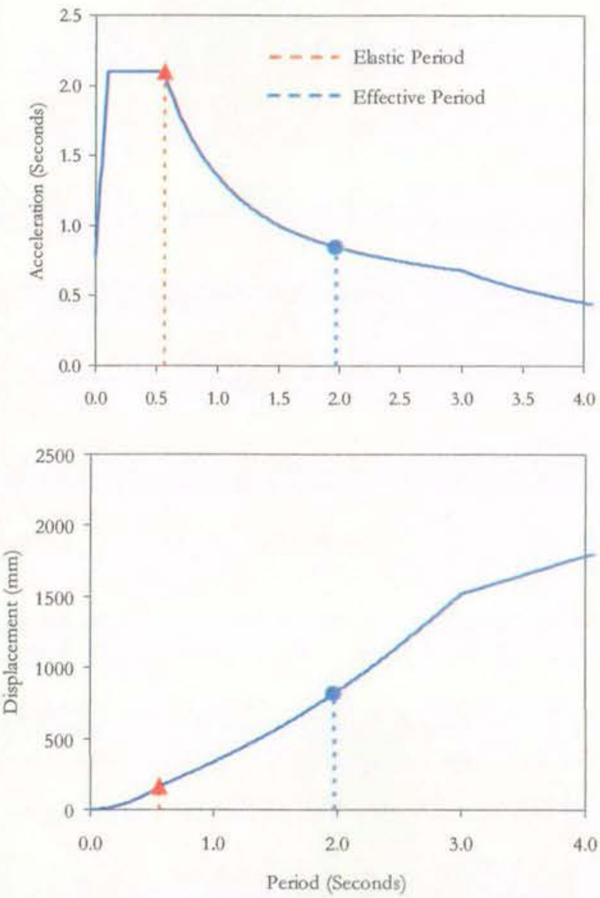

1. The initial period is 0.557 seconds and the yield coefficient $C_Y = 0.238$.

2. By iteration, the effective period is calculated to be 1.974 seconds. At this value of effective period, T_e, the design coefficient $C = 0.845$ (for Soil Class D, within

2 km of a fault). From this, the ductility factor is calculated as $R_E = 0.845 / 0.238 = 3.55$. (This correlates to the calculation of $T_e = 0.557 \times 3.55 = 1.97$ seconds).

3. At T_e, the displacement is calculated from the elastic coefficient as $0.845 \times 9810 \times 1.974^2/4\pi^2 = 818$ mm.

For this wall, the 7 time histories for the near fault Soil Class D motions produced maximum displacements ranging from 622 mm to 1276 mm, with a mean of 918 mm. The mean result is about 14% higher than the predicted value of 818 mm. The results, plotted in Figure 7-4, illustrate the wide variation in results between the different earthquakes, all scaled to the same spectrum. Given this variability, the 14% difference between the predicted and average value is within acceptable error limits.

Figure 7-4 Predicted versus Analysis Displacements

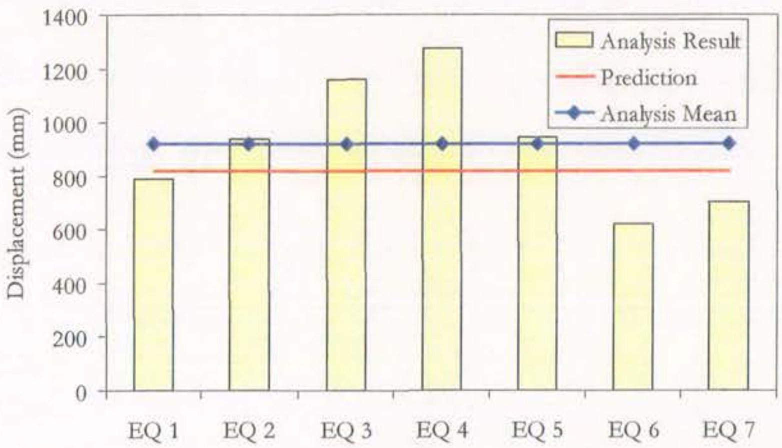

As discussed earlier, the equation for the effective period, T_e, is recursive and must be solved by iteration or other means. Table 7-1 summarizes a step-by-step procedure to solve for the displacement using spreadsheet tools:

1. Define initial data. Table 7-1 is set to solve for displacement for factors from 0.10 to 1.0 applied to the earthquake loads. Also required is the initial period, T_i, and the yield coefficient, C_y. (Table 7-1 is set for single or multi-story walls and so there is provision for coefficients C_0 and C_m. These are discussed later, but are set to 1.0 for a single story wall).

2. Initialise a factor on S_a to 1.0. This is the factor such that $C(T_i) \times \text{Factor} = C(T_e)$.

3. The first estimate of S_a is the factor times $C(T_i)$, where $C(T_i)$ is a function of the initial period and seismic load.

4. The R_E (ductility) factor is calculated as $R_E = C_m S_a/C_Y$.

5. An effective period is calculated as $T_e = T_i\, R_E$

6. A second estimate of S_a is $S_a{}^* = C(T_e)$, which is calculated from the design spectrum for the seismic load.

7. The ratio of S_a*/S_a is calculated. If not equal to 1.0, adjust the factor and return to Step 2.

8. Once convergence is obtained, calculate the roof displacement as $\Delta_{roof} = C_0 S_a T_e^2 g/4\pi^2$.

The example listed in Table 7-1 uses a macro to solve for all earthquake scale factors. If only a single value is to be solved, it is possible to adjust the factor on S_a manually until convergence is obtained. This is relatively quick as the factor is always positive and less than or equal to 1.0.

Table 7-1 Calculation of Effective Period

Input Data Provided by User				Iterative Loop to Solve for S_a						Output
Scale Factor On EQ	Initial Period T_i	Factor C_0	Factor C_m	Factor on S_a	S_a	R	Te	S_a*	Ratio	Δ-roof
0.100	0.557	1.000	1.00	1.00	0.210	0.881	0.557	0.210	1.00	16.2
0.200	0.557	1.000	1.00	0.78	0.329	1.382	0.770	0.329	1.00	48.5
0.300	0.557	1.000	1.00	0.66	0.416	1.743	0.971	0.415	1.00	97.3
0.400	0.557	1.000	1.00	0.58	0.490	2.054	1.144	0.490	1.00	159.3
0.500	0.557	1.000	1.00	0.53	0.556	2.333	1.300	0.556	1.00	233.4
0.600	0.557	1.000	1.00	0.49	0.617	2.589	1.442	0.617	1.00	319.0
0.700	0.557	1.000	1.00	0.46	0.676	2.837	1.580	0.676	1.00	419.6
0.800	0.557	1.000	1.00	0.44	0.734	3.081	1.716	0.735	1.00	537.5
0.900	0.557	1.000	1.00	0.42	0.791	3.316	1.847	0.791	1.00	670.4
1.000	0.557	1.000	1.00	0.40	0.845	3.545	1.974	0.845	1.00	818.6

The predicted displacements solved in Table 7-1 for scale factors from 0.10 to 1.00 are compared with the mean value from the analysis for this specific wall in Figure 7-5. (Note that the maximum factor of 1.0 produces the predicted value of 818 mm versus the mean analysis value of 919 mm discussed above). Predicted displacements for this case were between 1% and 22% lower than the mean analysis values.

Figure 7-5 Predicted Displacements Wall 2-1-B, Soil D

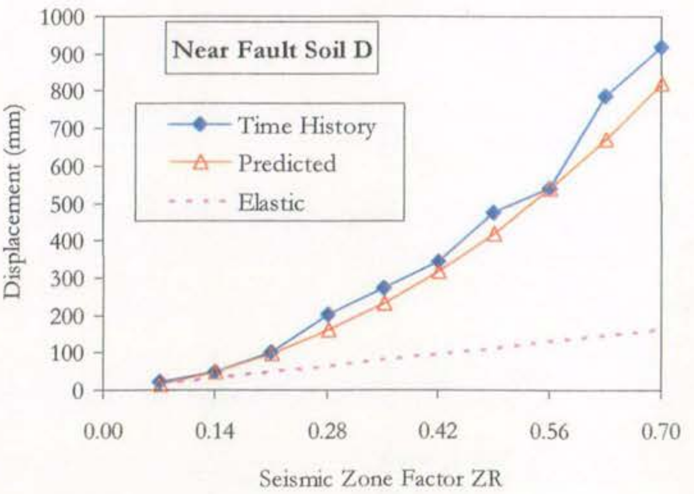

In Figure 7-6, the procedure has been repeated for each of the six variations of soil class and near fault conditions, a total of 60 data points. The difference between predicted and analysis displacements ranges from -31% to +20% with a mean difference of -9%.

Figure 7-6 Predicted Displacements; Wall 2-1-B

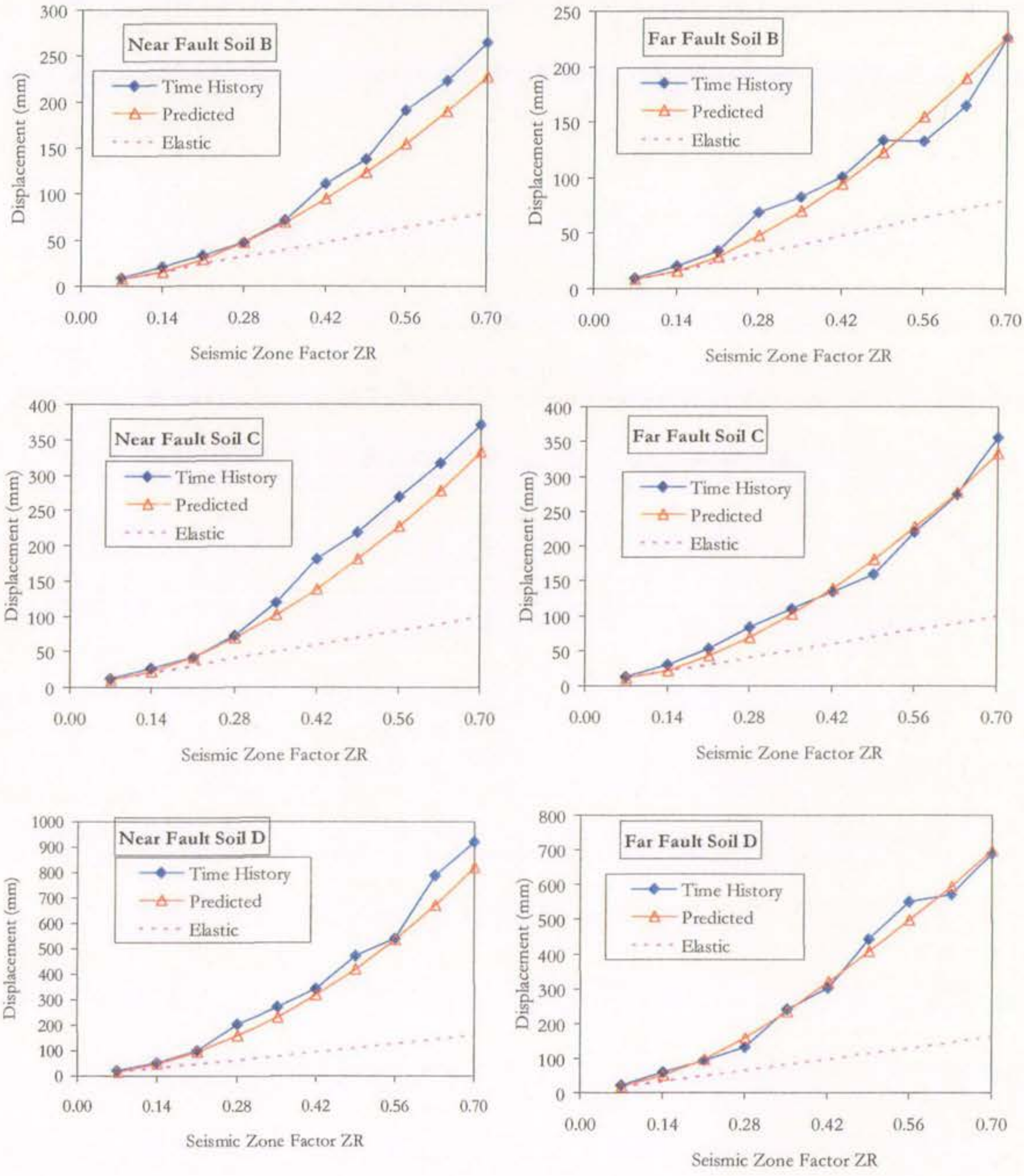

7.1.2 Multi-Story Walls

The procedure described above to predict maximum displacements is based on a single degree of freedom (SDOF) approximation to the wall. Multi-story walls have multiple degrees of freedom (MDOF) but can be approximated as a single degree of freedom system by adjusting the calculations using two factors defined by FEMA 356 for the nonlinear static procedure on which this procedure is based:

1. C_m, which is the effective mass excited by the fundamental mode in the direction being considered. This is obtained from the model analysis or alternatively tabulated values from FEMA 356 can be used (typically 1.0 for 1 or 2 story buildings, 0.8 or 0.9 for taller buildings).

2. C_0, a modification factor to relate the spectral displacement of an equivalent SDOF system to the roof of the MDOF system. This can be extracted from the modal analysis as the product of the participation factor times the mode shape component at roof level or, alternatively, tabulated values may be used. Values are 1.0 for single story buildings increasing with height in a range of between 1.2 and 1.5 for higher buildings.

The modifications to the procedure to include these two factors are:

a. The yield force is modified to incorporate the centroid of application of the lateral load being at less than full height, by dividing by C_0. Note that if C_0 is the maximum value of 1.5 then it is assumed than the lateral load is applied at 2/3 height, equivalent to a triangular distribution of load.

$$F_y = \frac{WL}{2\frac{H}{C_0}} \tag{7-10}$$

b. The strength ratio R_E (Step 4 in the procedure) is factored by the effective mass factor C_m to reflect less than 100% participation in the fundamental mode for multi-story buildings.

c. The roof displacement (Step 8 in the procedure) includes the C_0 factor to extrapolate the displacement at the centroid to the top of the building.

Figures 7-7 and 7-8 compare predicted displacements with mean displacements from the analysis for two different wall configurations. These demonstrate the range of displacements for flexible walls and stiff walls:

1. Figure 7-7 is a 3 story high 3.600 m long wall on medium clay springs. This wall has an aspect ratio of 3:1 and relatively soft springs and so has large displacements, up to 2265 mm for near fault motions when ZR is the maximum value of 0.70. The predicted displacements varied from the nonlinear analysis values by a range of -32% to +8%. As shown in Figure 7-7, the procedure identified the increase in inelastic displacements compared to elastic displacements very well and tended to give a "smoother" function than that shown by the nonlinear analyses.

2. Figure 7-8 is the equivalent series of plots for a single story high 14.400 m long wall on medium gravel springs. This wall has an aspect ratio of only 0.5:1 and relatively stiff springs and so has much smaller displacements, only 7.5 mm when ZR is the maximum value of 0.70. This is over two orders of magnitude less than the values in Figure 7-7 and yet the procedure also predicts these displacements well. The predicted values varied from the nonlinear analysis values by -49% to +27% although the maximum variations occurred when

displacements were very small. As shown in Figure 7-8, the procedure identified the sudden increase in inelastic displacements for this wall when the seismic amplitude reached the level where uplift occurred.

When comparing results, it is important to note that the nonlinear analysis results are not an exact solution, they are average results from seven time histories and there are also associated numerical errors with impacting analyses such as this. Therefore, a procedure to predict displacements could not be expected to produce an exact correlation with the nonlinear analysis results even if it were an exact procedure.

Figure 7-7 Predicted Displacements; Wall 2-3-B

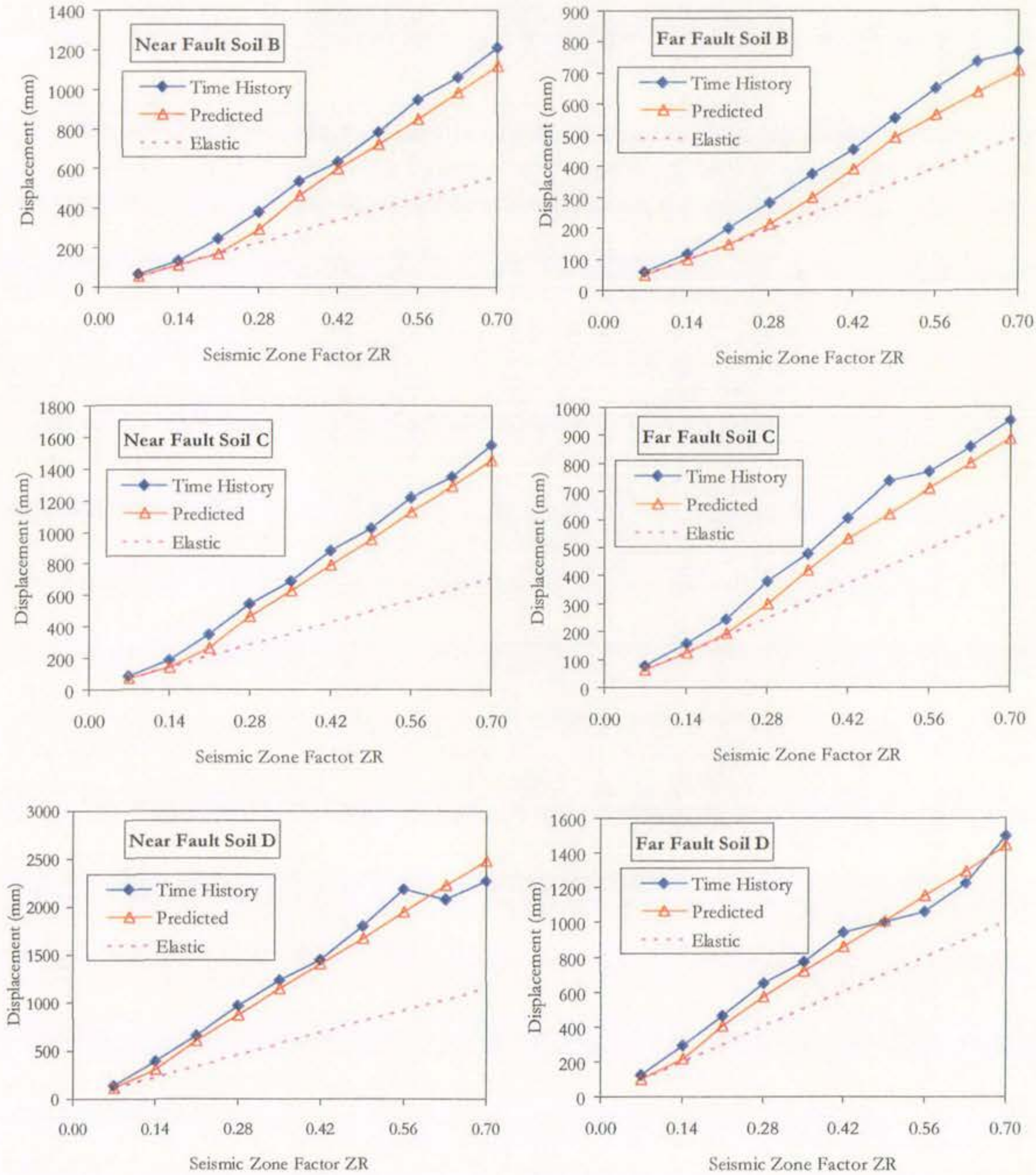

Figure 7-8 Predicted Displacements; Wall 3-1-E

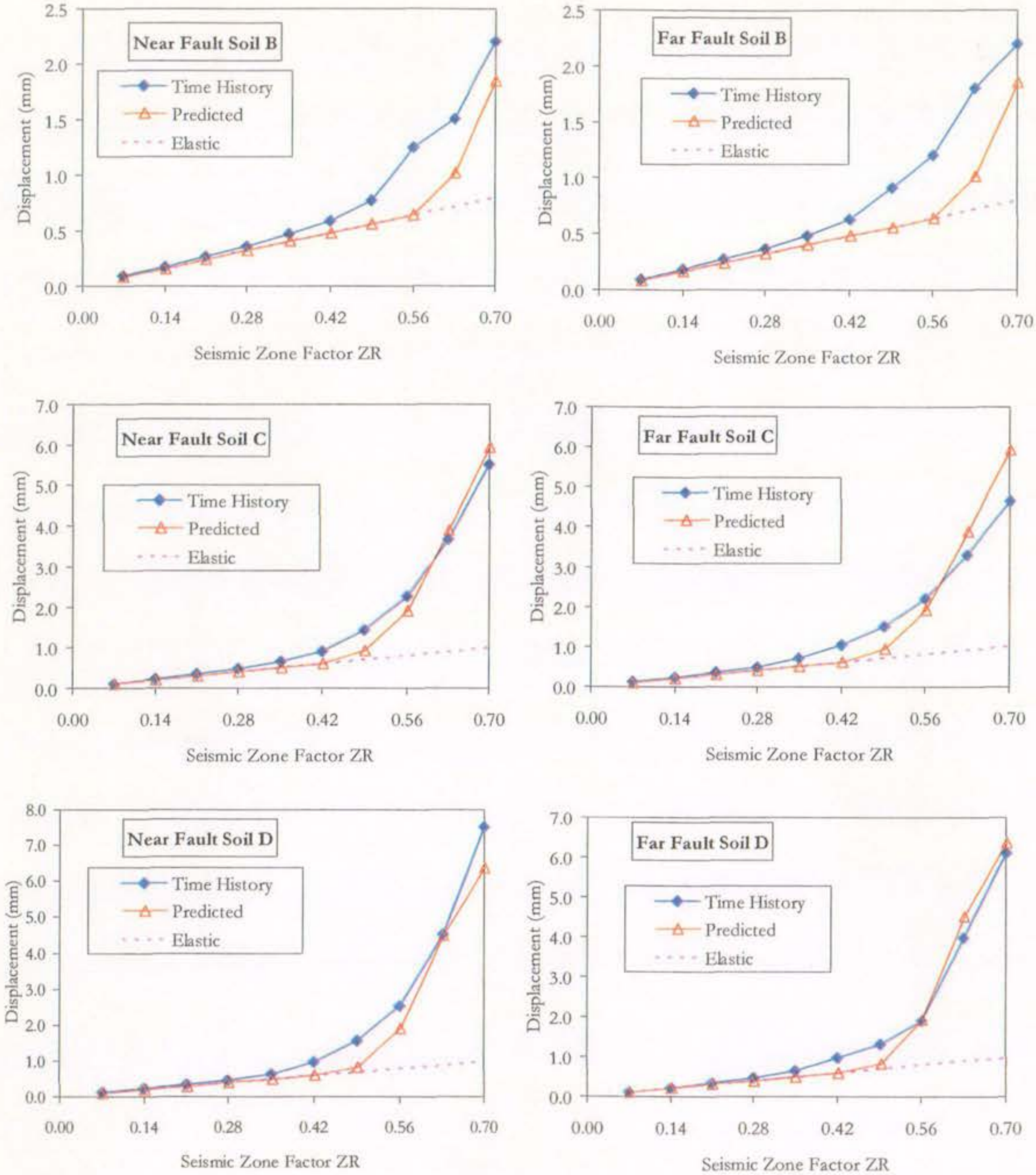

Appendix A contains a comparison of analysis displacements with predicted displacements using this procedure for all 40 wall configurations. These results have been used to derive the best fit relationship shown in Figure 7-9. The best-fit linear trend line has an equation of $y = 0.9812x$, which is remarkably close to the equation $y=1.00x$ which would indicate perfect correlation.

The results cover a very wide range of displacements, over three orders of magnitude, and so Figure 7-9 is changed to a log-log plot, in Figure 7-10, to show the correlation at smaller displacement amplitudes more clearly. This type of scale does tend to minimise the variation between predicted and measured values.

Figure 7-9 Predicted versus Analysis Displacements

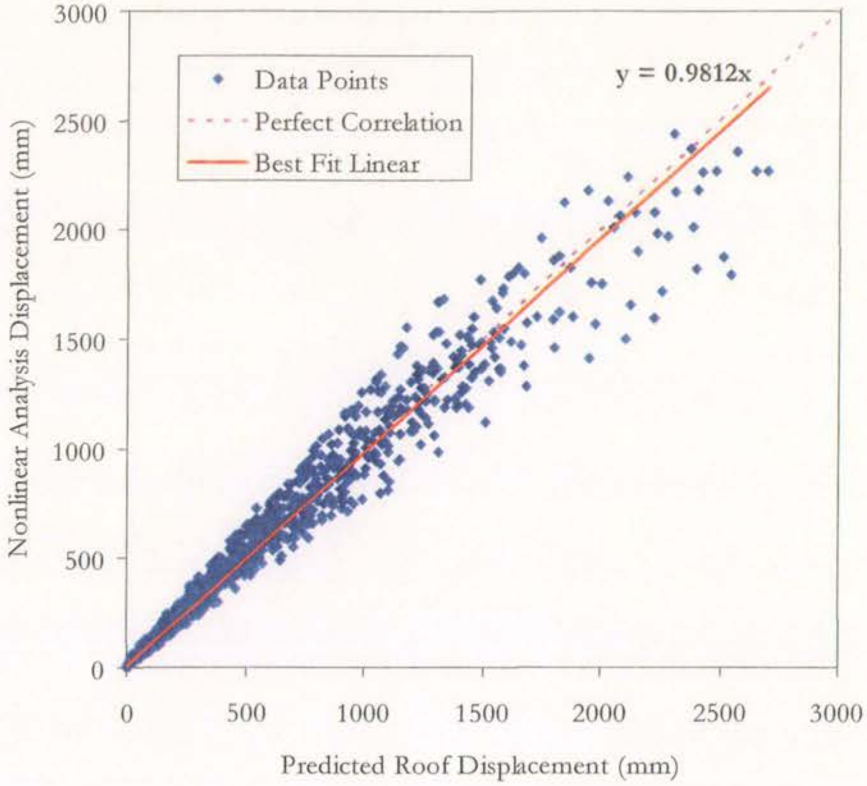

Figure 7-10 Predicted versus Analysis Displacements Log Plot

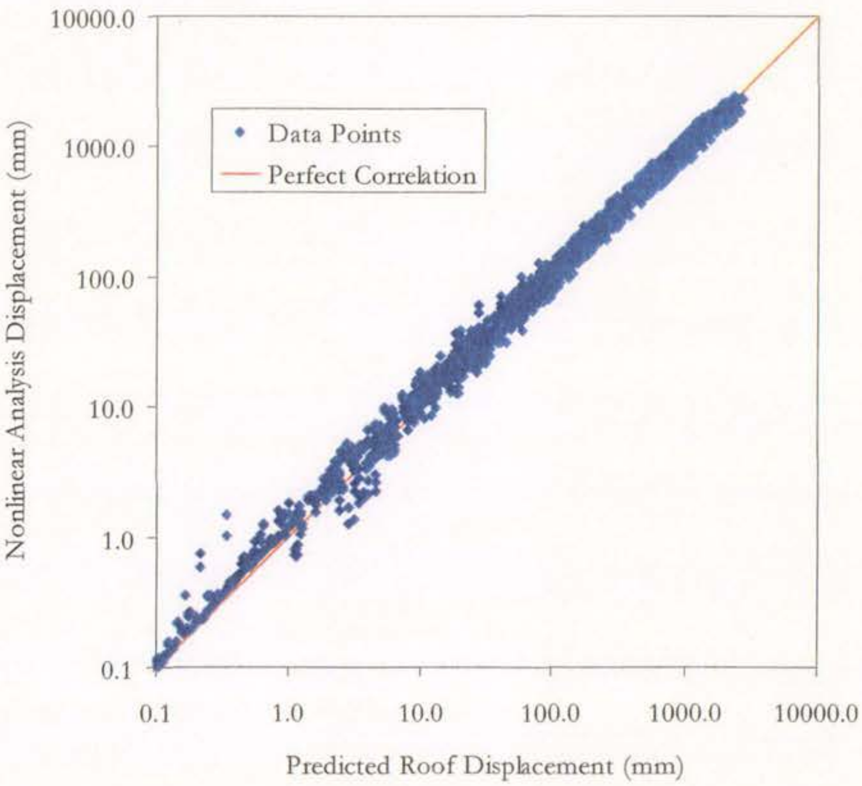

7.2 Effect of Seismic Weight and Wall Dead Load

The single wall models evaluated previously, and used to develop the design procedure, used a constant floor load of 10 KPa and an assumption that the total wall dead load corresponded to one-half the total seismic weight, on the assumption that orthogonal walls would support the other one-half of the seismic weight.

In order to check whether the design procedure was sensitive to these assumptions, the evaluation of Wall 1-3-B was repeated with two variations:

1. The seismic weight was reduced by a factor of 2.0, that is, a total floor seismic weight reduced from 10 KPa to 5 KPa. Distribution of weight to the walls was assumed the same, that is, the dead load was also reduced by a factor of 2.0.

2. The seismic weight was retained at 10 KPa but the dead load on the wall was reduced by a factor of 2.0, that is, assuming that part of the floor weight is supported by other elements such as columns.

The effect of these two variations on the capacity curve is illustrated in Figure 7-11. When the seismic weight is reduced by a factor of 2 the lateral coefficient is essentially the same, as it is reflects the ratio of dead load to seismic weight. However, the wall with reduced seismic weight is initially stiffer, and this is reflected in a shorter period. When the seismic weight is kept the same but the wall dead load reduced by a factor of 2.0 the wall lateral load also reduces by a factor of 2.0. The elastic period remains the same as it is a factor of spring stiffness and seismic weight, not dead load.

Figure 7-11 Effect of Seismic Weight and Wall Dead Load on Capacity Curve

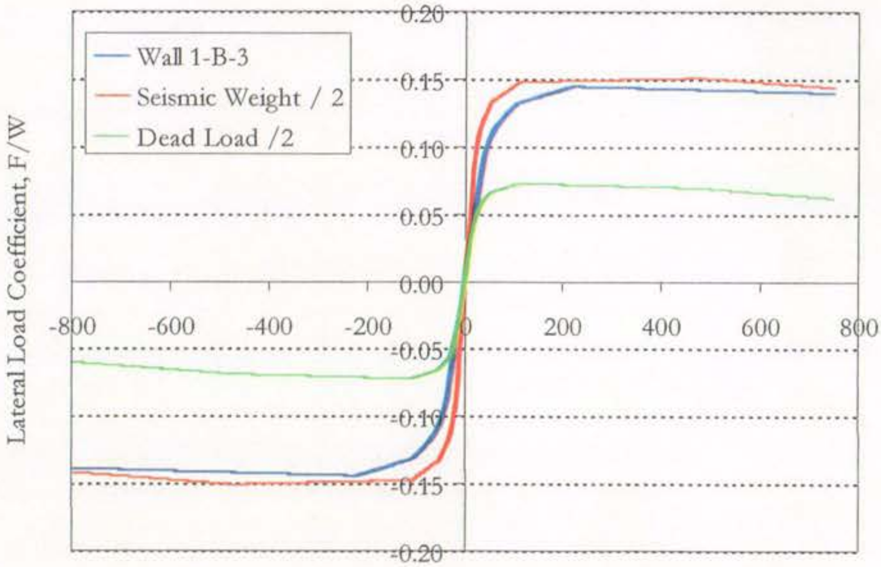

The effects of seismic weight and wall dead load, as derived from the comparisons in Figure 7-12, are:

1. When the seismic weight is reduced by a factor of 2.0 (0.5W in Figure 7-12), the displacements are reduced by approximately a constant ratio for all seismic amplitudes, with maximum displacements about 65% to 75% of the values with the full seismic weight.

2. When the seismic weight is the same but dead load on the wall reduced by a factor of 2.0 (0.5 DL in Figure 7-12) the displacements are much higher, with the ratio increasing with increasing earthquake amplitude. At ZR = 0.10 the displacements are equal as the wall does not rock but for high amplitudes the displacements with reduced dead load are almost twice as high as those for the original analysis.

3. The design procedure as described above is capable of accurately capturing these effects of seismic weight and dead load, as shown by the predicted displacements in Figure 7-12 (curves identified as 1-DOF).

Figure 7-12 Effect of Seismic Weight and Wall Dead Load on Displacements

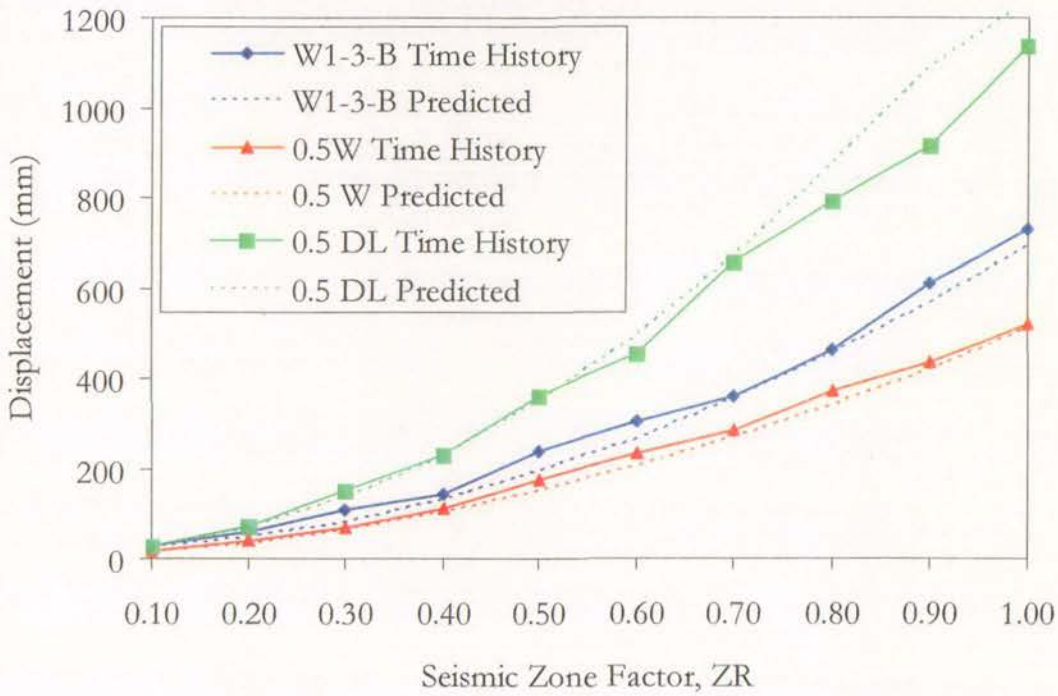

The reason for the increase in displacement with the decrease in dead load can be seen by the plots of effective period versus earthquake amplitude for the three configurations in Figure 7-13. For the reduced seismic weight the initial elastic period is reduced by $\sqrt{2}$ when the weight is halved and this ratio is approximately maintained in the difference in effective periods in Figure 7-13. When the seismic weight is kept the same but the dead load reduced the initial elastic period does not change. However, as the earthquake amplitude increases, and the extent of rocking also increases, the effective period increases much more rapidly for the configuration with the reduced dead load. As displacements are proportional to the square of the period, this period elongation causes the increases in displacements exhibited in Figure 7-12.

Figure 7-13 Effect of Seismic Weight and Wall Dead Load on Effective Period

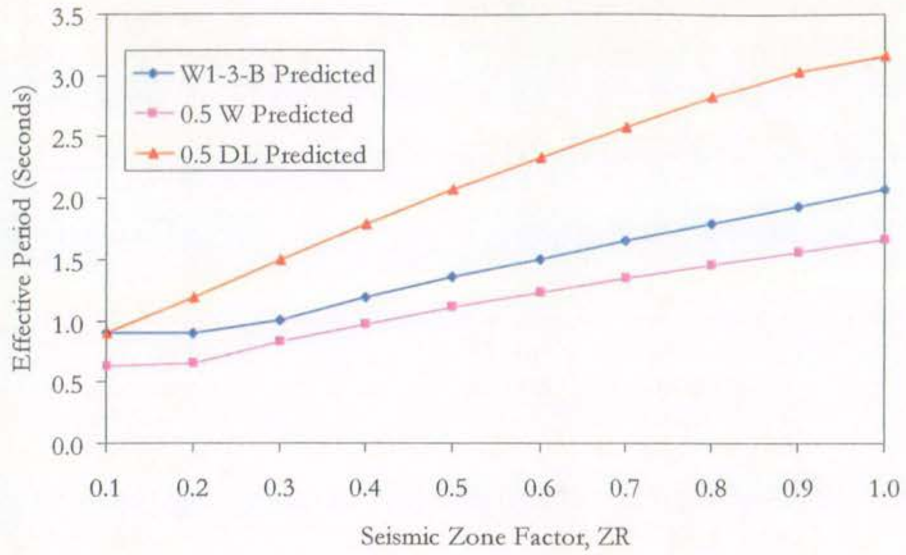

The evaluation of these variations in seismic weight and dead load has shown that the response is sensitive to both of these parameters, but also that the proposed design procedure incorporates both these variables and is able to accurately capture their effect on response.

7.3 Wall Ductility Factors

7.3.1 Ductility Definitions

Ductility is a measure of the extent of inelastic deformations beyond the elastic limit for either a structural component or a complete structure. Generally, it is expressed as a ratio of the maximum deformation to the yield deformation, defined by a symbol μ with a subscript indicating the type of deformation. Deformation may be translational (displacement ductility μ_Δ) or angular (rotation or curvature ductility, μ_θ or μ_φ respectively).

The New Zealand design code, NZ1170, defines a structural ductility factor, μ, and an inelastic spectrum scaling factor, k_μ which is numerically equal to the ductility factor for periods of 0.70 seconds or longer, where it is assumed that the assumption of equal elastic and inelastic displacements applies. For shorter periods the scaling factor is smaller than the ductility factor, based on an equal energy assumption. The design coefficient is obtained by dividing the elastic coefficient by the scaling factor k_μ.

Figure 7-14 illustrates the definitions used for structural ductility factor and displacement ductility for the purposes of this project.

1. The structural ductility factor is defined as the spectral acceleration coefficient at the elastic period of the structure divided by the force coefficient at the initiation of uplift, calculated from Equation (7-1).

3. For a given wall length and soil spring stiffness, maximum ductility values are relatively insensitive to the number of stories, especially for the softer springs where almost all the deformation is in the springs. For example, for the 3.600 m long wall on clay ductilities are between 4 and 6 for all heights from 1 to 6 stories.

7.3.3 Structural Ductility Factor

As discussed above, an alternative measure in elastic response is to use the ductility factor, the ratio of elastic force demand to the force capacity at the initiation of rocking. This is simpler to calculate than displacement ductility as it is a function of the wall properties alone, not seismic response.

Table 7-3 lists the structural ductility factors for each wall variation considered in this project assuming the spectral shape for Soil Class D. The values range from a minimum of 1 (squat walls on rock) to 20+ (slender walls on rock). Note that some of these walls may have excessive drifts under specific seismic input. These walls were excluded from the displacement ductilities tabulated in the preceding section but are not excluded from the calculation of structural ductility factors.

For a given wall size, the overturning moment capacity is generally independent of the spring stiffness but the period is strongly dependent on soil stiffness and so the spectral acceleration varies with soil stiffness. In general, the softer the soil the longer the period and the lower the spectral acceleration and so the ductility factor tends to reduce with reducing soil spring stiffness. This is not universally true as some walls have a short period and so remain on the spectral plateau even with the softer springs.

Table 7-3 Maximum Structural Ductility Factors for Soil Class D

Soil Spring Stiffness	7.200 m Wall Length Stories			3.600 m Wall Length Stories						14.400 m Wall Length Stories		
(kN/m)	1	2	3	1	2	3	4	5	6	1	2	3
Soft Clay K=2,000			5									
Clay K=10,000	4	8	8	9	8	8	9	9	8	2	4	5
Hard Clay K=40,000			10									
Soft Gravel K=40,000			11									
Sand/Gravel K=60,000	5	8	11	9	14	13	14	14	15	2	4	5
Hard Gravel K=80,000			11									
Rock K=1,000,000	3	8	11	9	15	20	22	20	20	1	3	4

7.4 Wall Shear Force Dynamic Amplification Factors

7.4.1 Maximum Amplification by Story

As discussed in Section 5.9, the dynamic inertia force distribution for multi-story walls varies from the static distribution, resulting in an increase in maximum shear force over what would be expected from a static analysis. This effect is not unique to rocking walls and is the reason NZS3101 defines a dynamic shear magnification factor for ductile shear walls.

As for the displacement ductility ratios in Table 7-2, the results used in this section are restricted to those from analyses in which the peak drift was within NZS 1170 limits (2.50% for motions without near fault effects and 2.50/0.67 = 3.73% for near fault motions).

Table 7-3 lists the maximum shear force amplification factor for each wall greater than one story high, where the amplification factor is defined as the maximum base shear force from the nonlinear analysis divided by the shear force calculated to initiate rocking, as defined in equation (7-10).

Table 7-4 Maximum Shear Force Amplification Factors

Soil Spring Stiffness	7.200 m Wall Length Stories		3.600 m Wall Length Stories					14.400 m Wall Length Stories	
(kN/m)	2	3	2	3	4	5	6	2	3
Soft Clay K=2,000		1.19							
Clay K=10,000	1.16	1.52	1.28	1.64	2.18	2.52	3.47	1.14	1.27
Hard Clay K=40,000		1.58							
Soft Gravel K=40,000		1.68							
Sand/Gravel K=60,000	1.30	1.78	1.53	1.94	2.93	3.89	4.72	1.25	1.37
Hard Gravel K=80,000		1.82							
Rock K=1,000,000	1.57	2.29	2.45	3.31	4.41	5.08	6.45	1.38	1.49

Table 7-3 shows definite trends for the amplification factors:

1. The amplification factor is strongly correlated to the number of stories, and increases with increasing number of stories for all walls and all soil spring stiffness values.

2. The amplification factor is relatively insensitive to the length of the wall for a specified number of stories.

3. The amplification factor increases with increasing soil spring stiffness but by a much lesser factor than the increase for increasing number of stories.

Figure 7-15 plots the shear amplification factors for all analyses which produced drifts within NZS1170 limits. These clearly show the dependence of the amplification on the number of stories. For ductile walls, NZS3101 defines an amplification factor as:

$$\omega_V = 0.9 + N / 10 \tag{7-11}$$

for buildings up to 6 stories. An equivalent function to envelope the results in Figure 7-11 would be

$$\omega_V = 0.5 + N \qquad \text{for } N > 1 \tag{7-12}$$

This would also apply for buildings up to 6 stories. Equation (7-12) provides factors which are much higher than for ductile walls, 2.5 compared to 1.1 for 2 story walls and 6.5 compared to 1.5 for 6 story walls.

Figure 7-15 Shear Magnification Factors

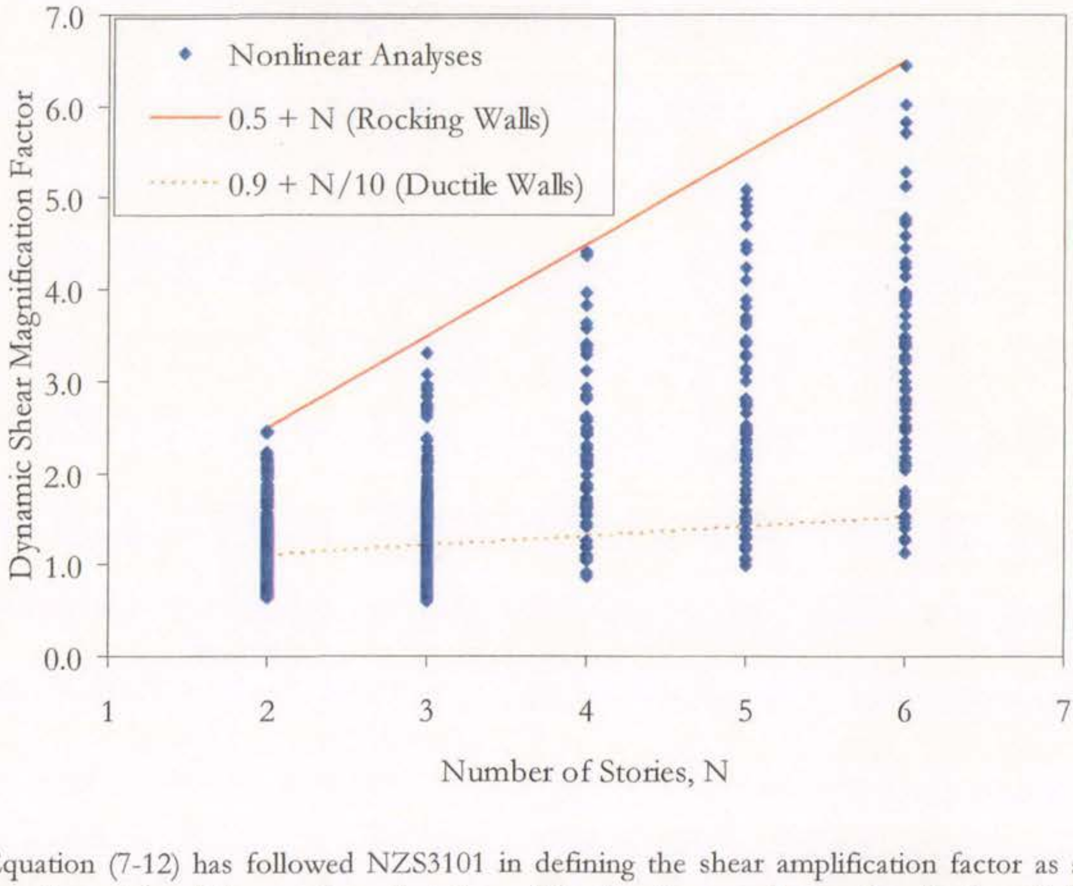

Equation (7-12) has followed NZS3101 in defining the shear amplification factor as a function solely of the number of stories. The function envelopes all walls for which drifts are within code limits, but it may be very conservative for walls for which drifts are much lower than code limits. This is examined below.

7.4.2 Effect of Displacement Ductility on Shear Amplification Factor

Figure 7-16 plots the shear magnification factor versus the nominal displacement ductility ratio, delineated by the number of stories. For each number of stories a best-fit linear function has been shown on the plot. The fit has been done subject to the constraint that the amplification is 1.0 at a ductility of 1.0.

The results appeared to show that the amplification was more a function of the number of stories than it was of the wall aspect ratio. When Figure 7-16 was re-formulated versus aspect ratio rather than number of stories the aspect ratios of 0.5 and 1.0 produced similar best-fit coefficients but the aspect ratio of 0.75 produced a higher coefficient than either. As the coefficients formed a more consistent function when calculated for the number of stories rather than aspect ratio, this former parameter was used to define the coefficients.

Figure 7-15 shows that the shear magnification factor is a function of ductility. It is only a weak function of ductility for the lower walls (2 and 3 stories) but becomes a stronger function as the wall height increases.

Figure 7-16 Ductility Factor Dependence of Shear Magnification Factors

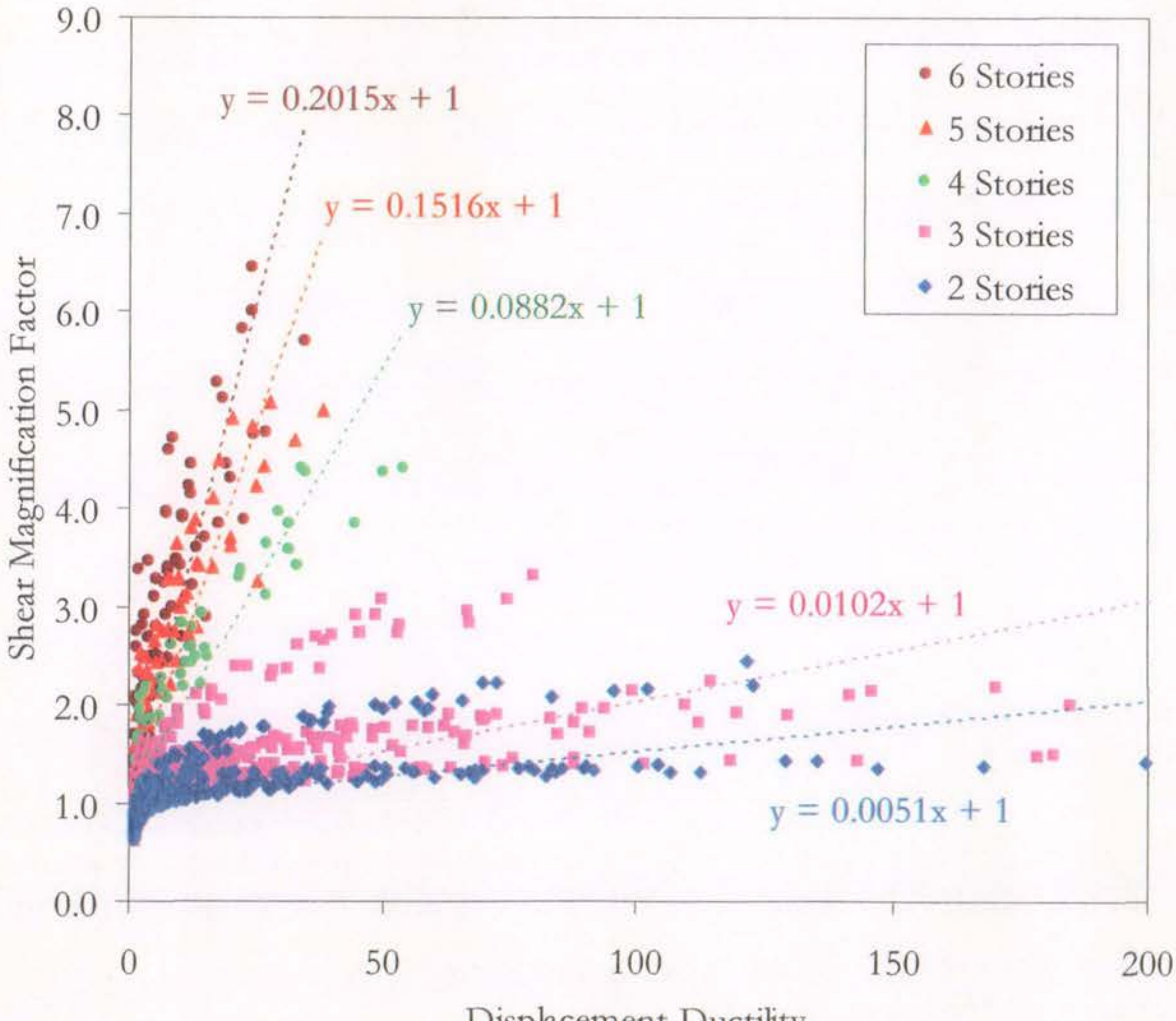

7.4.3 Effect of Ductility Factor on Shear Amplification Factor

Figure 7-17 plots the same shear amplification factors as in Figure 7-16 but as a function of the structural ductility factor rather than the displacement ductility ratio. As for Figure 7-16, best-fit linear curves are shown for each number of stories. These show a similar pattern to the previous plot, with coefficients which increase as the number of stories increases. Numerically, the values are quite different as ductility factors are an order of magnitude lower than displacement ductility ratios.

Figure 7-17 Displacement Ductility Dependence of Shear Magnification Factors

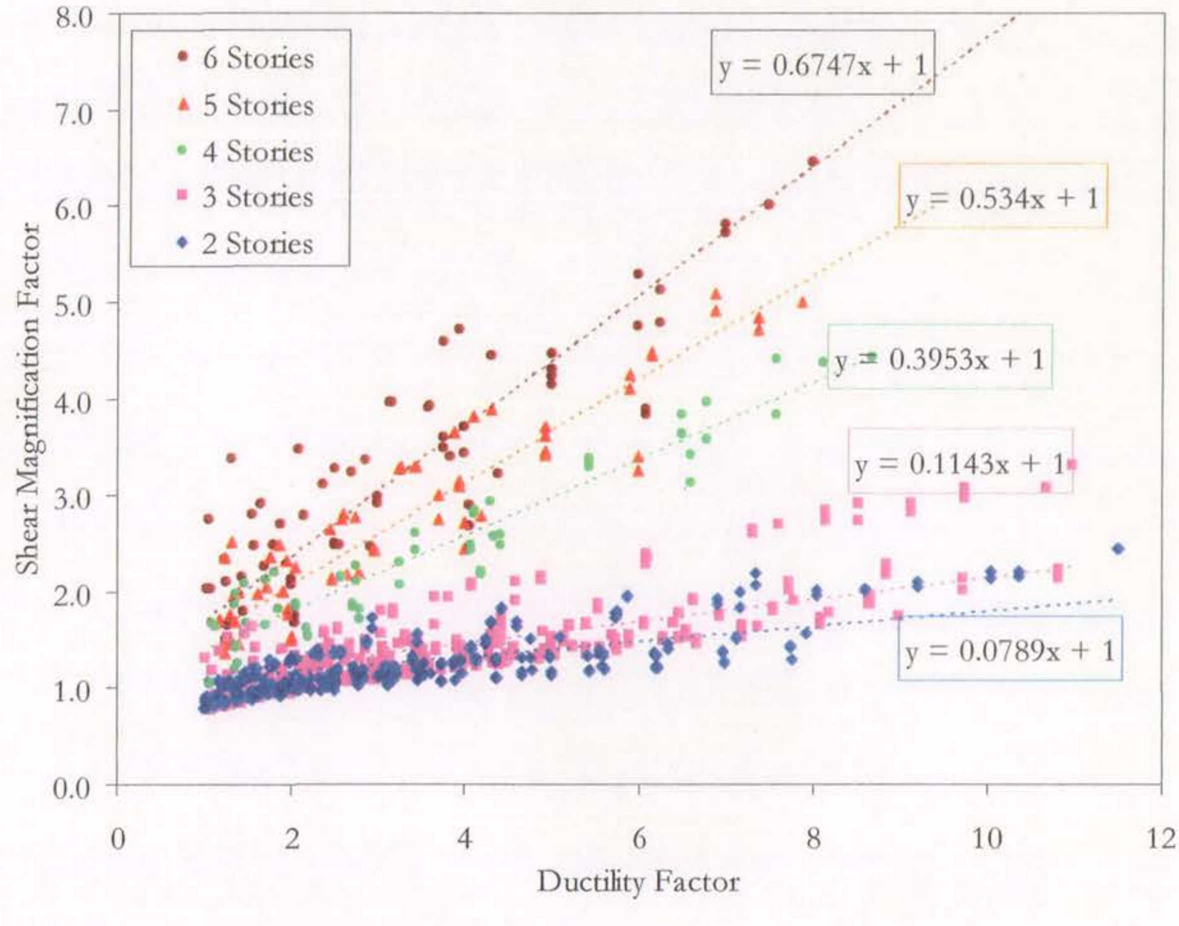

7.4.4 Tentative Equation for Shear Amplification

Table 7-5 provides numerical values of the best-fit linear relationships plotted in Figures 7-16 and 7-17. Also listed are the R-squared values, where R is the Pearson product moment correlation coefficient. Values of R-squared approaching unity indicate that the two sets of data are closely correlated, so values closer to unity indicate a better correlation.

For all number of stories, shear amplification factors were better correlated for the ductility factor than for the displacement ductility ratio. The correlation tended to be better for 4 stories or more than for the lower walls.

As the ductility factor is easier to calculate in a design office environment than displacement ductility ratio, and as it provides a better match to the data, the shear amplification function is formulated using this parameter.

Table 7-5 Best-Fit Parameters for Shear Amplification Factors

Number of Stories	Best-Fit Displacement Ductility		Best Fit Ductility Factor	
	Coefficient	R –Squared	Coefficient	R –Squared
2	0.0051	0.29	0.0789	0.57
3	0.0102	0.27	0.1143	0.60
4	0.0882	0.73	0.3953	0.92
5	0.1516	0.66	0.5340	0.86
6	0.2015	0.43	0.6747	0.73

Based on the plots in Figure 7-17, a formulation for the shear amplification factor would be based on a coefficient applied to the ductility factor with Equation (7-12) forming an upper limit:

$$\omega_V = 1 + a_{VN} DF \leq 0.5 + N \qquad \text{for } N > 1 \qquad (7\text{-}13)$$

If the shear amplification is a function of the rocking of the wall then it would be expected that the value would be unity for ductility factors up to 1, where rocking does not occur. This would imply that Equation (7-13) would be in the form $1 + a_{VN}$ (DF-1). However, as is apparent from Figure 7-17, the amplification factors are greater than 1 for DF = 1, especially for the taller walls. This is because the elastic shear distribution in the walls does not correspond to a uniform distribution because of higher mode effects, which is why the effect is more pronounced for taller walls.

Table 7-6 lists the coefficient, a_{VN}, to be applied to the ductility factor for each number of stories to that the calculated shear amplification will be at least 90% of the shear amplification ratio extracted from the analysis for 90% of the analysis values. For each number of stories, the ductility factor beyond which the upper limit applies is also listed.

Table 7-6 Shear Amplification Equation Parameters

Number of Stories	Coefficient on Ductility Factor, a_{VN}	Upper Limit on ω_V	Upper Limit at DF	Ratio of Predicted / Analytical			
				Number of Data Values	Number Prediction > 90% Analysis	Fraction Prediction > 90% Analysis	Average Prediction Analysis
1	0.000	1.0	-	-	-	-	-
2	0.100	2.5	15.0	338	314	93%	1.129
3	0.150	3.5	16.7	448	405	90%	1.176
4	0.400	4.5	8.8	65	58	89%	1.035
5	0.600	5.5	7.5	61	55	90%	1.077
6	0.900	6.5	6.1	64	57	89%	1.189

Also listed in Table 7-6, for all multi-story walls is (a) the number of data values for each value of the number of stories (b) the number and fraction of data points for which the predicted amplification from Equation (7-13) is at least 90% of the shear amplification recorded from the analysis and (c) the average ratio of predicted to analysis shear amplification.

Figure 7-18 compares the amplification factor calculated from Equation (7-13) with the data points extracted from the analyses for each variation of the number of stories. The upper limit governs only 5 and 6 story variations. The shear amplification factors required by Equation (7-13) will be conservative for some configurations, especially for the high structures with high ductility factors. It may be more effective to perform a specific evaluation for walls which fall into this category.

Figure 7-18 Shear Amplification Factors Verses Equation Values

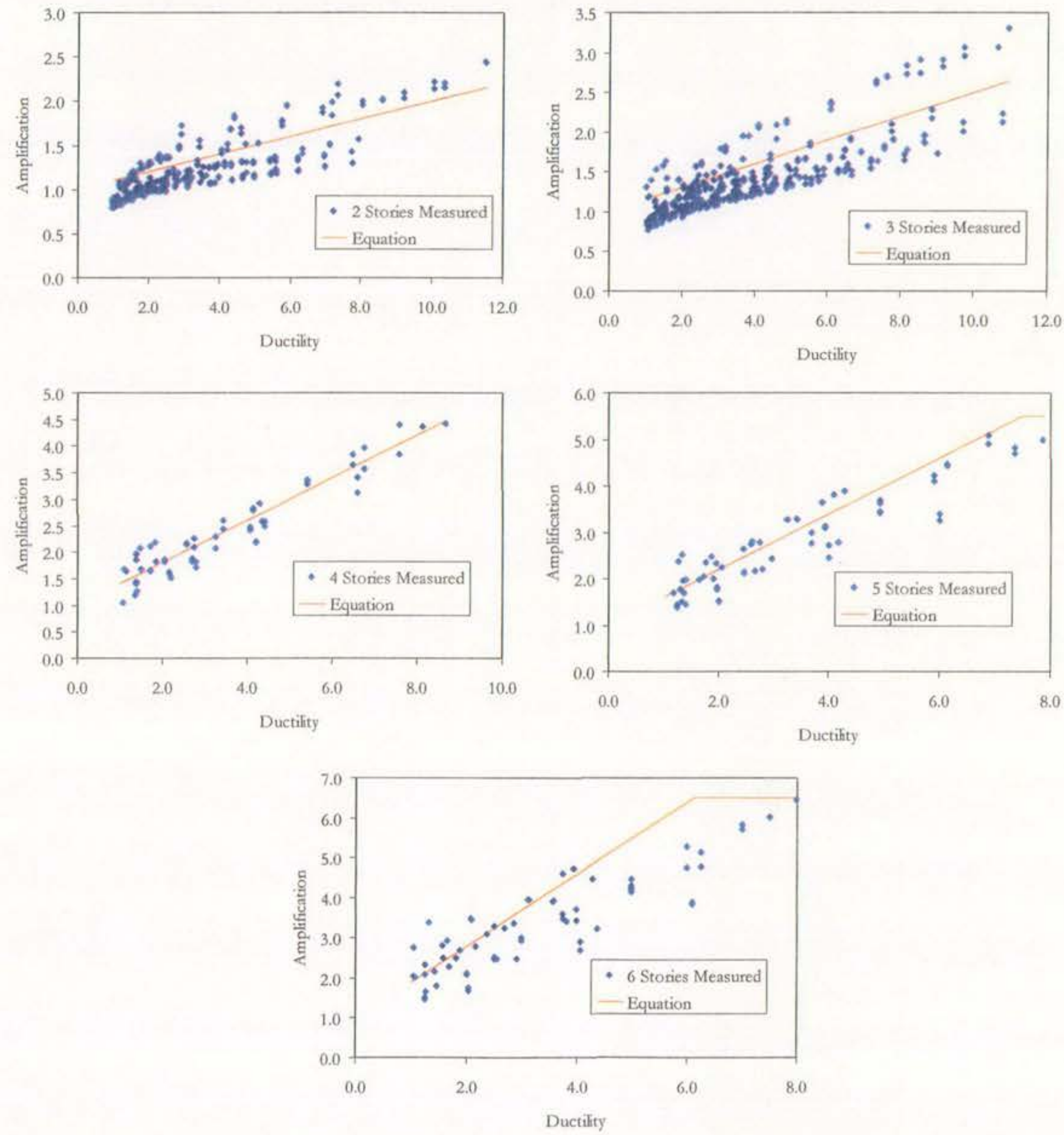

7.5 Wall Reaction Force

7.5.1 Concentration of Reaction

The wall reactions were discussed in detail in Section 5.10 of this report. As the wall rocks, the reaction force will be concentrated in the "end zone", which is defined as a footing length of B/6, where B is the footing width, as shown in Figure 5-1 which is reproduced from FEMA 356 Figure 4-5. The stress block approach which is in common use in design offices (see Section 6.5.2) is a representation of this concentration and is the recommended method of assessing reaction stresses.

For small ductilities the reaction force will be distributed over a longer compression block and the assumption of full gravity load on the stress block will be conservative (see Figure 5-31). It is beyond the scope of this development to derive a formulation for this reaction. If the reaction force is critical then the calculated displacement can be applied to a linear elastic model of the wall on springs and the reactions in tension identified and removed from the model. This will then give the compression force distribution.

7.5.2 Reaction Impact Factor

Section 5.10 described how the inclusion of vertical mass in the model gave rise to impact forces which increased the maximum reaction beyond the total gravity load. As discussed earlier, soil structure interaction is a complex process and includes other important effects, which as soil nonlinearity and radiation damping which were not included in the analysis. Therefore, the impact forces derived from the model are likely to be upper bound values and conservative for design.

7.5.2.1 Impact Factor Versus Soil Spring Type

The recorded impact factors increased with soil spring stiffness but the ductility also increases with soil spring stiffness. Because of this, the relationship between impact factor and ductility tended to be largely independent of soil spring stiffness.

Figure 7-19 plots the impact factor for Wall 1 for the three different soil springs against (a) displacement ductility and (b) against structural ductility factor. These plots show that the variability between soil spring types is not sufficient to justify attempting to differentiate impact factors as a function of soil spring. Therefore, in the following sections results for all spring types are combined as a data points for a specific wall.

7.5.2.2 Impact Factor Versus Displacement Ductility

Figures 7-20 and 7-21 plot the impact factors versus displacement ductility for the two walls which were evaluated including the effects of vertical mass (the 3 story wall 7.200 m long and the 2 story wall 14.400 m long). As the results appeared relatively independent of soil spring stiffness (Figure 7-19a) the results in the two figures combine results for soil springs B, E and G (medium clay, medium gravel and rock).

Figure 7-19 Impact Factors for Wall 1 Seismic Zone B
(a) Versus Displacement Ductility

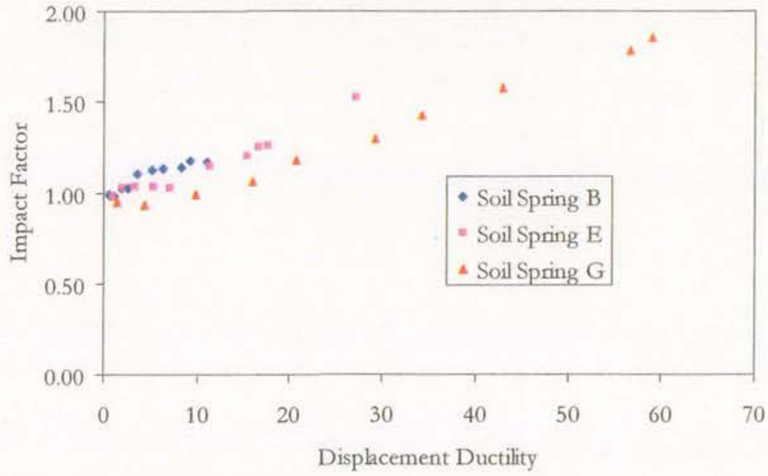

(b) Versus Structural Ductility Factor

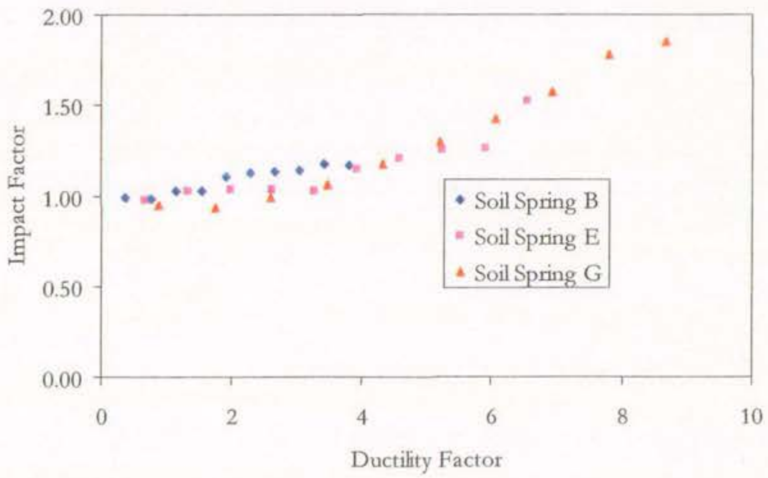

For each of the two walls in Figures 7-20 and 7-21, a best-fit linear curve has been fitted, with the intercept set at an impact factor of 1.0 at a ductility of 1.0. For Wall 1, the 7.200 m long 3 story wall plotted in Figure 7-20, the slope of the best fit line was 0.0094 and the correlation coefficient R^2 was 0.90, indicating a high degree of correlation between impact factor and ductility. For Wall 3, the 14.400 m long 2 story wall plotted in Figure 7-21, the slope of the best fit line increased to 0.0153 but the correlation coefficient R^2 was only 0.25, indicating less correlation between impact factor and displacement ductility.

Using the limited set of results available from Figures 7-17 and 7-18, and recognizing the wide scatter of results, a reasonable approximation for the impact factor, F_I, as a function of displacement ductility ratio, μ, would be:

$$F_I = 1.0 + 0.01\ (\mu - 1) \tag{7-14}$$

Figure 7-22 plots the analysis points from Figures 7-20 and 7-21 and also the function represented by Equation (7-13).

Figure 7-20 Impact Factors for Wall 1 L = 7.200 m

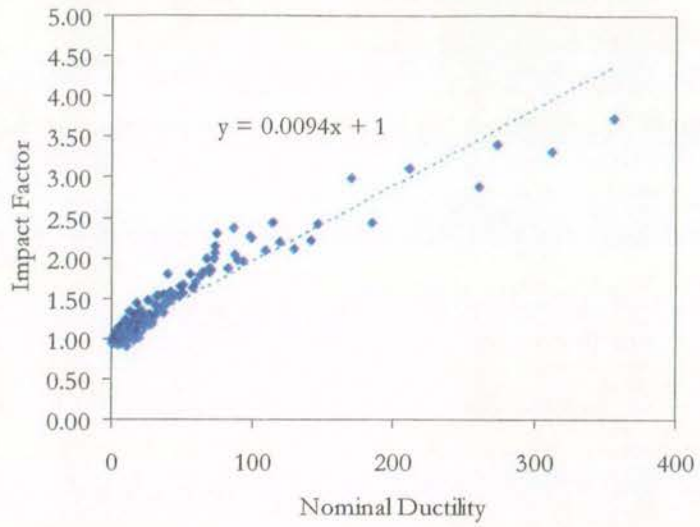

Figure 7-21 Impact Factors for Wall 3 L = 14.400 m

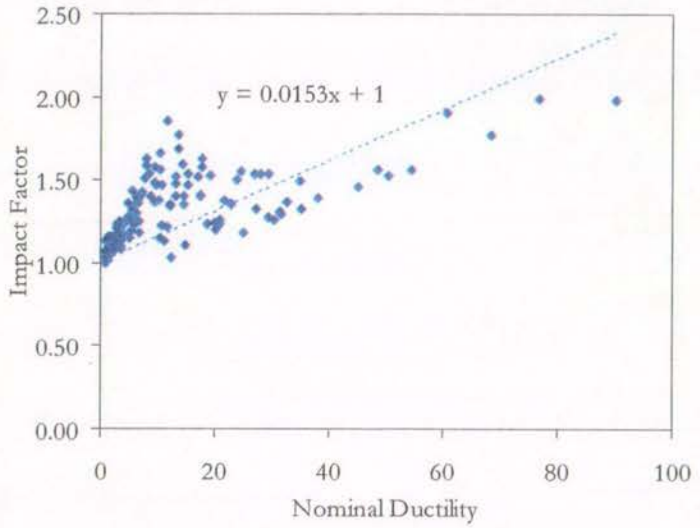

Figure 7-22 Fit with Suggested Formula

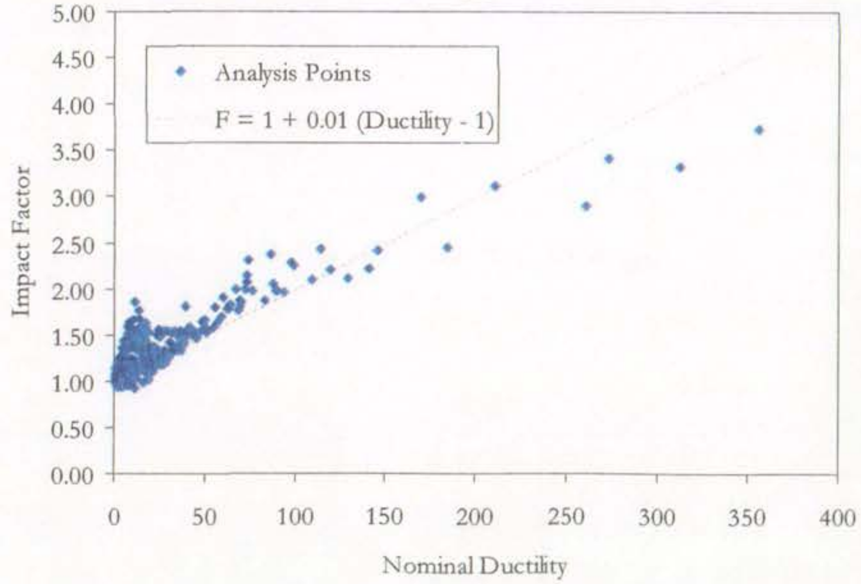

7.5.2.3 Impact Factor Versus Ductility Factor

Figures 7-22 and 7-23 plot the impact factors as in Figure 7-20 and 7-21 but versus structural ductility factor rather than displacement ductility and a best-fit linear curve has fitted as previously. For Wall 1, the 7.200 m long 3 story wall plotted in Figure 7-23, the slope of the best fit line was 0.1174 and the correlation coefficient R^2 was 0.73, indicating a reasonable degree of correlation between impact factor and ductility. For Wall 3, the 14.400 m long 2 story wall plotted in Figure 7-24, the slope of the best fit line increased to 0.2956 and the correlation coefficient R^2 was also 0.73.

For both these walls the correlation coefficient is 0.73, compared to coefficients of 0.90 and 0.25 respectively when the displacement ductility ratio was used. This suggests that the ductility factor is a better choice of parameter in that it has a wider range of applicability.

Figure 7-23 Impact Factors for Wall 1 L = 7.200 m

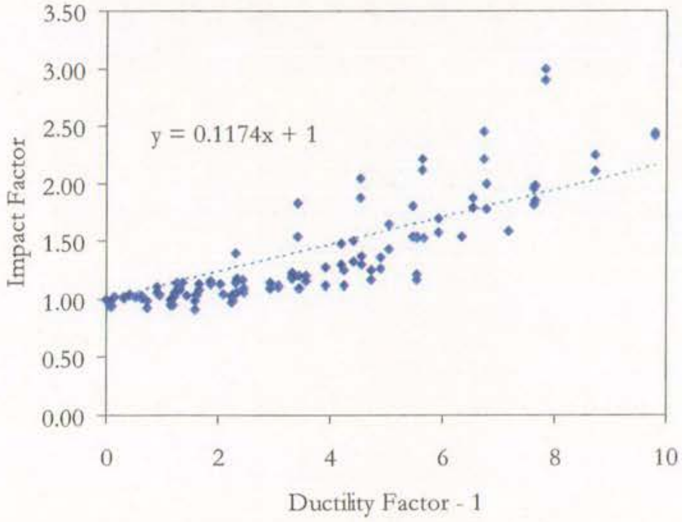

Figure 7-24 Impact Factors for Wall 3 L = 14.400 m

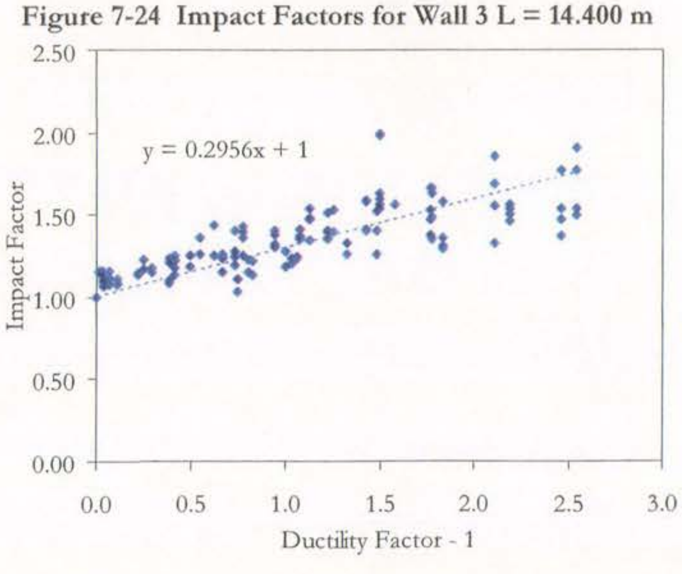

Using the limited set of results available from Figures 7-23 and 7-24, and recognizing the wide scatter of results, a reasonable approximation for the impact factor, F_I, as a function of displacement ductility, μ, would be:

$$F_I = 1.0 + 0.1336\ (\mu - 1) \geq 1.50 \qquad (7\text{-}15)$$

Figure 7-25 plots the analysis points from Figures 7-23 and 7-24 and also the function represented by Equation (7-15).

Figure 7-25 Fit with Suggested Formula

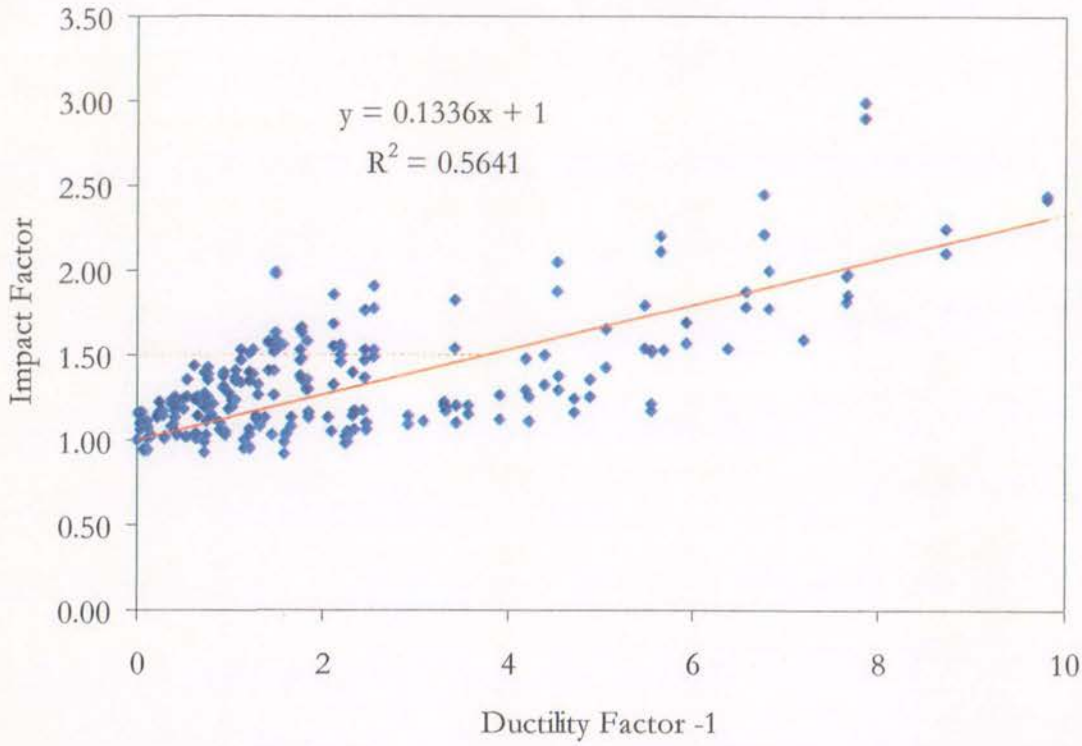

Although Equation (7-15) is a representation of the impact factors from the analyses, there is too much uncertainty in the procedures used here to recommend that these be used for design. The analyses with vertical mass did not include soil nonlinearity nor radiation damping, both of which would tend to reduce amplification.

8 MULTIPLE WALL ROCKING MODELS

8.1 Planar Walls in Series

The next level of structural complexity, above the single wall rocking models used to develop the design procedure, comprises multiple walls in the same plane. If the multiple walls are each of the same length then the response would be the same as for one wall, provided the response was uncoupled. If the walls differ in length then the response would be expected to differ from that of the individual walls. The latter configuration is examined in this section.

8.1.1 Analysis Model

To assess the response of multiple walls of unequal length, the combined wall shown in Figure 8-1 was used. This is formed as a combination of the three story configurations of both Wall 1 (length 7.200 m) and Wall 2 (length 3.600 m). Although a portion of floor slab is shown connecting the two walls in Figure 8-1, for analysis purposes this is assumed to have negligible flexural stiffness and is ignored in the evaluation.

The combined model was a direct combination of the individual models and used soil springs as described for the single wall models. It was assumed that there was an equal gravity load on each wall and that the total seismic mass was distributed to the walls by a diaphragm.

Figure 8-1 Combined Wall Model

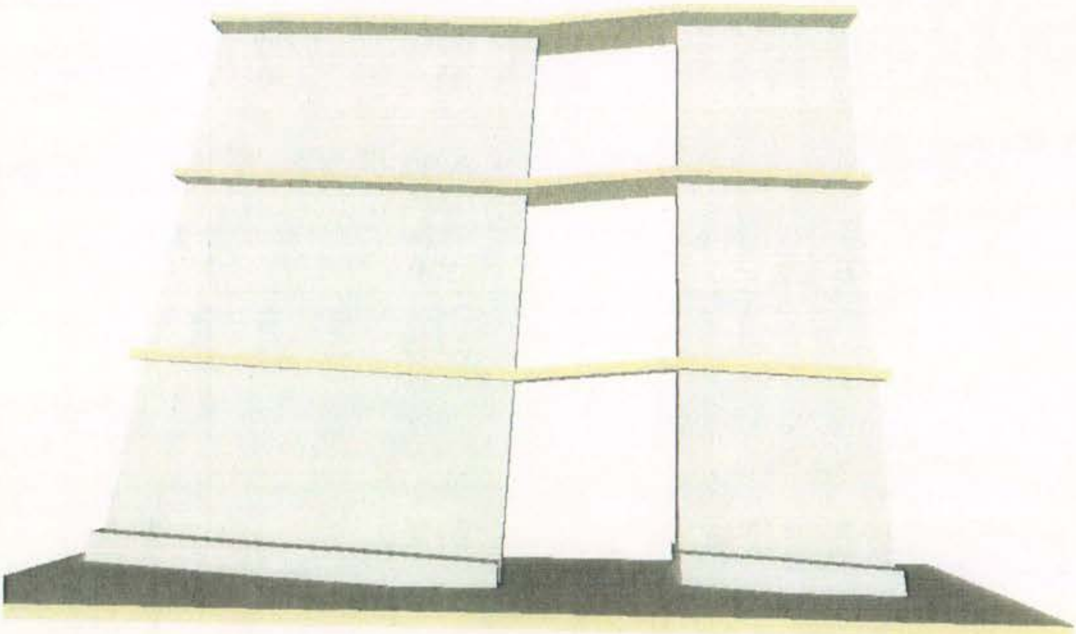

Table 8-1 lists the periods for the individual walls (extracted from Table 5-3) and the periods for the combined model. As expected, the periods for the combined wall were between those for the two component walls but closer to those of the longer wall.

Table 8-1 Wall Periods (Seconds)

ID	Spring Type	Wall 1 L = 7.200	Wall 2 L = 3.600	Wall 12 L = 3.600 + 7.200
B	Medium Clay	0.900	2.093	1.166
E	Medium Gravel	0.438	1.025	0.568
G	Rock	0.175	0.430	0.229

8.1.2 Calculation of Strength Properties

The bilinear properties were calculated using the same procedure as for single walls except that the yield force coefficient, C_Y, was based on the summation of the two walls. Table 8-2 summarizes the calculations for the three soil types. Note that only the period and the yield displacement were a function of soil type and so the capacity calculations are the same for all three spring types.

Table 8-2 Calculation of Bilinear Properties

	B Medium Clay	E Medium Gravel	G Rock	
C_0 = Mode Shape x PF = φPF		1.286		
Mass, M (tonne)		621		
Height, H (m)		10.800		
Period, T (seconds)	1.166	0.568	0.229	$\Delta_Y = \dfrac{9180MT}{4\pi^2}$
Displacement, Δ_Y	49.2	15.0	2.50	
Wall 1				$M_u = \dfrac{WL}{2}$
Length (m)		6.330		
Weight (kN)		1526		
Moment Capacity M_U (kN-m)		4828		$F_u = \dfrac{M_u}{(H/\varphi PF)}$
F_u = Force at M_U (kN)		575		
Wall 2				
Length (m)		3.433		
Weight (kN)		1526		
Moment Capacity M_U (kN-m)		2619		
F_u = Force at M_U (kN)		312		
Total Force (kN)		887		
Force Coefficient, C_Y (F/Mg)		0.146		=887/(9.81x621)

Figures 8-2 and 8-3 plot the capacity curves for soil types B (medium clay) and E (medium gravel) respectively. Each figure shows the capacity curves for both the individual walls and for the combined wall model. The bilinear properties, calculated as detailed in Table 8-2, are compared with the capacity curve obtained from the Nonlinear Static Procedure (NSP, or pushover analysis).

In a similar pattern as for the periods, the capacity curve for the combined wall falls between the curves for the two individual walls. For the stiffer soil springs (Figure 8-3) the NSP capacity eventually converges to the bilinear curve but for the softer springs (Figure 8-2) the bilinear curve over-estimates the capacity because the second order (P-Δ) effects are larger due to the high displacements.

Figure 8-2 Medium Clay Foundation Capacity Curve

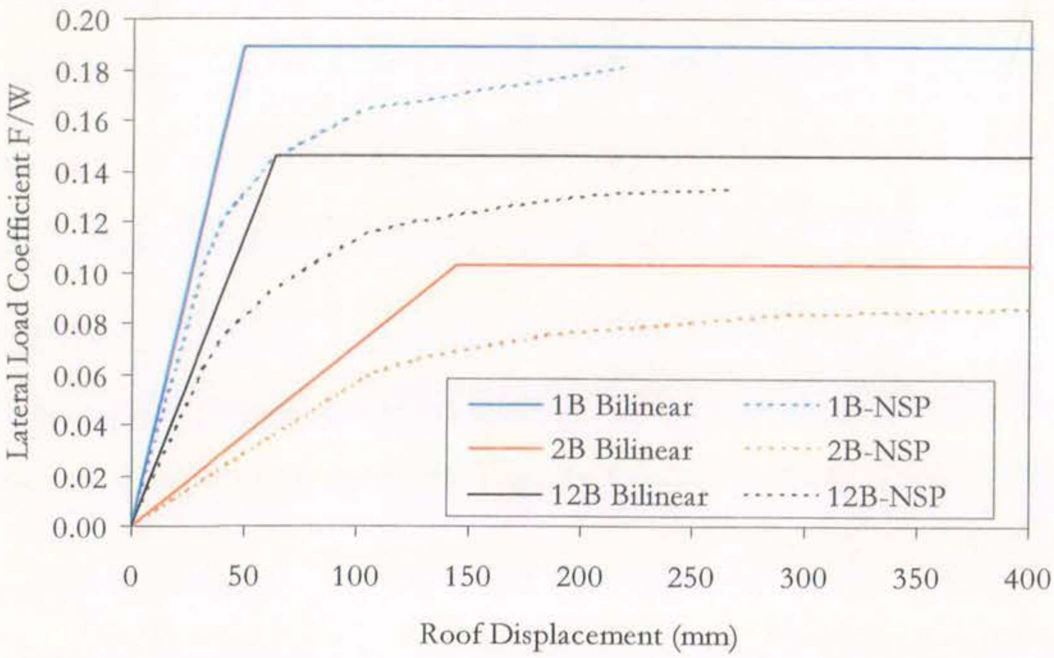

Figure 8-3 Medium Gravel Foundation Capacity Curve

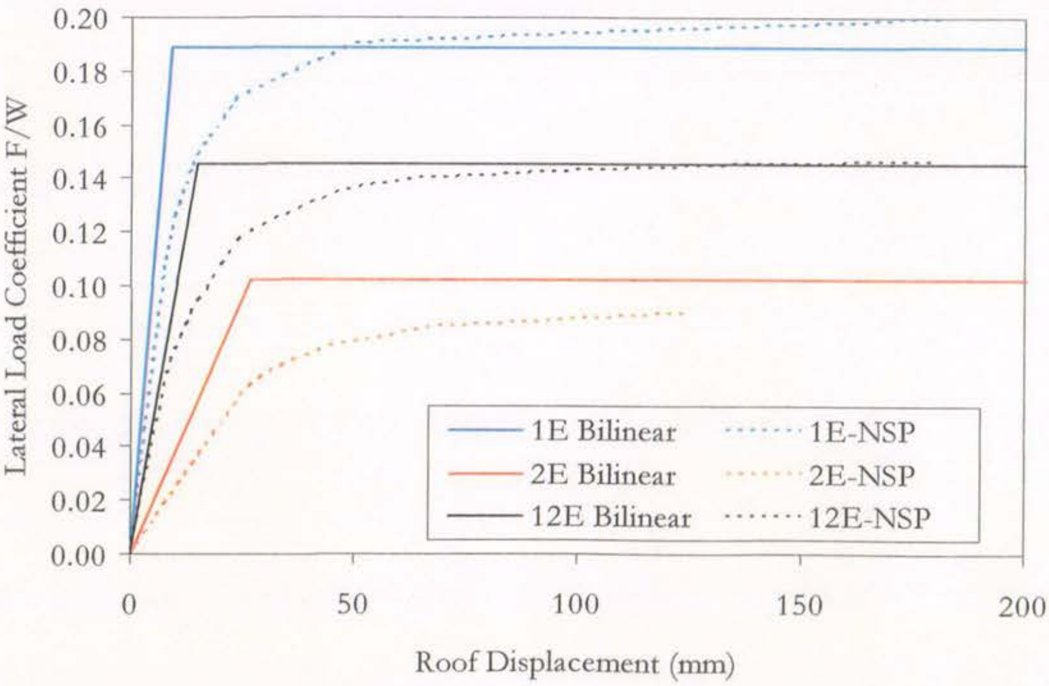

8.1.3 Time History Results

Figures 8-4 and 8-5 plot results for the medium gravel soil springs for two seismic zones, (1) Soil B far fault, which produces displacements up to 600 mm, and (2) Soil D near fault, which produces displacements over three times as high. Each figure plots the results for the individual walls (1 and 2) and the combined wall (12). At each earthquake amplitude, the results from the nonlinear analysis (ANSR) are compared with the displacements predicted from the design procedure (EQN).

As for the periods and the capacity curves described earlier, the displacements for the combined wall fall within those for the two individual walls. The displacements generally follow a similar pattern for all models, increasing at a higher rate than the increase in earthquake amplitude. It is also seen that the design procedures appear to be as accurate in predicting peak displacements for the combined model as they are for the individual walls.

Figure 8-4 Comparison Soil B Far Fault Medium Gravel

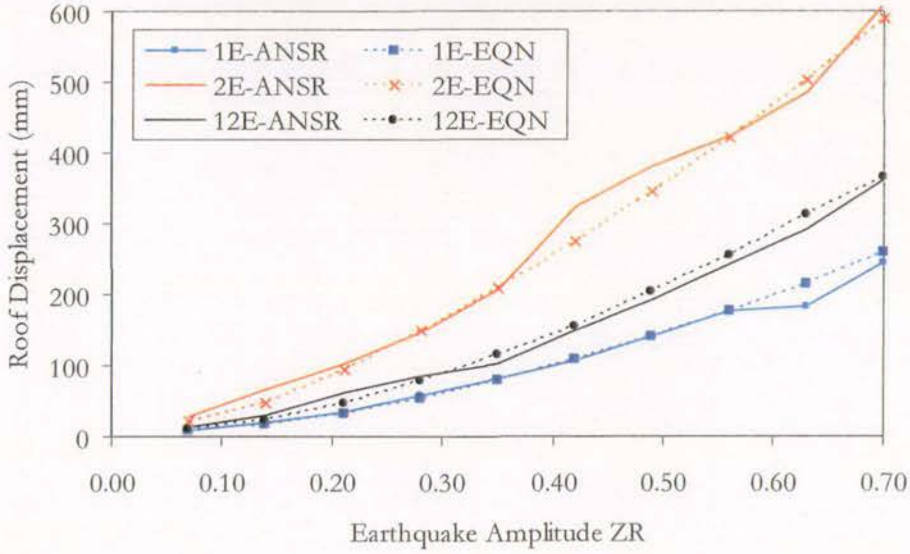

Figure 8-5 Comparison Soil D Near Fault Medium Gravel

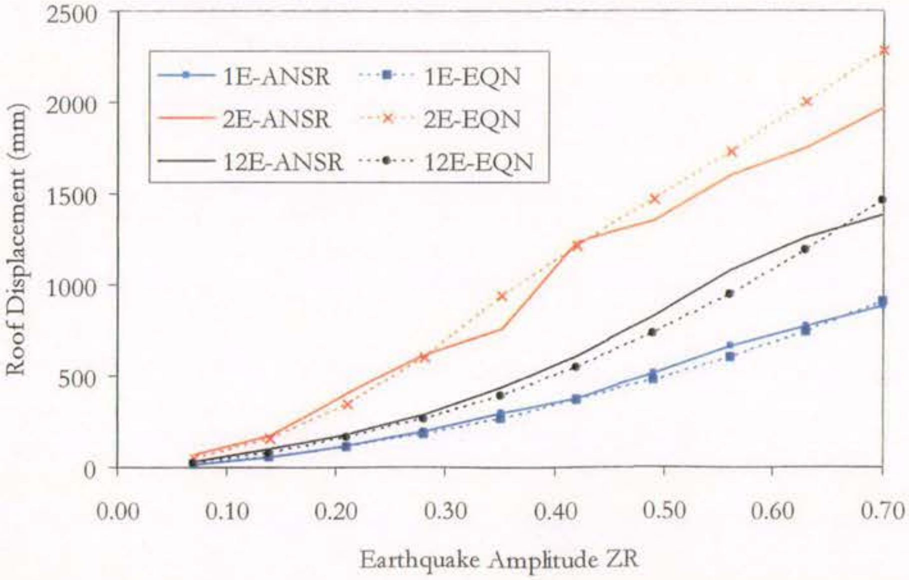

8.1.4 Comparison with Design Procedure Predictions

A detailed comparison of the displacements from the time history analysis and those predicted from the design procedure is contained in Appendix A, Figures A-41 to A-43. Figure 8-6 shows the comparisons for the soil springs corresponding to the medium gravel, the intermediate values, for all seismic soil types for both near fault and far fault conditions. Maximum displacements at ZR=0.7 range from less than 400 mm (far fault, Soil B) to over 1400 mm (near fault, Soil D). This shows that with some exceptions (chiefly the high amplitude motions for far fault Soil D) the design procedure provides an excellent predictor of maximum displacements, generally within 10% of the mean value from the nonlinear analysis.

Figure 8-6: Run 12-3-E 7.200 m + 3.600 m Wall Length 3 Story Medium Gravel

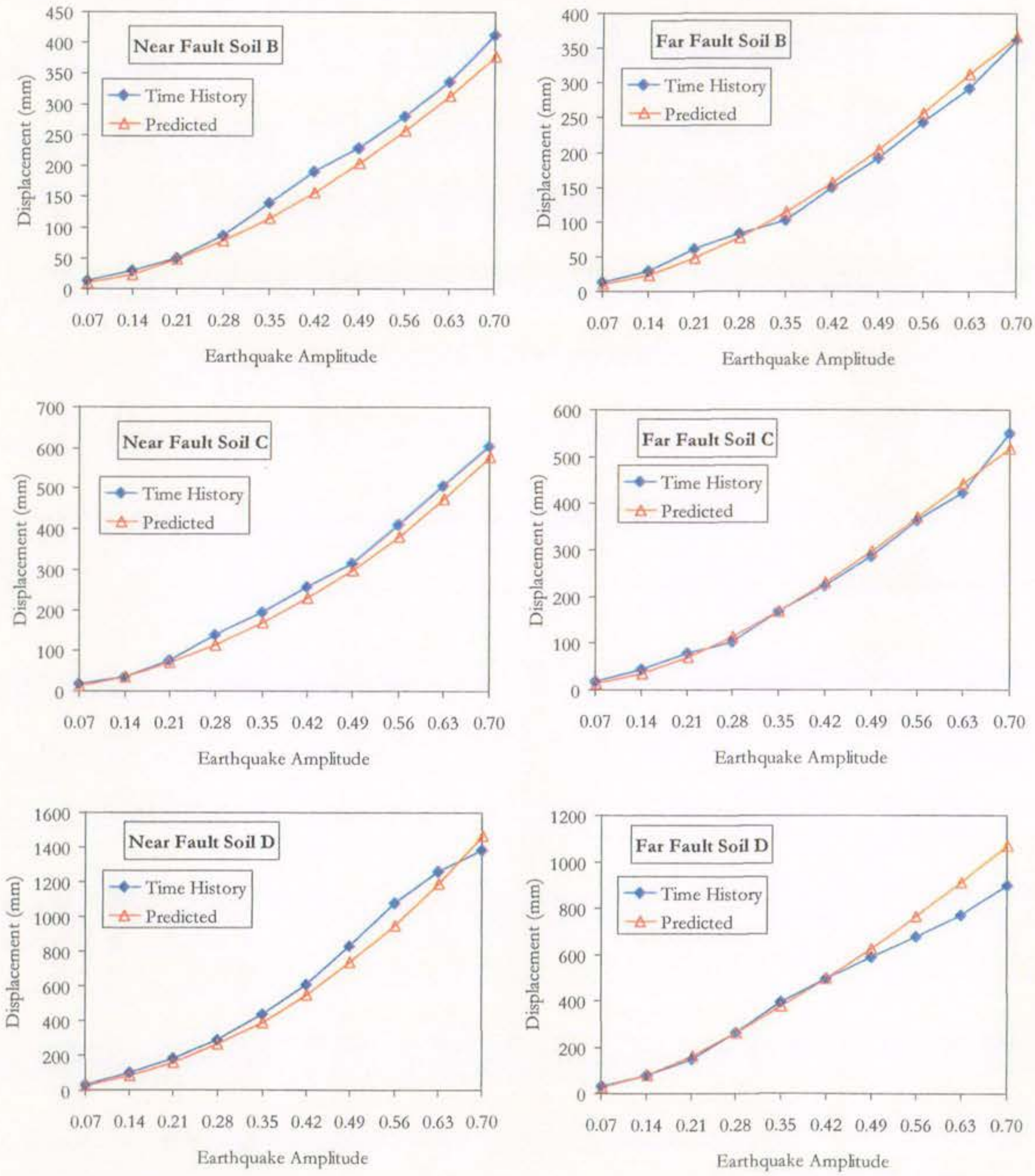

This analysis on a combined wall shows that the design procedure developed for single walls can also be applied to multiple planar walls, provided the initial period of the combined system is used and that the force coefficient is based on the sum of the ultimate (uplift) forces of the individual walls.

8.2 Characteristics of Non-Planar Walls

The planar single and multiple walls evaluated in the preceding sections share a number of characteristics which act to simplify the problem of evaluating response under earthquake loads:

1. The walls act in a single direction so there is no interaction with walls in the orthogonal direction. This allows the earthquake excitation to be considered as a single translational component.

2. The response of each individual wall is symmetric and so the response of the total system of planar walls is also symmetric. This results in a wall lateral strength which is independent of the direction of load.

3. There is no torsional component to response so the maximum displacement will be the same at all points on a floor.

It follows from these characteristics that the evaluation of non-planar walls will have to consider the multi-directional nature of seismic excitation; that the variation in strength with direction of earthquake will need to be considered and that displacements will need to incorporate an allowance for torsion.

These features of the response of non-planar walls add considerable complexities to the attempt to develop a simplified design procedure for rocking walls. As the wall configuration becomes more complex, there will be limits to when a simplified procedure can be used and beyond that point a specific time history evaluation will be needed.

In the following section, two commonly used configurations of non-planar walls are considered; firstly three-sided U-shaped walls (e.g. retail occupancies, with an open frontage) and, secondly, buildings with non-symmetrical wall layouts (different wall lengths on each elevation). The seismic response of these walls to increasing amplitude earthquake is evaluated and an attempt made to extend the design procedure developed for planar-walls to include non-planar effects.

8.3 U Shaped Walls

Buildings with walls on three sides with a largely open fourth wall are common in retail type occupancies and result in U-shaped wall configurations. Unlike the single and multiple planar walls considered previously, the response of U-shaped walls will be affected by the concurrent action of earthquake components in each translational direction and so the effect of simultaneously applied components needs to be considered in the evaluation process.

8.3.1 Analysis Model

Two wall layouts were selected, as shown in Figures 8-7 and 8-8:

1. A three story U shaped wall with a long dimension of 14.400 m (parallel to the open elevation) and a short dimension of 7.200 m (Figure 8-7).

2. A two story U shaped wall square in plan, with dimensions of 14.400 m in each direction (Figure 8-8).

Figure 8-7 Layout of 3 Story U Shaped Wall 7.200 m x 14.400 m

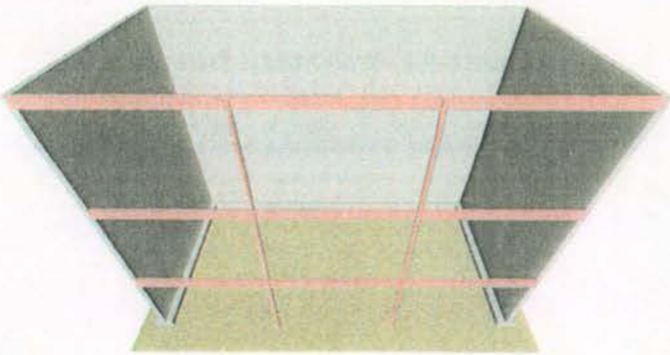

Figure 8-8 Layout of 2 Story U Shaped Wall 14.400 m x 14.400 m

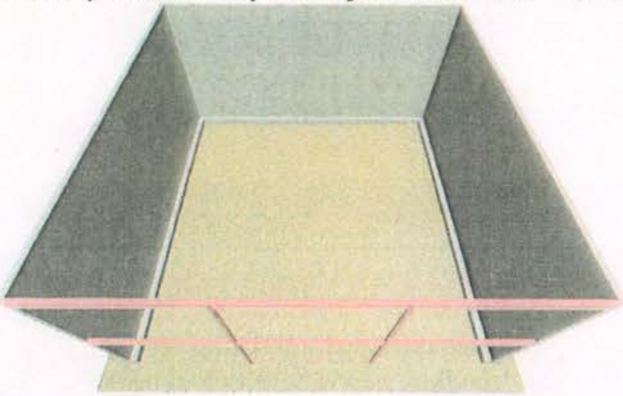

The model development generally followed the same principles as for the planar walls. For each model it was assumed that:

- The back wall was divided into 12 segments and the side walls into 6 segments, as shown in Figure 8-9 for the 7.200 m deep wall. The same numbering was used for both walls and so the side wall segment length was increased by a factor of 2 for the 14.400 m deep wall. The X axis was parallel to the open wall, as indicated in Figure 8-9.

- The floor seismic weight was 7.5 KPa at each floor for both buildings. The floor mass, and the rotational moment of inertia, was lumped at the geometric centroid of the building. For the variation with accidental eccentricity, the location of the centroid was moved parallel to each axis by an amount of 0.1 times the dimension of the building in that direction.

- The floors spanned across the building, from the front elevation (the open face) to the back elevation. Gravity loads were applied as uniform loads to beams along these two elevations at each floor level. Beam loads were 27 kN/m for the 7.200 m deep building and 54 kN/m for the 14.400 m deep building.

- Spring stiffness values were calculated as for individual walls. At column lines common to two walls the stiffness values for the individual walls were summed.

- Pinned columns were used at 3rd points along the front face to support part of the floor load. These columns did not contribute to the lateral strength of the building.

Figure 8-9 U-Wall Model Definition

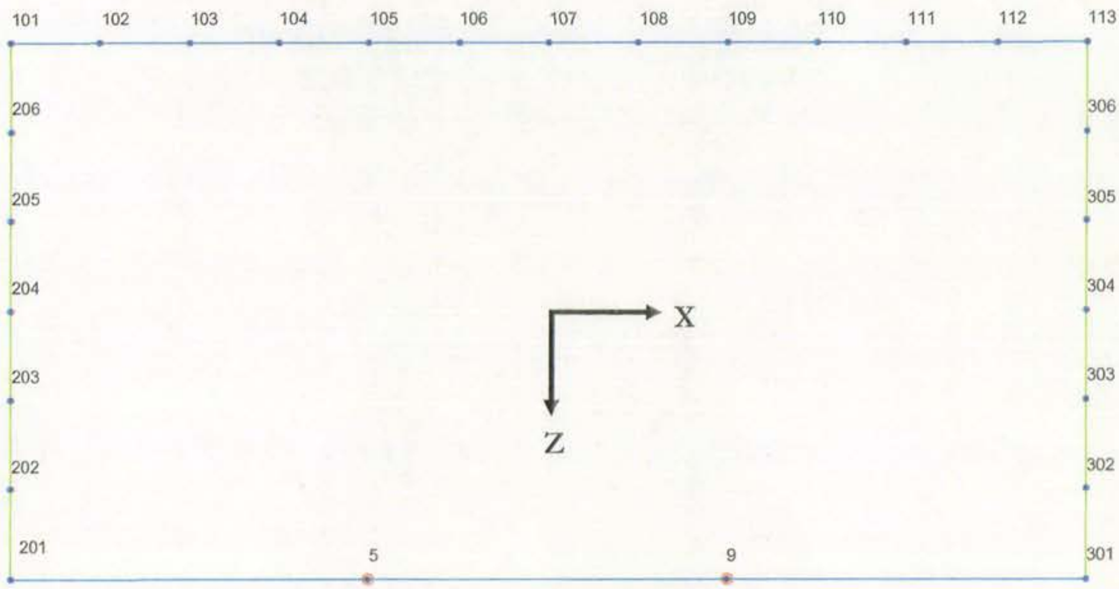

Each wall was evaluated for three different soil spring sets, B, E and G which correspond respectively to medium clay, medium gravel and rock in order of ascending stiffness.

8.3.2 Dynamic Properties

Table 8-3 lists the dynamic properties of the two different wall configurations for each spring set.

For the 7.200 m deep wall the periods in the X and Z directions are approximately equal whereas in the 14.400m deep wall the period in the Z direction (parallel to the side walls) is only about one-half the period in the other direction. This would appear to be counter-intuitive in that the 14.400 m deep configuration is square in plan and so equal periods would be expected in this building rather than the 7.200 m building which has a 2:1 aspect ratio. In other words, the 1:1 building has a period ratio of 2:1 and the 2:1 building has a period ratio of 1:1.

The reason for this apparent discrepancy is that, because of the effect of the soil springs, the period is proportional to the length of wall in each direction rather than the building dimension. For the 7.200 m building the length of wall in each direction is the same whereas for the 14.400 m wall there is twice the length of wall in the Z direction as in the X direction.

Table 8-3 Dynamic Properties of U-Shaped Walls

	7.200 m Deep U-Wall		14.400 m Deep U-Wall	
	X Direction	Z Direction	X Direction	Z Direction
Medium Clay Springs				
Period (seconds)	0.352	0.383	0.309	0.138
Effective Mass, M_{EFF}	49.1%	65.7%	78.1%	89.7%
Mode Shape x PF = φPF	0.739	0.989	1.042	1.194
Medium Gravel Springs				
Period (seconds)	0.220	0.188	0.164	0.074
Effective Mass, M_{EFF}	53.9%	76.6%	78.4%	90.1%
Mode Shape x PF = φPF	0.821	1.167	1.046	1.195
Rock Springs				
Period (seconds)	0.115	0.095	0.088	0.044
Effective Mass, M_{EFF}	59.3%	80.7%	79.8%	91.0%
Mode Shape x PF = φPF	0.951	1.286	1.067	1.196

The mode shapes are much more regular in the Z direction than the X direction, as indicated by the proportion of effective mass which is much higher in this direction (Table 8-3). The effective mass also tends to increase with increasing spring stiffness.

In the X direction the product of the mode shape component and the participation factor (φPF) is less than 1.0 for the walls 7.200 m deep. This appears to be a function of the low mass participation. This has an impact on the development of a design procedure to predict displacements as this factor is used to convert single degree of freedom displacements to roof displacements, and is discussed further later.

8.3.3 Wall Strength Properties

The strength properties of the two wall configurations were extracted from the model by applying a cyclic displacement trace at the top of the wall and recording the force at each step. Figures 8-10 and 8-11 plot the lateral load capacity of the 7.200 m and 14.400 m deep wall respectively, in both cases for the soil springs based on medium clay.

The two walls show characteristics which are a function of the U-shaped configuration:

1. For loads in the X direction, parallel to the open face, the strength is symmetrical, that is, the same in both directions. Although the two wall configurations have the same dimension along the X axis, and so the same length of wall resisting lateral loads, the 14.400 m deep wall has a load capacity almost

two times as high as the 7.200 m deep wall. This is because of the higher compression loads in the side walls to resist uplift in the 14.000 m wall.

2. For loads in the Z direction, parallel to the sides of the U, the strength is non-symmetrical. The strength is much higher when the wall pivots on the "front" face of the wall, that is, on the side wall ends adjacent to the open elevation, because the total compression resisting uplift is much higher on the back wall. The ratio between the maximum and minimum loads is approximately 3:1 for both walls. For the 7.200 m deep wall the Z capacity is less than the X capacity for both directions. The deeper wall has a Z capacity which exceeds the X capacity by about 50% in the stronger direction but is only about 50% of the X capacity in the weaker direction.

3. The loads in the X direction generally provide a positive stiffness to greater displacements than for loads in the Z direction. It is apparent from Figures 8-10 and 8-11 that secondary effects (P-Δ) are more complex for these walls than for the single walls. This is because of the more complex distribution of gravity loads and the presence of other elements (columns) to support part of the gravity loads.

Although the strengths of the U-shaped walls are more complex than the single values for the planar walls, the resistance to overturning is still provided by gravity loads and so the moment capacity can be calculated using the lever arms to the gravity loads. These calculations are provided later in this section.

The capacities in Figures 8-10 and 8-11 are for the medium clay springs, the most flexible. The capacity curves are generally similar for the other spring types, although the displacements at which uplift occurs reduce for the stiffer soil springs.

Figure 8-10 Lateral Capacity of 7.200 m Deep Wall on Medium Clay Soil Springs

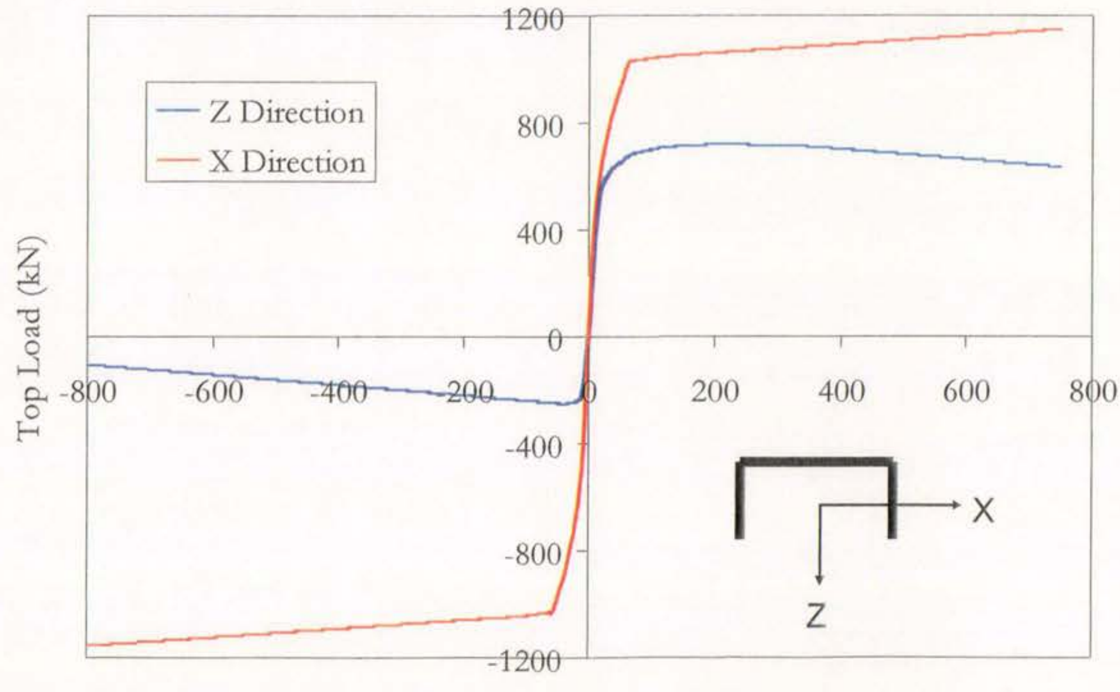

Figure 8-11 Lateral Capacity of 14.400 m Deep Wall on Medium Clay Soil Springs

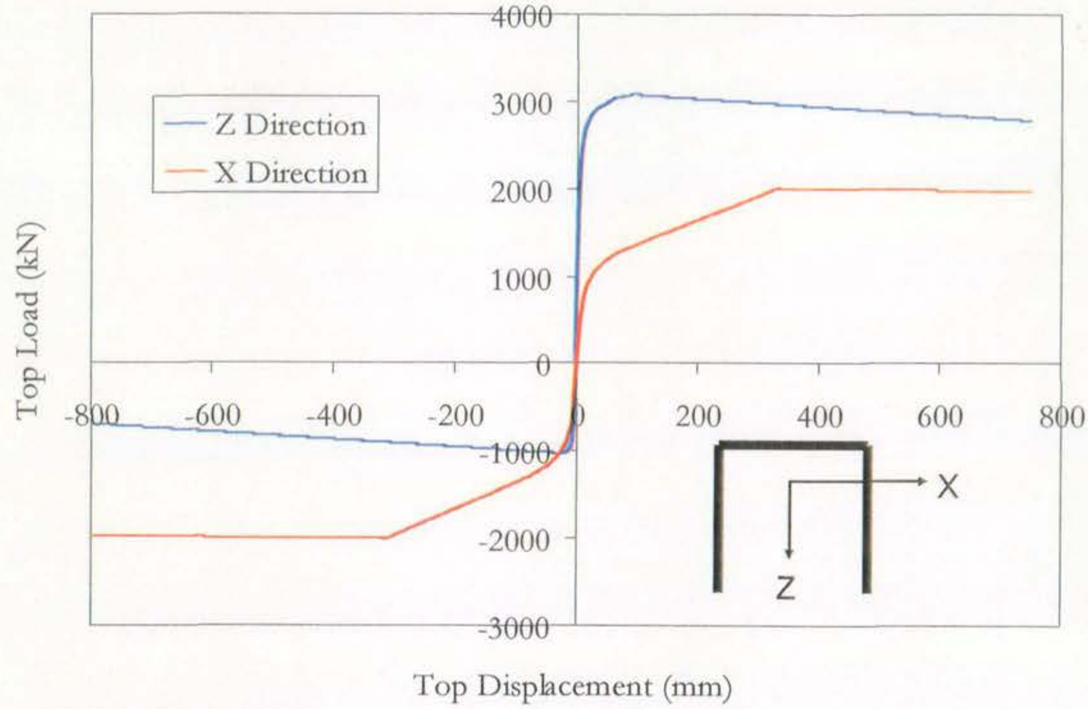

8.3.4 Time History Evaluation

The U-walls were evaluated for the variations in soil spring set and in earthquake load direction listed in Table 8-4:

1. For the model with no eccentricity (centroid at the calculated centre of mass) each of the three spring types was evaluated for three load directions (X and Z directions separately and then both simultaneously) for three spectrum shapes (Soil Classes B, C and D) in a near fault location. For each spring type and direction, this required a total of 210 time histories (3 spectrum shapes x 7 time histories x 10 earthquake amplitudes).

2. The analyses for the spectrum shape corresponding to Soil Class C were then repeated for two additional eccentricity configurations, with the mass centroid moved 0.1B in the positive and negative directions respectively. This provided an additional 140 time histories for each spring type and direction (1 spectrum shape x 7 time histories x 10 earthquake amplitudes x 2 eccentricities).

The same set of analyses was performed for both the 7.200 m and the 14.400 m deep walls. All analyses generally followed the solution procedures developed for the single walls:

- Rayleigh damping coefficients were calculated to provide 5% viscous damping at 1.5 times the calculated elastic period and at a period one-tenth this value. The elastic period was defined as the longer of the X and Z direction periods.

- All records were applied for a 50 second duration, which included the strong motion portion of all records.

- The integration time step was generally set at no longer than 1/200[th] of the fundamental period, where the period was the longer of the periods in the two directions.

Table 8-4 Time History Variations for U-Walls

	Calculated Centre of Mass	Positive Eccentricity	Negative Eccentricity
Soil Springs B (Medium Clay) E (Medium Gravel) G (Rock) Load Directions X (1 component) Z (1 component) XZ (2 components)	Near Fault B Near Fault C Near Fault D	Near Fault C	Near Fault C

For the analysis in the XZ load directions (both components applied simultaneously), the two components of each of the 7 earthquakes were individually scaled to match the target spectrum. A polar plot of the two components of one earthquake is shown in Figure 8-12. The XZ analysis essentially loads the walls with a continually varying angle of attack, and so is not the same as loading a wall along the diagonal.

Figure 8-12 Simultaneous Components of Caleta de Campos Earthquake, Mexico

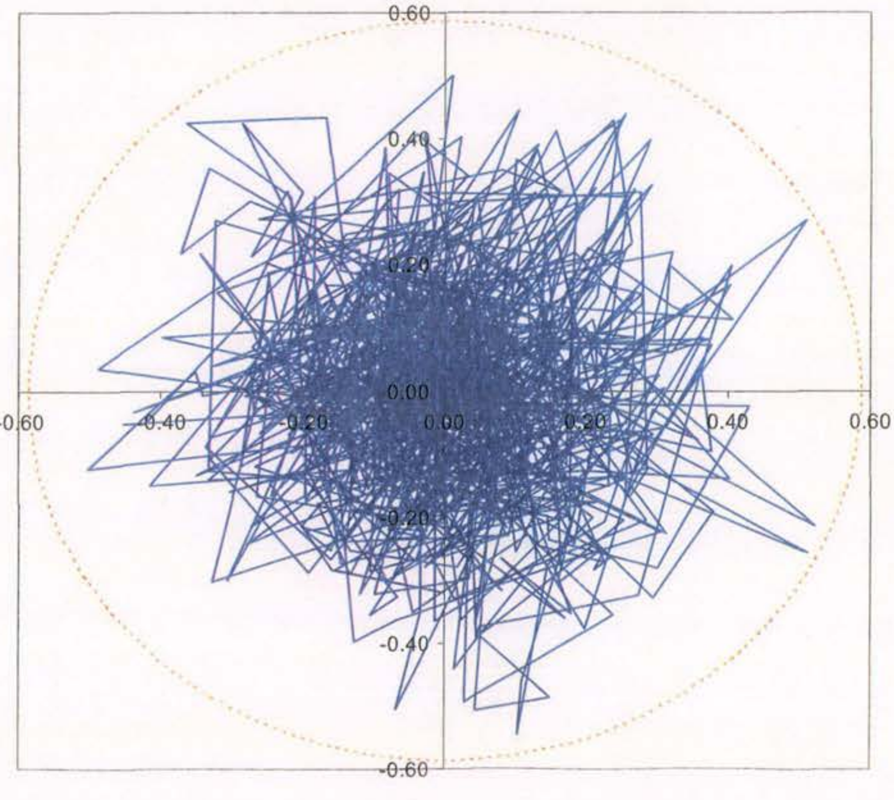

8.3.4.1 Processing Time History Results

As for the single wall models, a macro in the output workbook was used to read envelope values from each analysis and assemble the mean values from each set of 7 time histories. The macro included only analyses which terminated normally, that is, where the envelope time was 50 seconds. If 5 or more of a particular set terminated normally then the data point was accepted as valid, if less than 5 then the data point was discarded.

An example of the summary of results is given in Table 8-5, for the 7.200 m deep wall on the clay springs under the action of two simultaneously applied earthquake components. Note that for this example, there are no results for a scale factor of 1.0 for Near Fault Site Class D (the final line on the table). For the maximum amplitude considered (zone factor ZR = 0.7, scale factor = 1.0) the 7 earthquakes completed for Site Class B and C but only 3 of the 7 earthquakes completed for Site Class D. For this site class, the other 4 analyses terminated when displacements exceeded 5.0 m, indicating an overturning failure of the wall.

The processed data for each analysis contained the 10 columns of data in Table 8-5:

- The scale factor, where full scale is equivalent to ZR = 0.7 and so the incremental earthquake amplitude was ZR = 0.07.

- Maximum displacements anywhere on the floor plan in the X and Z directions, indicated as Δ_X and Δ_Z in Table 8-5 respectively.

- Displacement at the centre of mass of the floor plan in the X and Z directions, indicated as Δ_{XD} and Δ_{ZD} in Table 8-5, where the subscript indicates that this is the diaphragm displacement. These are always less than the maximum displacements, or equal to the maximum displacements if there is zero torsional response.

- The maximum base shear as a fraction of the seismic weight, V_X and V_Z in Table 8-5 for forces along each axis.

- The maximum number of simultaneously open gap elements, N_{OPEN}. There are a total of 25 gap elements supporting the wall and so a value of 24 would indicate that the complete wall was rocking on a corner of the wall. Note that although the actual number of open gaps for any particular run is an integer value, the values in Table 8-5 are the average of the 7 integer values and so are not generally an integer.

- The final column in Table 8-5 is the maximum compressive reaction on any of the 25 gap elements. The weight of the wall is 1555 kN and this forms the upper limit on the reaction, occurring when the wall rocks on one corner.

The data presented in Table 8-5 are for a single direction of load and a specific set of soil springs. For each of the two U-shaped walls there are a total of 9 similar sets of results (Soil sets B, E and G for each of X, Z and XZ directions of earthquake load). There are also 3 further sets of results for Soil Class C only for each of Soil sets B, E and G. These additional results contain results for the positive and negative accidental eccentricities respectively, each for the X, Z and XZ load directions.

Given the sheer volume of data represented by these 12 workbooks for each wall, only a summary is provided in this report. An attempt is made to extract trends which may be used to illustrate the effects of concurrency and eccentricity on peak wall response quantities.

Table 8-5 Time History Results: 3 Story U-Shaped Wall 7.200 m Deep Clay Springs XZ Load

Scale Factor	Δ_X	Δ_Z	Δ_{XD}	Δ_{ZD}	V_X	V_Z	δ_U	N_{OPEN}	Reaction
				Near Fault Soil B					
0.10	8.4	13.4	5.7	7.5	0.18	0.13	3.98	4.14	-320
0.20	15.9	28.9	11.3	20.9	0.29	0.25	13.90	10.57	-432
0.30	22.9	42.8	16.5	31.8	0.41	0.29	22.87	13.29	-519
0.40	31.7	68.6	22.8	55.0	0.52	0.34	39.23	16.71	-640
0.50	40.8	93.4	30.3	77.2	0.57	0.36	56.12	18.14	-732
0.60	52.6	116.3	39.4	95.0	0.61	0.37	71.81	18.71	-796
0.70	60.1	160.1	44.9	138.6	0.63	0.38	105.98	20.00	-863
0.80	81.0	227.9	60.4	198.0	0.65	0.42	145.83	21.14	-944
0.90	97.0	287.7	77.2	260.6	0.68	0.42	191.01	21.14	-1025
1.00	104.5	388.2	81.3	357.4	0.69	0.43	256.23	21.57	-1102
				Near Fault Soil C					
0.10	10.2	16.6	6.9	9.9	0.22	0.17	5.92	6.29	-350
0.20	20.1	38.2	14.3	26.9	0.35	0.28	19.72	12.86	-482
0.30	28.3	57.2	18.9	46.6	0.48	0.33	32.35	15.71	-579
0.40	40.7	94.3	30.2	79.4	0.56	0.36	56.68	18.14	-732
0.50	58.0	124.9	43.0	101.9	0.61	0.38	77.51	19.14	-813
0.60	82.1	214.4	62.1	186.5	0.63	0.40	134.10	19.86	-900
0.70	83.9	282.0	65.0	245.5	0.66	0.43	185.67	21.14	-1000
0.80	104.2	394.8	80.5	367.9	0.69	0.43	260.99	21.57	-1086
0.90	136.3	470.7	109.3	432.1	0.73	0.46	313.43	22.14	-1209
1.00	150.9	619.1	121.0	587.8	0.75	0.47	413.53	22.57	-1290
				Near Fault Soil D					
0.10	11.6	20.3	8.3	13.9	0.24	0.21	8.62	8.14	-376
0.20	25.6	54.4	18.6	43.8	0.42	0.32	30.57	15.29	-558
0.30	45.7	117.1	33.8	94.8	0.56	0.36	69.17	18.00	-745
0.40	70.2	204.3	51.7	177.3	0.62	0.40	128.69	20.00	-880
0.50	96.0	376.1	75.2	345.0	0.63	0.42	247.36	21.43	-1040
0.60	125.4	545.9	102.1	514.5	0.70	0.44	365.64	21.86	-1190
0.70	166.6	648.2	143.3	616.7	0.71	0.43	435.10	22.86	-1365
0.80	189.9	890.9	164.3	852.2	0.70	0.45	636.42	23.17	-1377
0.90	214.4	979.8	199.6	946.4	0.75	0.46	693.86	23.40	-1482
1.00									

The results in Table 8-5 can be presented graphically in a number of ways to help interpret the response. Two examples, for the same wall as tabulated in Table 8-5, are shown in Figures 8-13 and 8-14:

1. Figure 8-13 plots the X and Z displacements as a function of earthquake amplitude. For each direction both the diaphragm centroid displacement and the maximum displacements are plotted. The difference between the two represents the torsional component of displacement. For this wall, the torsional displacement tends to be approximately a constant ratio of the total displacement for the full range of amplitude.

2. Figure 8-14 plots the base shear against diaphragm displacement for each of soil types B, C and D. Plots are given for both the X and the Z directions. In general, the curves for each soil class overlay each other as the wall has a defined force-displacement relationship which is to a large extent independent of earthquake input.

Figure 8-13 Displacements: 3 Story Wall 7.200 m Deep Clay Springs XZ Load NF B

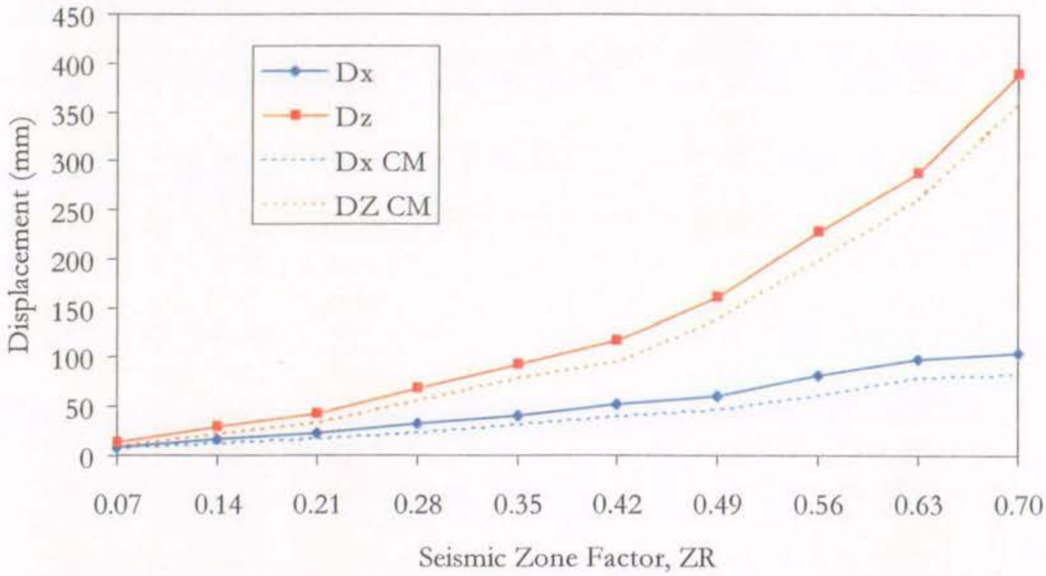

Figure 8-14 Shears: 3 Story Wall 7.200 m Deep Clay Springs XZ Load Near Fault

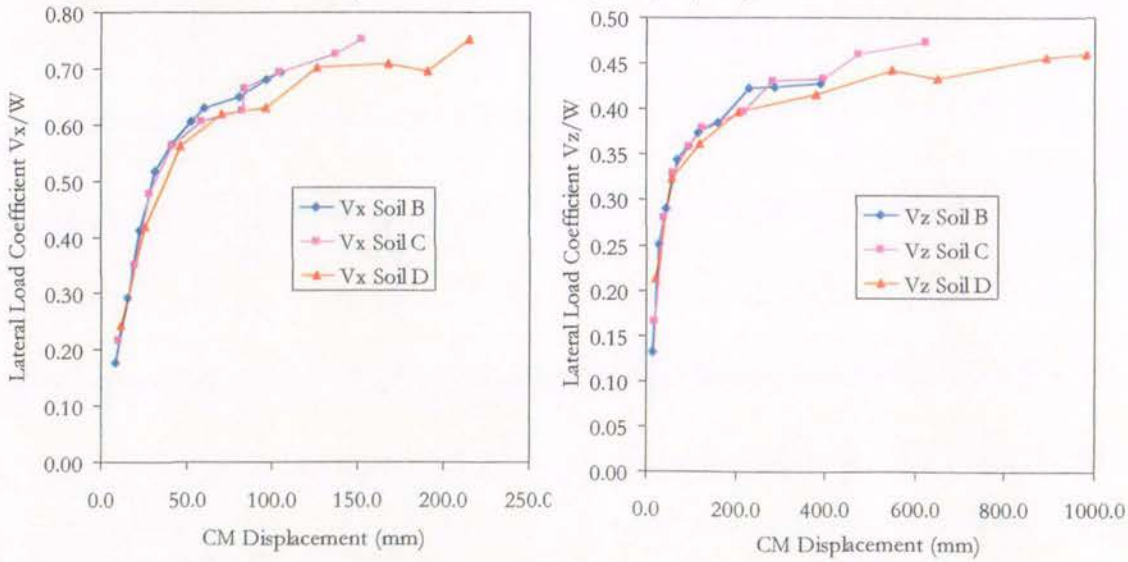

The capacity curve for the wall for which results are shown in Figures 8-13 and 8-14 is given in Figure 8-10. The capacity curve indicates an X strength of 1037 KN (0.67 W) and Z strengths in the two directions of 780 kN and 260 kN (0.50W and 0.17 W). The higher strength in the X direction than the Z direction is manifest as lower displacements in the X direction in Figure 8-13 and in the higher lateral load coefficients in the X direction in Figure 8-14.

The shear force coefficient recovered from the envelopes is the maximum value and so the plot of lateral load coefficient versus displacement for the Z direction in Figure 8-14 reflects the higher of the positive and negative strengths.

8.3.4.2 Effect of Concurrency

The effect of applying two horizontal components simultaneously is demonstrated in Figures 8-15 to 8-18 by plotting the displacements for three analyses, (a) one component applied along the X axis, (b) one component applied along the Z axis and (c) components applied along each axis simultaneously. For each variation, displacements are plotted at the centre of mass of the diaphragm (CM) and also the maximum at any location on the diaphragm (MAX). The difference between these two curves is an indication of the effect of torsion. All the analyses plotted in Figure 8-15 to 8-18 are for the configuration with the mass located at the calculated centroid so there is no "accidental" eccentricity added to the "natural" eccentricity.

These figures show some of the characteristics of concurrent response on three dimensional, non-symmetrical models:

- For the 7.200 m deep wall, Figures 8-15 and 8-16, the displacements normal to the direction of load are generally small (Z displacements due to X earthquake in Figure 8-15 and X displacements due to Z earthquake in Figure 8-16).

- For the 14.400 m deep wall, Figures 8-17 and 8-18, the displacements normal to the direction of load are also small for Z direction displacements (Z displacements due to X earthquake in Figure 8-17). However, for this wall X displacements due to Z earthquake (Figure 8-18) are higher than the Z displacements for low amplitude earthquakes and even for high amplitude earthquakes are a significant proportion of the Z displacements.

- When both components are applied simultaneously the displacements increase but generally by not a large fraction.

- In all cases the Z maximum displacement is almost identical to the Z centre of mass displacement, indicating almost no torsional response. In the X direction the maximum displacements are in all cases significantly higher than the centre of mass displacements. This is the expected response as the Z earthquake loads the structure along an axis of symmetry but the X earthquake does not.

Figure 8-15 7.200 m Deep Wall X Displacements Soil C NF

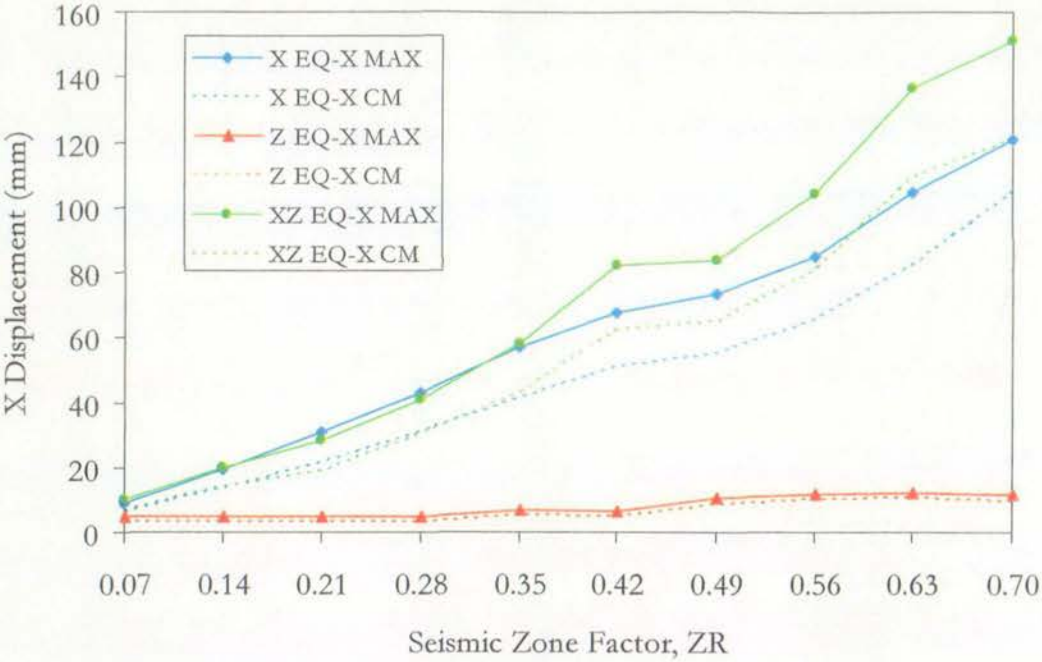

Figure 8-16 7.200 m Deep Wall Z Displacements Soil C NF

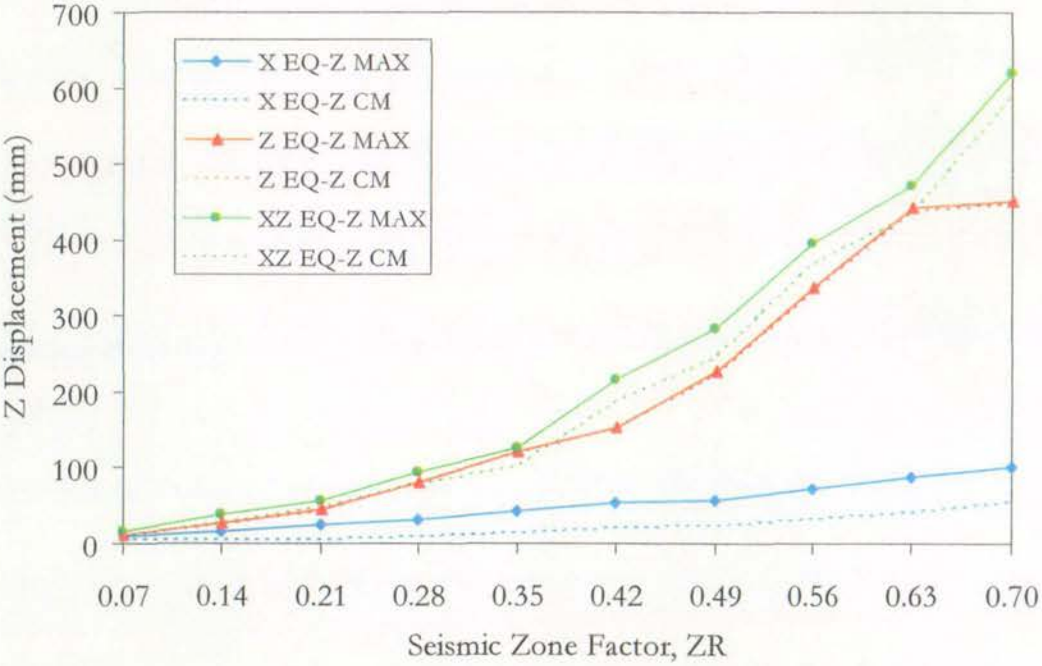

Figure 8-17 14.400 m Deep Wall X Displacements Soil C NF

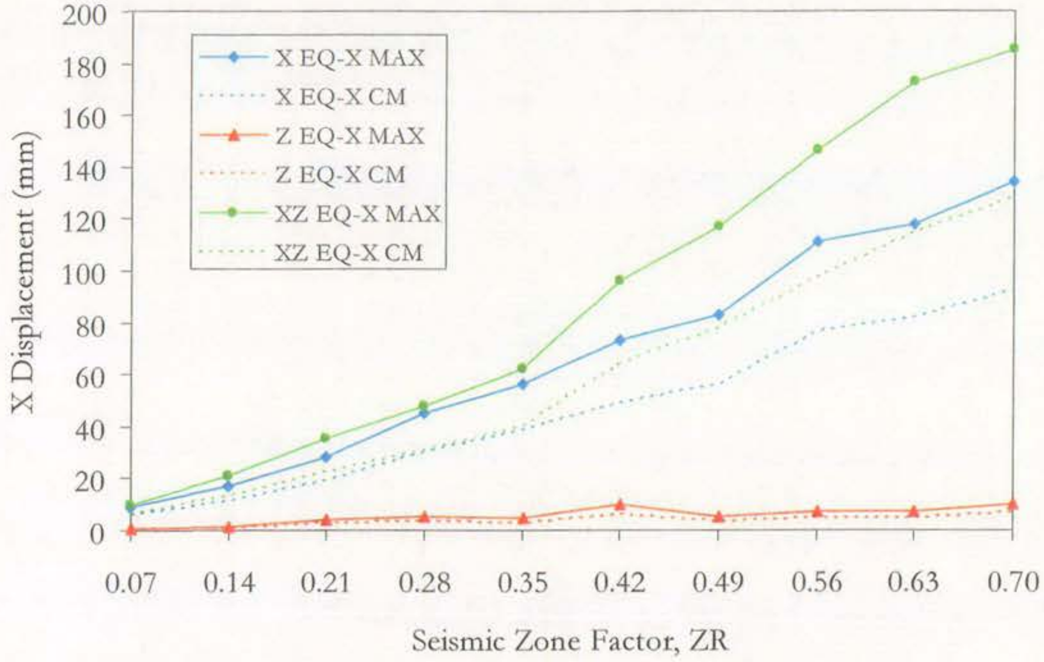

Figure 8-18 14.400 m Deep Wall Z Displacements Soil C NF

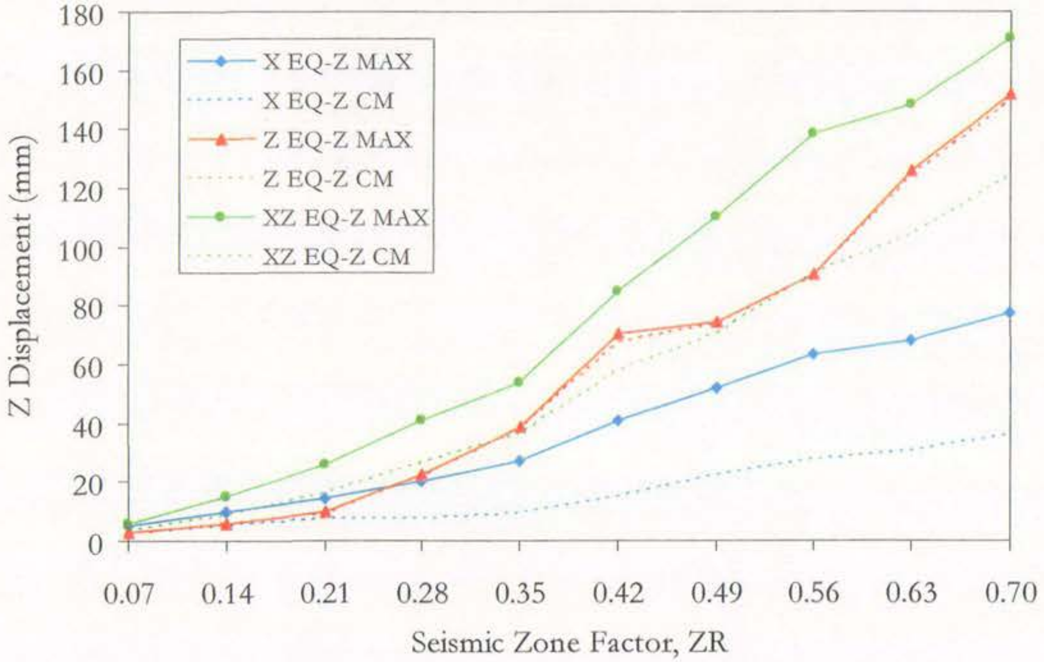

Table 8-6 summarizes the effects of torsion on the two depths of wall for all spring types, for the analyses using the calculated centre of mass location. For each wall, the ratio of maximum displacement at any location on the diaphragm to the centre of mass displacement is listed. The values are listed separately for the X direction and Z direction, in each case when a single earthquake component is applied in that direction and then when both components are applied simultaneously. All the values in Table 8-6 are the average from the three soil types and all ten earthquake amplitudes per soil type, a total of 30 data points.

1. For displacements in the X direction, torsion increases displacements by between 30% and 50%. The torsion is a weak function of soil stiffness, with a slight increase as the soil stiffness increases from clay to rock. There is essentially no difference in torsional displacements when the two components are applied simultaneously, with some values increasing slightly and others decreasing slightly. The differences between the 7.200 m deep and 14.400 deep wall are relatively small.

2. For displacements in the Z direction there is very little increase in displacements due to torsion when only the Z earthquake component is input. However, when both components are applied simultaneously there is a large increase due to torsion, ranging from a 22% to a 122% increase. The torsion effect is a strong function of soil spring stiffness and is higher for the 14.400 m wall than the 7.200 m wall.

The U-shaped walls are symmetrical for loading along the Z axis which is why there are small torsional increases for the case where a single component is applied along this axis.

Table 8-6 Torsional Displacements U-Shaped Walls

Wall Depth	Soil Spring Set	X Direction $\Delta_{XMAX}/\Delta_{XCM}$		Z Direction $\Delta_{ZMAX}/\Delta_{ZCM}$	
		X Earthquake	X + Z Earthquake	Z Earthquake	X + Z Earthquake
7.200 m	B Clay	1.34	1.32	1.05	1.22
	E Gravel	1.43	1.39	1.04	1.37
	G Rock	1.48	1.42	1.02	1.46
14.400 m	B Clay	1.47	1.50	1.04	1.61
	E Gravel	1.49	1.52	1.05	1.85
	G Rock	1.48	1.52	1.04	2.12

Table 8-7 summarizes the effects of two components of earthquake versus a single component on the two depths of wall for all spring types, for the analyses using the calculated centre of mass location. For each configuration, the ratio of 2-component displacement to 1-component displacement is listed, both for centre of mass (diaphragm) displacements and maximum displacements anywhere on the floor. As for Table 8-6, all the values in Table 8-7 are the average from the three soil types and all ten earthquake amplitudes per soil type, a total of 30 data points.

1. Two components applied simultaneously increase the displacements for both directions, all spring types and for both the centre of mass and maximum conditions.

2. The increases are a strong function of soil stiffness, with much higher increases on rock than on clay.

3. For the 7.200 m wall the increase is greater in the X than the Z direction but for the 14.400 m wall the opposite applies. The ratios are large numbers for the stiff soil

types in the X direction, with the 2-component earthquake producing displacements twelve times as high as the 1-component earthquake.

Table 8-7 Comparison of 2 Component and 1 Component Earthquakes U-Shaped Walls

Wall Depth	Soil Spring Set	X Direction Δ_{XZ}/Δ_X		Z Direction Δ_{XZ}/Δ_Z	
		Diaphragm Displacement	Maximum Displacement	Diaphragm Displacement	Maximum Displacement
7.200 m	B Clay	1.14	1.12	1.06	1.23
	E Gravel	1.37	1.33	1.00	1.33
	G Rock	2.00	1.91	1.16	1.73
14.400 m	B Clay	1.26	1.28	1.21	1.90
	E Gravel	1.34	1.37	2.09	3.73
	G Rock	1.70	1.73	6.07	12.02

The ratio between the Z displacements for the 1-component and 2-component earthquakes for the 14.400 m wall on rock is plotted for all 30 data points in Figure 8-19. The average of these data points is the 12.02 value listed in Table 8-7.

Figure 8-19 shows that the factors are higher for soil type D than soil types B or C and also that, regardless of soil type, the factor increases from a low value to a maximum at approximately one-half the maximum seismic amplitude after which it reduces.

Figure 8-19 Effect of 2-Component EQ : 14.4 m U-Shaped Wall on Rock

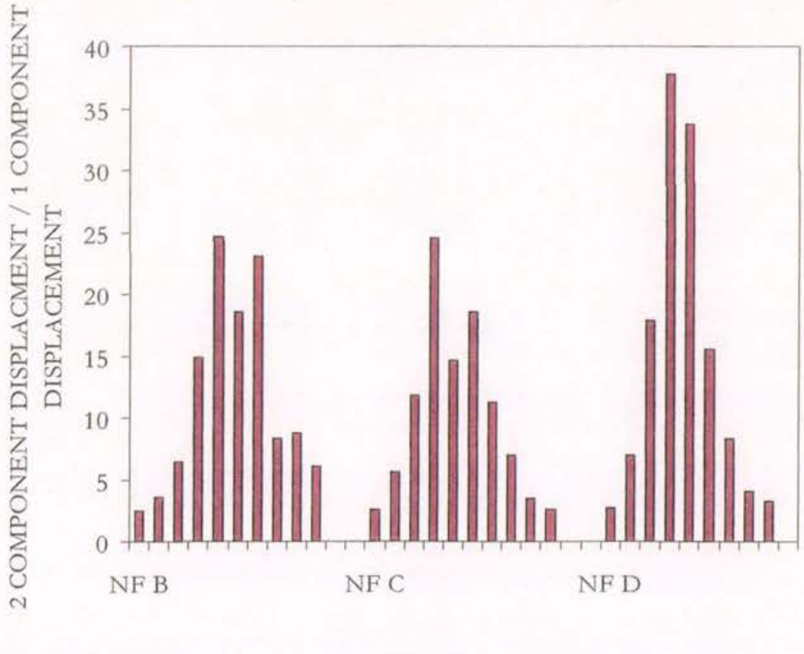

Figure 8-20 plots the Z displacements versus amplitude for the Soil Type D, for both the 1-component earthquake (Dz Z) and the 2-component earthquake (Dz XZ).

- At ZR = 0.35, one half the maximum amplitude, the 1-component displacement of 1.1 mm increases to 36.7 mm under 2 components, an increase by a factor of 33.4.

- At ZR = 0.70, the maximum amplitude, the 1-component displacement of 70.4 mm increases to 167.5 mm under 2 components, an increase by a factor of 2.4.

It appears that the major difference caused by the 2-component earthquake relative to the 1-component earthquake is that the simultaneous components initiate rocking at a lower earthquake amplitude and displacements increase rapidly once uplift occurs.

Figure 8-20 Displacements of 14.400 m U-Shaped Wall

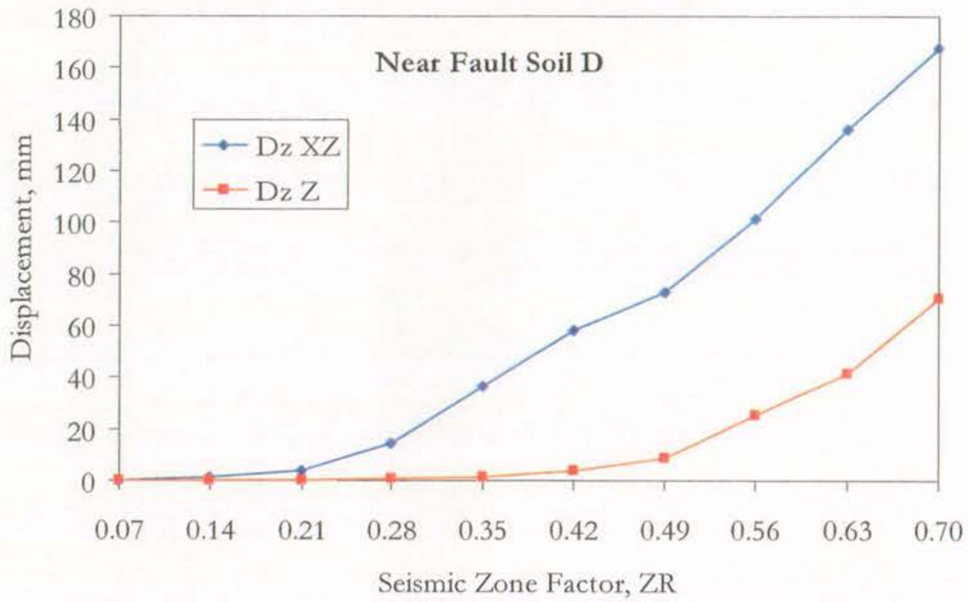

8.3.4.3 Effect of Mass Eccentricity

The effect of the NZS1170 specified accidental eccentricity of 0.10 times the structure dimension is demonstrated in Figures 8-21 to 8-24 by plotting the displacements for the calculated centre of mass and with the centre of mass moved by +10% and -10% of the structure dimension. The curves for no eccentricity on these figures match the plots for maximum displacement in Figures 8-15 to 8-18 above.

These figures show some of the effects of eccentricity on three dimensional, non-symmetrical models:

- For X displacements on the 7.200 m deep wall, the results in Figures 8-21 show that the results are relatively insensitive to eccentricity except when the earthquake is applied along the Z axis. In this last case the displacements are increased by a factor of 3 but the absolute values are quite small, much lower than when the load is applied along the X axis or concurrently along the X and Z axes.

- For Z displacements on the 7.200 m deep wall, the results in Figures 8-22 show that the results are relatively insensitive to eccentricity regardless of earthquake direction.

Figure 8-21 7.200 m Deep Wall Maximum X Displacements Soil C NF

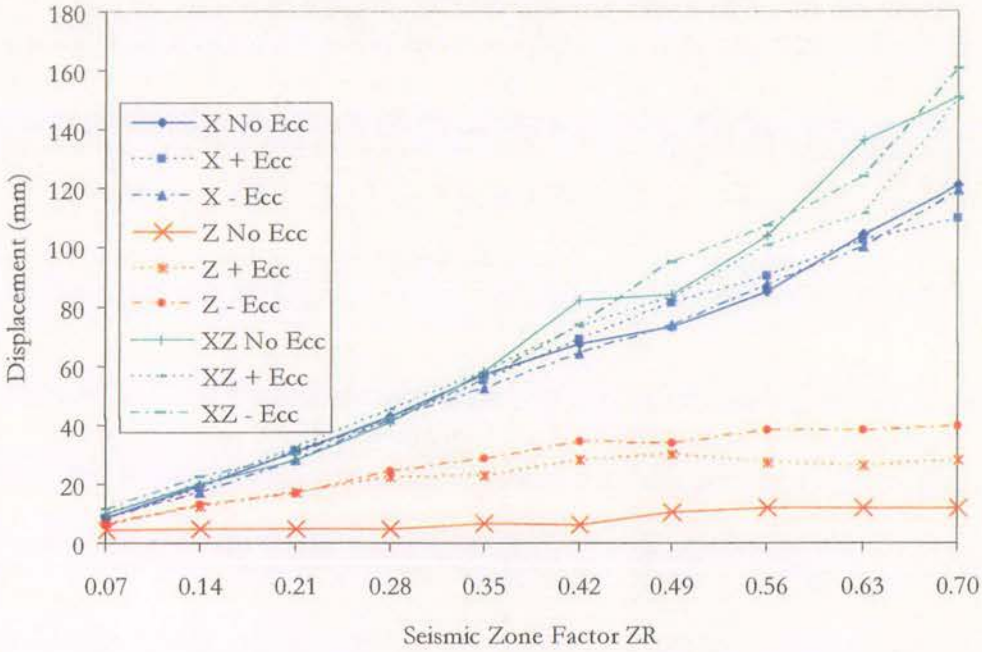

Figure 8-22 7.200 m Deep Wall Maximum Z Displacements Soil C NF

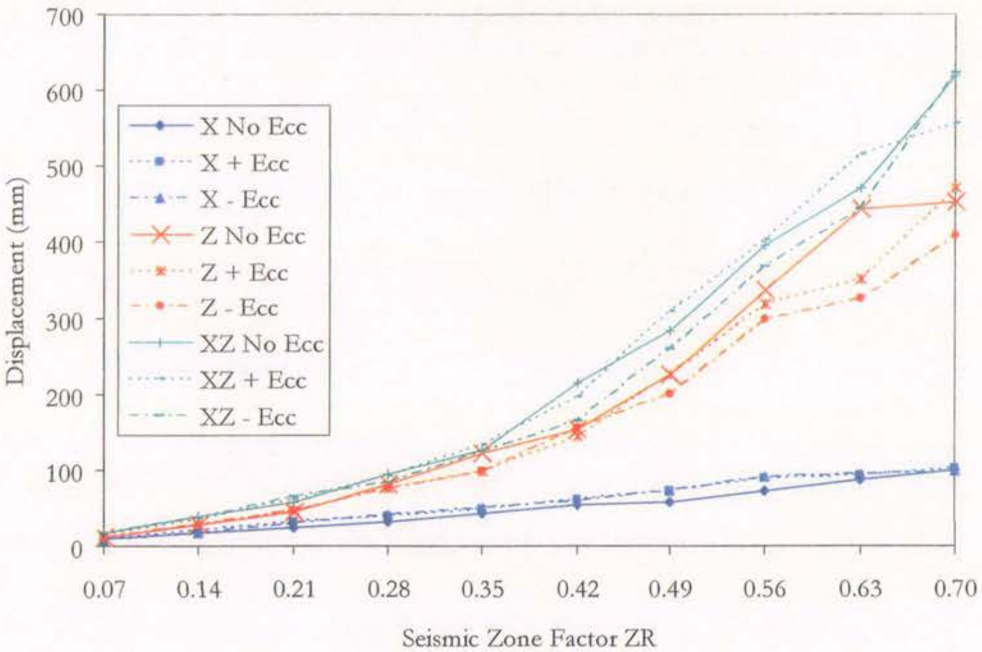

- For X displacements on the 14.400 m deep wall, the results in Figures 8-23 show a similar pattern to that for the 7.200 m wall. The results are relatively insensitive to eccentricity except when the earthquake is applied along the Z axis. In this last case the displacements are increased by a factor of over 3 but the absolute values are quite small, much lower than when the load is applied along the X axis or concurrently along the X and Z axes.

- For Z displacements on the 14.400 m deep wall, the results in Figures 8-24 show that the results are relatively insensitive to eccentricity regardless of earthquake direction, again similar results to that for the 7.200 m long wall.

Figure 8-23 14.400 m Deep Wall Maximum X Displacements Soil C NF

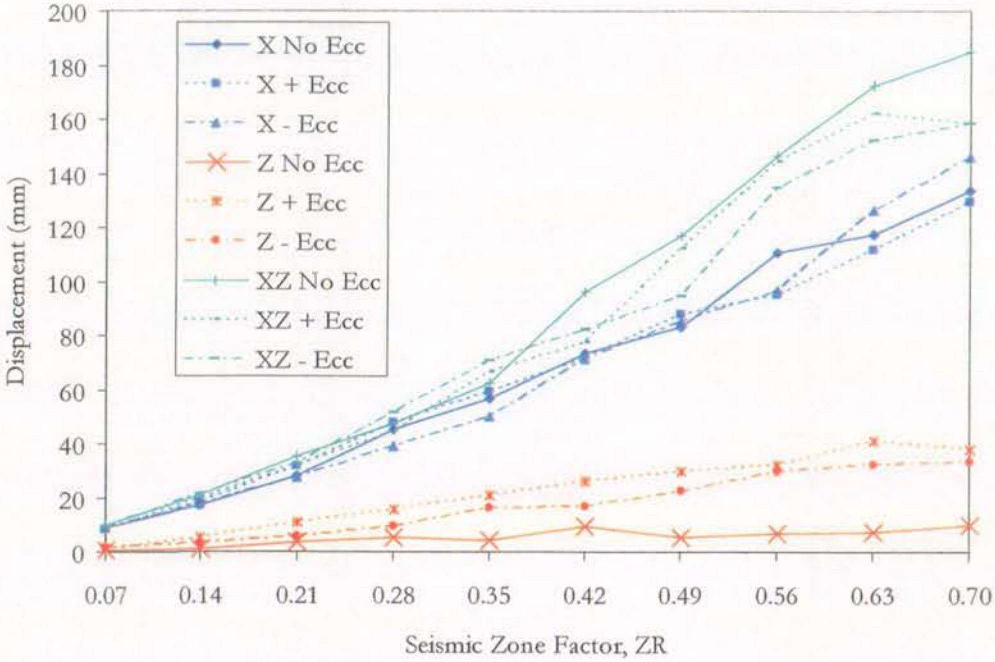

Figure 8-24 14.400 m Deep Wall Maximum Z Displacements Soil C NF

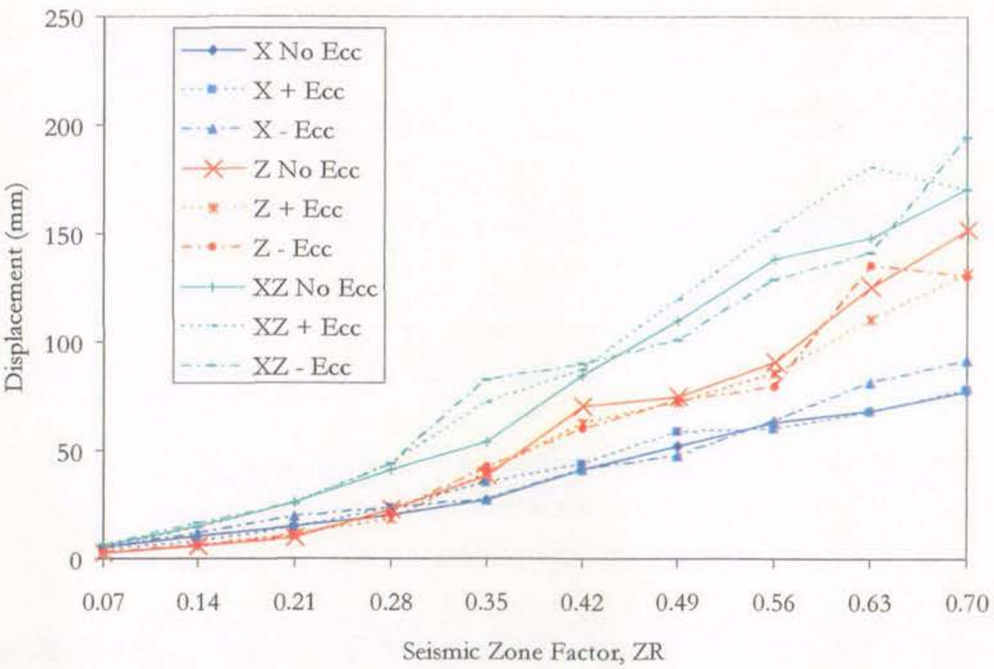

Tables 8-8 and 8-9 summarize the effects of eccentricity on maximum X and Z displacements respectively. For each configuration, the ratio is calculated as the maximum absolute displacements for either the positive or negative eccentricity analyses divided by the maximum absolute displacement for the analysis at the calculated centre of mass. All the values in Table 8-7 are the average from the three soil types and all ten earthquake amplitudes per soil type, a total of 30 data points.

The values in Table 8-8 and 8-9 show that on average the effects of accidental eccentricity are relatively low for the U-shaped walls, with a maximum effect of -3% and +20%. There are no clear patterns in terms of direction or whether 1 or 2 components are applied, although the effects of eccentricity do seem to be slightly more marked for the stiffer soil springs.

Table 8-8 Ratio of X Displacements with Eccentricity to No Eccentricity

Wall Depth	Soil Spring Set	X Maximum Displacement $\Delta_{MAX(E+,E-)}/\Delta_{E0}$		X Diaphragm Displacement $\Delta_{MAX(E+,E-)}/\Delta_{E0}$	
		X Earthquake	X + Z Earthquake	Z Earthquake	X + Z Earthquake
7.200 m	B Clay	1.00	1.05	1.02	1.10
	E Gravel	1.01	1.05	1.07	1.10
	G Rock	1.10	0.91	1.20	0.94
14.400 m	B Clay	1.03	0.97	1.07	1.04
	E Gravel	1.03	0.98	1.09	1.04
	G Rock	1.11	0.97	1.20	1.04

Table 8-9 Ratio of Z Displacements with Eccentricity to No Eccentricity

Wall Depth	Soil Spring Set	X Maximum Displacement $\Delta_{MAX(E+,E-)}/\Delta_{E0}$		X Diaphragm Displacement $\Delta_{MAX(E+,E-)}/\Delta_{E0}$	
		X Earthquake	X + Z Earthquake	Z Earthquake	X + Z Earthquake
7.200 m	B Clay	0.96	1.03	0.91	1.03
	E Gravel	0.98	1.09	0.89	1.15
	G Rock	1.01	0.97	0.86	1.06
14.400 m	B Clay	1.00	1.12	0.95	1.20
	E Gravel	0.99	1.13	0.90	1.29
	G Rock	1.21	1.05	0.99	1.33

8.3.5 Calculation of Strength Properties

The calculation of strength properties is more complex for non-planar and multiple walls than for single walls. The procedure used is tabulated in Table 8-10 for the 7.200 m deep wall and Table 8-11 for the 14.400 m wall. For each wall, the procedure followed was the same:

1. Obtain axial forces in each spring by performing a static gravity load analysis and tabulate along with coordinates of each spring.

2. Take moments about each of the two horizontal axes for both positive and negative sense of bending and calculate the position of the centroid. For moments about the Z axis (axis of symmetry) the centroid is at 7.200 m (midway along the back wall) for both the 7.200 m and 14.400 m walls.

3. Calculate the moment capacity as the total axial load times the distance to the centroid and the force capacity as the moment divided by the wall height.

Table 8-10 Calculation of Strength for 7.200 m Deep Wall

Column Number	Column Coordinate (m)		Spring Gravity Load, N (kN)	Moment about Z Axis		Moment about X Axis	
	X	Z		Positive N.X	Negative $N(X_{MAX}-X)$	Positive N.Z	Negative $N(Z_{MAX}-Z)$
101	0.000	7.200	148	0	2128	1064	0
113	14.400	7.200	180	2585	0	1292	0
102	1.200	7.200	45	54	593	323	0
103	2.400	7.200	46	110	552	331	0
104	3.600	7.200	47	169	508	338	0
105	4.800	7.200	48	230	460	345	0
106	6.000	7.200	49	293	410	351	0
107	7.200	7.200	50	357	357	357	0
108	8.400	7.200	50	423	302	362	0
109	9.600	7.200	51	490	245	367	0
110	10.800	7.200	52	558	186	372	0
111	12.000	7.200	52	627	125	376	0
112	13.200	7.200	53	696	63	380	0
201	0.000	0.000	51	0	739	0	369
301	14.400	0.000	53	765	0	0	383
202	0.000	1.200	55	0	798	66	332
203	0.000	2.400	59	0	852	142	284
204	0.000	3.600	63	0	906	226	226
205	0.000	4.800	67	0	960	320	160
206	0.000	6.000	70	0	1015	423	85
302	14.400	1.200	53	768	0	64	320
303	14.400	2.400	53	768	0	128	256
304	14.400	3.600	53	768	0	192	192
305	14.400	4.800	53	768	0	256	128
306	14.400	6.000	53	767	0	319	64
Sum			1555	11196	11199	8398	2799
Centroid (m) $= \dfrac{\sum NX}{\sum N}$				7.199	7.201	5.400	1.800
X_{MAX} Z_{MAX}	14.400	7.200					
Moment, M (kN-m) = Sum				11196	11199	8398	2799
Height, H (m)				10.8	10.8	10.8	10.8
Force, F (KN) = M/H				1037	1037	778	259

Table 8-11 Calculation of Strength for 14.400 m Deep Wall

Column Number	Column Coordinate (m)		Spring Gravity Load, N (kN)	Moment about Z Axis		Moment about X Axis	
	X	Z		Positive N.X	Negative $N(X_{MAX}-X)$	Positive N.Z	Negative $N(Z_{MAX}-Z)$
101	0.000	14.400	216	0	3103	3103	0
113	14.400	14.400	183	2640	0	2640	0
102	1.200	14.400	64	76	838	915	0
103	2.400	14.400	63	152	759	911	0
104	3.600	14.400	63	226	679	905	0
105	4.800	14.400	62	299	598	897	0
106	6.000	14.400	62	370	518	888	0
107	7.200	14.400	61	439	439	878	0
108	8.400	14.400	60	505	361	866	0
109	9.600	14.400	59	568	284	852	0
110	10.800	14.400	58	627	209	836	0
111	12.000	14.400	57	683	137	819	0
112	13.200	14.400	56	734	67	800	0
201	0.000	0.000	61	0	883	0	883
301	14.400	0.000	47	684	0	0	684
202	0.000	2.400	69	0	996	166	830
203	0.000	4.800	76	0	1100	367	733
204	0.000	7.200	84	0	1207	604	604
205	0.000	9.600	92	0	1321	881	440
206	0.000	12.000	100	0	1443	1202	240
302	14.400	2.400	64	922	0	154	768
303	14.400	4.800	80	1146	0	382	764
304	14.400	7.200	96	1377	0	688	688
305	14.400	9.600	113	1620	0	1080	540
306	14.400	12.000	130	1876	0	1564	313
Sum			2075	14943	14941	22396	7488
Centroid (m) $= \dfrac{\sum NX}{\sum N}$				7.200	7.200	10.792	3.608
X_{MAX} Z_{MAX}	14.400	14.400					
Moment, M (kN-m) = Sum				14943	14941	22396	7488
Height, H (m)				7.2	7.2	7.2	7.2
Force, F (KN) = M/H				2075	2075	3111	1040

The moments calculated in Tables 8-10 and 8-11 are compared with the capacity curves obtained from a pushover analysis in Figures 8-25 and 8-26 for the 7.200 m and 14.400 m long walls respectively, in each case for the Type B springs. The yield displacement is calculated from the elastic period, as described in Section 7 of this report.

The theoretical capacities for both walls provide a good match to the calculated strengths for loading in both directions and also accurately capture the difference in capacity for positive and negative bending for loading along the Z axis. The yield displacements are underestimated for all cases as they are based on the elastic period whereas under pushover loads the springs separate sequentially, providing continual softening.

Under an X direction load, the 14.400 m wall pushover curve, shown in Figure 8-26, exhibits a tri-linear type of capacity. The second stage of stiffness is when the springs along one flange separate simultaneously, after which the springs along the web separate sequentially. The 7.200 m wall exhibits this characteristic but to a much lesser extent because of the shorter flanges.

Figure 8-25 Calculated Strength for 7.200 m Deep Wall

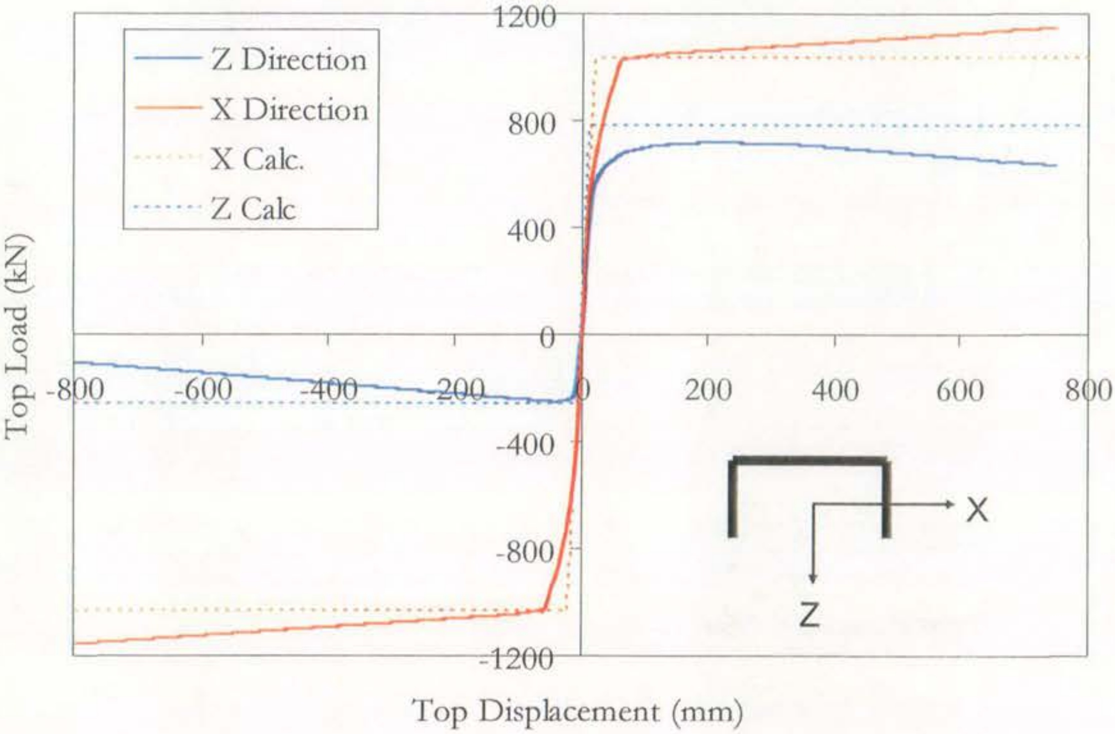

Figure 8-26 Calculated Strength for 14.400 m Deep Wall

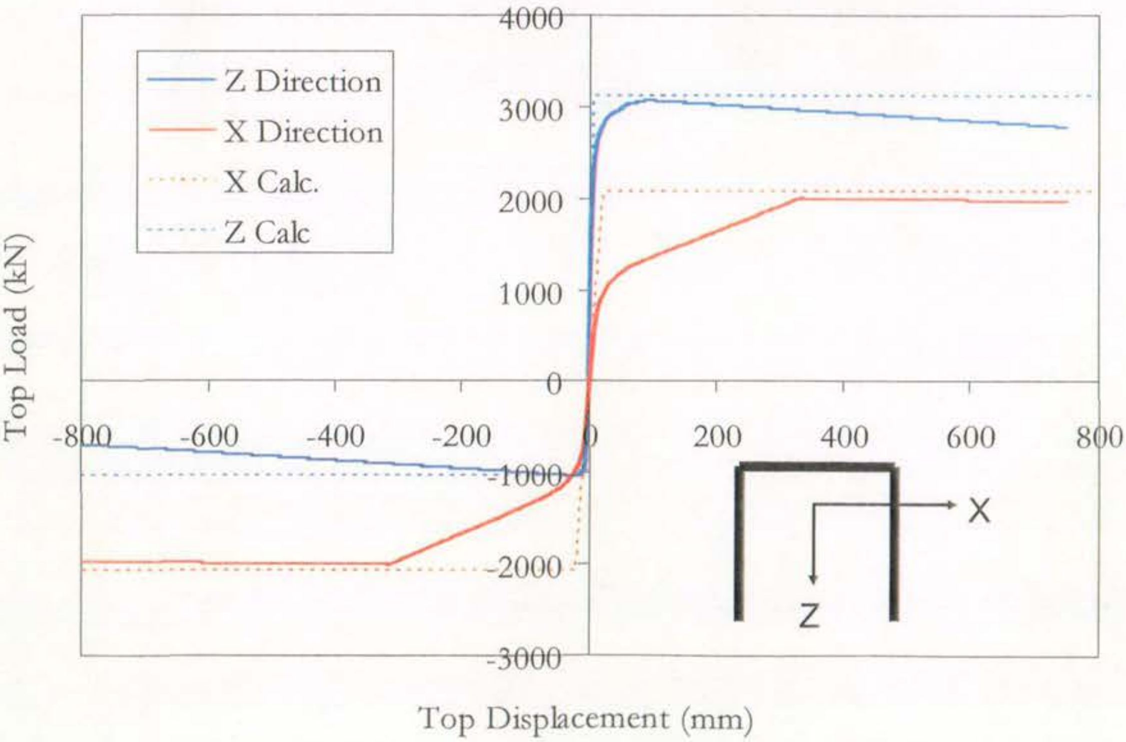

8.4 Non-Symmetrical Walls

There are a wide range of wall structures with non-symmetrical layouts of walls and it is not practical to develop design procedures which encompass all possible permutations. A single model with non-symmetrical walls was developed to assess where differences occurred compared to the planar wall and U-shaped wall models.

8.4.1 Analysis Model

The single wall layout as shown in Figure 8-27 was evaluated. This was a two story square building with 3.600 m long walls on two adjacent elevations and 7.200 m long walls on the other two adjacent elevations.

Figure 8-27 Layout of 2 Story Non-Symmetrical Wall Layout

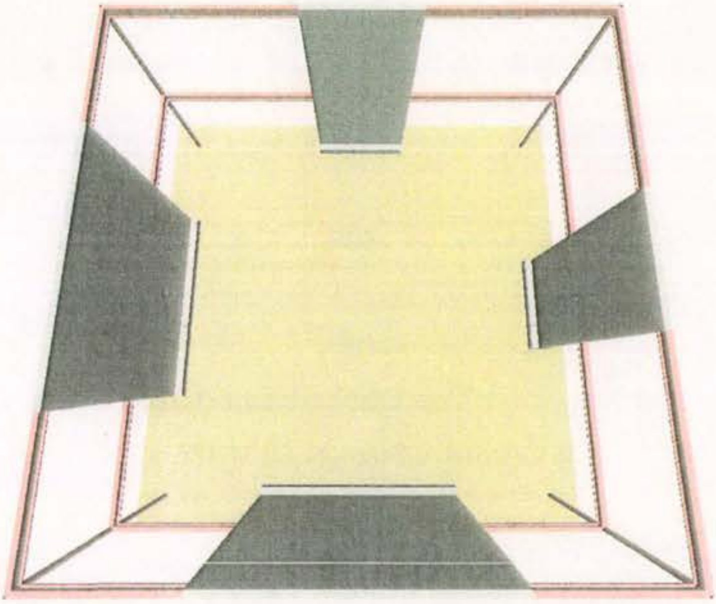

The model development followed the same principles as for the planar walls in terms of the gaps elements and spring stiffness values. Modelling features of the superstructure were:

- The 7.2 m walls were divided into 6 segments and the 3.6 m walls into 4 segments, as shown in Figure 8-28.
- The floor seismic weight was 7.5 KPa at each floor. The floor mass, and the rotational moment of inertia, was lumped at the geometric centroid of the building. For the variation with accidental eccentricity, the location of the centroid was moved parallel to each axis by an amount of 0.1 times the dimension of the building in that direction.
- Spring stiffness values were calculated as for individual walls.
- Pinned columns were used at the corners to support part of the floor load but these columns did not contribute to the lateral strength of the building.

- The floors were assumed to span two ways. Gravity loads were applied as uniform loads of 27 kN/m to beams along each of the four elevations at each floor level. The walls supported 69% of the total seismic weight and the four corner columns the remaining 31%.

Figure 8-28 Non-Symmetric Wall Model Definition

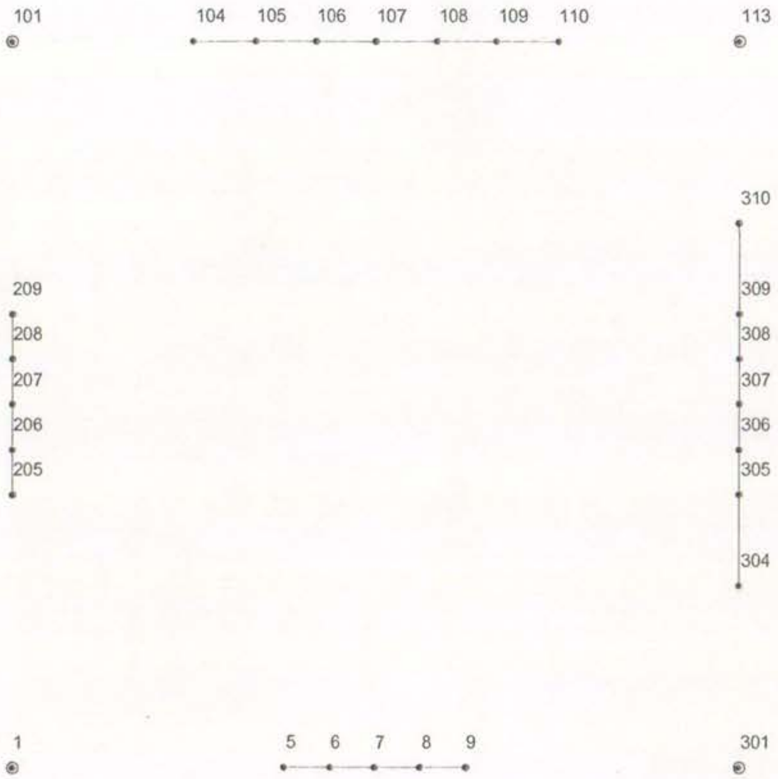

Each wall was evaluated for three different soil spring sets, B, E and G which correspond respectively to medium clay, medium gravel and rock in order of ascending stiffness.

8.4.2 Dynamic Properties

Table 8-3 lists the dynamic properties of the building for each spring set and the shape of the first two modes is plotted in Figures 8-29 and 8-30. The wall layout is such that the modal deformations are along the diagonals, at 45 degrees to the model coordinate axes. This is manifest by equal participation factors and equal effective mass factors in both the X and Z directions for the first two modes.

Because the first two modes have equal participation about both axes, the effective mass factors and the product of mode shape and participation factor, φPF, is low for all spring types compared to the single wall models, where the effective mass would typically be 95%-90% and φPF 1.2 for two story walls. This has an impact on the application of the design procedure to estimate displacements, as discussed later in this section.

Table 8-12 Dynamic Properties of Non-Symmetric Walls

	+X+Z Direction	-X+Z Direction
Medium Clay Springs		
Period (seconds)	0.648	0.758
Effective Mass, M_{EFF}	55.6%	53.9%
Mode Shape x PF = φPF	0.743	0.721
Medium Gravel Springs		
Period (seconds)	0.320	0.42
Effective Mass, M_{EFF}	47.0%	42.6%
Mode Shape x PF = φPF	0.633	0.577
Rock Springs		
Period (seconds)	0.138	0.203
Effective Mass, M_{EFF}	42.8%	35.3%
Mode Shape x PF = φPF	0.604	0.508

Figure 8-29 Non-Symmetric Wall Mode 1

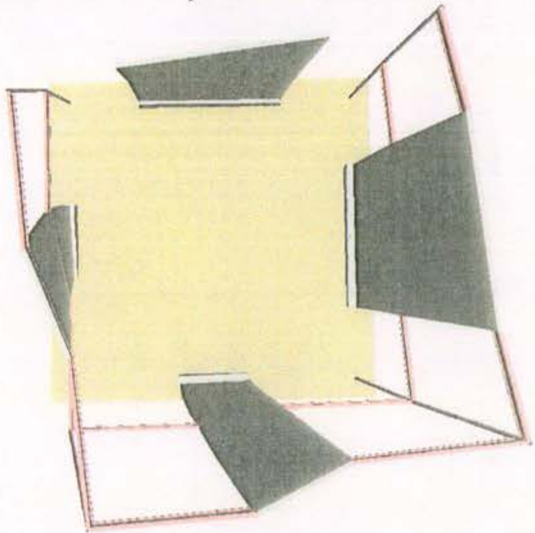

Figure 8-30 Non-Symmetric Wall Mode 2

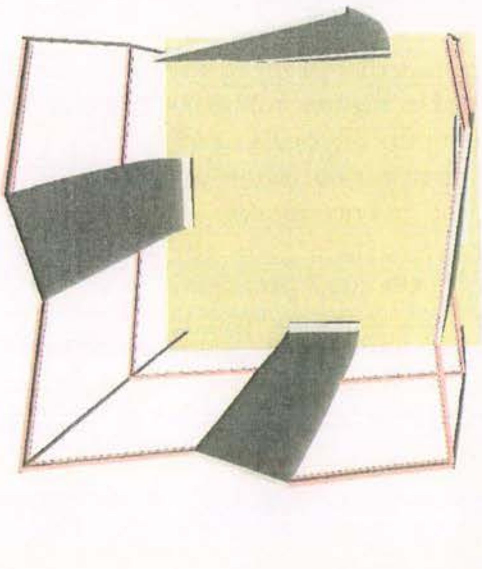

8.4.3 Wall Strength Properties

The strength properties of the wall were extracted from the model by applying a cyclic displacement trace at the top of the wall and recording the force at each step. Figure 8-31 plots the lateral load capacity for the soil springs based on medium clay for loads along each model axis. As the building has an equal total wall length in each direction the capacity curves are almost identical in the two directions.

Figure 8-31 Lateral Capacity of Non-Symmetrical Wall on Medium Clay Soil Springs

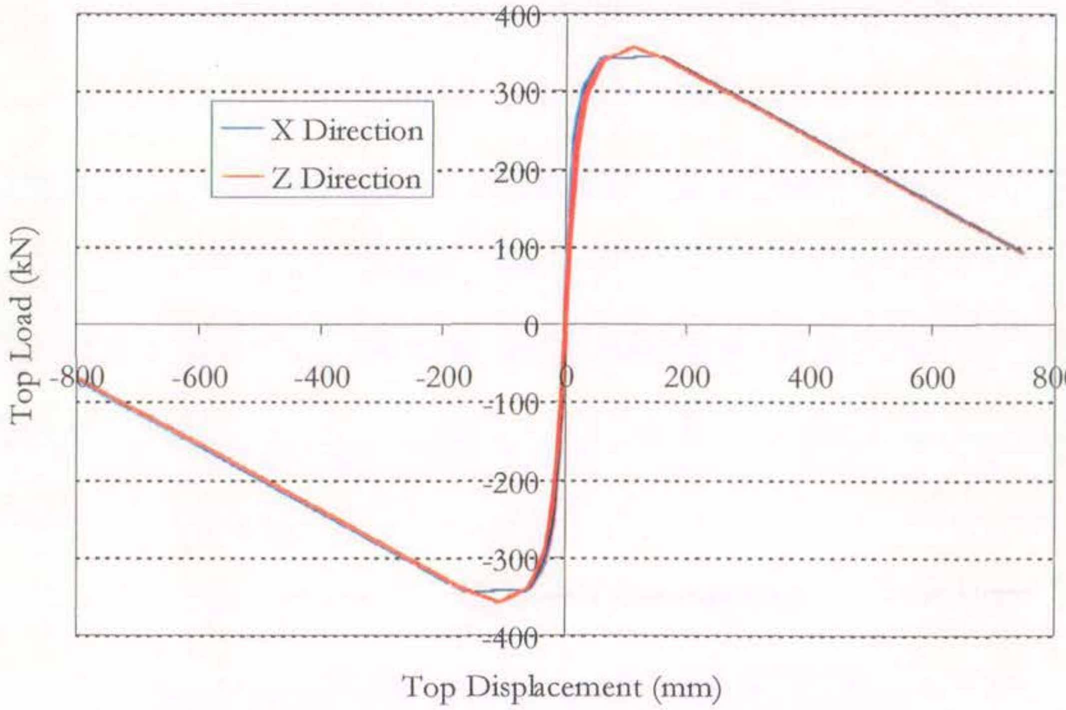

8.4.4 Time History Results

The non-symmetric wall was evaluated for the same variations as for the U-walls, as listed in Table 8-4 above. For the model with no accidental eccentricity, each of the three spring types was evaluated for three load directions (X and Z directions separately and then both simultaneously) for three spectrum shapes in a near fault location. The analyses for the spectrum shape corresponding to Soil Class C were then repeated for two additional eccentricity configurations, with the mass centroid moved 0.1B in the positive and negative directions respectively.

Results were processed as for the U-shaped walls above. Two examples of results obtained from the analyses are shown in Figures 8-32 and 8-33:

1. Figure 8-32 plots the X and Z displacements as a function of earthquake amplitude for the analysis with both components applied simultaneously. For each direction both the diaphragm centroid displacement and the maximum displacements are plotted. The difference between the two represents the

torsional component of displacement. For this wall, the torsional displacement with no accidental eccentricity is small for the full range of amplitude.

2. Figure 8-33 plots the base shear against diaphragm displacement for each of soil types B, C and D. Plots are given for both the X and the Z directions. The curves are approximately the same in both directions, as expected because of the equal strength shown in Figure 8-31. There are some inconsistencies at high amplitudes because not all 7 runs for a specific amplitude and soil class completed. The Soil B and Soil C curves follow the same trace but the response for Soil D appears to produce a lower base shear coefficient for a given displacement, indicating that the inertia load distribution is different for these records.

Figure 8-32 Displacements: Non-Symmetric Wall Clay Springs XZ Load NF B

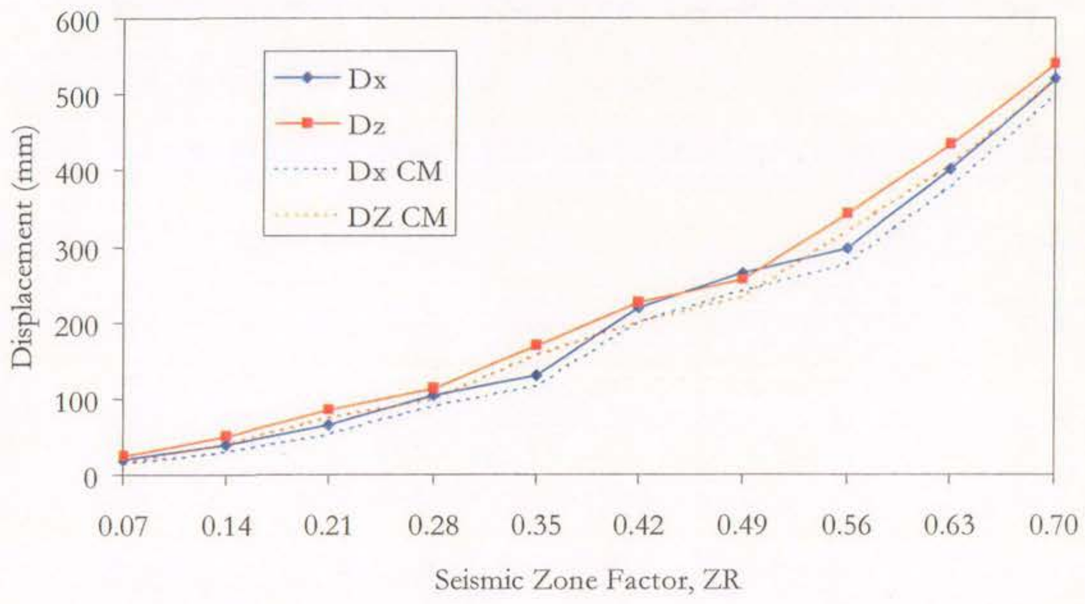

Figure 8-33 Shears: Non-Symmetric Wall Clay Springs XZ Load Near Fault

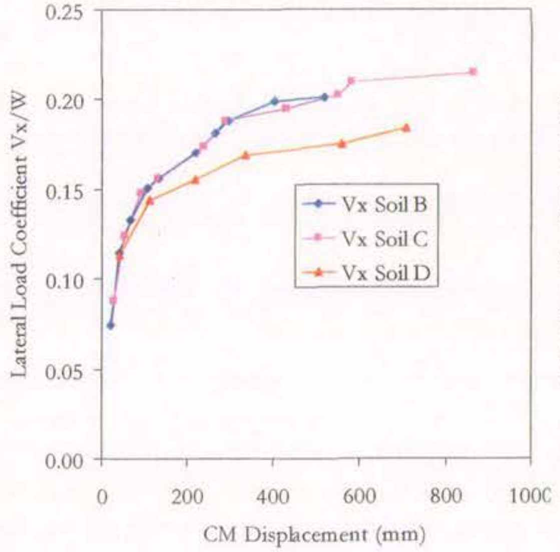

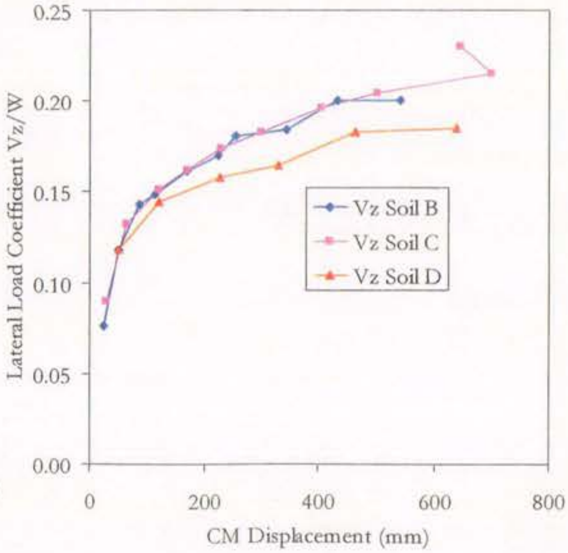

8.4.5 Effect of Concurrency

The effect of applying two horizontal components simultaneously is demonstrated in Figures 8-34 and 8-35 by plotting the displacements for three analyses, (a) one component applied along the X axis, (b) one component applied along the Z axis and (c) components applied along each axis simultaneously. For each variation, displacements are plotted at the centre of mass of the diaphragm (CM) and also the maximum at any location on the diaphragm (MAX). The difference between these two curves is an indication of the effect of torsion. The analyses plotted in Figures 8-34 and 8-35 are for the configuration with the mass located at the calculated centroid so there is no "accidental" eccentricity added to the "natural" eccentricity.

These figures show that:

1. The response is little affected by whether one or two components are applied simultaneously.

2. There is very little movement orthogonal to the direction of load, that is, there is a very small X displacement when the load is applied parallel to Z and vice versa.

3. There is almost no torsional response for the calculated centre of mass models, in that displacements at the centre of mass are almost identical to the maximum displacements at any location on the diaphragm.

4. The X and the Z displacements, shown in Figures 8-34 and 8-35 respectively, exhibit almost identical response characteristics.

Figure 8-34 Non-Symmetric Wall X Displacements Medium Clay Soil C NF

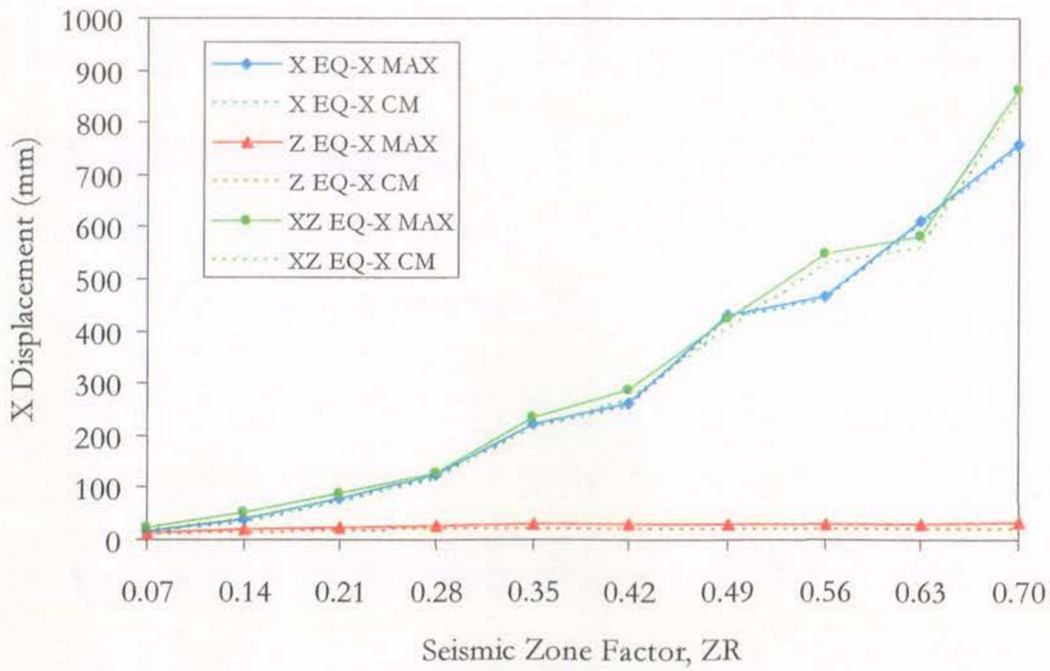

Figure 8-35 Non-Symmetric Wall Z Displacements Medium Clay Soil C NF

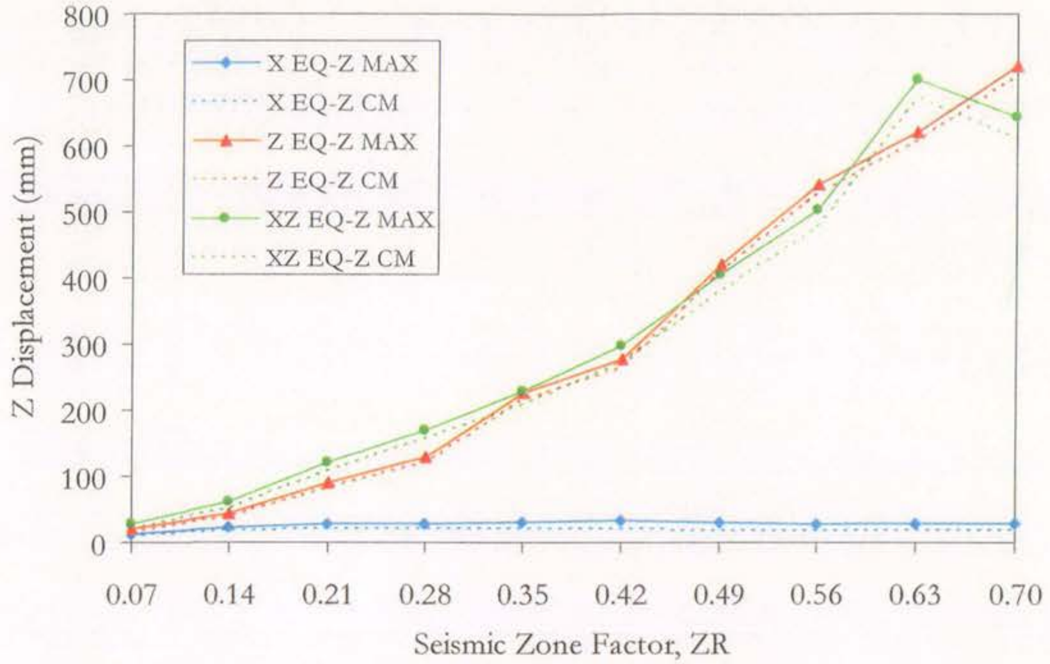

Table 8-13 summarizes the effects of torsion for all spring types, for the analyses using the calculated centre of mass location. For each wall, the ratio of maximum displacement at any location on the diaphragm to the centre of mass displacement is listed. The values are listed separately for the X direction and Z direction, in each case when a single earthquake component is applied in that direction and then when both components are applied simultaneously. All the values in Table 8-13 are the average from the three soil types and all ten earthquake amplitudes per soil type, a total of up to 30 data points. There are some trends apparent from Table 8-13:

1. The effect of torsion is consistently higher when two components are applied simultaneously then when a single component is applied.

2. The effect of torsion is consistently higher when the soil spring stiffness increases.

Table 8-13 Torsional Displacements: Non-Symmetric Wall

Wall Depth	Soil Spring Set	X Direction $\Delta_{XMAX}/\Delta_{XCM}$		Z Direction $\Delta_{ZMAX}/\Delta_{ZCM}$	
		X Earthquake	X + Z Earthquake	Z Earthquake	X + Z Earthquake
7.200 m	B Clay	1.07	1.15	1.07	1.13
	E Gravel	1.10	1.30	1.11	1.29
	G Rock	1.17	1.47	1.19	1.54

Table 8-14 summarizes the effects of two components of earthquake versus a single component, again for the analyses using the calculated centre of mass location. For each configuration, the ratio of 2-component displacement to 1-component displacement is listed, both for centre of mass (diaphragm) displacements and maximum displacements anywhere on the floor. As for Table 8-13, all the values in Table 8-14 are the average from the three soil types and all ten earthquake amplitudes per soil type, a total of up to 30 data points.

1. Two components applied simultaneously increase the displacements for both directions, all spring types and for both the centre of mass and maximum conditions.

2. The increases are a strong function of soil stiffness, with much higher increases on rock than on clay.

Table 8-14 Comparison of 2 Component and 1 Component Earthquakes Non-Symmetric Wall

Wall Depth	Soil Spring Set	X Direction Δ_{XZ}/Δ_X		Z Direction Δ_{XZ}/Δ_Z	
		Diaphragm Displacement	Maximum Displacement	Diaphragm Displacement	Maximum Displacement
7.200 m	B Clay	1.05	1.13	1.10	1.16
	E Gravel	1.05	1.25	1.13	1.31
	G Rock	1.28	1.62	1.28	1.65

Figure 8-19 plots the maximum Z direction factors for each soil class and seismic amplitude. The mean of the results in Figure 8-19 are those listed in Table 8-14 (1.16 for clay, 1.65 for rock). Figure 8-19 shows that the amplitude of the factors is generally similar for the three soil classes but is strongly influenced by the seismic amplitude, with high factors at low amplitude earthquakes reducing to unity at high amplitudes.

Figure 8-36 Effect of 2-Component EQ: Z Displacements for Non-Symmetric Wall

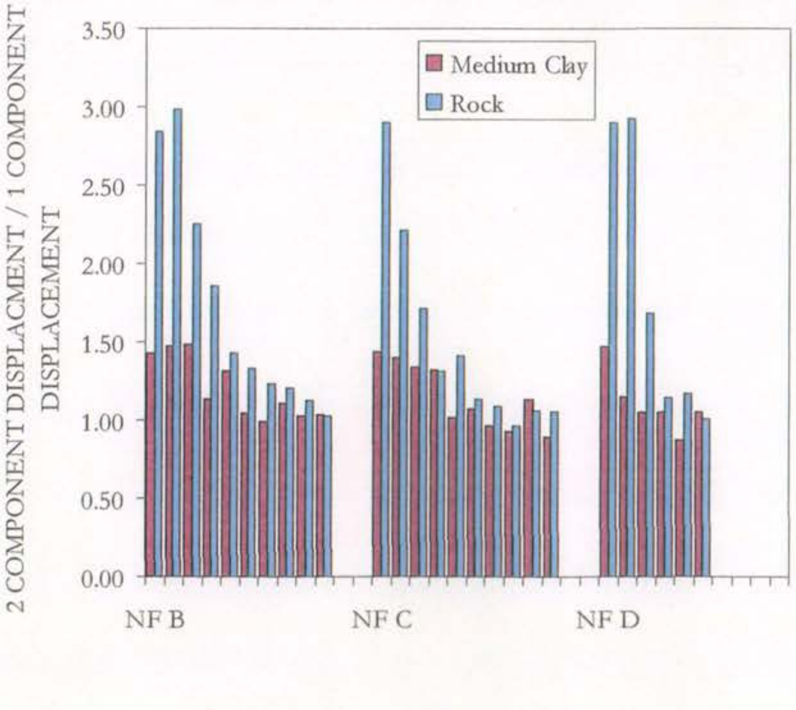

8.4.5.1 Effect of Mass Eccentricity

The effect of the NZS1170 specified accidental eccentricity of 0.10 times the structure dimension is demonstrated in Figures 8-36 and 8-37 which plot the displacements for the calculated centre of mass and with the centre of mass moved +10% and -10% of the structure dimension. The plots for no eccentricity match the plots for maximum displacement in Figures 8-34 and 8-35 above.

These plots show that the displacements are relatively insensitive to an accidental eccentricity with no clear pattern of increased displacement due to eccentricity.

Tables 8-15 and 8-16 summarize the effects of eccentricity on maximum X and Z displacements respectively. For each configuration, the ratio is calculated as the maximum absolute displacements for either the positive or negative eccentricity analyses divided by the maximum absolute displacement for the analysis at the calculated centre of mass. All the values are the average from the three soil types and all ten earthquake amplitudes per soil type, a total of 30 data points.

The values in Table 8-8 and 8-9 show that on average the effects of accidental eccentricity are relatively low for this wall, with a maximum effect of -8% and +14%., which is less than the variation between earthquake records. There are no clear patterns in terms of direction, number of components applied or soil spring stiffness value.

Table 8-15 Ratio of X Displacements with Eccentricity to No Eccentricity

Wall Depth	Soil Spring Set	X Maximum Displacement $\Delta_{MAX(E+,E-)}/\Delta_{E0}$		X Diaphragm Displacement $\Delta_{MAX(E+,E-)}/\Delta_{E0}$	
		X Earthquake	X + Z Earthquake	Z Earthquake	X + Z Earthquake
7.200 m	B Clay	1.07	0.92	1.07	0.98
	E Gravel	1.07	0.94	1.08	1.06
	G Rock	1.01	0.86	1.07	0.99

Table 8-16 Ratio of Z Displacements with Eccentricity to No Eccentricity

Wall Depth	Soil Spring Set	Z Maximum Displacement $\Delta_{MAX(E+,E-)}/\Delta_{E0}$		Z Diaphragm Displacement $\Delta_{MAX(E+,E-)}/\Delta_{E0}$	
		X Earthquake	X + Z Earthquake	Z Earthquake	X + Z Earthquake
7.200 m	B Clay	1.04	1.08	1.06	1.12
	E Gravel	1.06	0.99	1.07	1.08
	G Rock	1.03	0.94	1.11	1.14

Figure 8-37 Non-Symmetric Wall Maximum X Displacements Soil C NF

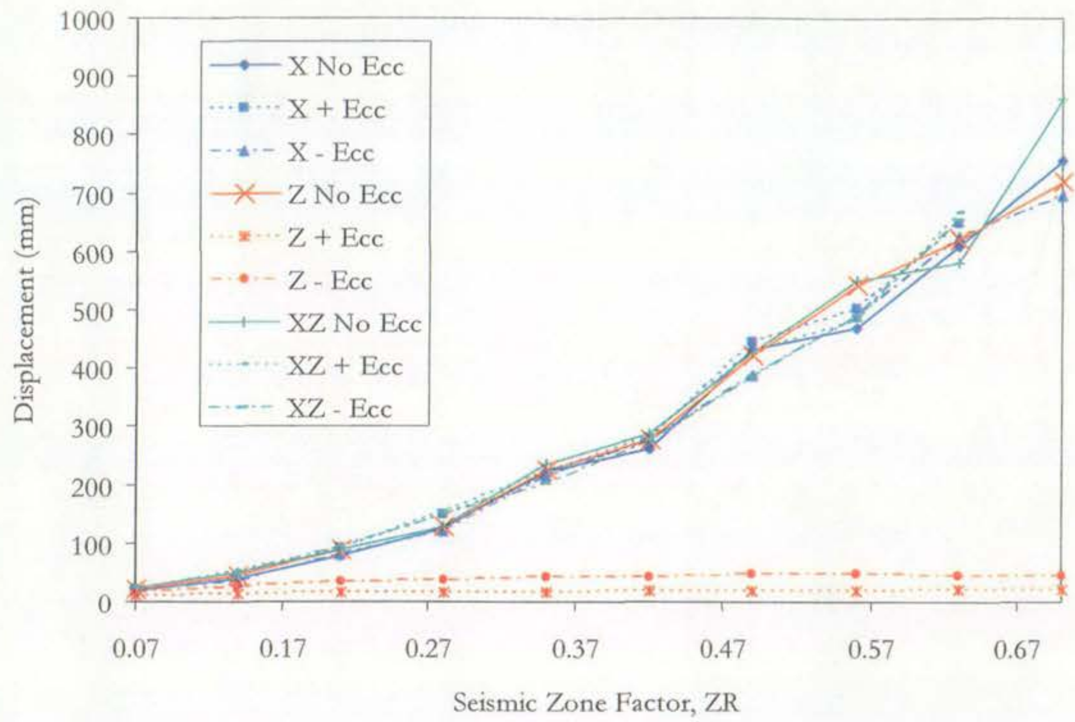

Figure 8-38 Non-Symmetric Wall Maximum Z Displacements Soil C NF

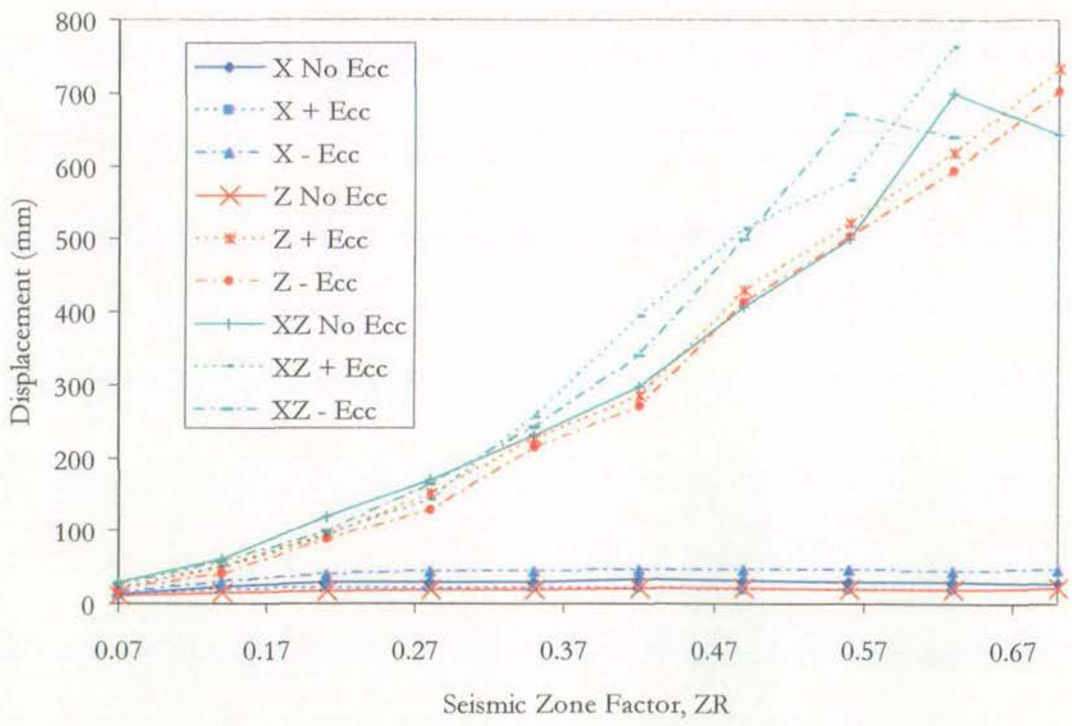

8.4.6 Calculation of Strength Properties

The wall layout for this building is such that the walls on all 4 elevations are independent and the calculated building strength is assembled as the sum of the strengths of the four walls, in a similar fashion as for multiple planar walls. The wall moments are summed in each direction to provide the total strength. As shown in Figure 8-28, the strength compares well with the results of the applied displacement pushover. The wall strengths are not quite identical because there is a difference in spacing of the gap elements on the two 7.200 m walls.

Table 8-17 Calculation of Strength for Non-Symmetric Wall

Column Number	Column Coordinate (m)		Spring Gravity	Wall Length, m		Wall Moment, kN-m	
	X	Z	Load, N (kN)	L_X	L_Z	M_X $=NL_X/2$	M_Z $=NL_Z/2$
5	5.400	0.000	118				
9	9.000	0.000	118				
6	6.300	0.000	83				
7	7.200	0.000	83				
8	8.100	0.000	83				
Sum			486	2.700	0.000	656	0
104	3.600	14.400	93				
110	10.800	14.400	93				
105	4.800	14.400	79				
106	6.000	14.400	79				
107	7.200	14.400	79				
108	8.400	14.400	79				
109	9.600	14.400	79				
Sum			583	6.000	0.000	1750	0
205	0.000	5.400	118				
209	0.000	9.000	118				
206	0.000	6.300	83				
207	0.000	7.200	83				
208	0.000	8.100	83				
Sum			486	0.000	2.700	0	656.1
304	14.400	3.600	94				
310	14.400	10.800	93				
305	14.400	5.400	79				
306	14.400	6.300	79				
307	14.400	7.200	79				
308	14.400	8.100	79				
309	14.400	9.000	79				
Sum			583	0.000	5.400	0	1574.6
Moment						2406	2231
Shear						334	310
V/W						0.107	0.099

Figure 8-39 Calculated Strength for Non-Symmetric Wall

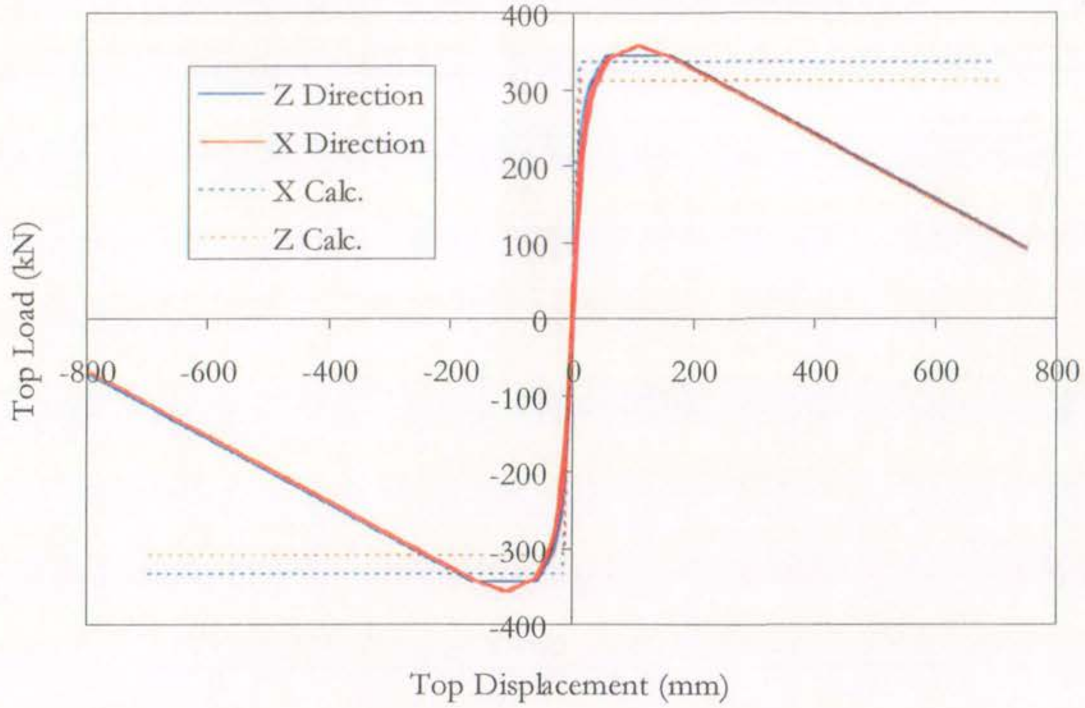

8.5 Assessment of Design Procedure for Non-Planar Walls

8.5.1 Predicted Displacements

Results from the three non-planar walls was assessed to determine whether the design procedure developed from the results on planar walls could be used to predict displacements for more complex systems. The effect of changing wall dynamic characteristics on the predicted displacements was assessed and it was concluded that the best match of predicted and analytical displacements was obtained by:

1. Using the fundamental period as calculated for each direction and the effective mass as calculated for this primary mode, the same as for planar walls.

2. Modifying C_0, the factor which relates the spectral displacement of a SDOF system to the roof of the MDOF system. For the single walls, this was defined as the product of the participation factor times the mode shape component at roof level, which produced values ranging from 1.0 for single story buildings increasing to a range of 1.2 to 1.5 for higher buildings. For the non-planar walls, the product was much less than 1.0 for the X direction of U-shaped walls and both directions of the non-symmetric walls (see Tables 8-3 and 8-12). The low values were in directions where more than one mode contributed to the response. It was found that better predictions where obtained where the values of C_0 were the sum of the mode shape component times participation factor for each mode which contributed significantly to response.

Other than the change to the method of calculating C_0, the procedure to estimate displacements was the same as for planar walls. The procedure was used to calculate displacements of the equivalent single degree of freedom structure and so does not include any torsional effects. For this reason, these results below compare predicted displacements with the analysis results at the centroid of the floor, not the maximum value. The effect of torsion is assessed separately.

The match of calculated displacements to analysis displacements ranged from very good (Figure 8-40, the symmetrical wall on soft springs) to very poor (Figure 8-41, the U-shaped wall with 14.400 m long flanges on stiff springs).

Figure 8-40 Non-Symmetrical Wall Medium Clay X Direction

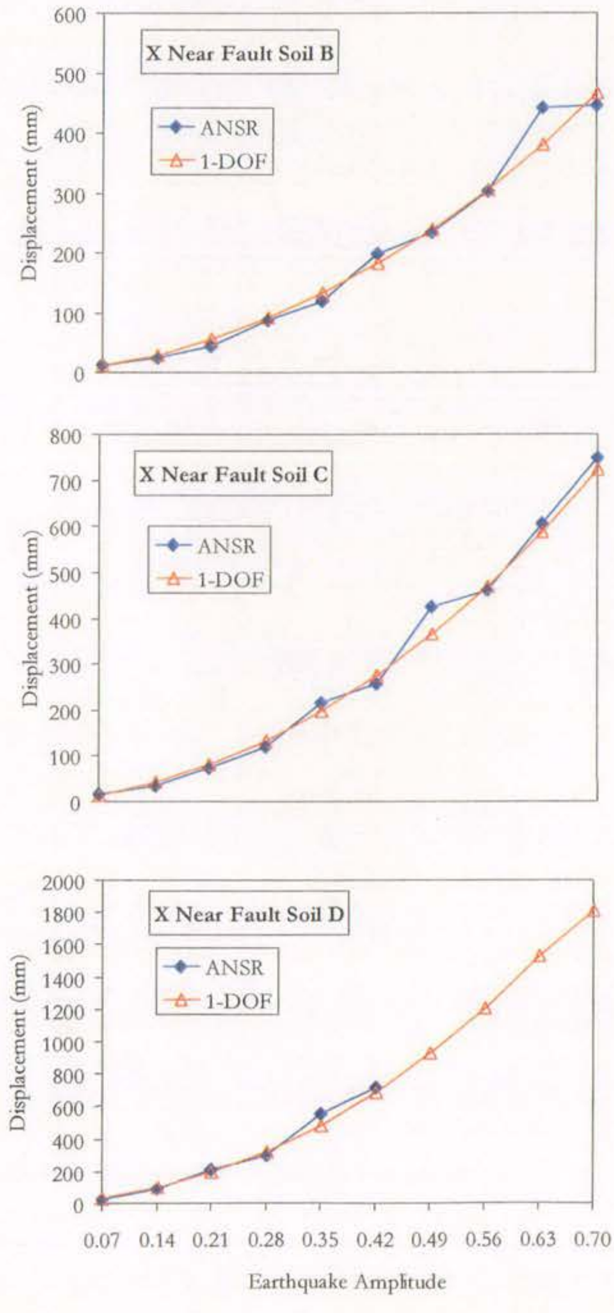

Figure 8-41 14.400 m U-Shaped Wall Rock Z Direction

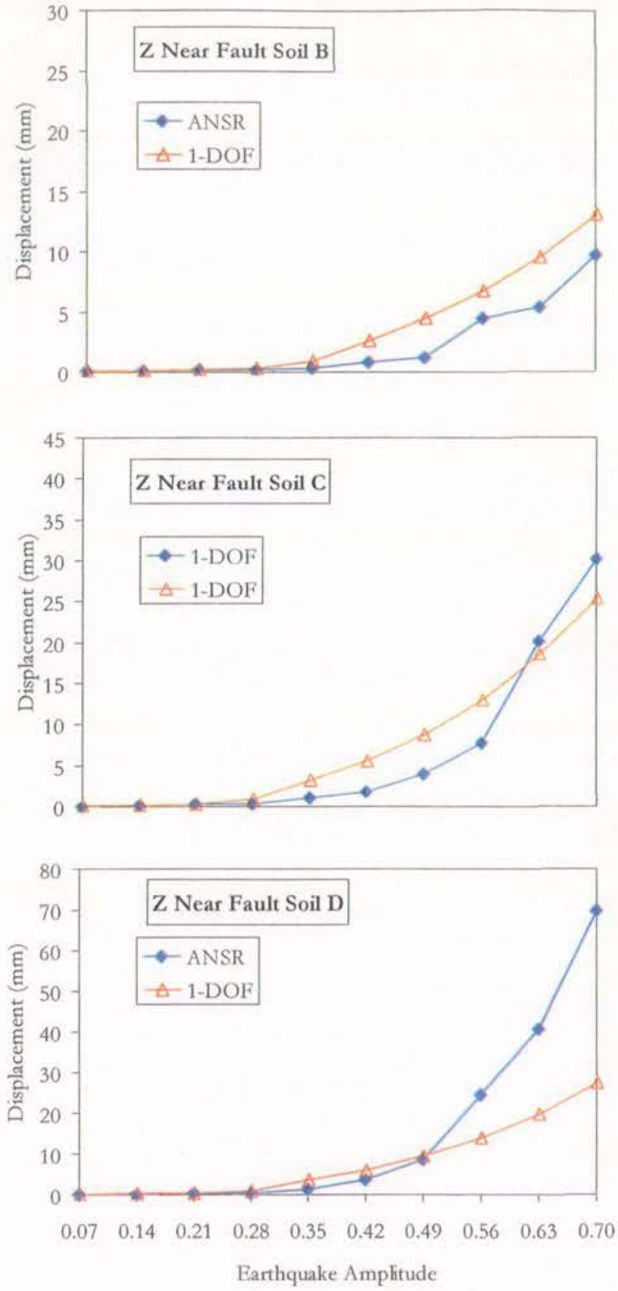

Figure 8-42 compares results for all analyses which produced drifts within the NZS1170 limit. Results are shown separately for each of the three walls and each direction of response.

1. For the U Shaped wall with 7.200 m deep flanges, the correlation was generally good for both directions except that the correlation was only fair in the Z direction when displacements were high, greater than about 150 mm. The procedure generally underestimated displacements, particularly in the Z direction.

2. For the U Shaped wall with 14.400 m deep flanges the correlation was poor for both the X and Z directions. The procedure tended to underestimate displacements in both directions

3. The correlation for the non-symmetrical wall was good for smaller displacements but only fair for higher displacements. The procedure tended to over-estimate displacements for lower values.

Figure 8-42 Comparison of Analysis and Measured Displacements

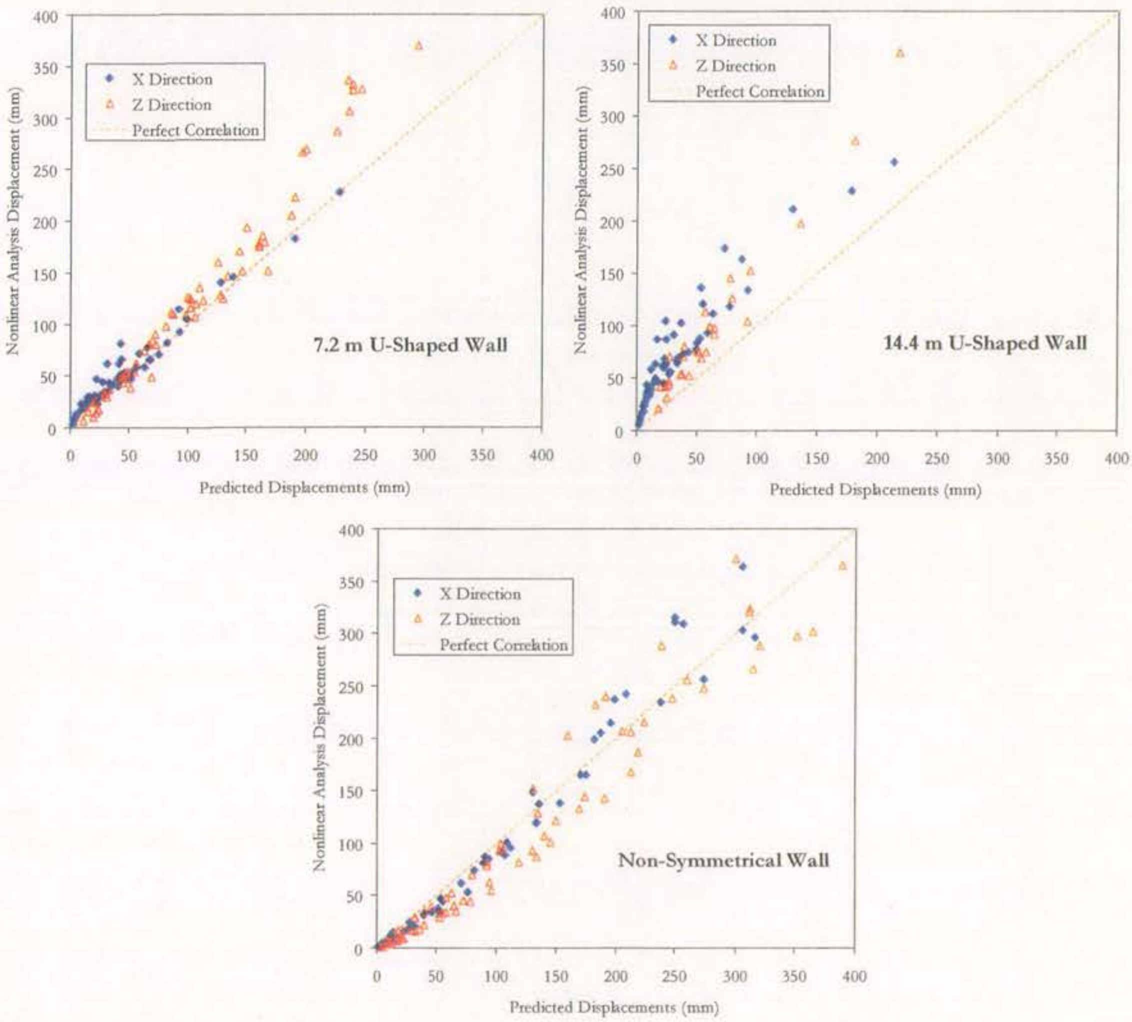

Figure 8-43 combines the results for all three walls and both directions, again restricted to the analyses where drifts were within NZS1170 limits. Although there is considerable scatter, the mean of all predictions provides a reasonable match with a best-fit linear curve having a slope within 6% of the ideal value.

Figure 8-44 presents the same results as Figure 8-43 but plotted log-log to more clearly show the results at smaller displacements. This type of plot shows that the scatter appears greater for small displacements, contrary to the results for the planar walls (see Figures 7-9 and 7-10).

Figure 8-43 Predicted Displacements for Non-Planar Walls

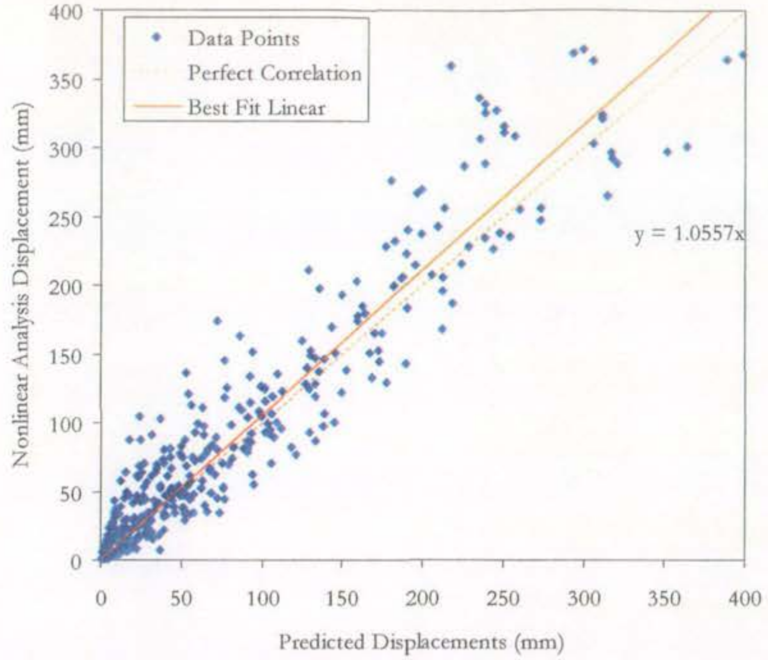

Figure 8-44 Predicted Displacements for Non-Planar Walls (Log Plot)

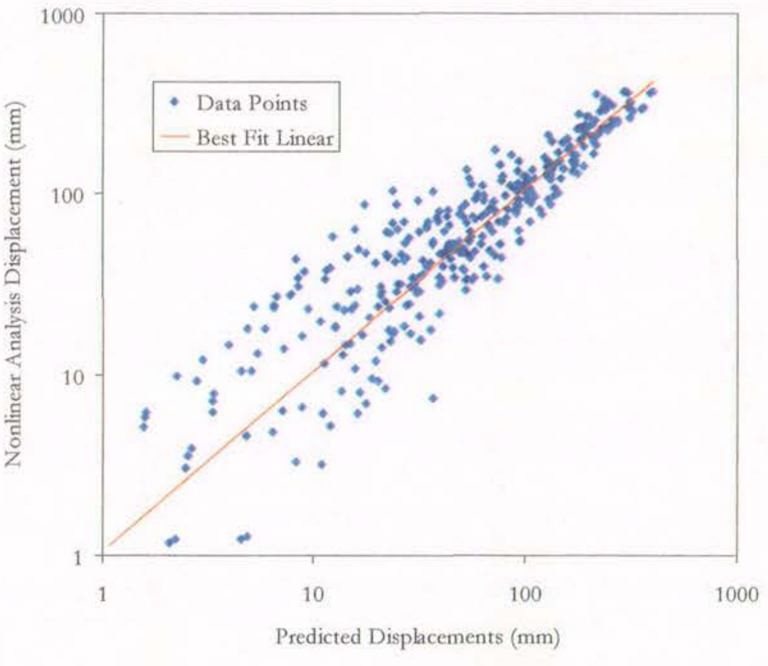

8.5.2 Dynamic Amplification Factors

Figure 8-45 compares the shear amplification factors required by the formula developed in Section 7.4 with the analysis results for each of the three walls. Generally, the formula provides a reasonable, and conservative, estimate of actual shear amplification. The formula appears to be more conservative for the 7.2 m U-Shaped wall and the non-symmetrical wall than the 14.4 m U-Shaped wall..

Figure 8-45 Shear Amplification Factors for Non-Planar Walls

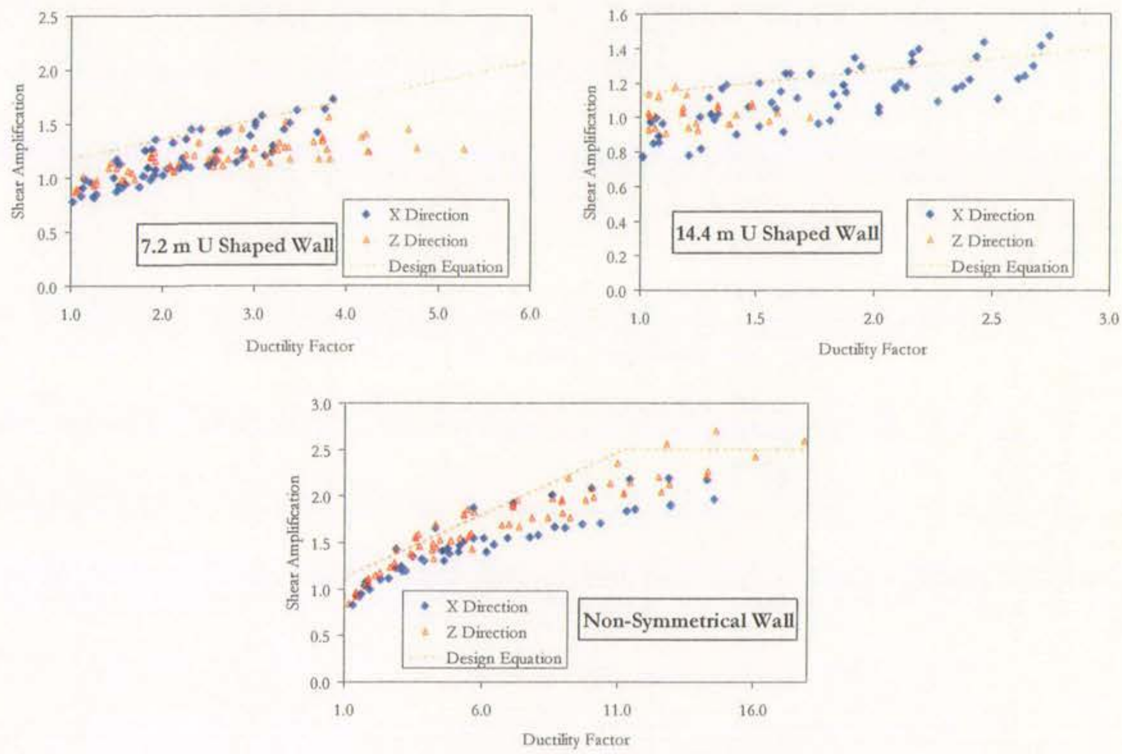

8.6 Effect of Torsion on Displacements

The number of non-planar walls evaluated in this project is too small to develop any detailed procedures for estimating torsional effects on displacements. The following discussion extracts general trends noted from the non-planar structures studied but details procedures would require a much more comprehensive suite of example structures.

Note that for the analysis, the eccentricity was modelled by moving the floor mass by the specified eccentricity but the gravity loads were not adjusted. For rocking walls, the lateral load resistance is proportional to the vertical load on the wall. Therefore, if the floor loads were moved so as to provide the accidental eccentricity then the centre of stiffness would tend to move so as to reduce the effects of accidental eccentricity. This effect was not included in this evaluation.

Table 8-18 lists the increases in X and Z displacements doe to torsion arising from two effects:

1. Due to actual eccentricity, by comparing the maximum displacement at the corner of the diaphragm with corresponding value at the centre of mass

2. Due to accidental eccentricity by comparing maximum displacements from the calculated centre of mass analysis with the maximum displacements from the analyses with the +0.1B and the -0.1B accidental eccentricity.

All cases are based on the results from the single earthquake component. Values listed are the average results over the three different spring types used for the analyses of each non-planar wall configuration.

Based on this extremely limited number of data points, some tentative patterns can be extracted:

1. The increase in maximum displacements, compared to the centre of mass displacement, is two times the actual eccentricity. The U-shaped walls (Wall ID 4 and 4B) have an actual eccentricity of 25% B for X loads and the displacement increase is 42% and 48%. The non-symmetrical wall structure (Wall ID 5) has 5% actual eccentricity in both directions and increases of 11% and 13% in the two directions respectively.

2. The increase in maximum displacements due to accidental eccentricity for any of the walls is numerically less than the eccentricity. A 10% accidental eccentricity produced up to a 7% increase in displacements.

Table 8-18 Torsional Displacements Due to 1-Component Earthquake

Wall ID	Calculated Actual Eccentricity		Ratio of Maximum Displacement to Centre of Mass Displacement		Increase in Maximum Displacement due to ±0.1B Accidental Eccentricity	
	X	Z	X	Z	X	Z
4	1.8 m (0.25B)	0	1.42	1.03	1.04	0.99
4B	3.6 m (0.25B)	0	1.48	1.04	1.05	1.07
5	0.65 m (0.05B)	0.65 m 0.05B	1.11	1.13	1.05	1.04

As discussed above, the effect of accidental eccentricity is likely to be less for rocking structures than for fixed base structures because an eccentricity in floor loads to cause a movement in the centre of mass will cause a corresponding movement in the centre of stiffness so as to minimise the effect of the eccentricity. Taking into account of this, a tentative recommendation for the increase in displacements for torsion is to allow for an increase equal to 2 times the actual eccentricity but not less than the accidental eccentricity, which is 10% for NZS1170 designs.

9 COMPARISON OF ROCKING AND YIELDING RESPONSE

The analyses performed in this study have demonstrated that the displacements of rocking walls are much higher than equivalent non-rocking walls. A design procedure was developed to predict displacements. This procedure produced a good match to the analysis results but the procedure differed markedly from other methods of predicting displacements in nonlinear systems, in particular the FEMA 356 and ATC 40 methods.

In order to ensure that the reason for this difference was because of the rocking mechanism, and not flaws in the analysis procedures used, two of the single wall examples were re-evaluated assuming that the walls were fixed at ground level and that the nonlinearity was due to plastic hinging at the base rather than be rocking.

9.1 Squat Wall

9.1.1 Model Configuration

The three story configuration of the 7.200 m long wall founded on rock springs was modified to a fixed base model. Strength properties were based on a steel reinforcing ratio of 0.25% throughout and nonlinearity was due to both shear cracking and flexural yielding. This procedure has been shown to be capable of predicting displacements accurately in a full size test of a yielding wall [21]. The wall configuration is shown in Figure 9-1.

Figure 9-1 Three Story Yielding Base Wall

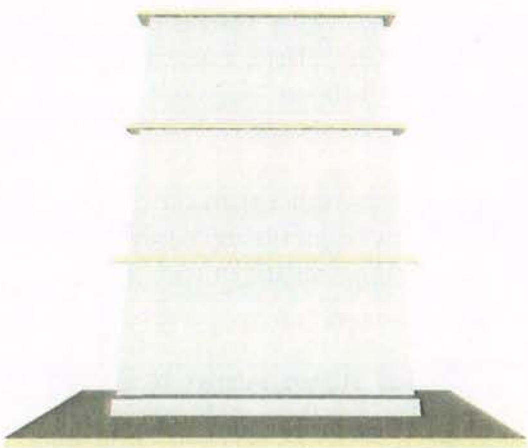

9.1.2 Wall Strength Characteristics

The wall hysteresis curve, shown in Figure 9-2, was generated by applying a cyclic displacement to the model. The cyclic response shows a "pinched" type hysteresis loop, typical of axially loaded reinforced concrete elements. The envelope strength shows a relatively strong bi-linear curve, with only slight softening due to shear cracking until a lateral load coefficient of 0.175 at 2 mm displacement, after which the outer flexural steel yields and there is a substantial reduction in stiffness.

Figure 9-2 Three Story Wall Response to Cyclic Displacements

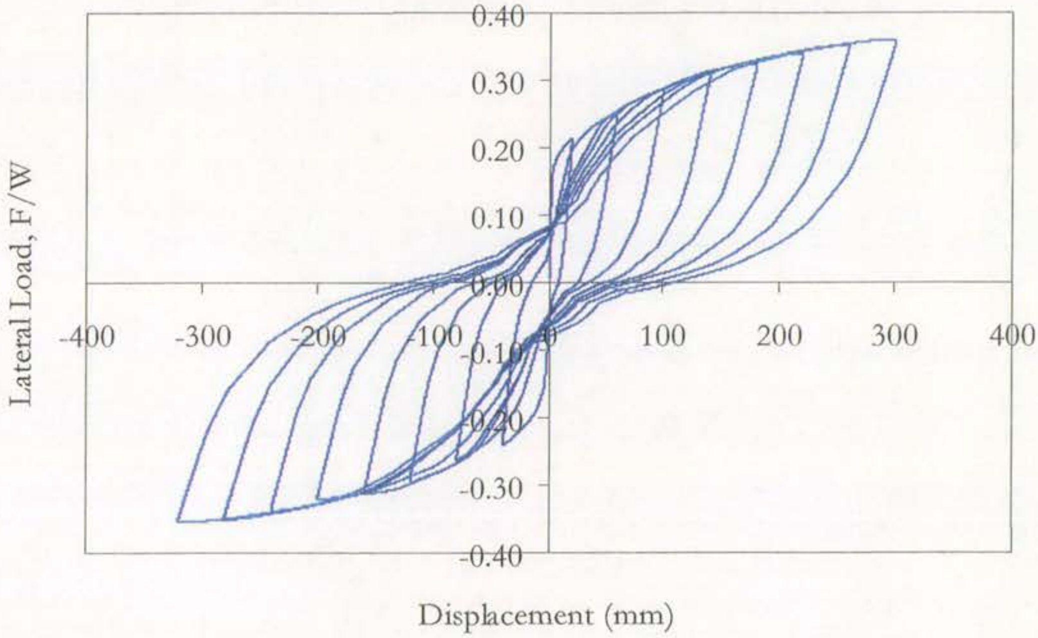

9.1.3 Time History Results

Figure 9-3 compares the maximum displacement at the top of the wall for the yielding model with the equivalent displacements obtained from the rocking model. Also included on Figure 9-3 is the baseline, elastic case where all nonlinearity in the model is inhibited. These plots show the different response characteristics of the rocking and yielding modes of response:

1. Yielding produces displacements higher than elastic response, an average of 3.3 times as high. The ratio increases with increasing earthquake amplitude. For the highest input, Near Fault D, the yielding displacements are 7.8 times as high as the elastic displacements.

2. Rocking produces even higher factors relative to elastic response, an average of 5.4 times as high. The ratio also increases with increasing earthquake amplitude. For the highest input, Near Fault D, the rocking displacements are 16.6 times as high as the elastic displacements.

3. For this wall, the rocking mode of response produces displacements higher than the yielding response by an average of 50%. Even though the displacements for both systems increase relative to the elastic case with increasing seismic input, the rate of change is higher for the rocking system. For the highest input, Near Fault D, the rocking displacements are 115% higher than the yielding displacements.

Figure 9-3 Comparison of Yielding and Rocking Displacements for Three Story Wall

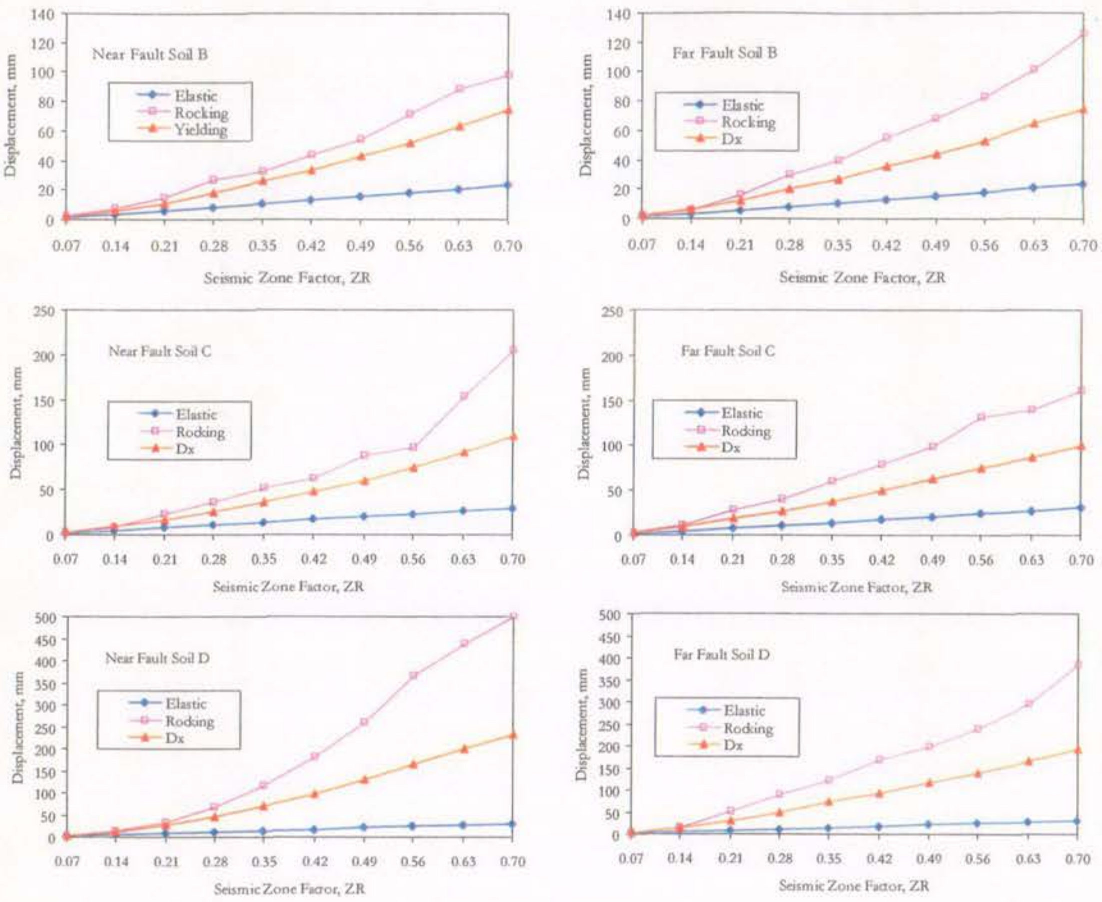

9.2 Slender Wall

Figure 9-4 Five Story Yielding Base Wall

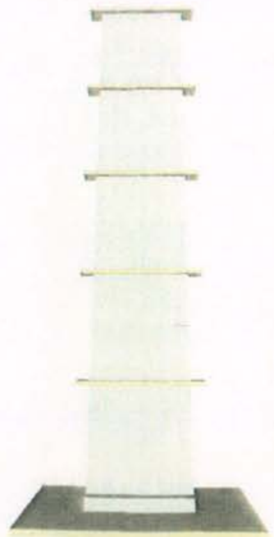

9.2.1 Model Configuration

The model of the five story configuration of the 3.600 m long wall on rock springs was also modified to a fixed base model. Strength properties were based on a steel reinforcing ratio of 1.0% throughout and nonlinearity was due to both shear cracking and flexural yielding. The wall configuration is shown in Figure 9-4.

9.2.2 Wall Strength Characteristics

The wall hysteresis curve, shown in Figure 9-5, was generated by applying a cyclic displacement to the model. As for the preceding wall, the cyclic response shows a "pinched" type hysteresis loop, typical of axially loaded reinforced concrete elements. The envelope strength again shows a relatively strong bi-linear curve, with only slight softening due to shear cracking up to a lateral load coefficient of 0.05 at 9mm displacement, after which the outer flexural steel yields and there is a substantial reduction in stiffness.

Figure 9-5 Five Story Wall Response to Cyclic Displacements

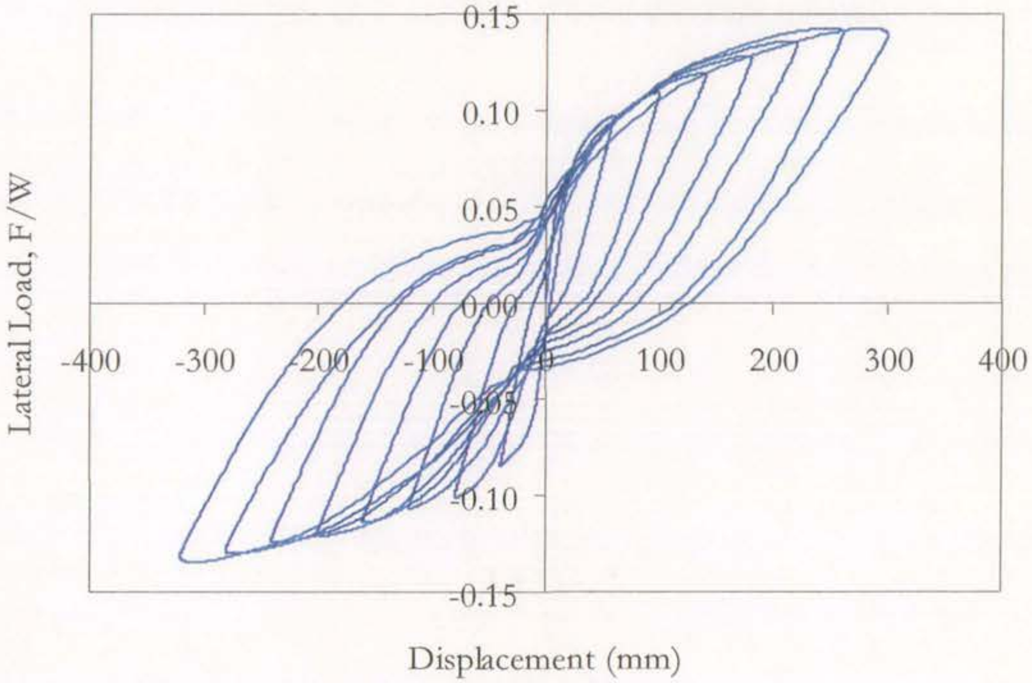

9.2.3 Time History Results

Figure 9-6 compares the maximum displacement at the top of the wall for the yielding model with the equivalent displacements obtained from the rocking model. Also included on Figure 9-6 is the baseline, elastic case where all nonlinearity in the model is inhibited. In general, these plots show the similar response characteristics to the three story wall results plotted in Figure 9-3 but with less pronounced differences:

1. Yielding produces higher displacements higher than elastic response, an average of 1.66 times as high. The ratio increases with increasing earthquake amplitude. For the highest input, Near Fault D, the yielding displacements are 2.58 times as high as the elastic displacements.

2. Rocking produces slightly higher factors relative to elastic response, an average of 2.18 times as high. However, the ratio of rocking displacements does not consistently increase with increasing earthquake amplitude. The highest ratio of rocking to rocking displacements, 3.4, occurs for ZR=0.35 for Near Fault D. At the highest amplitude, ZR=0.70, the ratio has reduced slightly to 2.9.

3. As for the 3 story wall, the rocking mode of response produces displacements higher than the yielding response, although in this case by an average of 30%. For the mid-point of the input the rocking displacements are 50% higher than the yielding displacements.

Figure 9-6 Comparison of Yielding and Rocking Displacements for Five Story Wall

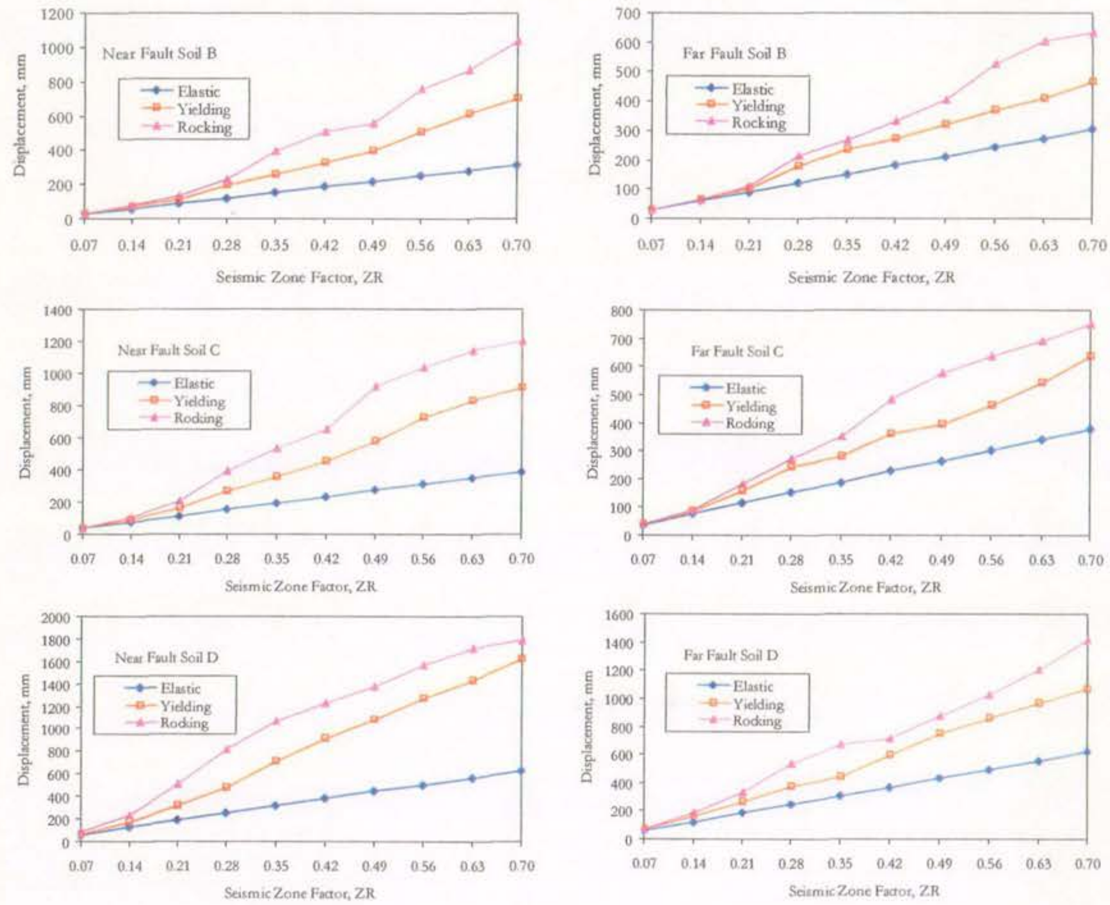

9.3 Summary of Yielding Versus Rocking Response

A limited study of two walls has demonstrated that permitting the base of the wall to rock results in higher displacements for all levels of seismic input compared to an equivalent yielding wall. The amount of increase is a function of both wall type and seismic input. For the 3 story wall the average increase was 50% and maximum 115%. For the 5 story wall the increase was less but still substantial, 30% on average and 50% maximum. This illustrates why procedures developed to estimate displacements in yielding systems require modification to be used for rocking system.

As a side issue, these analyses demonstrated that the response of yielding cantilever shear walls will be much higher than for equivalent elastic walls. Displacements averaged 3.3 times as high for the 3 story wall and 1.66 times as high for the 5 story wall.

10 TENTATIVE DESIGN GUIDELINES FOR ROCKING STRUCTURES

10.1 Summary of Design Procedure

The steps below summarize the tentative design procedure developed for rocking structures. As noted in the preceding sections, the procedure provides a good estimate of displacements for a wide range of single walls and can be extended to multiple planar walls. The procedure can be used for structures comprising multiple non-planar walls but the accuracy will be less, especially for wall layouts which produce significant torsion.

1. Define the Foundation Size

For elastic (non-rocking) response, the required foundation width can be calculated from the applied elastic seismic load, $V_E = C_d(T_1)$ Mg, the wall length at foundation level, L, and the soil ultimate bearing capacity, q_c, as $B = \dfrac{W}{q_c(L - \dfrac{2V_E H}{WC_O})}$. (See Step 3 below for definition of C_O).

For a rocking wall, the foundation length and/or width will be set at some value smaller than those defined above and the performance will be checked at the ductility factor resulting from the rocking wall, following the steps listed below.

The absolute minimum foundation width is $B > \dfrac{W}{q_c L}$ so the starting point must be larger than this. To calculate the width for a specific ductility factor, DF, set $V_E = V_E/DF$ in the equation for B above.

2. Calculate the Compression Block Size

Calculate the length of the compression block as $c = \dfrac{W}{q_c B}$

3. Soil Spring Stiffness

Foundation stiffness properties can be calculated using the spring definition from FEMA 256 Figure 4-5 (reproduced as Figure 5-1 in this report) or other sources. For New Zealand site, a typical range of soil properties is:

Soils and gravels, G = 40,000 to 80,000 kN/m^2, υ = 0.3 to 0.4

Clays (undrained case), G = 2,000 to 20,000 kN/m^2, υ = 0.5

4. Wall Rocking Strength

Calculate the yield force $F_y = \dfrac{W(L-c)}{2\dfrac{H}{C_0}}$ and the yield coefficient $C_y = \dfrac{F_y}{Mg}$ where M is the seismic mass tributary to the wall. For non-planar walls, such as C shaped and L shaped sections, the moment capacity, $\dfrac{W(L-c)}{2}$ in the equation above, can be calculated by taking moments of the reaction forces at individual springs about the wall centroid. The coefficient C_0 relates spectral displacement to the roof displacement of multi- story walls. It has a value of 1.0 for single story buildings and increases with height to a range of between 1.2 and 1.5 for higher buildings. FEMA 356 provides tabulated values.

5. Estimate Period

Either extract the period from a linear elastic model of the wall or use the approximate formulas in Section 10.3. The soil spring stiffness, required for period calculations, can be calculated from FEMA 356 procedures, as above.

6. Seismic Displacements

The single degree of freedom displacement $\Delta = C(T_e)g\dfrac{T_e^2}{4\pi^2}$ from which the displacement at the top of the wall is calculated as $\Delta_{TOP} = \Delta C_0$.

The effective period is calculated from the elastic period as $T_e = T_i R_E$; R_E is the response reduction factor $R_E = \dfrac{C_m C(T_e)}{C_y}$; C_m is the effective mass factor obtained from a modal analysis or alternatively tabulated values from FEMA 356 (typically 1.0 for 1 or 2 story buildings, 0.8 or 0.9 for taller buildings). Note that the equation for effective period is recursive as R_E is a function of T_e which is the unknown variable.

7. Structural Ductility Factor

Structural ductility factor DF = C (T_i) / C_Y

8. Dynamic Amplification Effects on Wall Shear

$V_U = F_Y \omega_V$

$\omega_V = 1 + a_{VN} DF \leq 0.5 + N$ for N > 1 story
$= 1.0$ for N = 1 story

N	a_{VN}
1	0.00
2	0.10
3	0.15
4	0.40
5	0.60
6	0.90

9. Torsional Increase in Displacements

The number of 3D structures evaluated was insufficient to fully develop procedures to estimate increases in displacement due to torsion. The limited studies suggest the higher of two factors:

1. Increase the displacements by two times the calculated actual eccentricity. If the calculated eccentricity is 0.20B, allow for a 40% increase in displacements.

2. If the actual eccentricity is less than 5%, increase the displacements by the same factor as the accidental eccentricity. That is, allow a 10% increase in displacements due to 0.10B eccentricity.

10. Assess Performance

The performance of the wall, as defined by maximum displacements and dynamic amplification effects, is assessed to determine whether it achieves the project design objectives. If not, the foundation size is adjusted and the procedure repeated from Step 2 above. Increasing the foundation size decreases the ductility factor, which reduces both displacements and dynamic amplification effects.

10.2 Response Versus Ductility Factor

The extent of rocking depends on the ductility factor, that is, the ratio of elastic seismic load to the lateral load causing uplift of the wall. As discussed earlier in this report, earlier New Zealand codes permitted uplift provided the ductility factor associated with this uplift did not exceed 2. In this section, the impact of ductility factors up to 2 on response is assessed.

10.2.1 Displacements

The procedure developed in the preceding sections was used to develop curves of the ratio of rocking displacement to the displacement if the wall were inhibited from rocking, as plotted in Figure 10-1. This figure plots the ratio of displacements for a range of initial elastic periods and all soil classes. All curves on Figure 10-1 assume that rocking occurs at a load level of 0.5 C(T) where C(T) is the elastic spectrum coefficient for horizontal loading as defined by NZS1170. This is the definition of Ductility Factor 2 (DF 2).

The curves are plotted separately for sites > 100 km from active faults (FF) and for sites within 2 km of active faults (NF). Figure 10-1 shows a number of trends:

1. The rocking displacement is in all cases greater than or equal to the elastic displacements. That is, the effect of rocking is never to reduce displacements.

2. For short periods, a rocking structure will have displacements 4 times that of a non-rocking structure. This applies for periods in the range of 0.10 to 0.15 for soil types B & C, 0.10 to 0.25 for soil type D and 0.10 to 0.50 for soil type E. For this period range, the response is not affected by near fault effects.

3. The ratio of rocking to elastic displacements reduces from 4.0 to a value of 1.64 at periods of 0.30 (soil B & C), 0.60 (soil D) and 1.0 (soil E). The ratio remains at this value of 1.64 to a period of 1.0 seconds for all soil types. The curves are identical for both FF and NF locations up to the 1.0 second period.

4. For elastic periods beyond 1.0 seconds at FF sites the ratio of rocking to elastic displacement continues to decrease until the displacements are the same (ratio = 1.0) for periods of 3 seconds or longer, the constant displacement period of the NZS1170 spectra.

5. For elastic periods beyond 1.0 seconds at NF sites the ratio of rocking to elastic displacement increases from 1.64 to reach a peak ratio of 1.95 at a period of 1.90 seconds for all soil types. After the 1.90 second period the ratio decreases until the displacements are the same (ratio = 1.0) but this occurs at periods of 5 seconds or longer, as the constant displacement period of the NZS1170 spectra does not occur until the near fault factor reaches a constant value at 5.0 seconds. Although the near fault factor does not exceed 1.0 until periods of 1.50 seconds, the rocking displacements are increased beyond periods of 1.0 seconds because at this elastic period the effective period of a DF 2.0 system reaches 1.50 seconds.

Figure 10-1 Effect of Soil Class on Rocking Displacements

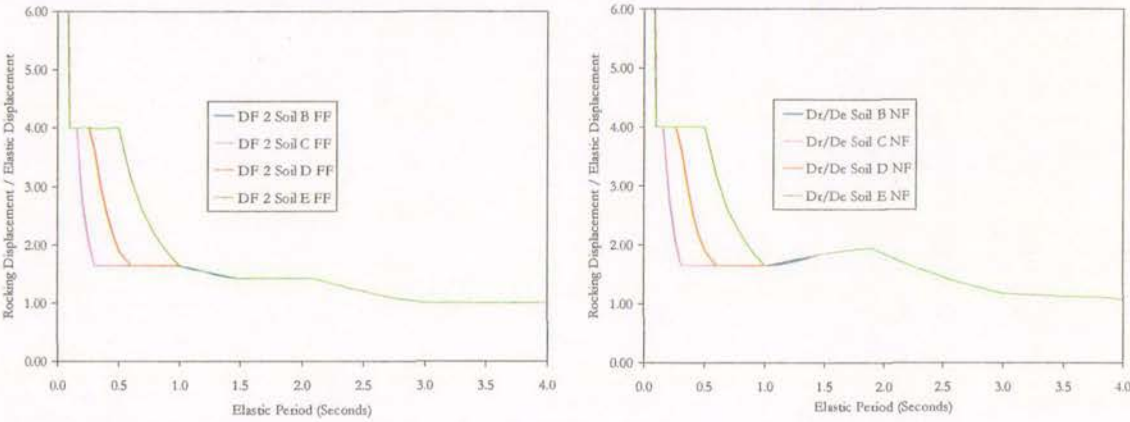

Figure 10-2 and 10-3 illustrate the effect of increasing ductility factor (DF) on displacements for sites distant from faults and near to faults respectively. All the curves on these two figures are for a seismic zone factor ZR = 0.40, site class C. For other ZR values the displacements will be proportionate to the plotted values.

Figure 10-2 demonstrates the effect of the extent of rocking, as defined by increasing DF, on a site where the near fault factor is 1.0 at all periods. The maximum displacement for all ductilities converges on the constant displacement value, which is 394 mm for this zone and is reached at a period of 3.0 seconds for an elastic system (DF = 1.0). As the ductility factor increases, the displacements increase at a faster rate such that the peak displacement is reached at shorter periods, as short as 1.0 second for a DF 8 system.

The effect of increasing ductility on a particular system can be assessed by reading the plot vertically from a particular elastic period. For example, an elastic system with a 1.0 second period will have a displacement of 118 mm. This increases to 158 mm at DF 1.5, to 194 at DF 2 and reaches a maximum of 391 mm at DF 8. The displacement at DF 2 is 1.64 times the elastic value, the factor which applies in a period range of 0.30 to 1.0 seconds as discussed above.

Figure 10-2 Effect of Ductility on Rocking Displacements: Distant from Fault Soil C

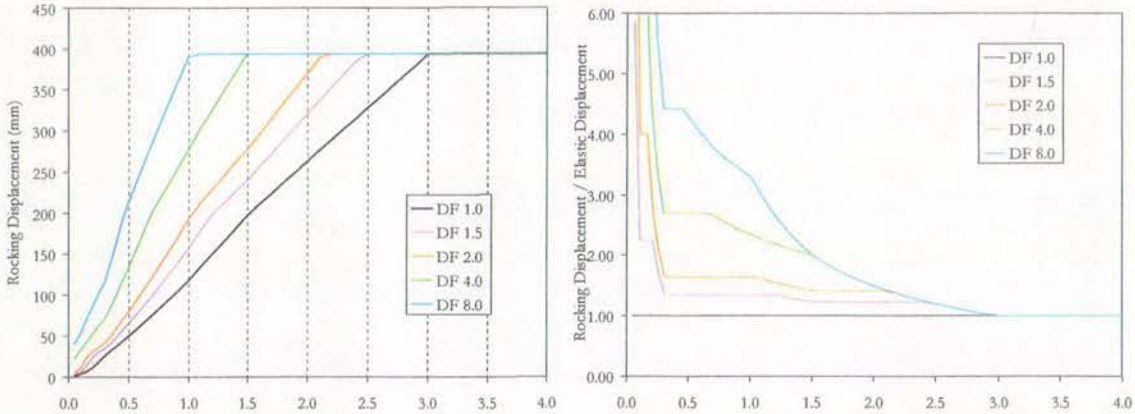

Figure 10-3 demonstrates the effect of the extent of rocking on a site with the maximum near fault factor. The maximum displacement for all ductilities converges on the constant displacement value, which at 677 mm is higher than the far fault value of 394 mm by the maximum near fault factor of 1.72 and which is reached at periods of 5.0 seconds for an elastic system. As the ductility factor increases, the displacements increase at a faster rate such that the peak displacement is reached at shorter periods, as short as 1.8 seconds for a DF 8 system.

For the elastic system with a 1.0 second period the displacement is 118 mm, the same as for the fault distant site. For low ductility factors the increase is the same as for the fault distant curves, to 158 mm at DF 1.5 and to 194 at DF 2 as above. As the ductility factor exceeds 4 the period lengthening is such that the displacements are influenced by the near fault factor (> 1.50 seconds). The maximum displacement at DF 8 is 571 mm, which is 46% higher than the fault distant value of 391 mm.

Figure 10-3 Effect of Ductility on Rocking Displacements: Near Fault Soil C

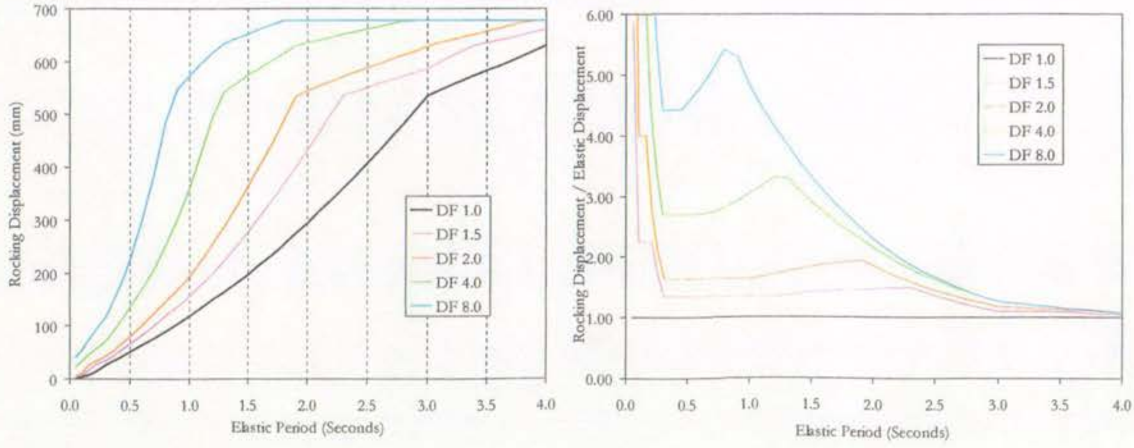

10.2.2 Dynamic Amplification Factors

A procedure to calculate dynamic shear amplification due to rocking, as a function of the ductility factor, was developed in Section 7. These values are higher than those specified by NZS3101 for ductile walls. Table 10-1 compares the dynamic amplification factors for rocking and ductile walls for varying number of stories, all for ductility factor 2. The values for the ductile wall are constant for all ductility values, the rocking values increase with increasing ductility. The values are plotted in Figure 10-4.

At ductility factor 2 the rocking amplification factors are only about 10% higher than for ductile wall for 2 and 3 story walls but for higher walls the factors are much higher, 87% greater for 6 story walls.

Table 10-1 Shear Wall Dynamic Amplification Factors

Number of Stories	Shear Amplification for Rocking at Ductility Factor = 2.0	Ductile Wall Dynamic Amplification Factor	Increase in Factor due to Rocking
2	1.20	1.10	1.09
3	1.30	1.20	1.08
4	1.80	1.30	1.38
5	2.20	1.40	1.57
6	2.80	1.50	1.87

Figure 10-4 Comparison of Ductile and Rocking Amplification Factors

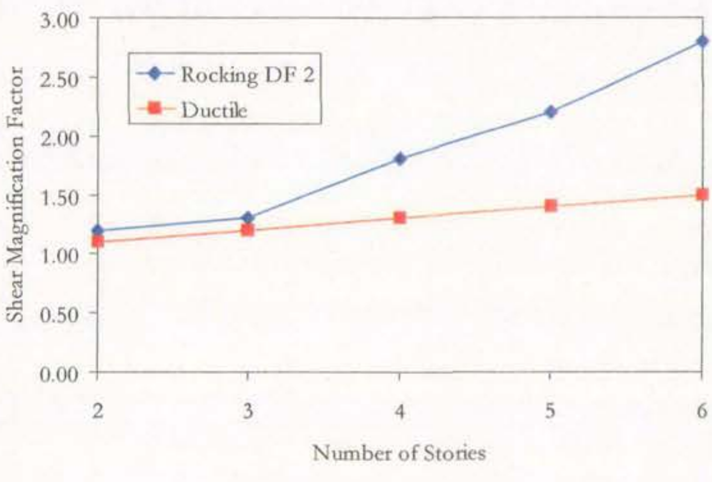

10.2.3 Summary of Effect of Rocking at Ductility Factor 2

The evaluations reported above have shown that permitting uplift at load levels corresponding to one-half the design load level, equivalent to ductility factor 2, influences both the displacements and shear forces:

1. Displacements are equal to or higher for a rocking structure than for an equivalent non-rocking system. The increase in displacements is greatest for structures on stiff springs (e.g. rock sites), where the displacements may be 4 times higher or more. Note however that on such stiff sites the displacements are generally small so the

amplification of displacements may not have much effect. For soft springs, such that the elastic period is 1 second or more, rocking displacements are up to 1.64 times elastic displacements for sites distant from a fault and up to 2.0 times higher at near fault locations.

2. Shear forces are increased by dynamic amplification factors which are higher than for ductile walls. At DF 2 the increase is less than 10% for 2 or 3 story structures but increases with height to an increase of 87% for 6 story structures.

10.3 Design Aids

The aim of the development of the design guidelines for rocking structures was to develop procedures for use in design offices. The following sections discuss the development of design aids to enable the procedures to be implemented using spreadsheet solutions. In general, the equations are simple enough to be implemented by a designer with a basic understanding of engineering mechanics. Two steps are more complex, the calculation of period and the calculation of rocking displacement. Spreadsheet implementations of these two steps are described below.

10.3.1 Calculation of Period

If the wall is stiff relative to the soil springs, as will often by the case for squat walls or soft soil conditions, then the period can be calculated using relatively simple calculations, using the procedure shown schematically in Figure 10-5.

Figure 10-5 Procedure for Calculating Period

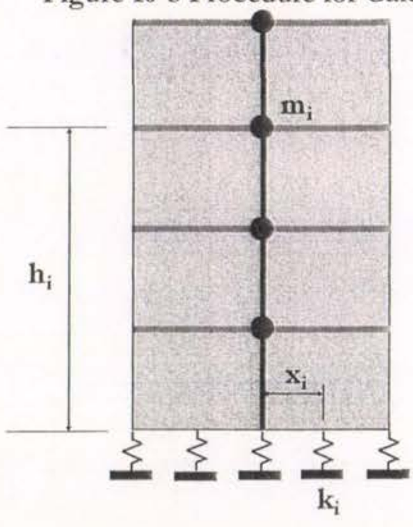

$$K_R = \sum k_i x_i^2$$

$$M_R = \sum m_i h_i^2$$

$$T_i = 2\pi \sqrt{\frac{M_R}{K_R}}$$

The steps in calculating the period are:

1. Calculate the stiffness of each soil spring using the FEMA equations (see Figure 5-1 in this report).

2. Calculate the stiffness and mass properties as listed in Equations (10-1) and (10-2) respectively:

$$Rotational\ Stiffness\ K_R = \sum k_i x_i^2 \tag{10-1}$$

$$Rotational\ Mass\ Inertia\ M_R = \sum m_i h_i^2 \tag{10-2}$$

3. From these, the rocking period can be calculated from Equation (10-3):

$$Rocking\ Period\ T_I = 2\pi \sqrt{\frac{M_R}{K_R}} \tag{10-3}$$

These equations are implemented on the workbook referred to above, as reproduced in Figure 10-6. The spreadsheet calculations are based on an assumption of 7 springs under the wall, with properties based on FEMA-356 Figure 4-5, reproduced as Figure 5-1 in this report. The spring properties are calculated from the soil shear modulus and Poisson's ratio provided by the user.

Figure 10-6 Spreadsheet Calculation of Wall Period

Period of Rigid Wall on Flexible Soil Springs

Foundation Length (m)	3.600
Foundation Width (m)	1.000
Number of Stories	3
Story Height (m)	3.600
Height of Wall, m	10.800
Floor Area, m^2	207.36
Seismic Weight, Kpa	5.000
Seismic Mass per Floor (t)	105.7
Soil G Values	60000
Poisson's Ratio	0.35

Calculation of Effective Stiffness				
Spring	l	k	x	kx^2
1	0.167	105077	-1.717	309656
2	0.653	44025	-1.307	75167
3	0.653	44025	-0.653	18792
4	0.653	44025	0.000	0
5	0.653	44025	0.653	18792
6	0.653	44025	1.307	75167
7	0.167	105077	1.717	309656
Sum				807228

Calculated Effective Stiffness, K	807228	
Calculated Effective Mass, M	19176	
Calculated Period	**0.968**	**Seconds**

Calculation of Effective Mass			
Floor	h	m	mh^2
1	3.60	106	1370
2	7.20	106	5479
3	10.80	106	12327
4			
5			
6			
7			
8			
9			
10			
Sum			19176

	G Kpa	Poisson's Ratio
Clay Lower Level	2000	0.50
Clay Mean Level	10000	0.50
Clay Upper Level	20000	0.50
Sand & Gravel Lower Level	40000	0.35
Sand & Gravel Mean Level	60000	0.35
Sand & Gravel Upper Level	80000	0.35

The example period calculated in Figure 10-6 is for the 3.600 m long 3 story wall on Medium Gravel springs. The analysis model for this wall was modified such that the wall was rigid and the periods are as listed in Table 10-2. It is seen that the formula can predict the analysis period within 1% for the range of soil properties considered in this study.

Table 10-2 Comparison of Calculated Periods for Rigid Wall on Springs

Set	Soil Type	Period Calculated From		Formula
		Formula	Rigid Wall Model	Model
A	Clay Lower Level	4.652	4.614	1.008
B	Clay Mean Level	2.080	2.062	1.009
C	Clay Upper Level	1.471	1.459	1.008
D	Sand & Gravel Lower Level	1.186	1.177	1.008
E	Sand & Gravel Mean Level	0.968	0.961	1.008
F	Sand & Gravel Upper Level	0.839	0.833	1.007
G	Rock	0.237	0.238	0.997

Table 10-2 compares the periods when the wall is rigid. This wall has a length of 3.600 m and is 3 stories high so is relatively flexible even with a fixed base, with a fixed base period of 0.356 seconds.

In Table 10-3, the results from the formula for the rigid wall model are compared with periods from the flexible wall model. This shows that the match is good for the softer springs but as the soil spring increases the error increases until the formula predicts a period only 55% of the analysis period for the stiffest springs, defined as set G.

The match can be improved by using the square root of the sum of the squares (SRSS) of the period based on a rigid wall and the period for the fixed base wall. The results in Table 10-3 show that the SRSS calculation of period is within1% of the model period for all soil spring variations.

Table 10-3 Comparison of Calculated Periods for Flexible Wall on Springs

Set	Period Calculated From		Formula	Wall	SRSS	SRSS
	Formula T_S	Flexible Wall Model	Model	Period T_W	$\sqrt{T_s^2 + T_W^2}$	Model
A	4.652	4.627	1.005	0.356	4.666	1.008
B	2.080	2.093	0.994	0.356	2.111	1.008
C	1.471	1.502	0.979	0.356	1.514	1.008
D	1.186	1.229	0.965	0.356	1.238	1.008
E	0.968	1.025	0.945	0.356	1.032	1.007
F	0.839	0.906	0.926	0.356	0.911	1.006
G	0.237	0.430	0.552	0.356	0.428	0.995
Rigid		0.356				

10.3.2 Rocking Displacement

The tentative design procedures for rocking structures are based on simple formulations which can be solved in a design office environment. Because the equation for effective period is recursive some automated procedure such as Excel© /Goal Seek is helpful.

Figure 10-7 shows an example screen for a workbook implementation of the design procedure. (A copy of this workbook is available from the authors on request).

Figure 10-7 Workbook Calculation of Rocking Displacement

1. Set Seismic Parameters	
Hazard Factor, Z	0.20
Return Period Factor, R	1.00
Site Subsoil Class	C
Structural Performance Factor, S_p	0.70
Distance to Fault	2

3. Define Wall Geometric & Mass Details					
Stories :	3	Wall 1	Wall 2	Wall 3	Wall 4
Wall Length, m		3.600	3.600		
Wall Height, m		10.800	10.800		
Gravity Load on Wall, KN		510	510		
Seismic Mass on Wall, t		208			

2. Define Wall Dynamic Properties	
Elastic Period, T_1	0.800
C_M = Effective Mass (see Table Cell Q10	0.900
C_0 = Phi x PF for default values)	1.200
Displacement at F_U	19.1

Calculated Capacity Curve				
Ultimate Moment, M_U	918	918	0	0
Force at M_U, F_U	102	102	0	0
Force / Seismic Weight	0.100			

Solve

Wall Will Rock at 0.6 of Design Load
increasing displacement by a factor of 1.50 to 56.5 mm
Ductility Factor 2.0 Shear Amplification Factor = 1.30
Displacement Ductility 2.96

Scale Factor	Effective Period T_{EFF} (Seconds)	Spectral Acceleration at $T_{EL} \times S$ $C(T_{EL})S$	Coefficient C0	Coefficient Cm	Response Reduction Factor R	Displacement at Top of Wall	Elastic Displacement
0.100	0.800	0.020	1.200	0.90	0.177	3.8	3.8
0.200	0.800	0.039	1.200	0.90	0.354	7.5	7.5
0.300	0.800	0.059	1.200	0.90	0.532	11.3	11.3
0.400	0.800	0.079	1.200	0.90	0.708	15.0	15.0
0.500	0.800	0.098	1.200	0.90	0.886	18.8	18.8
0.600	0.828	0.115	1.200	0.90	1.035	23.5	22.5
0.700	0.905	0.126	1.200	0.90	1.131	30.7	26.3
0.800	0.976	0.136	1.200	0.90	1.221	38.6	30.0
0.900	1.044	0.145	1.200	0.90	1.306	47.2	33.8
1.000	1.109	0.154	1.200	0.90	1.387	56.5	37.6

Spectral Acceleration at T_{EFF} C(Teff)	Spectrum Scale Factor S	Convergence Ratio	Displacement Ratio Rock at
0.020	1.00	1.00	1.00
0.039	1.00	1.00	1.00
0.059	1.00	1.00	1.00
0.079	1.00	1.00	1.00
0.098	1.00	1.00	1.00
0.115	0.97	1.00	1.04
0.126	0.91	1.00	1.17
0.136	0.86	1.00	1.28
0.145	0.82	1.00	1.40
0.154	0.78	1.00	1.50

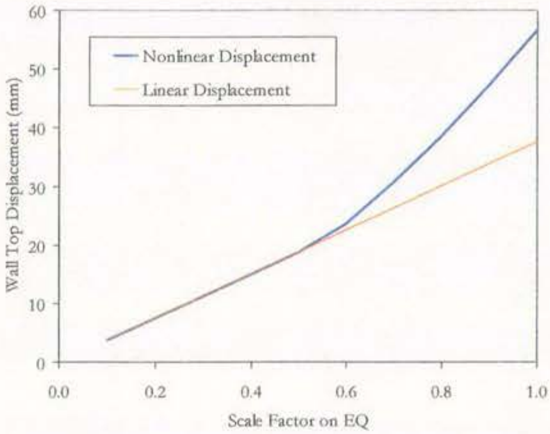

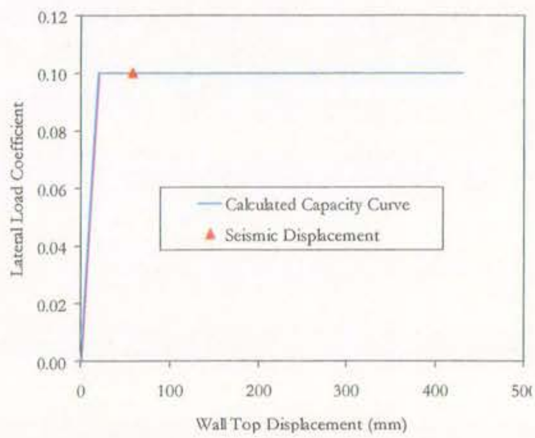

The input is described by three sections (cells coloured pale yellow in Figure 10-7):

1. Seismic parameters, which are the parameters prescribed by NZS1170. The spreadsheet is set up for the spectral shapes described by NZS1170 but the spectra portion of the calculations could be replaced with those from other sources. The parameters entered in this section define the acceleration and displacement spectrum, as listed and plotted on the *Spectra* sheet in the workbook.

2. Wall dynamic parameters, which are the elastic period, T_1, and FEMA factors C_M (effective mass factor) and C_0 (roof displacement factor). The ideal way to extract these properties is from a modal analysis of the structure, and this will be required

for complex structures. For simpler structures, the preceding section provides a procedure to estimate the period for walls where flexibility is provided by soil springs. FEMA-356 provides tabulated values of C_M and C_0, which are reproduced on the worksheet.

3. Wall geometric and mass details. These include length and height, gravity load and seismic mass. The workbook allows for up to 4 individual walls but assumes that these are planar or part of a symmetric structure as no allowance is made for torsion. Gravity loads are applied to each wall independently, but seismic mass is a single floor mass applying to the entire structure.

When the input data is complete, a "Solve" button is used to activate a macro which solves for displacements at increments of the design earthquake, at scale factors from 0.10 to 1.0. This button is also used to update results when input data changes.

The results of the solution are contained in a message box, which lists the fraction of the design load at which rocking will occur; whether the wall will rock; the ductility factor; shear amplification factor and displacement ductility.

The results are also plotted, the left hand plot comparing nonlinear displacements with linear displacements for increasing earthquake amplitude and the right hand plot showing the capacity curve and the location of the seismic displacement on the curve.

10.4 Theoretical Basis of Procedure

The procedure to estimate the maximum displacement of a rocking wall was developed empirically considering variations of a number of procedures used in other situations to calculate nonlinear response. The best solution was found to be a variation of the secant stiffness method where a substitute elastic structure was defined by an effective period, T_e. The effective period of the substitute structure was defined as $T_e = T_i R_E$ where T_i is the initial elastic period of the system and R_E is the ductility factor at the effective period.

The direct proportionality of T_e to R_E was unexpected as the effective stiffness, K, is inversely proportional to R for a yielding system. Because the period is inversely proportional to $\sqrt{K}$ it was expected that T_e would be proportional to $\sqrt{R}$, not R.

On further examination, as discussed in the following sections, it was found that the equation $T_E = T_I R_E$ is equivalent to the equation $T_E = T_I \sqrt{R_I}$ but only when the spectral acceleration is inversely proportional to the period, the constant velocity period of the spectrum. The form $T_E = T_I R_E$ is more complex in that it is recursive but applies for all portions of the spectrum, not solely the constant velocity portion.

10.4.1 Substitute Structure at Initial Period

The equal displacement theory, used in codes such as NZS1170 for moderate and long period structures (greater than 0.70 seconds for Soil Types A to D), assumes that the displacement of the yielding system will be equal to that of an equivalent elastic system. Using this assumption, an effective stiffness can be defined as the secant stiffness to the intersection of the yield level and a displacement equal to that of the elastic system, as shown in Figure 10-8.

Figure 10-8 Definition of Effective Stiffness

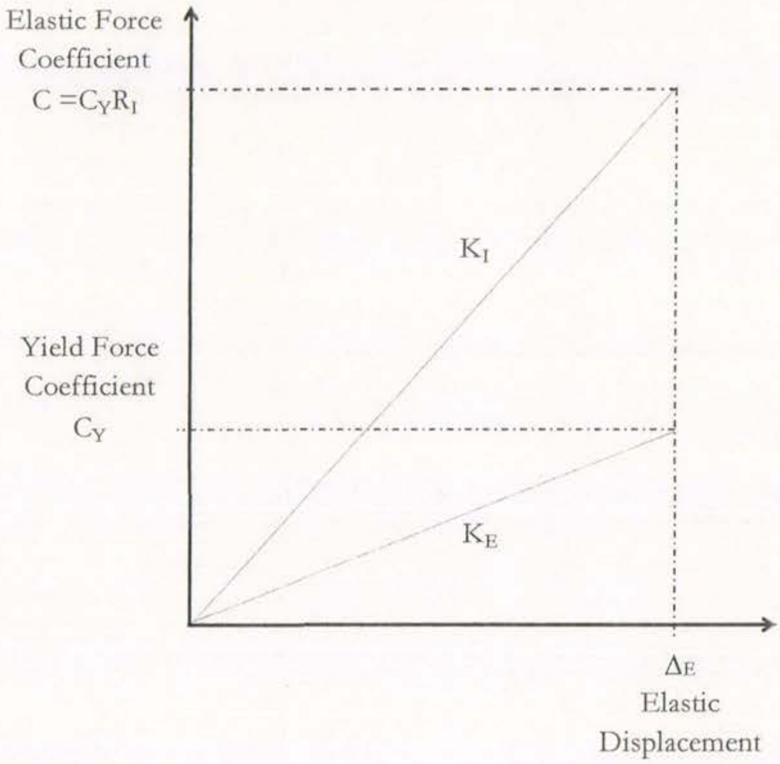

From Figure 10-8, the effective stiffness for a specified the yield coefficient can be expressed as a fraction of the initial stiffness and ductility factor, R_I:

$$K_E = \frac{K_I}{R_I} \tag{10-4}$$

The dynamic equation of motion defines an elastic system period, T, in terms of mass, M, and stiffness, K, as:

$$T = 2\pi\sqrt{\frac{M}{K}} \tag{10-5}$$

From which the stiffness can be expressed as a function of mass and period:

$$K = \frac{4\pi^2 M}{T^2} \tag{10-6}$$

Substituting the relationship from Equation (10-6) for both the initial and the effective stiffness in Equation (10-4) provides:

$$\frac{4\pi^2 M}{T_E^2} = \frac{4\pi^2 M}{R_I T_I^2} \tag{10-7}$$

Cancelling out common terms,

$$\frac{1}{T_E^2} = \frac{1}{R_I T_I^2} \tag{10-8}$$

Rearranging Equation (10-8), the effective period can be defined as a function of R as:

$$T_E = T_I \sqrt{R}_I \tag{10-9}$$

The effective period is therefore defined as the initial period times the square root of the ductility factor, where the ductility factor is based on the elastic response at the initial period.

10.4.2 Substitute Structure at Effective Period

The formulation developed as part of the design procedure was not based on the initial ductility factor but was rather based on the ductility factor at the effective period defined as:

$$R_E = \frac{C(T_E)}{C_Y} \tag{10-10}$$

To correlate Equation (10-10) with Equation (10-9), consider the constant velocity portion of the response spectrum plotted in Figure 10-9. This example is from NZS1170 Soil C but most design spectra have a segment where the acceleration is inversely proportional to T.

Fore the curves in Figure 10-9, when the period is in the range of 1.5 seconds to 3.0 seconds the spectral coefficient, C(T), at a specific period, T, is defined as the acceleration at period 1.5 seconds, C(1.5) divided by T:

$$C(T) = \frac{C(1.5)}{T} \tag{10-12}$$

From this relationship, the coefficients at two periods within the constant velocity range are related by the expression:

$$C(T_I) = C(T_E)\frac{T_E}{T_I} \tag{10-13}$$

Squaring both sides of Equation (10-9) above,

$$T_E^2 = T_I^2 R_I \tag{10-14}$$

Substituting the definition of initial ductility factor $R_I = \dfrac{C(T_I)}{C_Y}$ (Figure 10-8) gives

$$T_E^2 = T_I^2 \frac{C(T_I)}{C_Y} \tag{10-15}$$

Figure 10-9 NZS1170 Spectrum Z =0.14 Soil C Distant From Fault

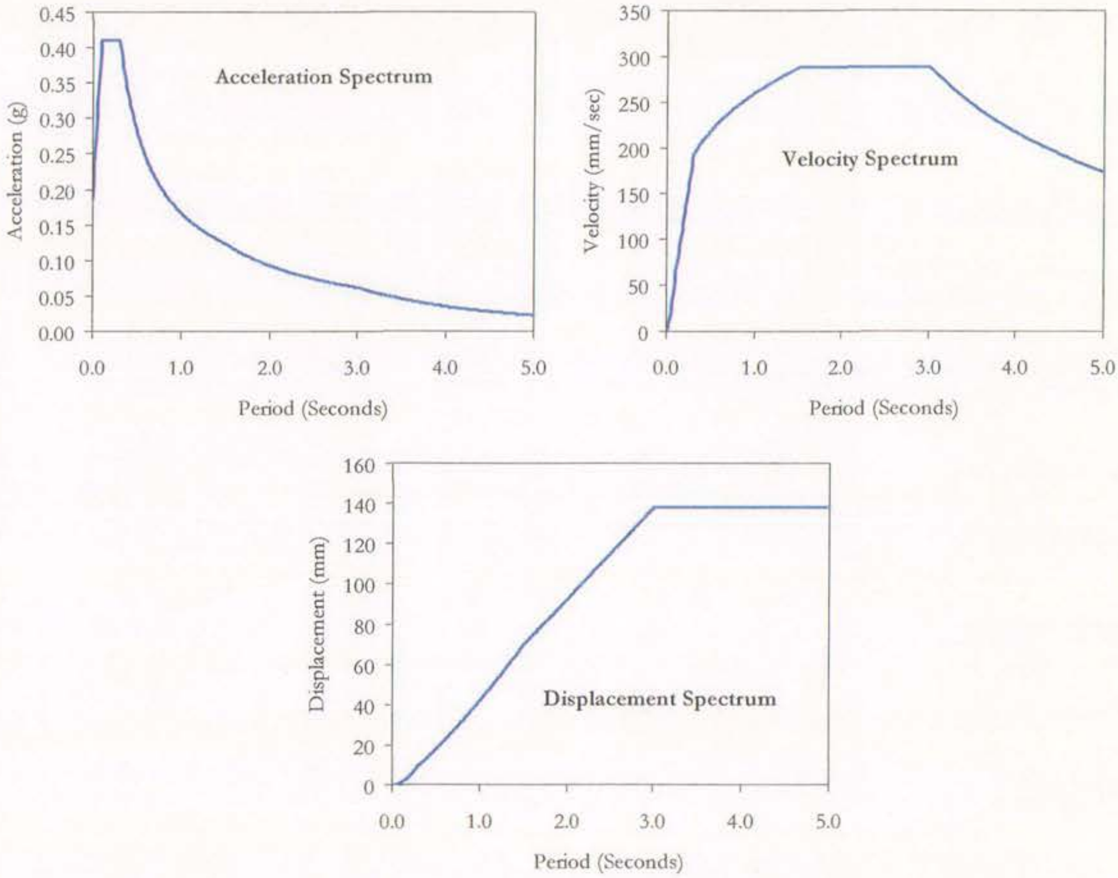

Replacing the definition of $C(T_I)$ from Equation (10-13) gives

$$T_E^2 = \frac{T_I^2}{C_Y} C(T_E) \frac{T_E}{T_I} \tag{10-16}$$

This simplifies to:

$$T_E = T_I \frac{C(T_E)}{C_Y} \tag{10-17}$$

From Equation (10-10) $\dfrac{C(T_E)}{C_Y} = R_E$ and so Equation (10-17) can be reduced to:

$$T_E = T_I R_E \tag{10-18}$$

This is the formulation developed in the design procedure developed previously. Therefore, for the constant velocity portion of the spectrum,

$$T_E = T_I R_E = T_I \sqrt{R_I} \tag{10-19}$$

From which it can be deduced that, in the constant velocity segment of the response spectrum, $R_E = \sqrt{R_I}$.

Therefore, either Equation (10-9) or Equation (10-18) can be used, and will produce the same result, if the acceleration coefficient is inversely proportional to period.

10.4.3 Capacity Spectrum Representation

The relationship between the ductility factors at the initial and effective periods in the constant velocity portion, represented by Equation (10-19), can be shown graphically using the capacity spectrum approach, discussed previously in Section 2.4. The capacity spectrum plots spectral acceleration versus spectral displacement. In this type of plot, radial lines through the origin represent different periods.

<u>Distant from Fault</u>

A capacity spectrum representation is shown in Figure 10-10 for a wall with an initial period of 1.50 seconds and a rocking coefficient of 0.10. The capacity spectrum is for NZS1170 Soil Class B greater than 20 km from a fault and so the acceleration is inversely proportional to period.

Figure 10-10 Capacity Spectrum Distant From Fault

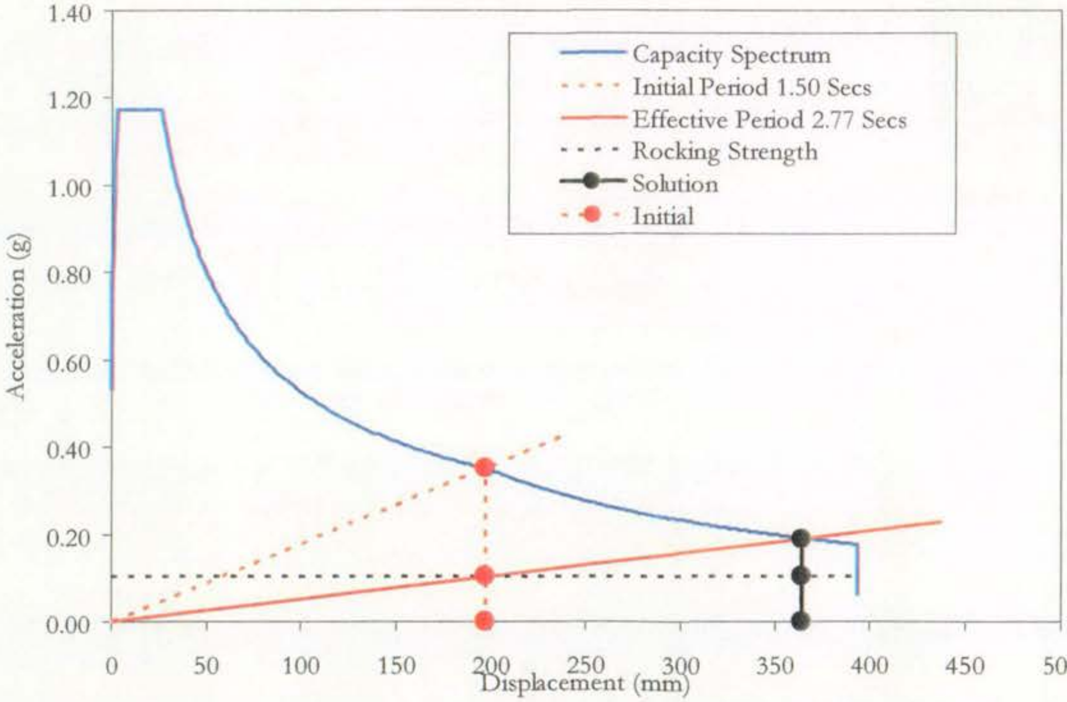

At the initial period of 1.50 seconds, the spectral acceleration is 0.352 and the initial ductility R_I = 0.352 / 0.100 = 3.52. From Equation (10-9) $T_E = T_I \sqrt{R_I}$ = 1.50 x √3.52

= 2.814 seconds. At this effective period, 2.814 seconds, the spectral acceleration is 0.1876 and the effective ductility factor R_E = 0.1876 / 0.100 = 1.876. From Equation (10-18) $T_E = T_I R_E$ = 1.50 x 1.876 = 2.814 seconds, the same results as obtained from Equation (10-9).

Near Fault

Figure 10-11 plots the same spectrum conditions as for Figure 10-10 except that it is assumed that the site is within 2 km of an active fault and so the spectrum coordinates are scaled by the near fault factor, N(T,D), for periods of 1.50 seconds or longer. At the initial period of 1.50 seconds the coefficient is the same as for the fault distant site and so Equation (10-9) would produce the same effective period, 2.814 seconds, as above. The use of Equation (10-18) requires an iterative solution which provides a period of 3.227 seconds. At 1.50 seconds the displacement is 197 mm, increasing to 485 mm at 2.814 seconds and to 557 mm at 3.227 seconds. Therefore, Equation (10-18) produces displacements 15% higher.

Figure 10-11 Capacity Spectrum Near Fault

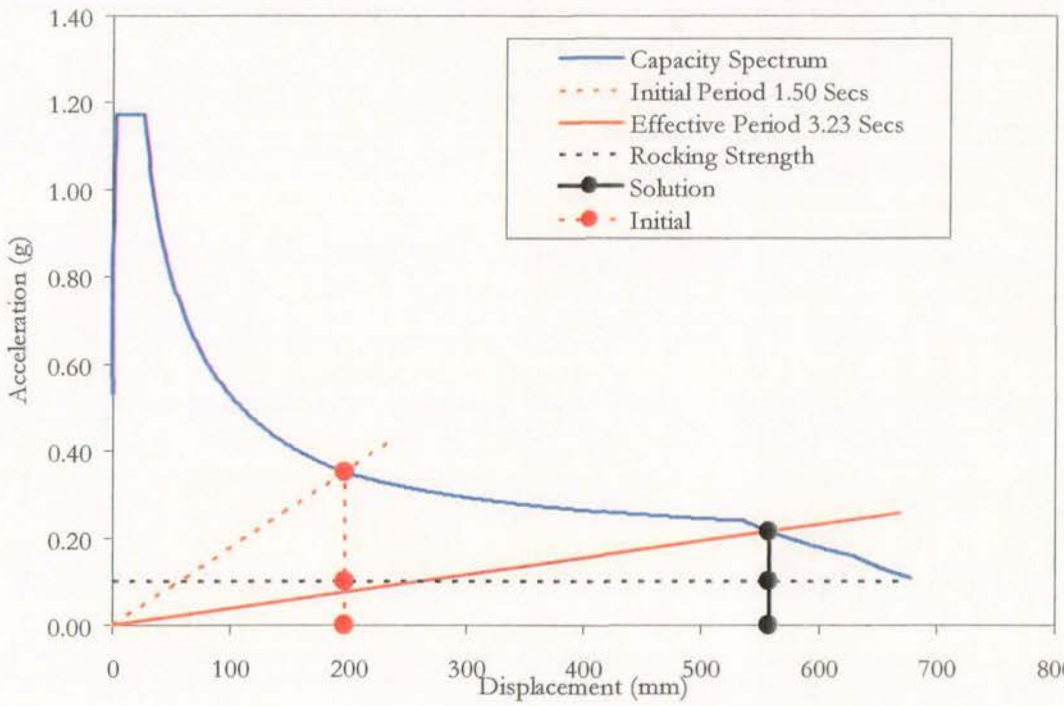

10.4.4 Comparison of Initial and Effective Period Equations

Equation (10-9) is much simpler to apply than Equation (10-18) as it is not recursive. The initial period and the initial ductility factor, R_I, can be calculated from properties of the wall and the elastic spectrum so iterative procedures are not needed. The reason that the more complex Equation (10-18) is used here is that it provides solutions where the acceleration coefficient is not inversely proportional to period. For example, short period walls or walls where response is influenced by the near fault coefficient. This is illustrated by three examples, where the displacements were calculated using both equations and the predictions compared with mean results from the times history analyses. The comparisons are presented in Figures 10-12 to 10-14. Each figure shows results for amplitudes ranging from ZR = 0.07 to 0.70 and for Site Classes B, C and D at both near fault and fault distant sites.

Short Period Wall

Figure 10-12 presents the results for a short period wall. The response plotted is for Wall 1, the 7.200 m long wall, 2 stories high on rock springs. This wall has an elastic period of 0.102 seconds and a rocking strength coefficient of 0.265. The calculated period of response ranged from 0.102 to 0.269 seconds using Equation (10-9) and from 0.102 to 0.640 seconds using Equation (10-18). The plateau of equal acceleration on the NZS1170 spectra for these soil types extends to 0.30 seconds for Class B and C and to 0.56 seconds for Class D so the response predicted by the initial ductility equation is on the plateau of the spectra for all amplitudes and classes. The response predicted by the effective ductility equation is on the falling branch for higher earthquake amplitudes.

For this wall, the use of the initial ductility as in Equation (10-8) severely underestimates the response for all amplitudes other than the very small values. The effective ductility Equation (10-18) provides a good match at all amplitudes.

Medium Period Wall

Figure 10-13 presents the results for a medium period wall, Wall 1, the 7.200 m long wall, 3 stories high on clay springs. This wall has an elastic period 0.645 seconds and a rocking strength coefficient of 0.189. The calculated period of response ranged from 0.645 to 1.881 seconds using Equation (10-9) and from 0.645 to 2.277 seconds using Equation (10-18), on the falling branch of the spectra.

For this wall, the use of the initial ductility in Equation (10-8) predicts smaller displacements than the effective ductility Equation (10-18) at all amplitudes. Both equations provide a generally similar match to the analyses results for fault distant locations but equation (10-18) provides a better match for near fault locations, especially for the softer soil classes.

Long Period Wall

Figure 10-14 presents the results for a long period wall, Wall 2, the 3.600 m long wall, 6 stories high on gravel springs. This wall has an elastic period 2.098 seconds and a rocking strength coefficient of 0.056. The calculated period of response ranged from 2.098 to 6.902 seconds using Equation (10-9) and from 2.098 to 6.078 seconds using Equation (10-18). In all cases the period was on the falling branch of the spectra and extended to the equal displacement portion of the spectra (3.0 seconds fault distant, 5.0 seconds near fault).

For these long periods the two methods produces almost identical responses for both near fault and far fault locations and provide a good match to the analysis results.

Figure 10-12 Comparison of Two Equations: Short Period Response

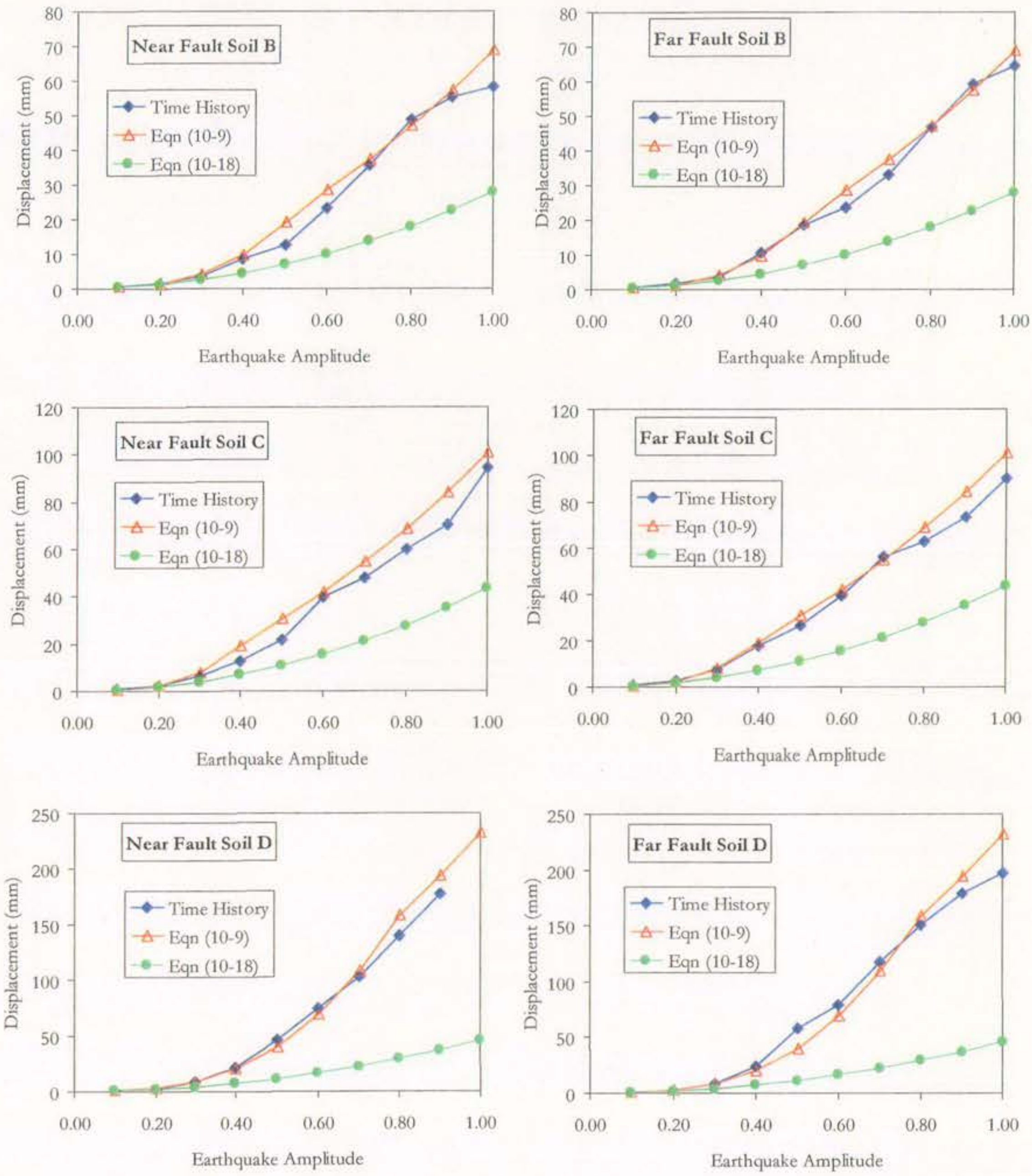

Figure 10-13 Comparison of Two Equations: Medium Period Response

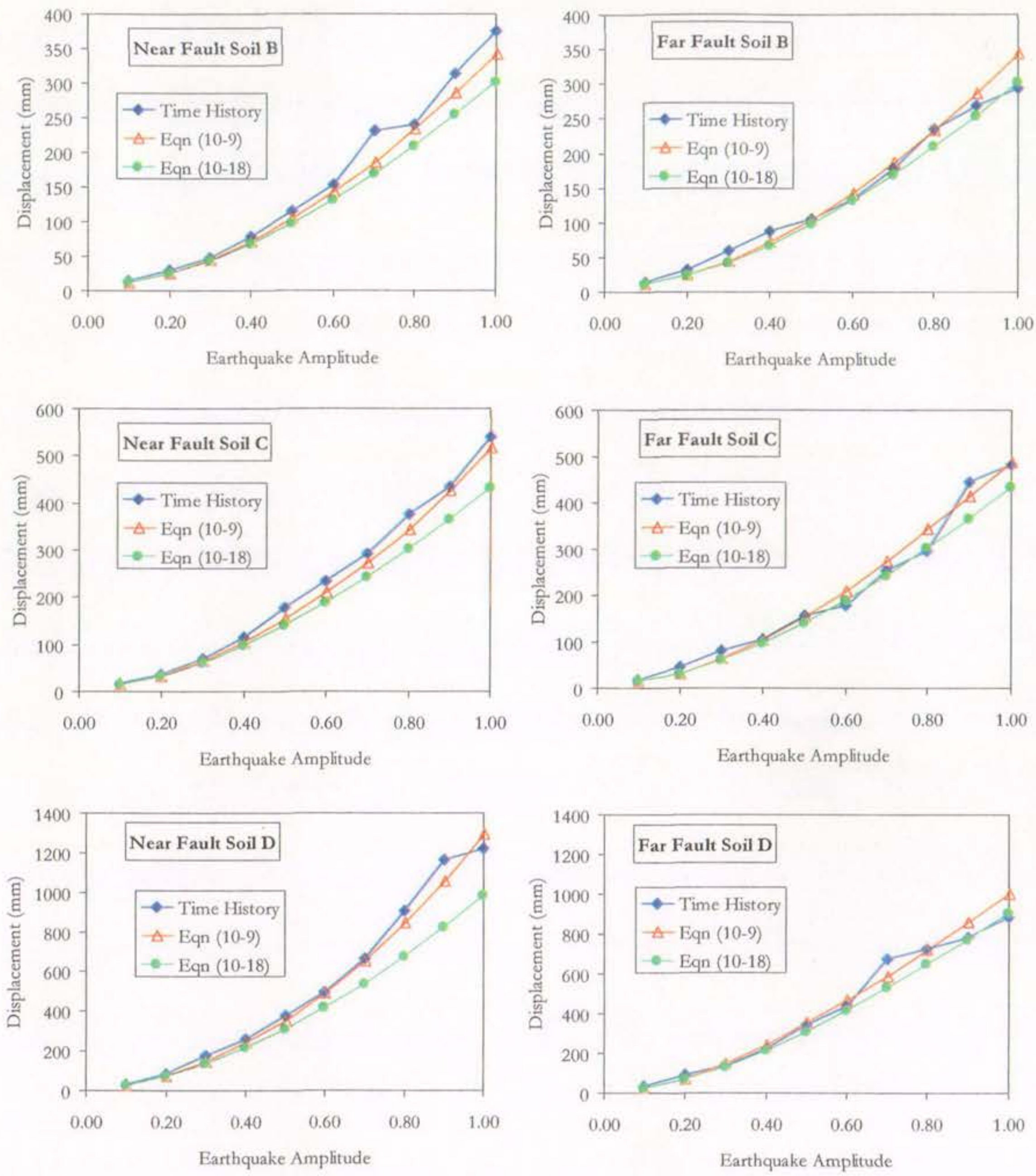

Figure 10-14 Comparison of Two Equations: Long Period Response

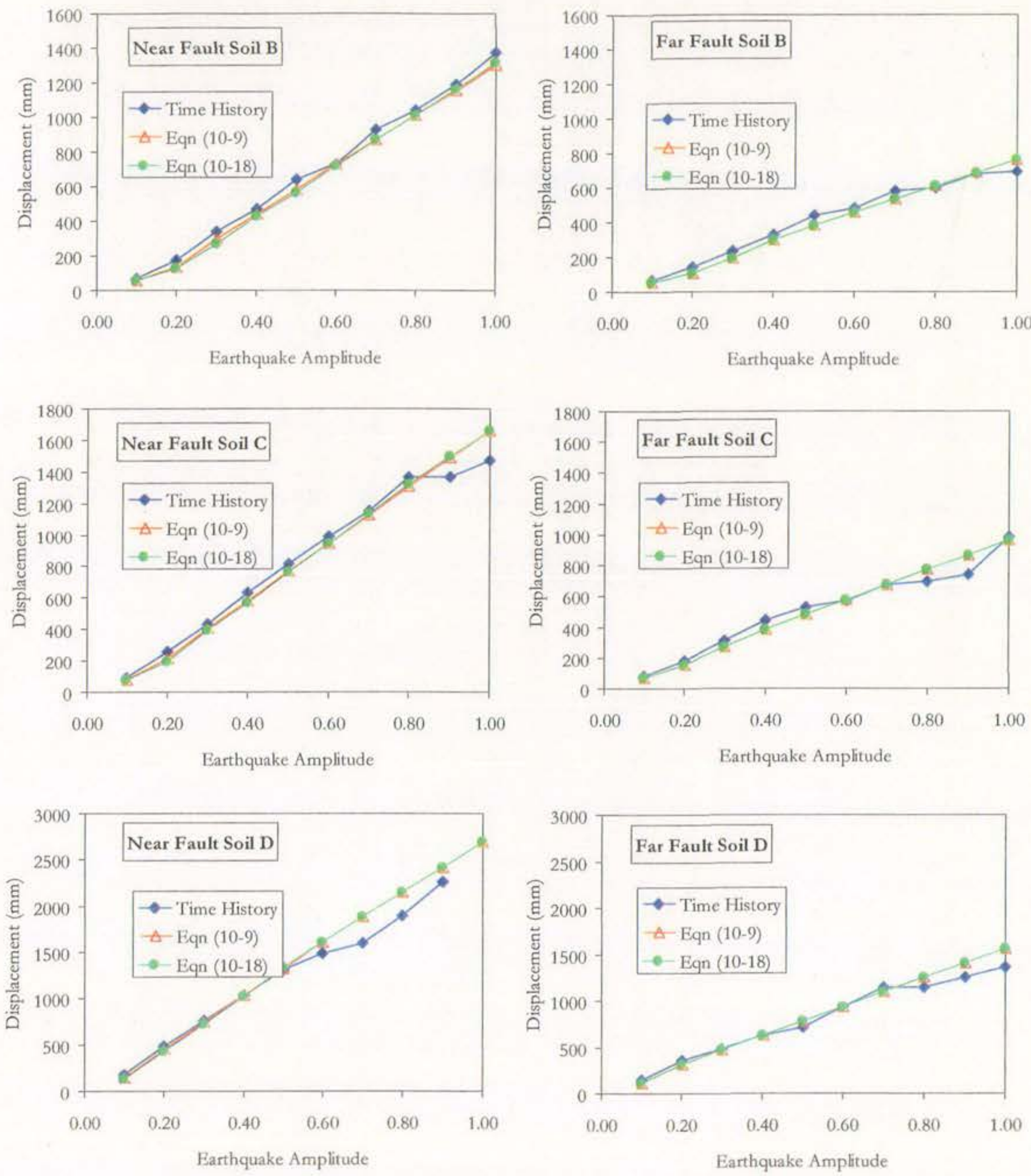

11 FUTURE RESEARCH REQUIREMENTS

The research on rocking structures reported here has served to illustrate the complexity of response of even what appear to be relatively simple rocking systems. Although it is considered that the tentative design procedure developed here will be helpful in design office environments, in terms of being better than ignoring the effects of uplift, there are a number of outstanding issues which future research could address. Some of these items will be clarified by research programs already underway on rocking systems.

11.1 Shear Amplification Factor

A tentative function to estimate dynamic amplification of shear forces was developed. The function was derived using an ad hoc approach and a more systematic approach using more sophisticated statistical techniques, such as the reliability index, would provide a more robust function.

In terms of dynamic amplifications, extremely large values were recorded for the taller walls (more than 3 stories). The shear distributions did not violate equilibrium and so were admissible from an engineering mechanics viewpoint. However, such large values have not been discussed in the literature and independent verification of the dynamic amplification would be useful. Two of the analyses for the 6 story wall were repeated using flexural elements rather than panel elements to represent the wall and similar dynamic amplification factors were recorded, confirming that the large factors are not a function of the element formulation.

11.2 Non-Planar Walls

Most of the development effort in this project was restricted to single walls. The procedures developed for single walls are applicable to multiple planar walls but only a limited number of examples of non-planar multiple wall structures were considered.

The design procedures did not match the non-planar configurations as well as the planar walls, especially for walls with a high degree of natural eccentricity. Future research to extend the number of examples of non-planar walls and refine procedure for this type of structure would be useful.

For the analyses in this project, accidental eccentricity was modelled by moving the floor mass by the specified eccentricity but no adjustment was made to the gravity loads. For rocking walls, the lateral load resistance is proportional to the vertical load on the wall. Therefore, if the floor loads were moved so as to provide the accidental eccentricity then the centre of stiffness would tend to move so as to reduce the effects of accidental eccentricity. This effect should be the subject of further study.

11.3 Period of Rocking Walls

Procedures have been provided to estimate the period of rigid rocking walls on specified soil springs, and also to modify the calculated period to incorporate the effect of wall flexibility. The simplified procedures have been checked on a single model and their applicability to a wider set of rocking structures needs to be assessed. Also, the procedure applies only to symmetrical walls or arrangements of walls. The method needs to be extended to walls where the periods include a torsional component.

11.4 Case Studies

The design procedures were applied to three configurations of non-planar wall buildings but they need to be checked using case studies of actual uplifting structures.

11.5 Soil Pressures and Effect of Soil Yielding

The example wall structures evaluated generally used the same width foundation, resulting in a constant soil pressure, for all sub-soil conditions. The scope of the studies could be extended to examine the effect of varying foundation width on response. The design procedures could be used as a relatively simple method for performing these studies.

All analyses used in this research to develop the guidelines assumed linear elastic soil springs, even though it is known that soil plasticity will modify response. The nonlinearity of foundation soil is a complex phenomena and research is required into appropriate ways to model this effect before the assessment of nonlinearity on response can be quantified.

11.6 Impact Effects and Soil-Structure Interaction

Uplifting is a dynamic procedure and so the foundation pressures will be influenced by impact effects as the gap closes at a particular velocity. The impact effects were examined in a superficial manner in this study and it was obvious that a simplified procedure, as is obtained by incorporating vertical mass in the model, is not reliable enough to gain useful design information. The modelling procedure used results in high frequency vibrations of individual springs and does not take account of important items such as the continuum nature of the soil springs which couples response of the springs; radiation damping which acts to reduce impact forces and soil-structure interaction where the response of the rocking wall modifies the input. Further research on all these topics is required.

11.7 Uplifting Framed Structures

The research here has concentrated on a common subset of rocking structures, shear wall type buildings. Frame structures form another subset of uplifting structures, where exterior and corner columns may be subject to tension. If a tension capacity is not provided at these locations then uplift will occur. This research focussed on rocking walls as the effects of rocking are likely to be more severe than in frames because a larger proportion of the foundation will separate from the ground. Future research should extend these procedures to assess whether they can be extended to include framed structures.

12 SUMMARY AND CONCLUSIONS

12.1 Evaluation Procedure

This study has examined the response of a range of rocking walls of various lengths, heights and soil stiffness values. The response was calculated using the nonlinear time history method of analysis. This method of analysis was shown to provide a reasonable representation of rocking response by comparing results with observed experimental results, although the Rayleigh damping mechanism was not an accurate representation of the energy loss due to rocking impacts and so limited the accuracy of the method.

The study used a series of sets of time histories. Each set comprised seven earthquake records each frequency scaled to match a spectra shape as defined by NZS1170, for both near fault and distant from fault locations. Generation of nonlinear response spectra using these motions demonstrated that use of average results from the seven scaled records produced a smooth curve and removed the variability associated with individual records. For this reason, the use of average results from seven records was adopted to define input for the wall evaluations.

12.2 Single Wall Response

The results of analyses of a series of single wall configurations showed that the displacement response was highly nonlinear once rocking occurred. For the highest seismic coefficients in New Zealand (represented by ZR = 0.70, the upper limit) displacements of the rocking wall were over 5 times the displacement for an equivalent elastic system.

As the earthquake amplitude increased the period of response lengthened, which was a major influence on the increased displacements. The rocking strength of the wall formed a limit to the base shear, and also maximum accelerations, for single story walls. However, for the multi-story walls higher mode deformed shapes were excited, causing dynamic amplification of shear forces and accelerations. Dynamic amplification was a strong function of the amplitude of rocking.

As expected, displacements were strongly related to the soil spring values and the seismic soil class, with large increases as the springs or soil conditions became softer. In the most extreme conditions, a wall displacement of 98 mm on rock springs and soil class B increased to 2438 mm for the same wall on soft clay, soil class D, an increase by a factor of more than 24. Near fault effects influenced response for period beyond 1.50 seconds and so were also very dependent on soil stiffness. The response of walls on rock tended to be insensitive to near fault effects but walls on soft springs were very sensitive, with displacements increasing by more than 50%.

Wall displacement was also very sensitive to the aspect ratio and height (represented by the number of stories). For the three story walls, there was an increase in displacements by a factor of about 5 when the aspect ratio increased from 0.25 to 0.50 and an increase by about 10 as the aspect ratio increased further to 1.00. The ratio was sensitive to earthquake magnitude and tended to decrease proportionately as the earthquake magnitude increases.

The wall reaction forces followed a pattern which was predictable from the engineering mechanics of rocking. With increasing displacement the reaction became successively more concentrated on the springs close to the compression edge of the wall. Eventually, as foundation separation increased the full weight of the wall was concentrated on the outermost spring and this formed the upper limit.

12.3 Impact Forces on Rocking Walls

The usual method of modelling for dynamic analysis specifies horizontal seismic mass but does not include vertical mass. Because of this, impact effects do not occur when the springs close as inertia forces are the product of vertical mass and vertical acceleration.

The analyses of a three story wall on two spring types were repeated with vertical mass included and these showed increases in maximum springs forces as the wall "bounced" on the soil spring. For the clay springs the spring period was about 0.38 seconds and the compression force varied by about $\pm 100\%$ from the mean value, which is the value when vertical mass is not included in the model. For the rock foundation the "bouncing" was much more pronounced, with a period of only about 0.10 seconds and an amplitude up to -100% and 300% of the values when vertical mass is excluded from the analysis. The negative variation is limited to -100% as at this point the gap re-opens and the force remains at zero.

Soil structure interaction is a complex process and includes important effects not included in this model, such as soil nonlinearity (strain dependence of properties) and radiation damping. These effects would tend to inhibit the resonance and so the maximum amplification of reaction forces is likely to be less than is obtained by including full vertical mass.

12.4 Design Actions on Single Walls

The results from the evaluations of single wall models were used to develop methods for deriving design actions on this type of wall. The resisting mechanism provided by the weight on the wall was derived using engineering mechanics. It was found that the displacement from the analysis could be predicted accurately by using an effective period defined as the initial elastic period times the response modification factor, R, which corresponds to the ductility factor. The single degree of freedom solution could be extended to multi-story walls using the FEMA factors C_0 and C_M to represent respectively the increase of displacement from centroid to roof and the effective mass excited in the fundamental mode.

The design shear force for the multi-story walls was higher than the static shear required to initiate rocking because of dynamic amplification effects. These effects were a strong function of the ductility factor.

12.5 Response of Multiple Wall Buildings

The evaluation was extended by considering a limit set of buildings comprising multiple planar walls and non–planar wall configurations, including two layouts of U-shaped walls.

These evaluations showed that it was possible to extend the procedures to develop design action for single walls to include multiple planar walls and symmetrical wall configurations with an acceptable level of accuracy. However, as the walls became more non-symmetrical the ability of the procedure to predict displacements decreased. Tentative recommendations to incorporate the effects of torsion were formulated but these require confirmation from a larger set of example buildings.

12.6 Comparison of Rocking and Yielding Response

A limited study was performed to evaluate two walls with both rocking and yielding base conditions. This demonstrated that permitting the base of the wall to rock resulted in higher displacements for all levels of seismic input, as a function of both wall type and seismic input. For a 3 story wall the average increase was 50% and for a 5 story wall the increase was less, 30% on average. This illustrated why procedures developed to estimate displacements in yielding systems require modification to be used for rocking system.

12.7 Tentative Design Procedure

The results from the single and multiple wall evaluations were used to develop a step-by-step tentative design procedure for rocking walls. The procedure provides a good estimate of displacements for a wide range of single walls and can be extended to multiple planar walls. The procedure can be used for structures comprising multiple non-planar walls but the accuracy will be less, especially for wall layouts which produce significant torsion.

Design aids were developed to enable the procedures to be implemented for design office use. In general, the equations are simple enough to be implemented by a designer with a basic understanding of engineering mechanics. Two steps are more complex, the calculation of period and the calculation of rocking displacement. Spreadsheet implementations of these two steps were provided.

12.8 Future Research

The research performed on rocking structures served to illustrate the complexity of response of even what appear to be relatively simple rocking systems. Although it is considered that the tentative design procedure developed here will be helpful in design office environments, in terms of being better than ignoring the effects of uplift, a number of outstanding issues which future research could address were identified, such as shear amplification factors; soil-structure interaction and impact effects and the effect of partial uplift on frame structures. Some of these items will be clarified by research programs already underway on rocking systems.

12.9 Effect of Ductility Factor 2 on Response

As discussed in the introduction, the predecessor to the current loading code was interpreted as requiring no special design provisions for rocking structures provided that uplift occurred at a level of seismic load no less than 50% of the full elastic load. This effectively permitted an elastic ductility factor of 2.0.

The design procedure was used to evaluate the effect of rocking for systems with a ductility factor 2, the limit permitted by the previous code. This showed that there were effects on both the displacements and shear forces:

1. Displacements are equal to or higher for a rocking structure than for an equivalent non-rocking system. The increase in displacements is greatest for structures on stiff springs (e.g. rock sites), where the displacements may be 4 times higher or more. Note however that on such stiff sites the displacements are generally small so the amplification of displacements may not have much effect. For soft springs, such that the elastic period is 1.0 second or more, rocking displacements are up to 1.64 times the elastic displacements for sites distant from a fault and up to 2.0 times higher at near fault locations.

2. Shear forces are increased by dynamic amplification factors which are higher than for ductile walls. At DF 2 the increase is less than 10% for 2 or 3 story structures but increases with height to an increase of 87% for 6 story structures.

These conclusions suggest that uplift corresponding to ductility factors of 2.0 be permitted provided the effect of a possible increase in displacement is assessed and that an increased dynamic amplification factor is used for the wall if it exceeds 3 stories in height.

13 REFERENCES

[1] Standards New Zealand, 1992. *Code of Practice for General Structural Design and Design Loadings for Buildings*, NZS 4203:1992, Standards New Zealand.

[2] Standards New Zealand. 2002. *Structural Design Actions, Parts 5 Earthquake Actions – New Zealand,*, NZS1170.5:2004, Standards New Zealand.

[3] M J N Priestley, R. J. Evison, A. J. Carr, 1978, *Seismic Response of Structures Free to Rock on Their Foundations*, Bulletin of the New Zealand National Society for Earthquake Engineering, Vol. 11, No. 3, September.

[4] ASCE, American Society of Civil Engineers, 2000. *Prestandard and Commentary for the Seismic Rehabilitation of Buildings*, prepared for the SAC Joint Venture, published by the Federal Emergency Management Agency *FEMA-356*, Washington, D.C.

[5] Nicos Makris & Dimitrios Konstantinidis, 2001, The *Rocking Spectrum and the Limitations of Design Guidelines*, PEER Report 2005/04 Pacific Earthquake Engineering Research Center College of Engineering University of California, Berkeley, August.

[6] J. Zhang1 and Nicos Makris, 2001, *Rocking Response Of Free-Standing Blocks Under Cycloidal Pulses*, ASCE Journal of Engineering Mechanics, Vol. 127, No. 5, May.

[7] Housner, G.W, 1963, *The behaviour of Inverted Pendulum Structures During Earthquakes*, Bulletin of the Seismological Society of America, Vol.53, No.2, February.

[8] C. S Yim, A. K. Chopra and J. Penzien, 1980, *Rocking Response Of Rigid Blocks To Earthquakes*, Earthquake Engineering and Structural Dynamics, Vol. 8, 565-587.

[9] Ishiyama, Y, 1982, *Motions Of Rigid Bodies And Criteria For Overturning By Earthquake Excitations*, Earthquake Engineering and Structural Dynamics, Vol. 10, 635-650.

[10] Psycharis, I. N., 1982, *Dynamic Behavior of Rocking Structures Allowed to Uplift*, EERL Report 81-02, California Institute of Technolohy, Pasadena, California.

[11] Huckelbridge, Arthur A, *Earthquake Simulation Tests of a Nine Story Steel Frame with Columns Allowed to Uplift*, Earthquake Engineering Research Center, Berkeley, CA, Report No. UCB/EERC-77-23, August, 1977.

[12] Ma, Q., Wight, G.D., Butterworth, J., and Ingham, J.M, *Assessment of Current Procedures for Predicting the In-Plane Behaviour of Controlled Rocking Walls,* Proceedings of the 8th U.S. National Conference on Earthquake Engineering, San Francisco, California, April, 2006.

[13] ElGawady, M.A., Ma, Q., Butterworth, J., and Ingham, J.M, *The Effect of Interface Material on the Dynamic Behaviour of Free Rocking Blocks*, Proceedings of the 8th U.S.

National Conference on Earthquake Engineering, San Francisco, California, April, 2006.

[14] C. Harden, T. Hutchinson, G. Martin, B. L. Kutter, 2005, *Numerical Modeling of the Nonlinear Cyclic Response of Shallow Foundations,* PEER Report 2005/04 Pacific Earthquake Engineering Research Center College of Engineering University of California, Berkeley August.

[15] B. L. Kutter, G. Martin, T. Hutchinson, C. Harden, S. Gajan, J. Phalen, 2006, *Workshop on Modeling of Nonlinear Cyclic Load-Deformation Behavior of Shallow Foundations,* PEER Report 2005/14 Pacific Earthquake Engineering Research Center College of Engineering University of California, Berkeley March.

[16] Chad William Harden & Tara Hutchinson, 2007, *Beam-on-Nonlinear-Winkler-Foundation Modeling of Shallow Rocking-Dominated Footings*, SEAOC 2007 Convention Proceedings.

[17] Donald L. Anderson, 2003, *Effect of Foundation Rocking on the Seismic Response of Shear Walls*, Canadian Journal of Civil Engineering, 30:360-365.

[18] ATC *Seismic Evaluation and Retrofit of Concrete Buildings*, Applied Technology Council, California, November, 1996

[19] Mondkar, D.P. and Powell, G.H., 1979, *ANSR II Analysis of Non-linear Structural Response User's Manual*, EERC 79/17, University of California, Berkeley, July.

[20] Kelly, T.E. 2000, *Performance Based Evaluation of Existing Buildings : Nonlinear Pushover and Time History Analysis : Reference Manual.* Revision 5, November, Holmes Consulting Group.

[21] Kelly, T. E., *A Blind Prediction Test Of Nonlinear Analysis Procedures For Reinforced Concrete Shear Walls,* Bulletin of the New Zealand Society for Earthquake Engineering, Vol. 40, No. 3, September, 2007.

[22] Rayleigh, Lord, 1877 *Theory of Sound (two volumes).* New York

[23] Opus International Consultants *Methodology for the Assessment of Face Loaded Unreinforced Masonry Walls Under Seismic Loading,* Report prepared for the EQC Research Foundation, May, 2000.

[24] Makris, N. and Roussos, Y., 1998, *Rocking Responseand Overturning of Equipment Under HorizontalPulse-Type Motions,* Pacific Earthquake Engineering Research Center, Berkeley, CA.

[25] Yim, S. C. and Chopra, A. K., 1985, *Simplified Earthquake Analysis of Multistory Structures with Foundation Uplift*, Journal of Structural Engineering, American Society of Civil Engineers, New York, New York, Vol. 111, No. 12, pp. 2708-2731.

[26] Kelly, T. E. *Earthquake Resistance of Unreinforced Masonry Buildings*, New Zealand National Society for Earthquake Engineering, Conference Proceedings, Rotorua, New Zealand, March, 1995.

APPENDIX A

DETAILED RESULTS

NOTES:

1. In the tables and plots in this appendix, the earthquake scale factors are normalized such that a value of 1.0 corresponds to the upper limit on the seismic zone factor in NZS1170, ZR = 0.70.

2. In all Figures, two curves are plotted. The curves labelled "Time History" represent the mean results from 7 nonlinear time history analyses. The curves labelled "1-DOF" are the displacements predicted from the equations presented in this report, which are based on a single degree of freedom (1-dof) equivalent elastic system approximation.

LIST OF TABLES

LIST OF FIGURES

Table A- 1 Displacements Wall 1 7.200 m 1 to 3 Stories Near Fault Springs B,E,G

Scale	Single Story			Two Story			Three Story		
Factor	Clay	Gravel	Rock	Clay	Gravel	Rock	Clay	Gravel	Rock
Soil Class B									
0.10	3.1	0.7	0.1	10.6	4.3	0.6	21.6	9.6	2.0
0.20	6.4	1.4	0.1	21.4	10.5	1.5	44.3	20.2	6.9
0.30	11.8	2.4	0.2	36.8	19.2	3.6	77.7	32.1	14.5
0.40	19.0	4.4	0.4	51.5	28.7	8.5	115.3	52.5	26.7
0.50	25.6	9.1	0.8	69.1	38.3	12.7	142.4	67.1	32.1
0.60	32.7	13.1	1.3	90.0	45.3	23.3	213.7	106.3	43.9
0.70	41.3	18.5	2.6	130.3	60.6	35.7	264.7	155.2	53.8
0.80	46.9	24.7	5.9	157.2	66.6	48.8	341.9	167.8	71.0
0.90	57.2	38.1	8.9	199.1	89.7	55.2	378.9	214.3	88.5
1.00	74.1	46.9	12.3	287.4	109.6	58.4	458.9	287.5	98.3
Soil Class C									
0.10	3.9	0.8	0.1	13.2	5.4	0.8	27.0	12.3	2.7
0.20	8.6	1.9	0.2	28.5	14.6	2.3	59.1	25.6	8.5
0.30	16.9	4.1	0.3	48.0	25.9	6.6	106.9	48.6	22.2
0.40	25.8	8.8	0.8	69.2	38.4	12.7	142.0	67.6	35.2
0.50	34.2	14.1	1.4	96.4	52.9	21.7	236.8	112.6	52.2
0.60	46.3	23.3	4.4	164.2	65.0	39.7	304.3	148.3	62.0
0.70	55.2	32.8	8.6	206.8	83.7	47.9	362.1	191.0	87.1
0.80	78.1	45.7	13.7	288.6	109.2	59.9	463.8	296.1	97.0
0.90	75.2	49.4	18.3	308.3	155.5	70.3	609.1	327.2	153.2
1.00	87.1	65.2	27.5	376.4	165.7	94.6	728.3	377.4	204.5
Soil Class D									
0.10	3.9	0.8	0.1	21.3	5.4	0.8	44.9	18.9	2.8
0.20	8.9	1.9	0.2	52.8	18.8	2.3	118.4	54.9	13.4
0.30	18.3	4.3	0.3	107.0	38.9	8.0	223.3	117.5	31.5
0.40	32.6	10.6	0.9	167.3	68.0	20.8	341.7	195.5	67.4
0.50	55.1	17.1	2.1	259.7	125.5	45.7	468.5	295.7	116.3
0.60	80.7	36.0	6.6	356.8	177.3	74.7	676.8	378.5	181.4
0.70	127.5	57.2	13.1	448.0	224.6	103.0	864.1	515.4	258.8
0.80	152.4	64.4	24.9	561.4	369.2	139.7	1165.4	663.5	365.3
0.90	191.6	110.4	38.3	720.6	459.2	177.5	1475.9	775.5	437.3
1.00	258.7	132.9	59.6	796.2	530.7	219.1	1587.2	884.8	498.7

Table A- 2 Displacements Wall 1 7.200 m 1 to 3 Stories Far Fault Springs B,E,G

Scale	Single Story			Two Story			Three Story		
Factor	Clay	Gravel	Rock	Clay	Gravel	Rock	Clay	Gravel	Rock
Soil Class B									
0.10	3.1	0.7	0.1	10.7	4.1	0.6	23.2	8.9	2.0
0.20	6.6	1.5	0.1	23.1	10.8	1.7	46.9	20.1	5.9
0.30	12.4	2.6	0.2	40.9	19.3	3.5	74.8	34.6	15.9
0.40	19.9	5.4	0.4	56.3	31.5	10.6	117.3	56.5	30.3
0.50	28.0	9.7	0.7	86.1	45.0	18.5	160.1	80.9	40.0
0.60	30.8	16.1	1.7	115.1	59.6	23.5	189.1	107.0	55.2
0.70	47.3	19.9	3.0	131.6	81.6	32.9	247.8	140.2	67.8
0.80	61.4	27.8	5.9	161.6	97.2	46.8	276.7	177.3	82.9
0.90	67.7	38.1	10.6	198.0	111.6	59.2	315.1	184.0	101.4
1.00	81.4	48.4	15.3	213.4	139.1	64.3	394.3	245.4	125.4
Soil Class C									
0.10	3.8	0.9	0.1	13.4	5.2	0.8	29.0	11.2	3.0
0.20	9.4	2.0	0.2	30.5	14.1	2.6	60.5	26.2	11.1
0.30	17.2	4.2	0.3	53.5	26.4	7.6	104.0	52.5	27.2
0.40	28.0	10.8	0.7	85.9	45.1	17.8	160.4	77.7	40.2
0.50	39.2	16.2	2.2	118.0	62.7	26.3	198.2	115.1	60.2
0.60	54.1	22.3	4.3	142.6	84.7	39.2	245.4	153.7	78.3
0.70	64.1	36.1	9.2	191.9	112.2	55.9	292.9	183.0	97.6
0.80	78.7	47.7	16.3	215.5	138.1	62.8	392.1	241.6	131.4
0.90	86.6	61.9	23.9	230.6	150.8	73.1	503.2	302.7	139.0
1.00	115.1	65.1	29.8	306.7	185.7	90.2	675.9	356.6	160.4
Soil Class D									
0.10	3.8	0.9	0.1	22.9	5.3	0.8	47.6	17.3	3.1
0.20	9.5	2.1	0.2	55.4	17.9	2.4	120.8	54.3	12.7
0.30	19.2	5.0	0.3	119.7	51.5	8.6	183.1	103.5	51.9
0.40	40.7	10.9	0.7	153.2	99.0	23.7	278.3	155.2	90.1
0.50	79.3	19.7	1.8	207.6	143.4	57.6	392.6	244.7	122.8
0.60	117.4	36.1	5.9	266.7	177.0	78.8	618.3	335.6	167.7
0.70	153.4	64.0	11.7	411.0	193.7	117.6	739.2	454.1	198.3
0.80	186.4	98.2	24.7	456.7	255.8	149.8	832.1	606.3	238.2
0.90	210.8	134.9	35.1	664.5	295.5	178.5	968.6	659.2	295.1
1.00	229.1	148.4	52.6	715.5	361.4	197.2	1173.2	670.4	383.0

Table A- 3 Displacements Wall 1 7.200 m Long 3 Stories Springs A,C,D,F

Scale Factor	Near Fault				Far Fault			
	Soft Clay	Hard Clay	Soft Gravel	Hard Gravel	Soft Clay	Hard Clay	Soft Gravel	Hard Gravel
Soil Class B								
0.1	61.8	14.3	11.1	7.7	55.9	14.9	11.3	7.9
0.2	123.6	30.0	24.6	17.8	111.9	32.4	26.4	17.6
0.3	185.9	46.5	40.7	27.8	167.9	60.0	44.4	31.0
0.4	258.2	77.6	58.6	45.4	227.5	87.8	78.1	50.8
0.5	367.3	114.1	82.6	60.9	287.7	105.3	98.3	77.4
0.6	468.9	152.8	142.9	91.9	380.2	133.3	119.5	96.6
0.7	594.6	231.5	165.8	119.6	460.9	177.7	164.6	138.4
0.8	751.5	239.7	248.4	153.2	545.7	234.3	186.4	151.1
0.9	908.2	313.9	275.3	179.8	631.8	268.2	231.6	180.0
1.0	1060.3	375.1	323.3	249.8	742.8	293.3	274.1	201.5
Soil Class C								
0.1	77.7	17.9	14.0	9.8	70.3	18.6	14.3	10.1
0.2	155.4	37.7	32.3	23.3	140.6	45.9	36.8	23.1
0.3	239.4	68.5	54.8	41.6	213.2	80.6	68.2	46.7
0.4	371.6	113.9	82.7	61.0	289.5	105.5	98.4	77.0
0.5	502.6	177.6	133.0	100.7	411.1	156.8	126.4	108.8
0.6	681.2	234.0	218.1	135.9	502.4	177.0	173.5	135.4
0.7	878.1	291.9	277.2	176.6	607.7	252.6	215.1	173.4
0.8	1067.6	376.6	320.9	249.4	753.9	293.4	274.5	219.4
0.9	1196.4	433.1	377.2	306.6	842.4	443.6	334.6	259.5
1.0	1355.5	539.0	455.8	357.4	945.4	482.2	411.9	325.3
Soil Class D								
0.1	125.6	30.6	24.3	13.4	113.5	34.0	26.4	14.4
0.2	263.9	82.7	57.8	45.2	230.8	92.5	73.1	50.8
0.3	479.8	174.6	124.4	76.9	389.9	140.7	121.9	96.7
0.4	775.1	255.5	260.4	171.4	562.0	225.8	176.1	149.4
0.5	1078.1	375.4	329.1	281.8	774.8	342.9	279.4	215.4
0.6	1315.7	491.6	434.1	395.7	916.6	436.2	378.4	306.0
0.7	1474.7	666.0	579.8	490.1	1169.3	669.2	476.8	385.5
0.8	1961.5	907.9	670.6	624.9	1270.2	725.6	609.4	492.7
0.9	2133.0	1164.8	920.3	670.3	1393.3	780.5	704.9	604.1
1.0	2437.8	1217.8	1072.9	827.2	1511.7	879.7	779.9	708.9

Table A- 4 Displacements Wall 2 3.600 m 1 to 3 Stories Near Fault Springs B,E,G

Scale Factor	Single Story			Two Story			Three Story		
	Clay	Gravel	Rock	Clay	Gravel	Rock	Clay	Gravel	Rock
Soil Class B									
0.10	9.2	3.6	0.5	30.8	12.2	3.9	66.4	26.2	9.4
0.20	20.6	10.3	1.5	62.4	29.4	12.9	136.3	66.1	20.5
0.30	33.4	18.4	5.3	103.6	50.4	20.3	246.7	120.3	39.8
0.40	47.7	25.0	9.9	163.2	95.4	31.3	381.3	166.0	76.9
0.50	72.0	40.9	19.2	219.9	148.7	46.9	537.2	257.8	135.5
0.60	111.1	43.5	24.8	314.9	185.0	72.4	635.5	394.2	180.2
0.70	137.7	61.9	35.5	435.9	229.4	102.5	782.0	463.5	214.2
0.80	190.3	89.7	41.0	603.1	290.9	138.1	947.7	664.3	314.2
0.90	223.3	102.9	56.1	575.5	369.2	214.7	1057.9	762.9	374.5
1.00	264.4	132.2	71.3	727.6	455.0	255.3	1211.5	767.2	411.9
Soil Class C									
0.10	11.5	4.7	0.7	38.5	15.7	5.9	83.5	33.2	11.8
0.20	26.4	13.4	2.6	83.9	39.2	17.6	189.5	91.7	31.7
0.30	41.4	24.5	8.2	145.8	81.1	33.8	348.9	151.0	72.7
0.40	72.0	40.7	20.4	216.7	154.3	46.1	540.8	261.7	133.0
0.50	120.1	47.5	29.5	335.6	192.8	74.6	688.2	425.2	188.2
0.60	180.7	72.3	38.2	505.7	254.7	119.6	879.2	608.3	250.6
0.70	218.5	99.5	52.9	665.1	367.0	200.9	1026.2	648.5	350.6
0.80	268.5	125.5	71.0	718.3	466.6	255.2	1219.3	799.9	432.4
0.90	316.1	172.5	82.2	769.9	511.2	296.6	1346.4	1012.5	533.5
1.00	371.2	247.8	104.7	945.8	742.1	343.3	1545.9	1276.4	664.2
Soil Class D									
0.10	21.2	4.9	0.7	63.5	30.3	6.4	139.5	68.3	21.5
0.20	50.1	20.1	2.8	167.5	100.7	32.9	392.0	170.0	86.2
0.30	100.6	48.7	12.2	322.0	187.6	75.8	656.0	407.4	177.8
0.40	203.2	85.1	37.3	615.1	286.1	122.8	970.3	620.2	315.5
0.50	272.9	154.7	52.9	790.4	464.0	258.1	1236.8	758.7	444.6
0.60	344.0	230.7	84.0	848.3	594.7	337.4	1446.2	1236.7	727.5
0.70	473.9	310.0	126.7	1325.4	829.2	396.0	1800.2	1350.0	894.9
0.80	541.0	391.9	172.6	1711.3	1078.5	528.8	2179.8	1604.1	1077.8
0.90	787.8	436.2	206.0	1877.1	1113.9	675.0	2073.6	1751.9	1219.5
1.00	918.5	497.9	258.2	2066.5	1503.4	793.0	2265.4	1968.1	1323.0

Table A- 5 Displacements Wall 2 3.600 m 1 to 3 Stories Far Fault Springs B,E,G

Scale Factor	Single Story			Two Story			Three Story		
	Clay	Gravel	Rock	Clay	Gravel	Rock	Clay	Gravel	Rock
Soil Class B									
0.10	9.5	3.8	0.5	30.5	13.0	4.3	59.7	27.7	9.1
0.20	20.0	10.4	1.8	64.3	32.8	14.4	119.3	65.1	25.7
0.30	33.9	20.4	4.4	102.0	60.8	25.5	198.8	101.7	46.8
0.40	68.3	30.6	12.3	153.5	79.0	36.9	281.2	147.8	76.8
0.50	82.8	46.1	19.4	226.2	104.3	56.9	374.5	205.9	110.1
0.60	100.8	60.9	30.1	304.3	158.6	82.4	453.2	324.4	156.4
0.70	133.5	78.3	38.3	337.6	210.8	105.7	553.5	381.3	209.9
0.80	133.1	97.8	46.0	419.0	287.3	126.2	650.4	424.3	234.2
0.90	165.1	117.6	53.0	419.7	333.3	152.5	735.3	484.4	311.4
1.00	226.1	126.5	65.8	506.5	353.3	183.9	769.7	609.9	352.9
Soil Class C									
0.10	11.8	4.9	0.7	38.1	16.7	5.9	75.0	35.7	12.1
0.20	29.1	15.3	3.2	87.4	50.0	19.5	155.1	82.4	37.9
0.30	52.8	28.3	10.6	134.9	74.1	38.4	245.4	141.6	63.2
0.40	82.9	46.8	18.2	224.7	104.7	56.0	377.9	200.7	100.3
0.50	110.0	62.0	32.6	332.5	171.1	82.8	477.4	352.3	173.3
0.60	134.4	88.5	45.1	383.4	228.4	110.8	605.4	415.1	227.8
0.70	158.5	104.6	48.4	456.0	324.8	146.9	737.1	452.6	285.7
0.80	220.6	125.9	67.1	507.2	354.2	184.2	771.0	583.0	362.2
0.90	274.1	148.5	83.7	636.1	432.3	231.2	859.4	716.3	404.3
1.00	356.1	174.7	99.6	615.8	511.8	258.1	951.4	822.8	485.9
Soil Class D									
0.10	20.6	5.2	0.7	65.5	34.0	6.8	121.3	65.8	22.4
0.20	57.4	21.4	3.4	153.8	83.1	42.8	293.9	149.9	77.2
0.30	93.9	66.6	12.3	314.8	172.1	80.5	461.3	313.0	147.8
0.40	132.6	97.6	40.8	411.9	281.3	124.2	650.6	428.1	248.8
0.50	241.6	121.2	66.4	520.5	399.7	175.8	776.5	614.2	361.8
0.60	301.6	168.1	93.1	591.3	491.1	254.6	946.5	789.5	451.2
0.70	441.5	207.9	108.4	951.5	624.9	346.6	1001.2	910.9	570.2
0.80	551.6	289.1	125.7	1034.2	649.9	403.7	1063.7	949.9	672.0
0.90	571.4	371.7	151.1	1082.4	799.3	448.6	1222.3	1057.7	751.7
1.00	687.4	432.2	187.5	1186.6	927.6	491.1	1497.4	1185.1	797.0

Table A- 6 Displacements Wall 2 3.600 m 4 to 6 Stories Near Fault Springs B,E,G

Scale	Four Stories			Five Stories			Six Stories		
Factor	Clay	Gravel	Rock	Clay	Gravel	Rock	Clay	Gravel	Rock
Soil Class B									
0.10	89.1	34.9	15.5	122.9	51.2	27.5	138.3	70.6	35.0
0.20	179.6	79.5	48.0	247.1	121.2	77.4	277.5	175.4	91.8
0.30	290.1	141.0	100.6	401.7	236.9	133.9	442.1	342.7	193.6
0.40	443.3	249.9	145.2	602.2	389.6	229.7	647.7	469.9	330.9
0.50	626.8	419.2	213.9	744.0	494.3	394.8	791.9	639.1	440.5
0.60	835.7	419.7	304.1	915.3	593.7	503.0	991.5	731.4	552.3
0.70	967.3	549.5	427.5	1024.5	805.3	552.3	1159.2	930.7	762.7
0.80	1172.3	689.1	519.1	1268.8	940.9	757.8	1313.9	1040.2	895.2
0.90	1284.5	981.8	673.6	1459.7	1132.9	868.8	1555.9	1191.1	972.5
1.00	1338.9	1134.1	708.0	1523.2	1183.9	1035.4	1672.8	1369.1	1078.6
Soil Class C									
0.10	112.1	43.7	20.4	154.6	64.4	37.2	173.8	88.8	44.6
0.20	231.3	113.0	65.2	314.5	157.3	107.0	356.1	257.0	120.4
0.30	404.7	225.8	129.4	577.2	333.4	204.7	603.9	433.3	299.0
0.40	630.9	420.5	213.4	759.7	493.2	396.2	792.3	636.3	423.3
0.50	845.2	476.1	303.8	967.2	645.4	530.4	1048.1	818.2	596.6
0.60	1083.8	591.6	482.2	1144.2	908.3	648.4	1256.7	992.5	862.0
0.70	1261.6	910.4	657.9	1431.5	1086.1	916.8	1462.8	1150.0	958.3
0.80	1344.3	1139.1	721.8	1532.7	1217.2	1034.5	1672.5	1363.6	1081.5
0.90	1517.1	1246.3	933.5	1602.2	1426.0	1137.1	1771.6	1367.6	1187.7
1.00	1708.7	1383.1	1102.3	1798.3	1545.9	1200.9	1828.2	1471.4	1362.4
Soil Class D									
0.10	80.7	49.8	251.2	123.9	79.4	281.6	179.3	94.1	
0.20	262.3	151.1	607.7	411.9	236.8	652.6	480.3	338.7	
0.30	475.2	320.7	938.5	665.8	507.4	1008.8	764.8	505.8	
0.40	769.2	575.1	1302.7	964.0	818.2	1337.9	1039.3	913.5	
0.50	1167.8	764.3	1533.5	1267.6	1070.1	1684.0	1316.4	1100.3	
0.60	1368.3	1075.2	1733.6	1457.7	1229.5	1785.8	1485.6	1308.1	
0.70	1576.2	1273.3	2124.5	1621.5	1376.6	1828.0	1602.4	1459.9	
0.80	1757.8	1280.3	2242.7	1655.6	1565.1	2076.4	1900.2	1497.2	
0.90	1981.6	1409.4	2371.3	2006.1	1719.2	2180.0	2258.6	1820.8	
1.00	1874.7	1598.1		2270.0	1789.5			2265.2	

Table A- 7 Displacements Wall 2 3.600 m 4 to 6 Stories Far Fault Springs B,E,G

Scale Factor	Four Stories			Five Stories			Six Stories		
	Clay	Gravel	Rock	Clay	Gravel	Rock	Clay	Gravel	Rock
Soil Class B									
0.10	71.6	36.7	16.8	88.4	51.9	28.6	82.2	63.9	35.4
0.20	143.2	75.0	46.2	176.8	116.7	64.3	164.4	141.7	83.0
0.30	219.8	138.4	76.9	269.4	182.1	110.9	246.7	237.5	167.5
0.40	309.7	224.4	119.6	373.3	271.7	212.9	330.8	331.1	229.8
0.50	425.8	284.0	211.6	458.4	393.4	268.5	427.8	442.2	272.4
0.60	576.2	348.9	262.3	533.0	456.4	331.9	550.9	479.5	382.9
0.70	651.8	427.0	327.0	599.9	483.0	405.4	639.7	580.1	493.7
0.80	688.9	487.4	387.2	715.0	625.0	526.7	700.7	602.2	536.1
0.90	729.5	664.1	464.5	789.6	672.0	603.7	801.5	683.3	597.5
1.00	842.1	718.2	500.7	891.8	733.6	632.1	881.8	694.5	656.2
Soil Class C									
0.10	90.0	46.6	23.1	111.1	65.4	36.2	103.4	80.3	45.7
0.20	180.7	102.1	58.5	222.6	154.0	89.8	206.9	178.8	120.3
0.30	292.6	218.2	109.5	352.8	243.1	181.4	311.3	310.3	205.2
0.40	428.7	291.3	213.6	460.9	403.1	271.6	430.9	443.9	264.2
0.50	602.9	371.4	285.3	549.7	510.0	350.4	587.8	530.1	407.0
0.60	664.7	417.6	333.5	663.4	572.6	481.0	676.2	571.5	536.9
0.70	723.2	565.7	446.6	777.3	660.2	576.7	783.9	676.1	584.3
0.80	845.0	720.8	513.0	890.1	742.8	634.0	888.6	695.1	663.6
0.90	888.5	743.2	583.3	1068.2	854.1	691.7	1017.7	742.0	760.1
1.00	873.5	843.4	685.8	1171.5	899.2	747.1	1167.5	985.1	877.2
Soil Class D									
0.10	145.7	75.4	46.5	179.8	121.1	65.6	168.0	143.8	83.6
0.20	320.5	223.0	117.9	380.0	271.4	189.3	338.2	353.2	232.0
0.30	584.9	359.0	262.7	539.4	470.8	327.4	570.4	485.4	392.8
0.40	691.0	502.5	366.1	734.7	632.0	531.3	722.2	627.2	549.9
0.50	859.0	720.9	483.7	911.9	773.5	664.9	904.0	710.7	658.4
0.60	870.0	814.8	656.6	1145.5	870.2	711.2	1089.8	931.0	863.6
0.70	986.4	945.5	725.0	1256.7	1015.9	872.2	1175.0	1139.8	981.2
0.80	1304.0	1117.3	810.4	1374.9	1166.4	1020.2	1277.1	1146.3	1212.2
0.90	1476.6	1218.9	981.9	1421.0	1370.9	1203.3	1392.0	1252.8	1284.7
1.00	1487.5	1383.2	1117.1	1488.7	1531.1	1416.1	1639.6	1360.9	1348.1

Table A- 8 Displacements Wall 3 14.400 m 1 to 3 Stories Near Fault Springs B,E,G

Scale Factor	Single Story			Two Story			Three Story		
	Clay	Gravel	Rock	Clay	Gravel	Rock	Clay	Gravel	Rock
Soil Class B									
0.10	0.5	0.1	0.0	3.0	0.7	0.1	7.4	2.1	0.3
0.20	1.0	0.2	0.0	6.1	1.4	0.2	15.1	4.6	0.7
0.30	1.5	0.3	0.1	10.2	2.4	0.3	23.9	9.7	1.5
0.40	2.1	0.4	0.1	16.0	3.9	0.4	36.6	15.9	2.4
0.50	2.9	0.5	0.1	22.9	5.2	0.6	46.0	28.0	4.4
0.60	4.1	0.6	0.1	33.0	11.1	1.1	51.9	33.6	8.7
0.70	5.5	0.8	0.1	41.4	16.0	1.9	79.7	46.2	11.9
0.80	7.3	1.2	0.2	47.0	23.7	2.3	91.4	52.3	19.0
0.90	9.0	1.5	0.2	59.4	27.7	4.7	93.9	64.5	26.3
1.00	11.7	2.2	0.3	69.9	32.1	8.2	124.4	73.0	32.8
Soil Class C									
0.10	0.6	0.1	0.0	3.7	0.9	0.1	9.3	2.6	0.4
0.20	1.2	0.2	0.0	8.3	1.9	0.2	19.9	6.8	0.9
0.30	1.9	0.3	0.1	14.4	3.5	0.4	33.8	15.4	2.2
0.40	2.9	0.5	0.1	22.9	5.2	0.6	45.8	27.2	4.4
0.50	5.0	0.6	0.1	35.2	11.3	1.1	62.0	35.9	9.2
0.60	6.0	0.9	0.1	46.5	17.3	2.0	82.9	52.3	14.8
0.70	8.4	1.4	0.2	58.8	26.6	4.2	94.6	61.0	24.3
0.80	11.1	2.3	0.3	70.6	34.7	8.4	122.1	70.2	31.2
0.90	20.9	3.7	0.4	85.7	44.3	14.0	148.3	76.7	49.2
1.00	22.7	5.5	0.6	99.9	53.3	19.5	204.7	102.3	61.4
Soil Class D									
0.10	0.6	0.1	0.0	3.7	0.9	0.1	11.1	2.7	0.4
0.20	1.2	0.2	0.0	8.0	1.9	0.2	26.9	7.3	1.0
0.30	1.9	0.3	0.1	15.1	3.5	0.4	48.7	14.0	2.2
0.40	3.0	0.5	0.1	24.4	6.4	0.6	97.7	27.5	5.0
0.50	4.9	0.6	0.1	50.1	11.8	1.3	118.0	56.0	10.6
0.60	6.1	1.0	0.1	62.4	19.2	2.7	163.9	79.7	18.2
0.70	9.1	1.6	0.2	97.0	30.8	6.0	270.7	103.6	40.7
0.80	12.9	2.5	0.4	130.6	56.7	11.8	300.9	143.7	61.4
0.90	20.3	4.5	0.7	174.0	81.4	20.3	358.7	206.3	82.9
1.00	35.7	7.5	1.5	205.3	109.0	30.7	550.3	258.5	124.8

Table A- 9 Wall 3 14.400 m 1 to 3 Stories Far Fault Springs B,E,G

Scale	Single Story			Two Story			Three Story		
Factor	Clay	Gravel	Rock	Clay	Gravel	Rock	Clay	Gravel	Rock
Soil Class B									
0.10	0.5	0.1	0.0	3.2	0.7	0.1	7.5	2.2	0.3
0.20	1.0	0.2	0.0	6.6	1.5	0.2	15.5	5.1	0.7
0.30	1.5	0.3	0.0	11.2	2.8	0.3	25.0	9.4	1.3
0.40	2.2	0.4	0.1	18.3	4.4	0.5	37.0	18.9	2.7
0.50	3.3	0.5	0.1	26.2	5.9	0.7	47.1	27.1	4.2
0.60	4.5	0.6	0.1	37.2	10.1	1.0	65.1	36.6	8.3
0.70	6.6	0.9	0.1	46.5	18.4	1.6	87.7	50.1	16.5
0.80	8.1	1.2	0.2	56.4	26.4	2.6	104.3	62.2	24.0
0.90	12.0	1.8	0.2	76.7	25.9	4.5	122.3	80.6	31.8
1.00	14.7	2.2	0.2	77.4	41.2	7.5	160.9	81.6	39.0
Soil Class C									
0.10	0.6	0.1	0.0	3.9	0.9	0.1	9.4	2.8	0.4
0.20	1.3	0.2	0.0	8.8	2.1	0.2	20.9	6.6	1.0
0.30	2.0	0.3	0.1	14.9	3.8	0.4	32.0	16.7	2.0
0.40	3.2	0.5	0.1	27.4	5.5	0.7	47.1	26.3	4.3
0.50	5.2	0.7	0.1	39.0	12.0	1.3	69.0	40.0	9.3
0.60	7.1	1.0	0.1	52.3	22.2	2.2	96.3	59.8	18.3
0.70	10.0	1.5	0.2	68.9	31.5	4.3	110.9	67.1	29.0
0.80	15.3	2.2	0.2	77.2	39.2	8.0	160.4	81.6	40.1
0.90	21.3	3.3	0.4	100.5	49.5	12.2	199.8	105.2	49.1
1.00	32.6	4.7	0.5	113.2	58.9	21.8	228.7	125.9	52.8
Soil Class D									
0.10	0.6	0.1	0.0	3.9	0.9	0.1	11.1	2.8	0.4
0.20	1.3	0.2	0.0	8.8	2.1	0.2	25.9	6.6	1.0
0.30	2.0	0.3	0.1	16.2	3.8	0.4	52.8	17.5	2.2
0.40	3.2	0.5	0.1	29.4	6.0	0.6	103.7	31.0	4.3
0.50	5.0	0.6	0.1	53.2	12.2	1.1	154.2	76.2	12.5
0.60	6.3	1.0	0.2	96.0	22.1	2.1	189.1	122.2	22.5
0.70	10.5	1.3	0.2	128.4	37.8	5.0	255.1	155.6	40.7
0.80	16.0	1.9	0.4	167.9	57.4	10.1	302.2	198.1	71.0
0.90	24.5	4.0	0.6	197.6	87.6	15.2	340.3	223.0	100.3
1.00	38.9	6.1	1.0	255.9	123.2	36.1	427.7	274.4	127.1

Figures A- 1 Run 1-1-B 7.200 m Wall Length 1 Story Medium Clay

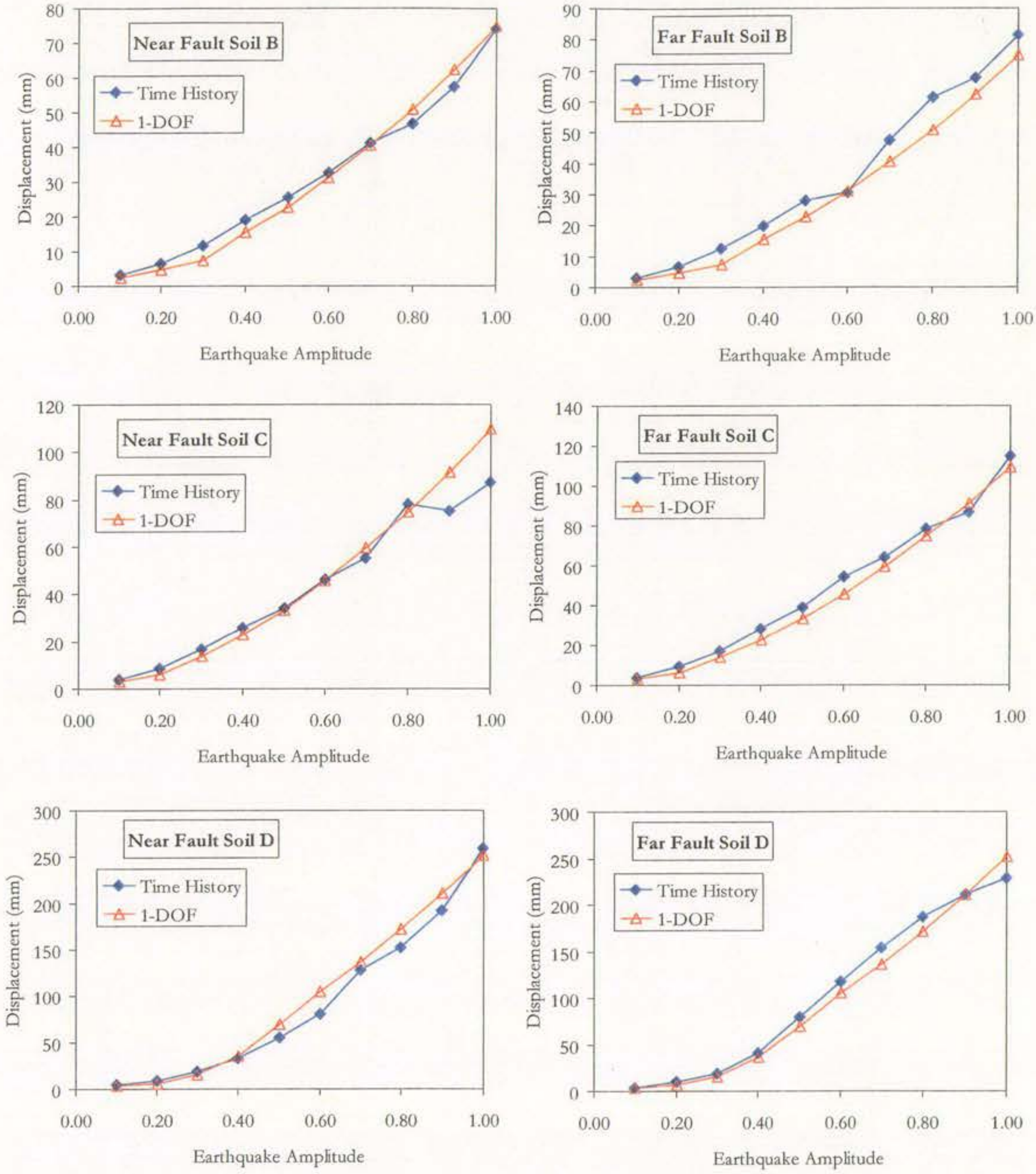

Figures A- 2 Run 1-1-E 7.200 m Wall Length 1 Story Medium Gravel

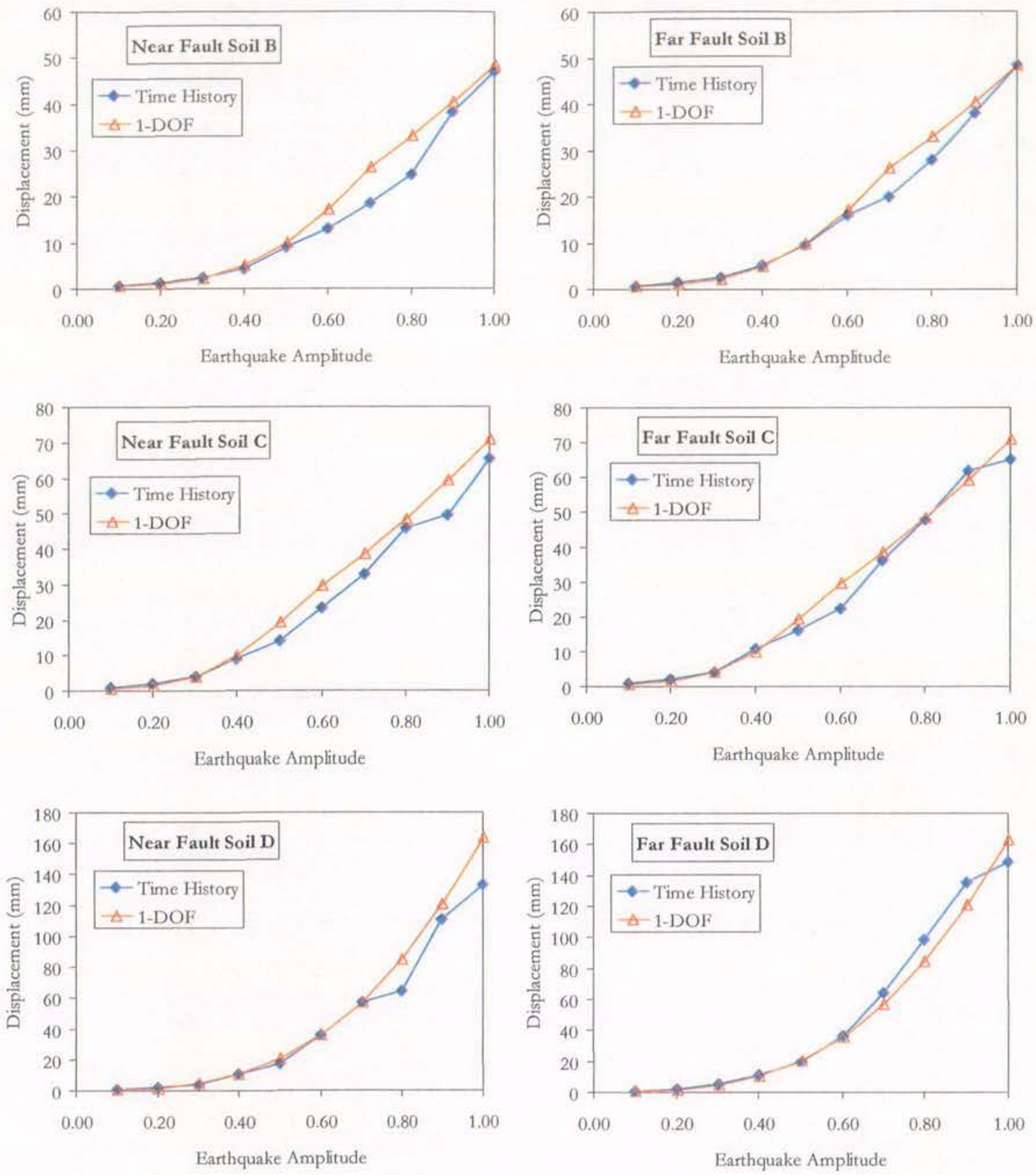

Figures A- 3 Run 1-1-G 7.200 m Wall Length 1 Story Rock

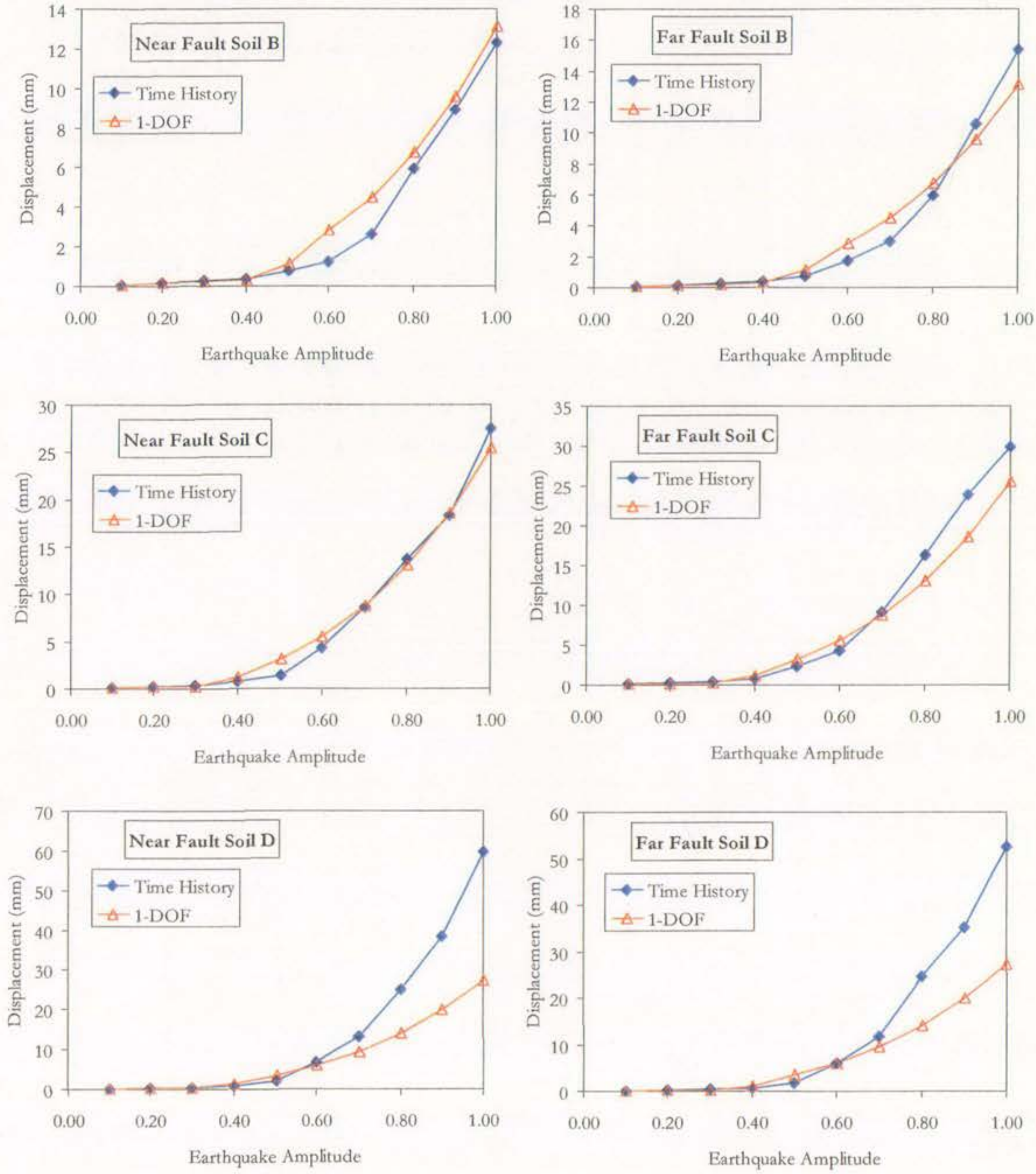

Figures A- 4 Run 1-2-B 7.200 m Wall Length 2 Story Medium Clay

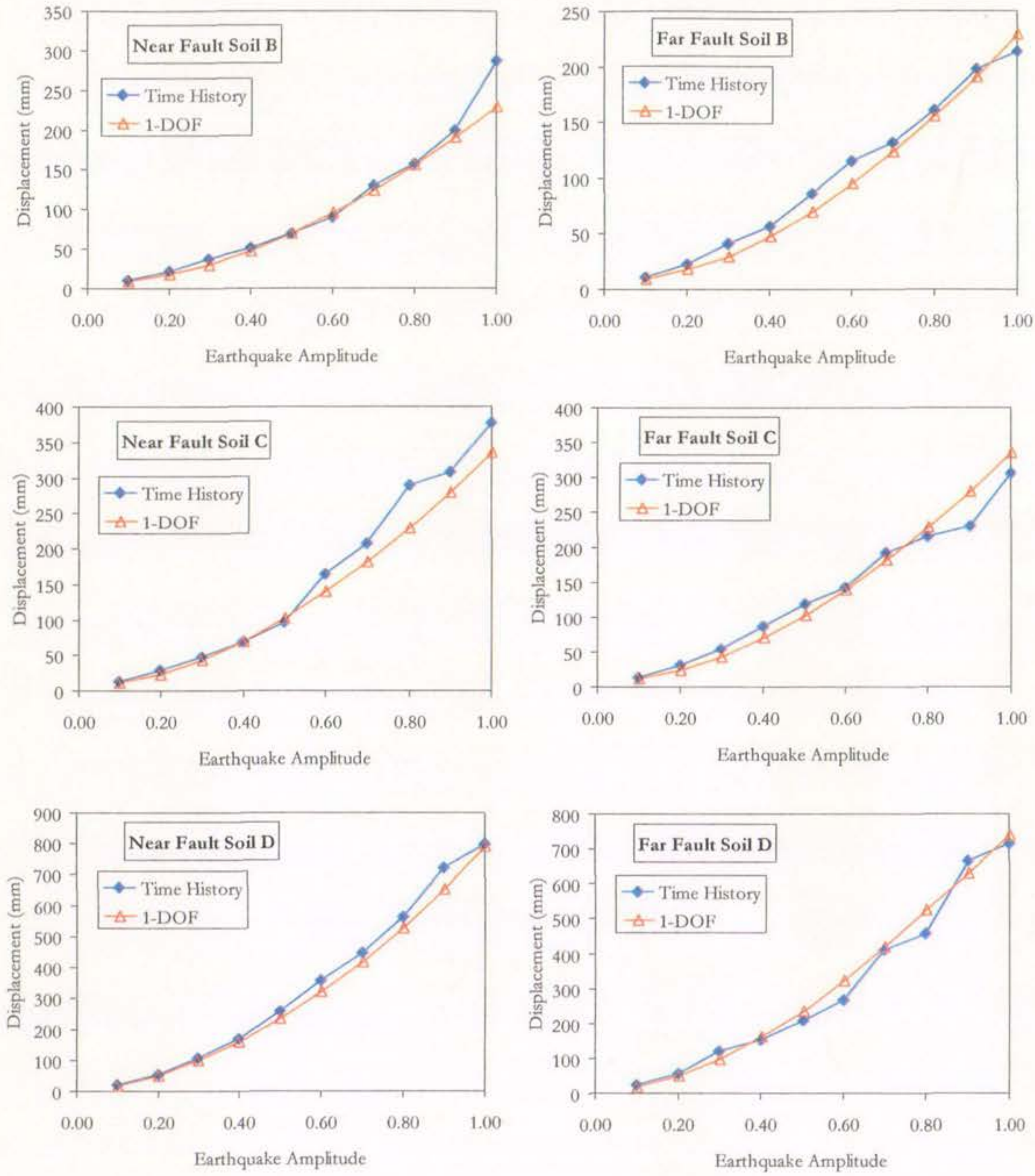

Figures A- 5 Run 1-2-E 7.200 m Wall Length 2 Story Medium Gravel

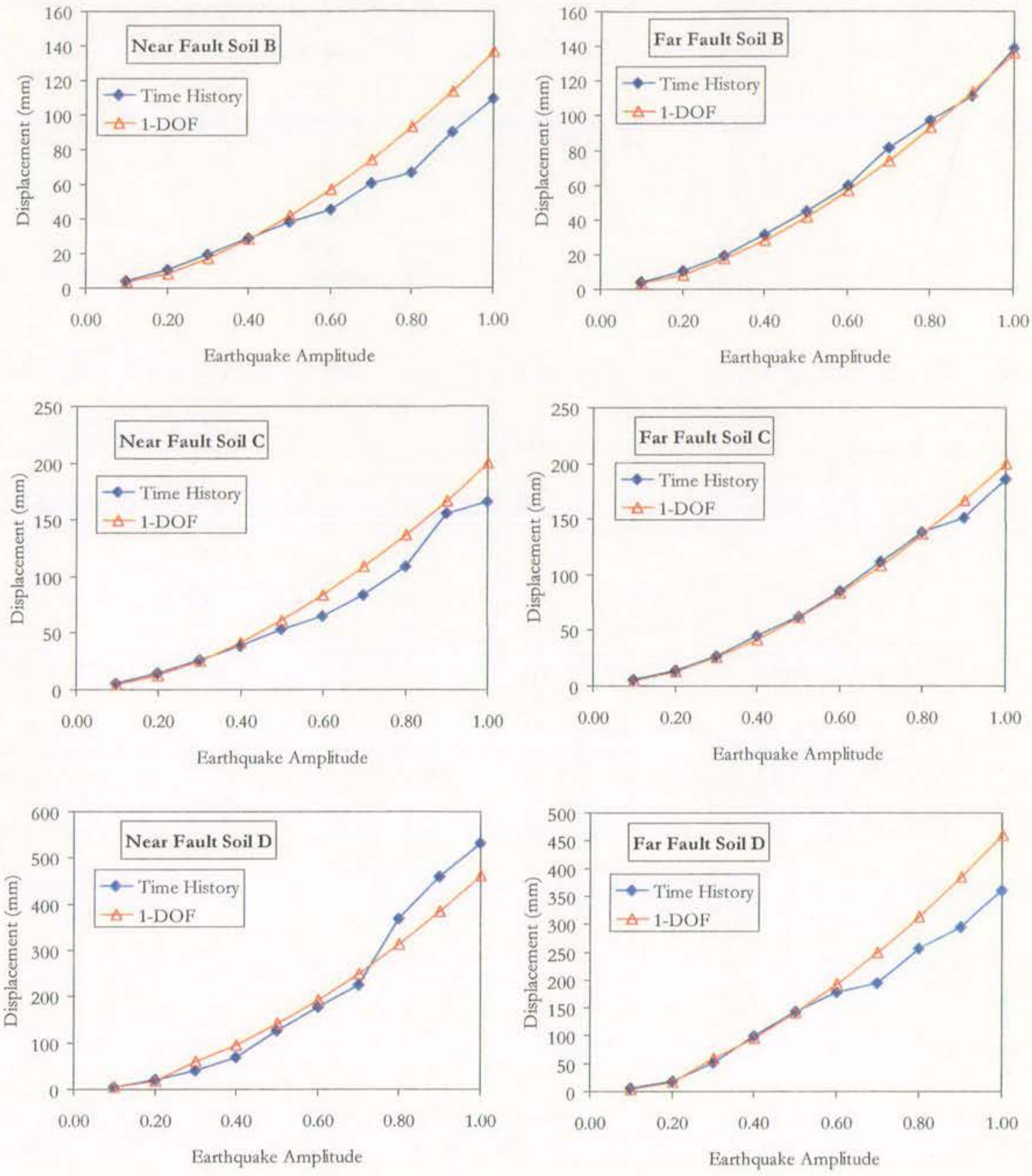

Figures A- 6 Run 1-2-G 7.200 m Wall Length 2 Story Rock

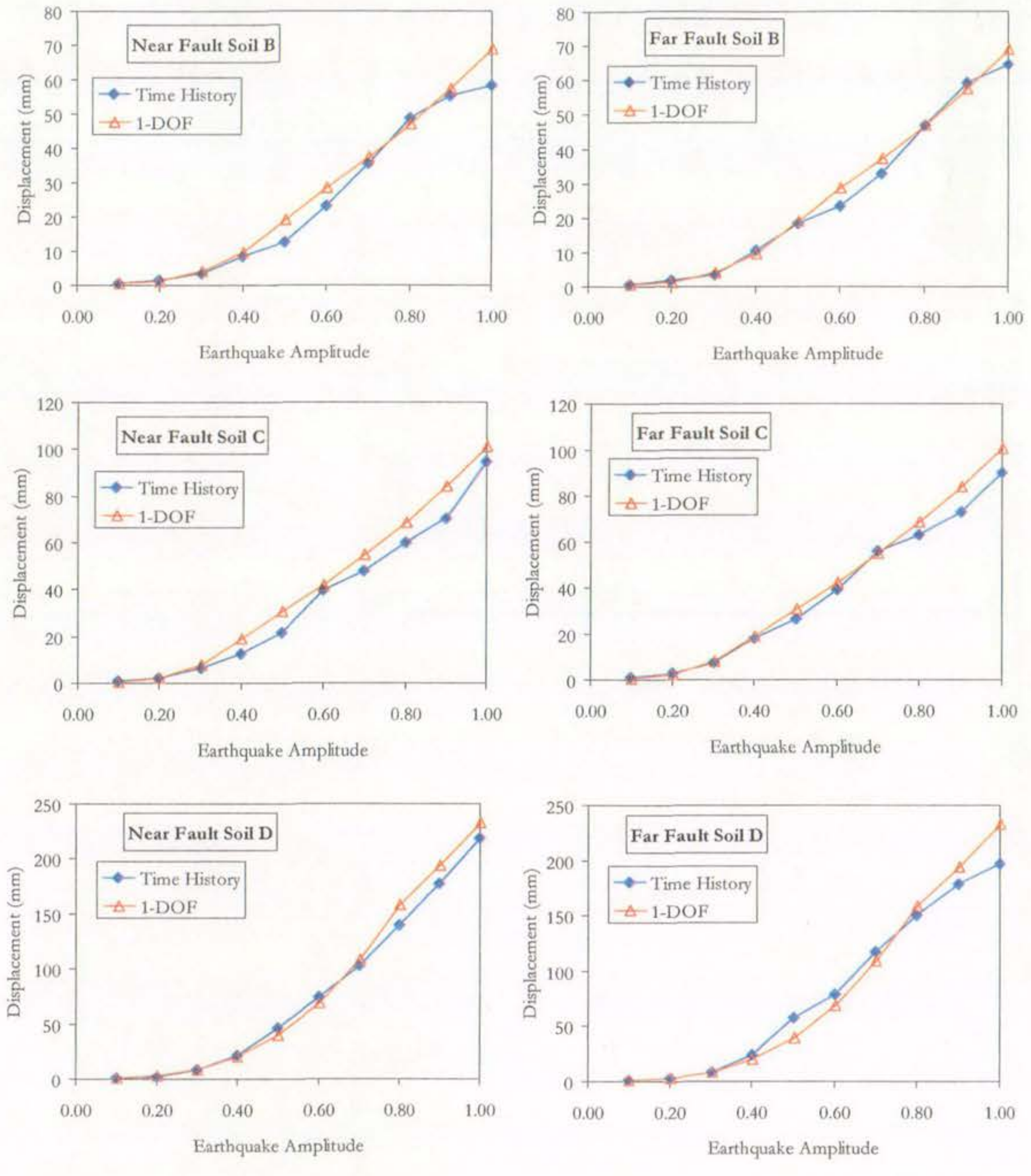

Figures A- 7 Run 1-3-A 7.200 m Wall Length 3 Story Firm Clay

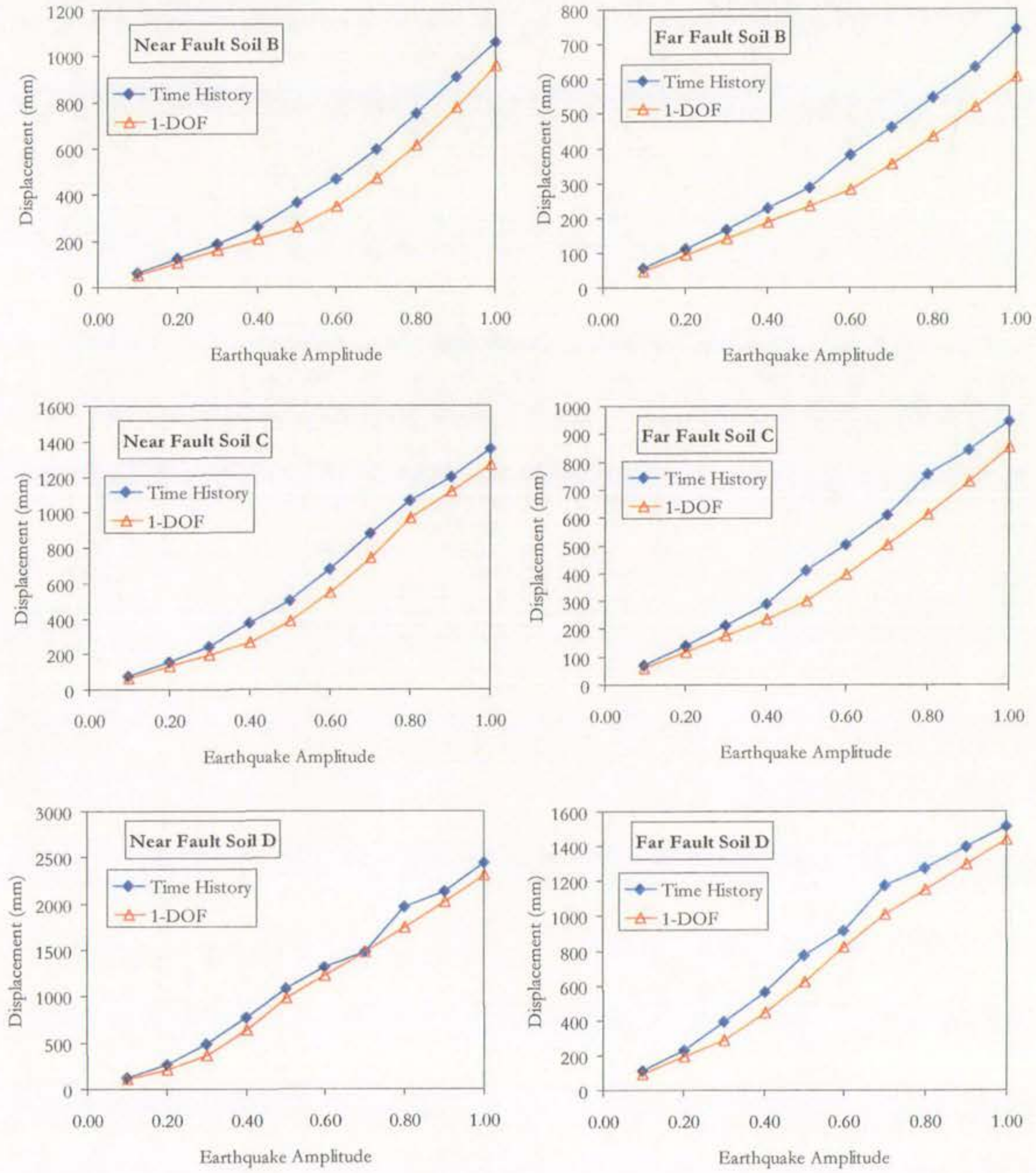

Figures A- 8 Run 1-3-B 7.200 m Wall Length 3 Story Medium Clay

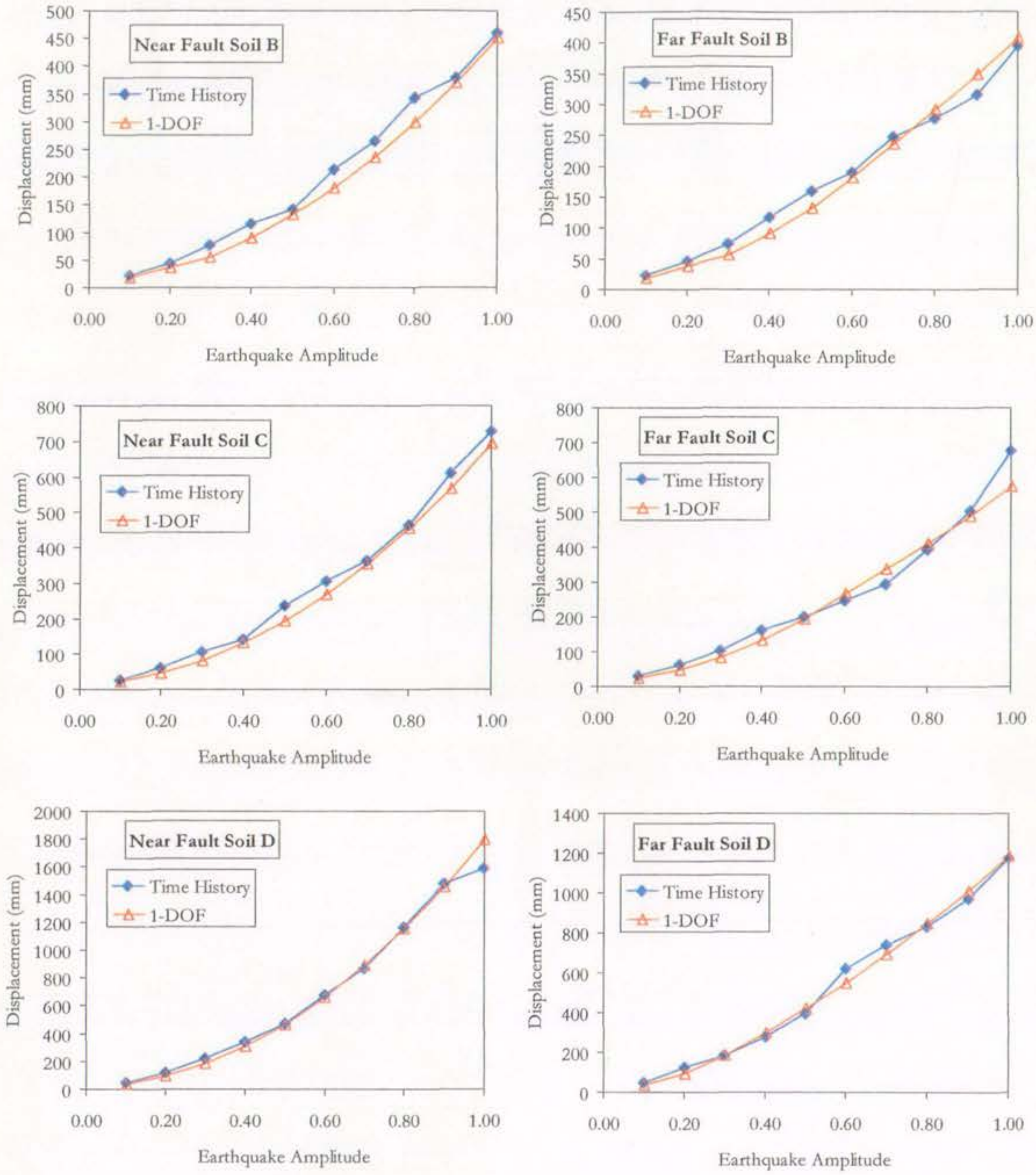

Figures A- 9 Run 1-3-C 7.200 m Wall Length 3 Story Soft Clay

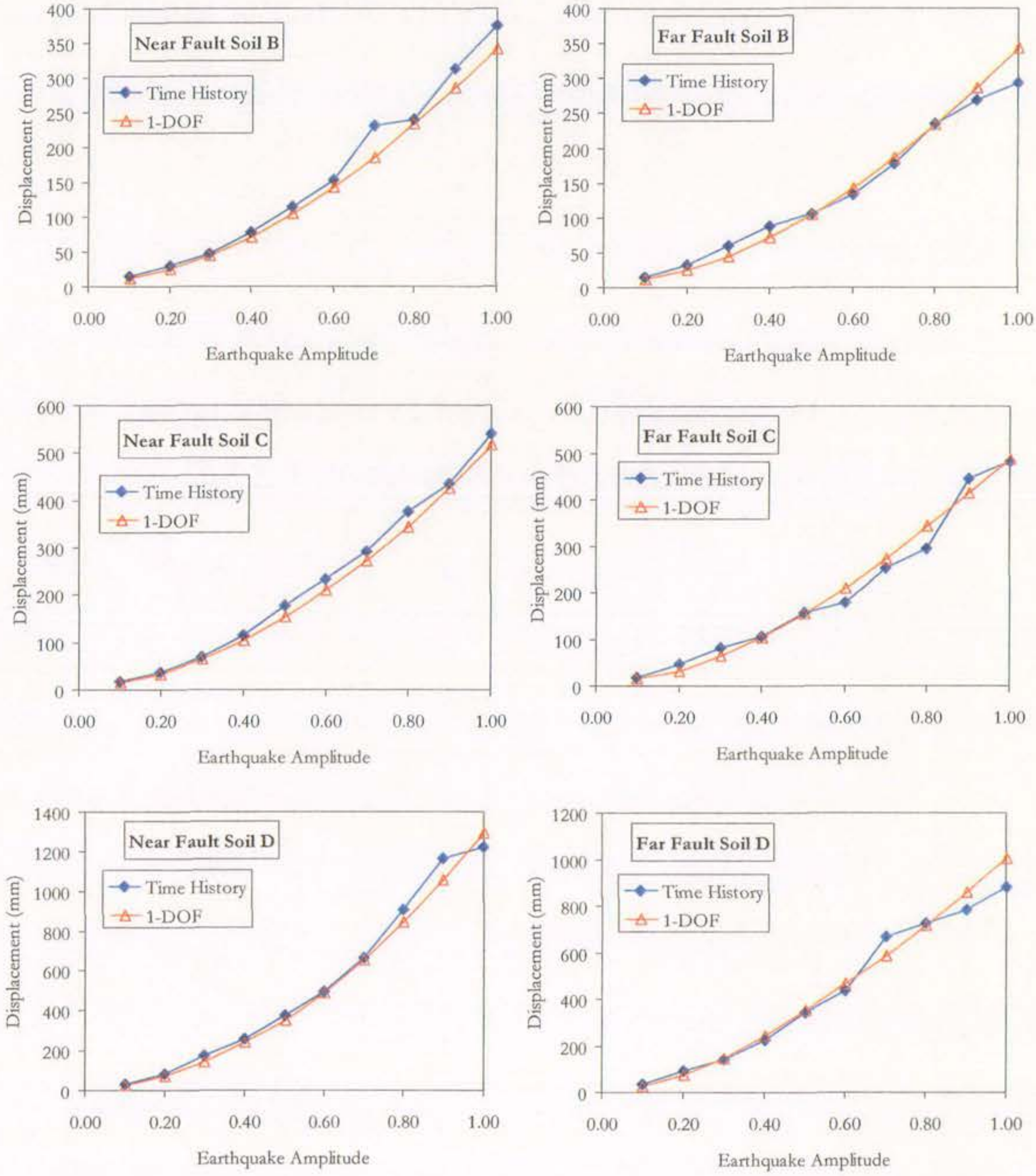

Figures A- 10 Run 1-3-D 7.200 m Wall Length 3 Story Firm Gravel

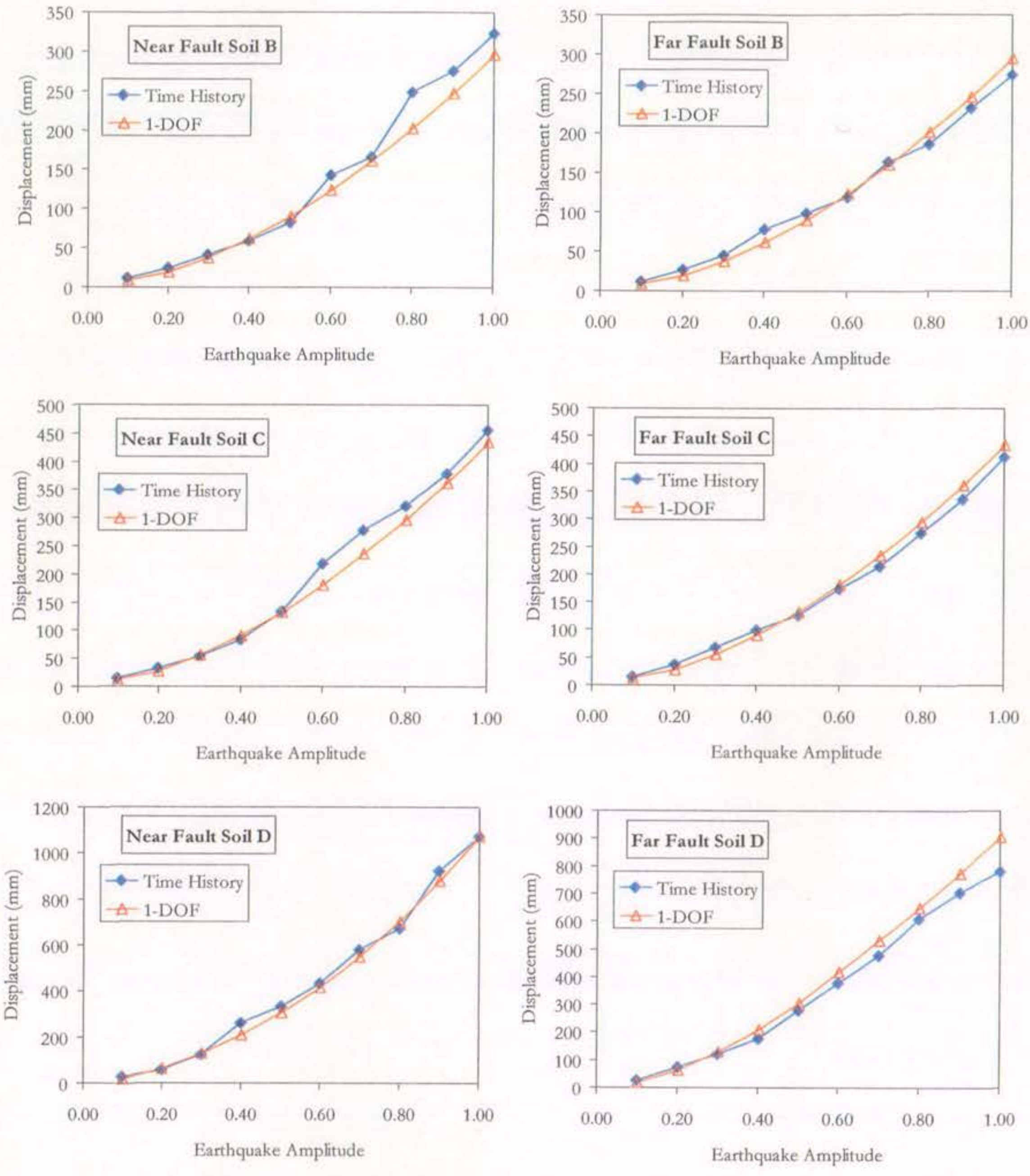

Figures A- 11 Run 1-3-E 7.200 m Wall Length 3 Story Medium Gravel

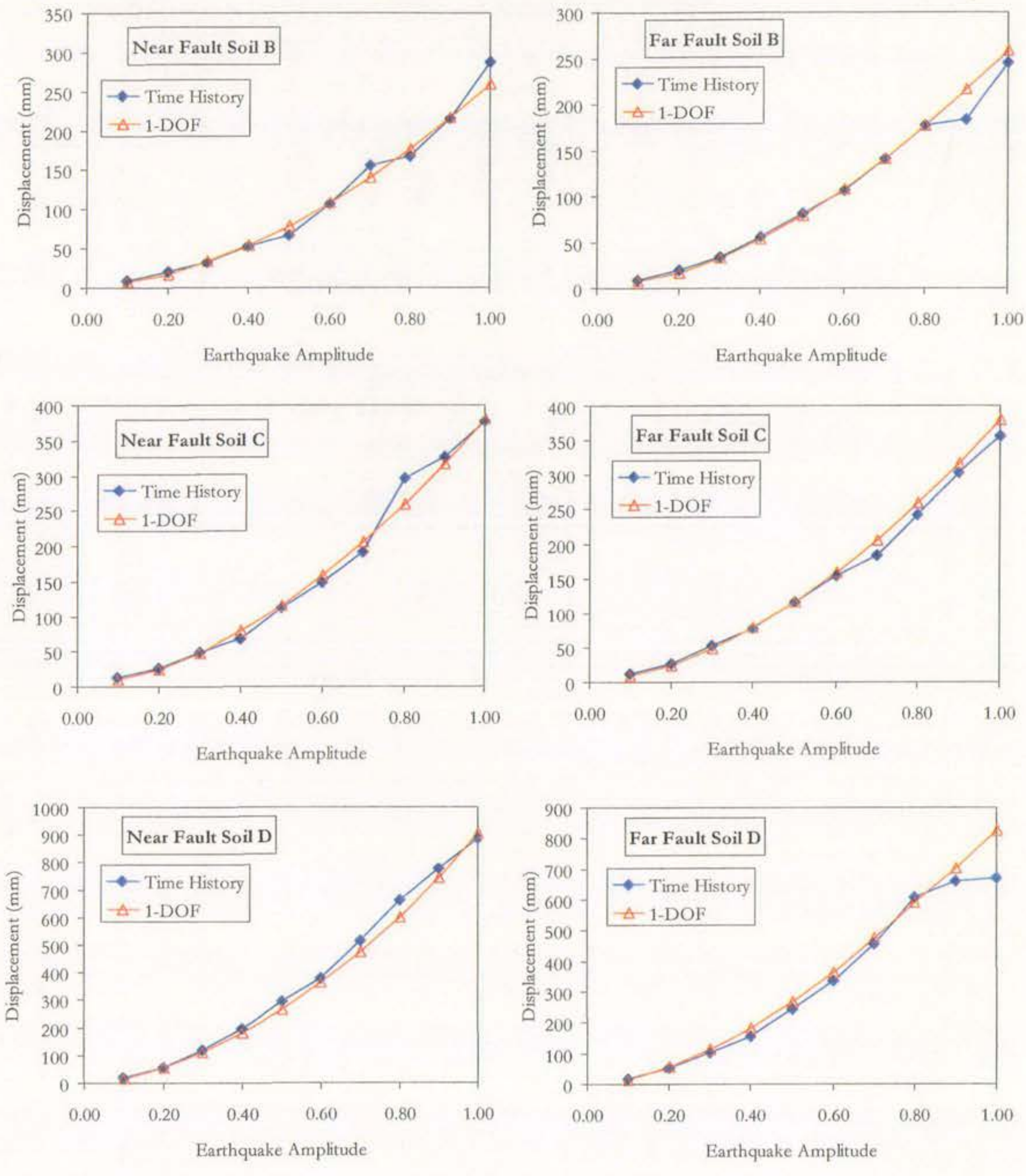

Figures A- 12 Run 1-3-F 7.200 m Wall Length 3 Story Loose Gravel

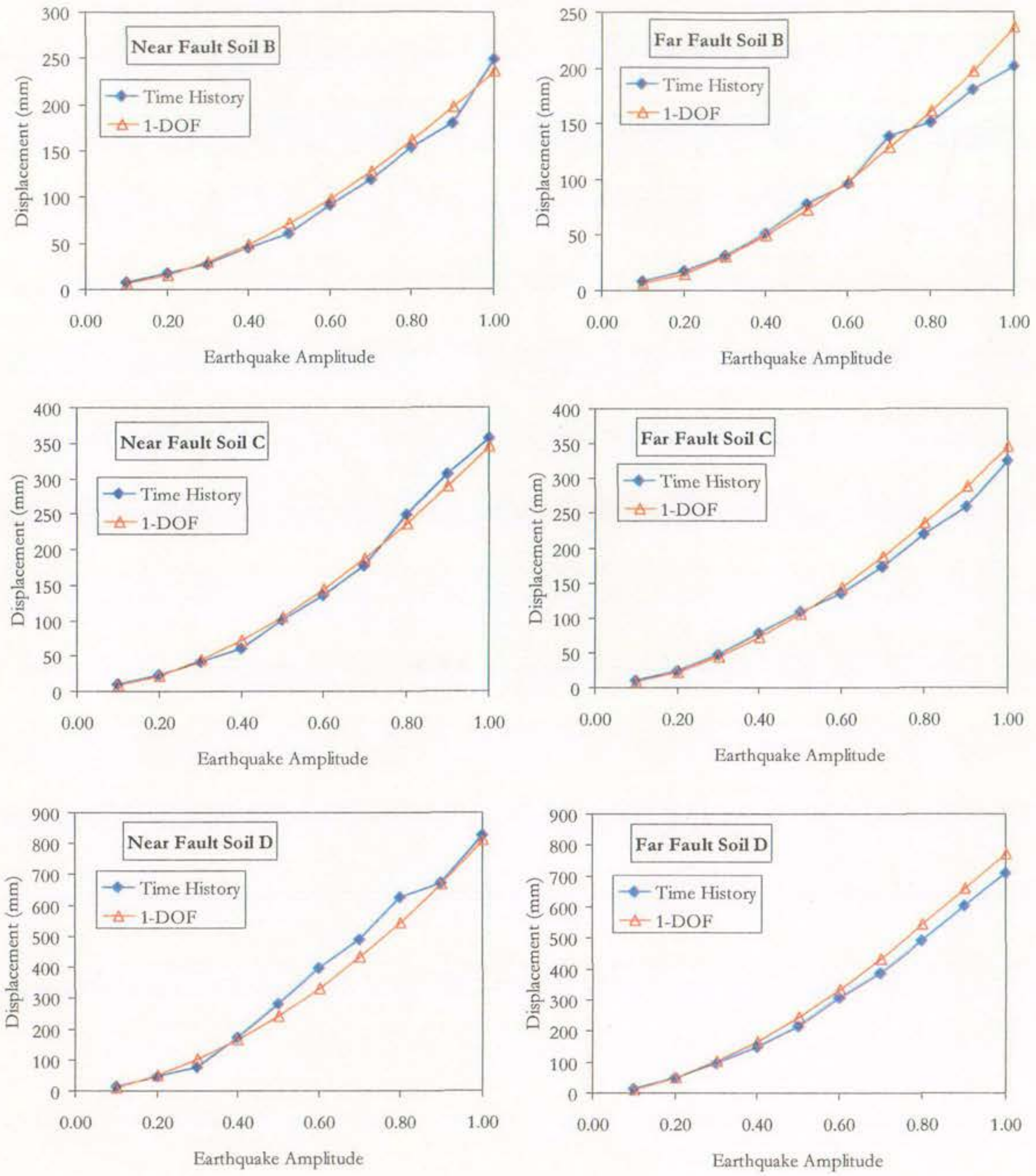

Figures A- 13 Run 1-3-G 7.200 m Wall Length 3 Story Rock

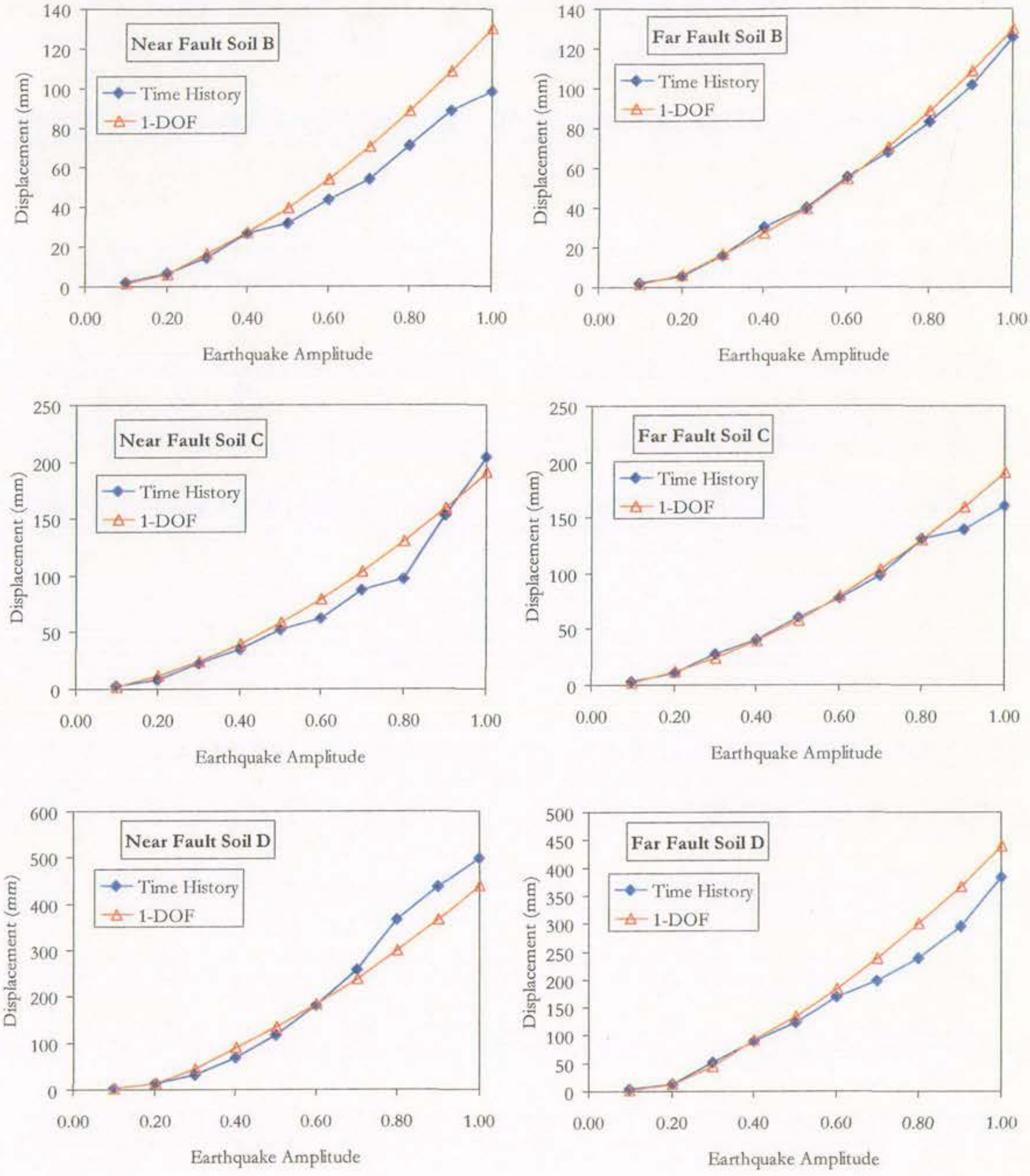

Figures A- 14 Run 2-1-B 3.600 m Wall Length 1 Story Medium Clay

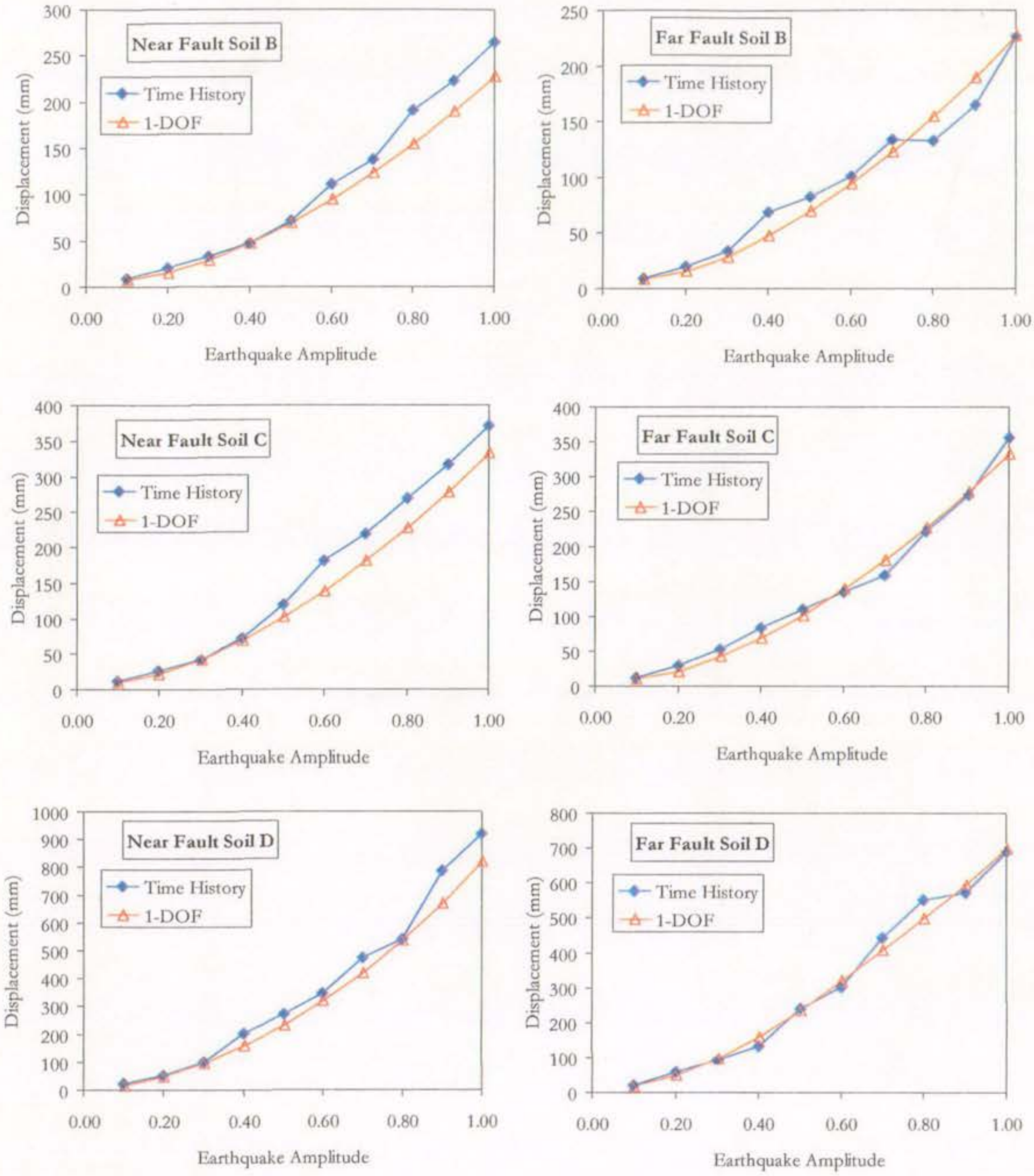

Figures A- 15 Run 2-1-E 3.600 m Wall Length 1 Story Medium Gravel

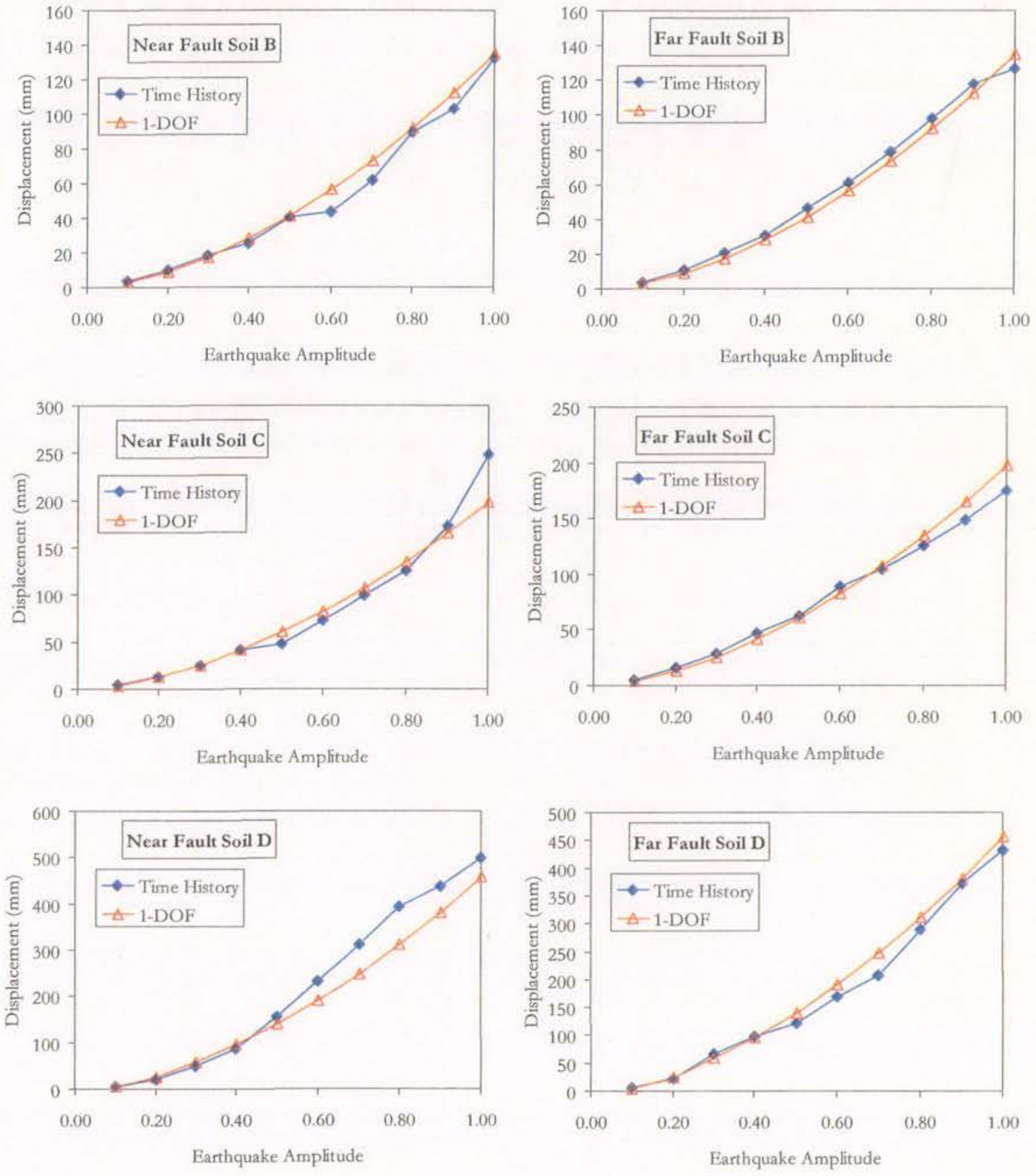

Figures A- 16 Run 2-1-G 3.600 m Wall Length 1 Story Rock

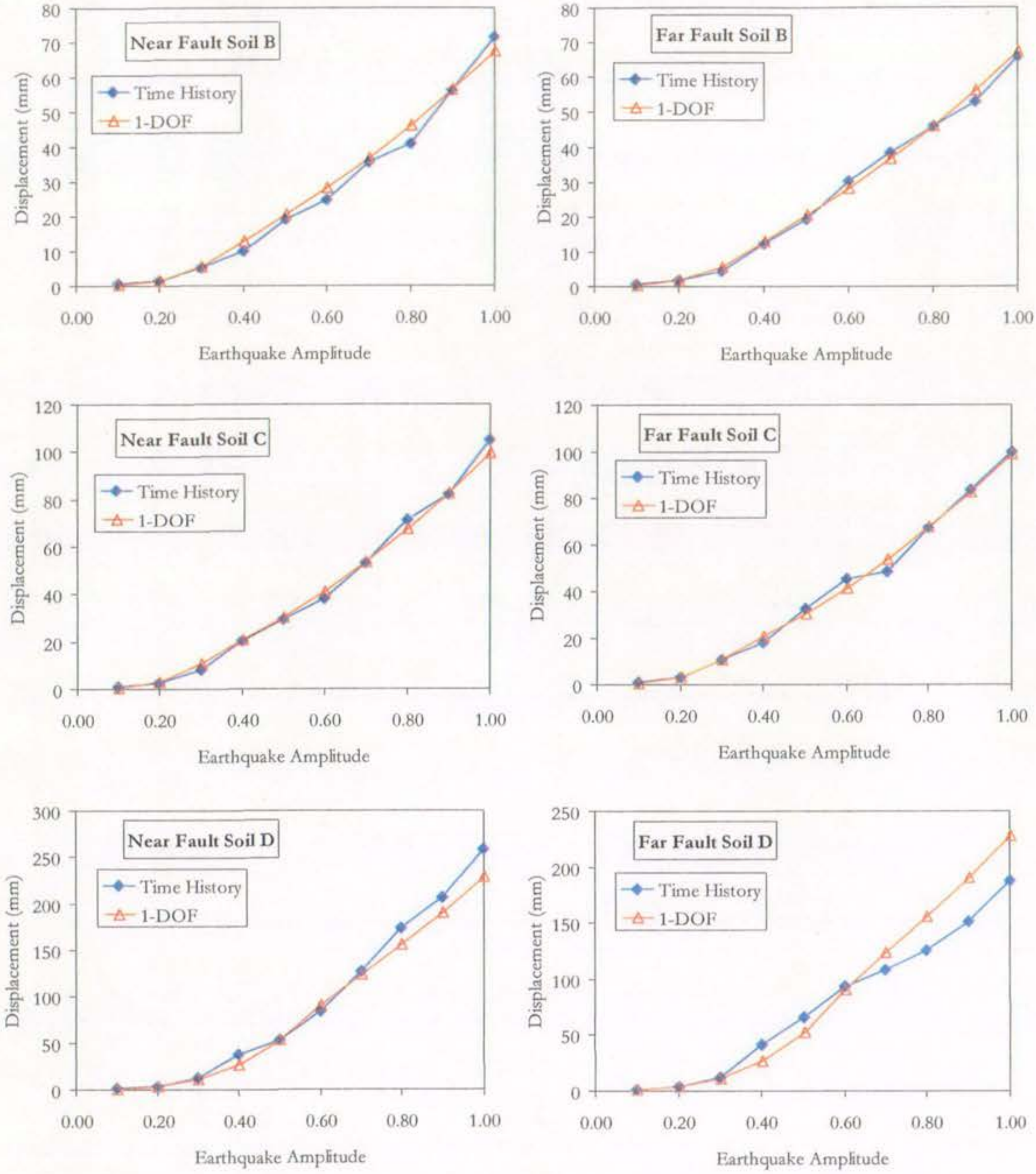

Figures A- 17 Run 2-2-B 3.600 m Wall Length 2 Story Medium Clay

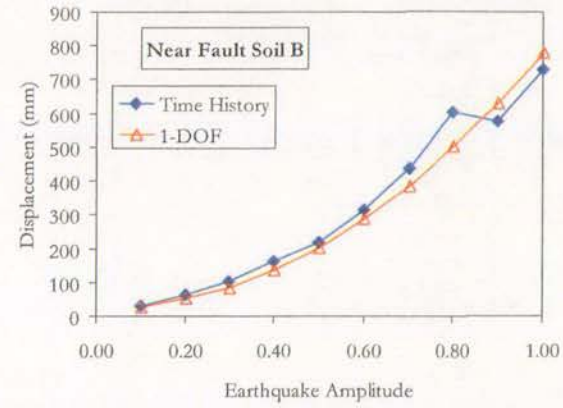

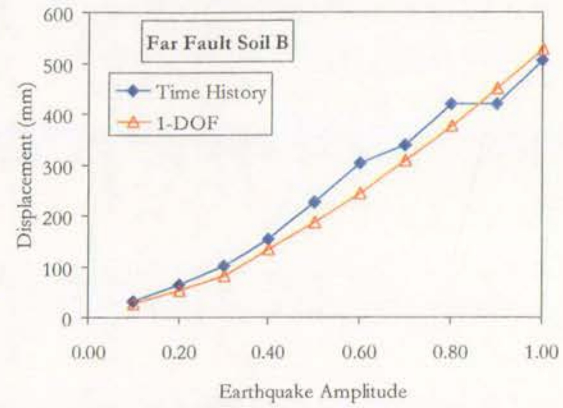

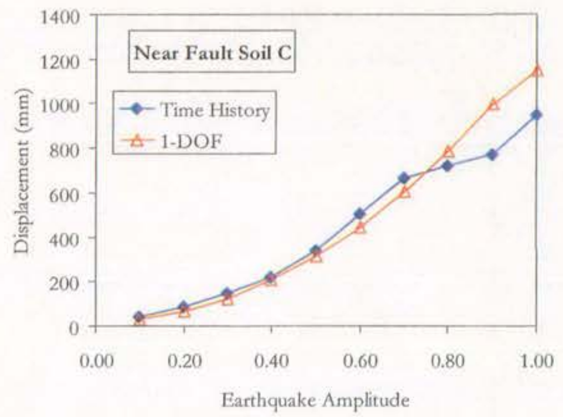

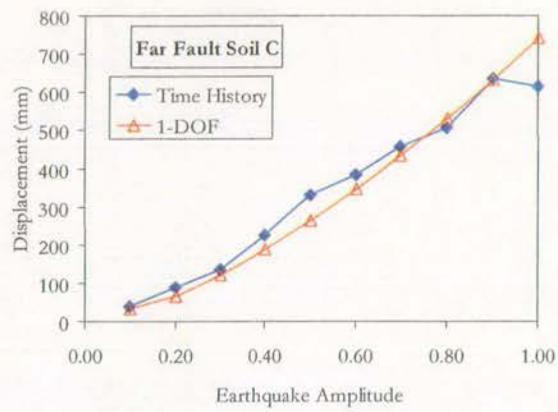

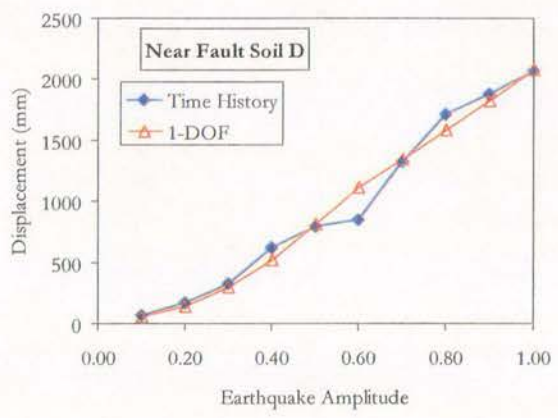

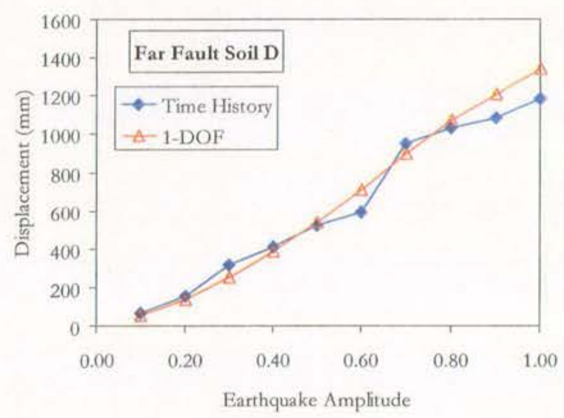

Figures A- 18 Run 2-2-E 3.600 m Wall Length 2 Story Medium Gravel

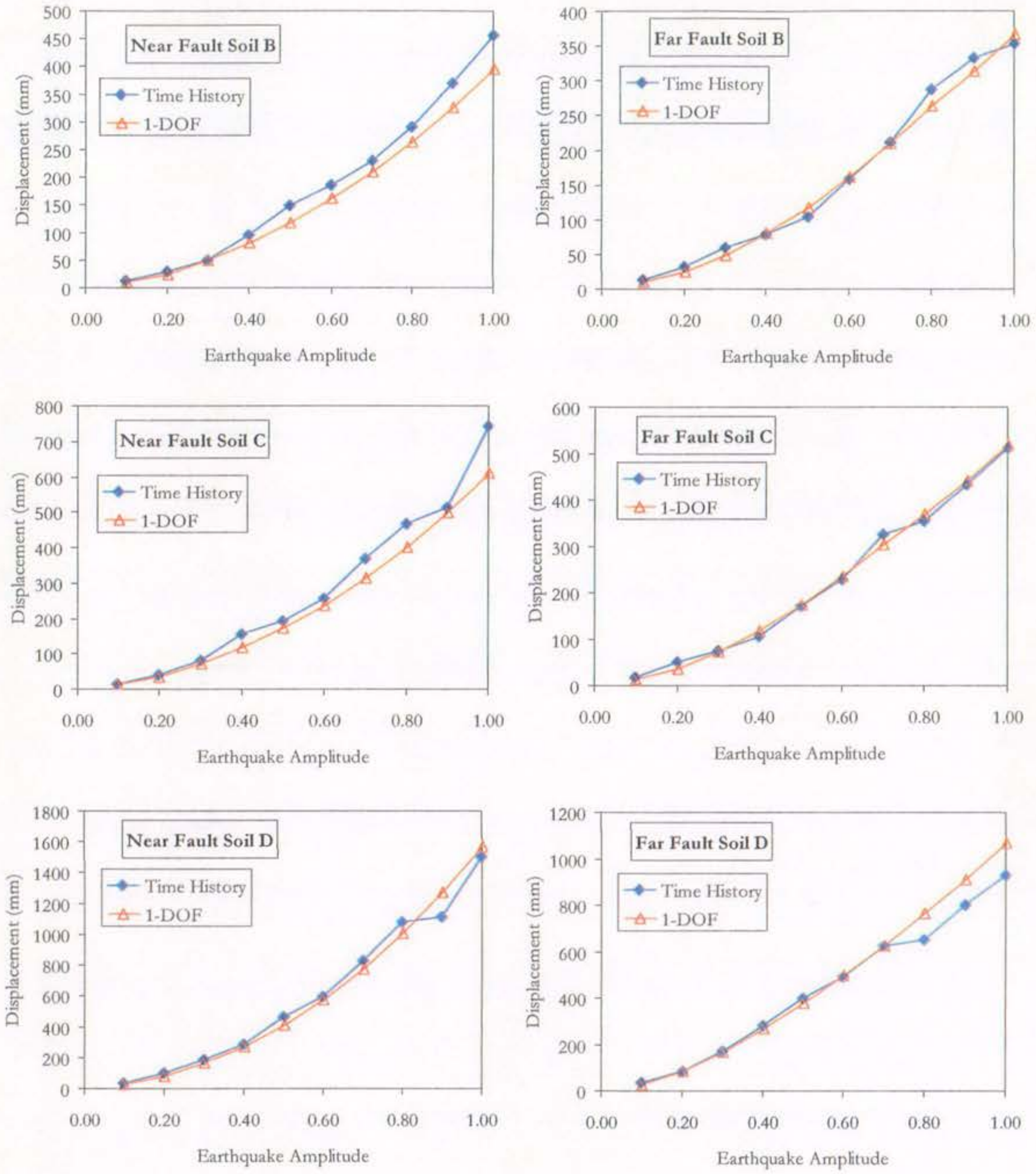

Figures A- 19 Run 2-2-G 3.600 m Wall Length 2 Story Rock

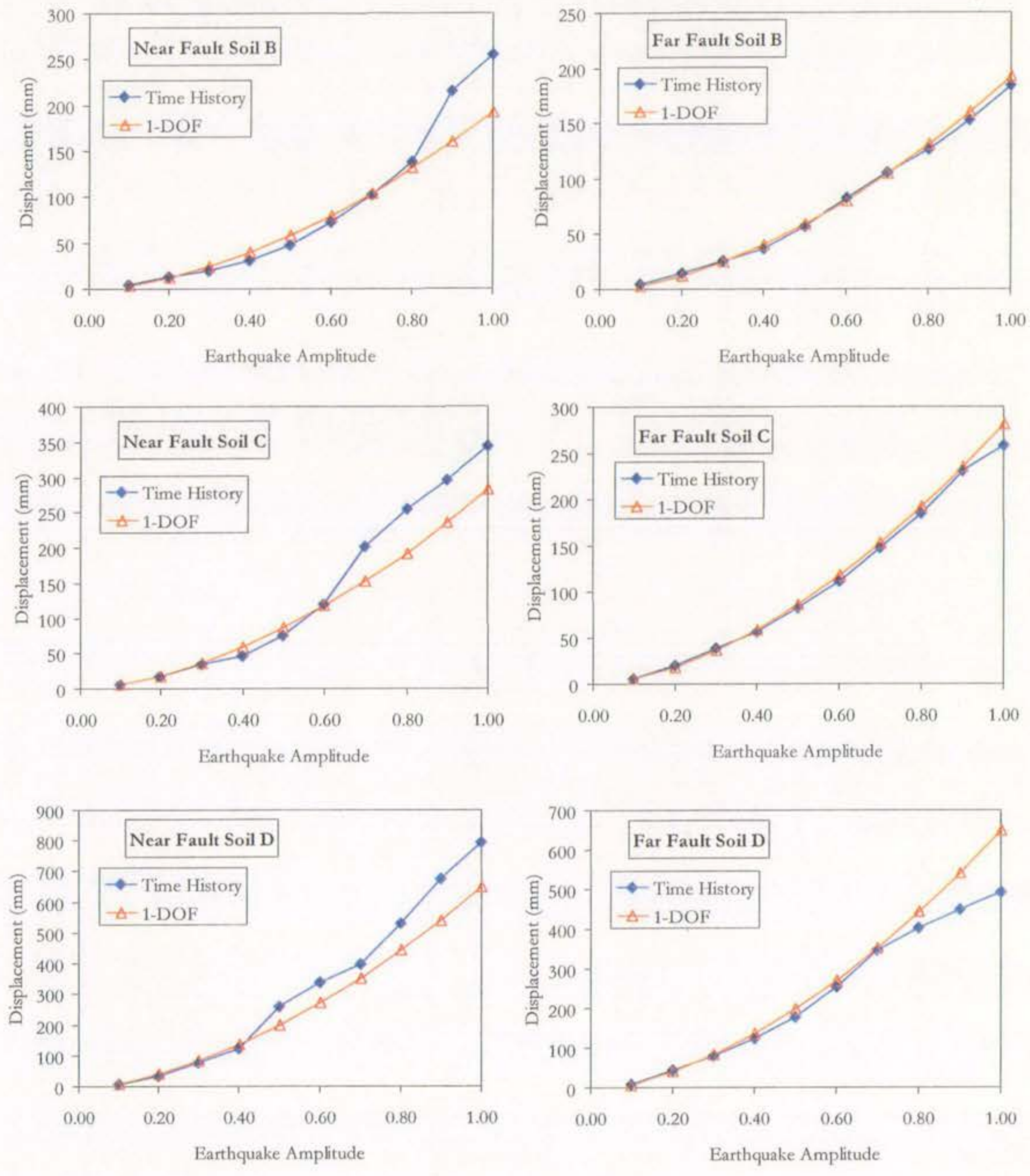

Figures A- 20 Run 2-3-B 3.600 m Wall Length 3 Story Medium Clay

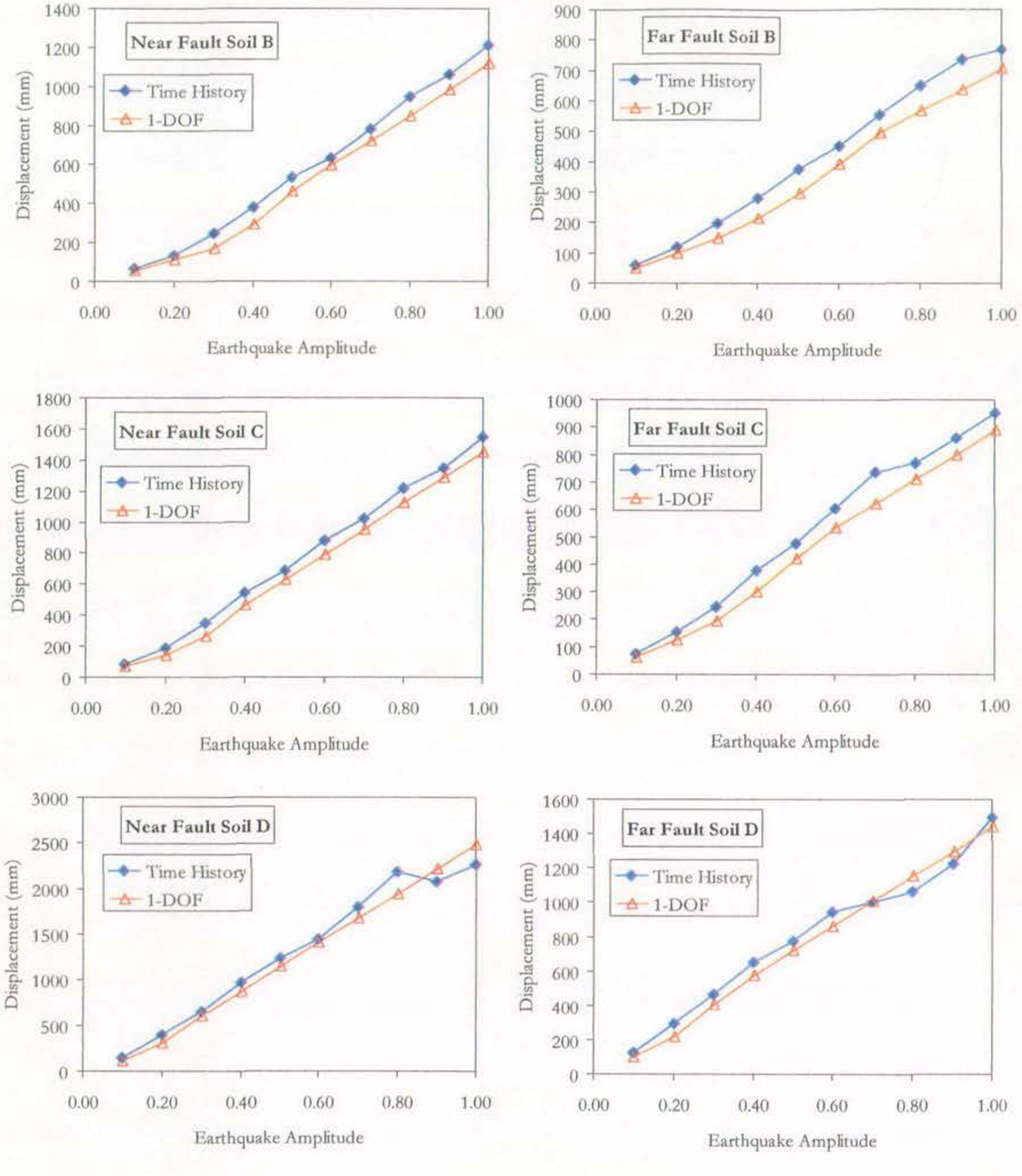

Figures A- 21 Run 2-3-E 3.600 m Wall Length 3 Story Medium Gravel

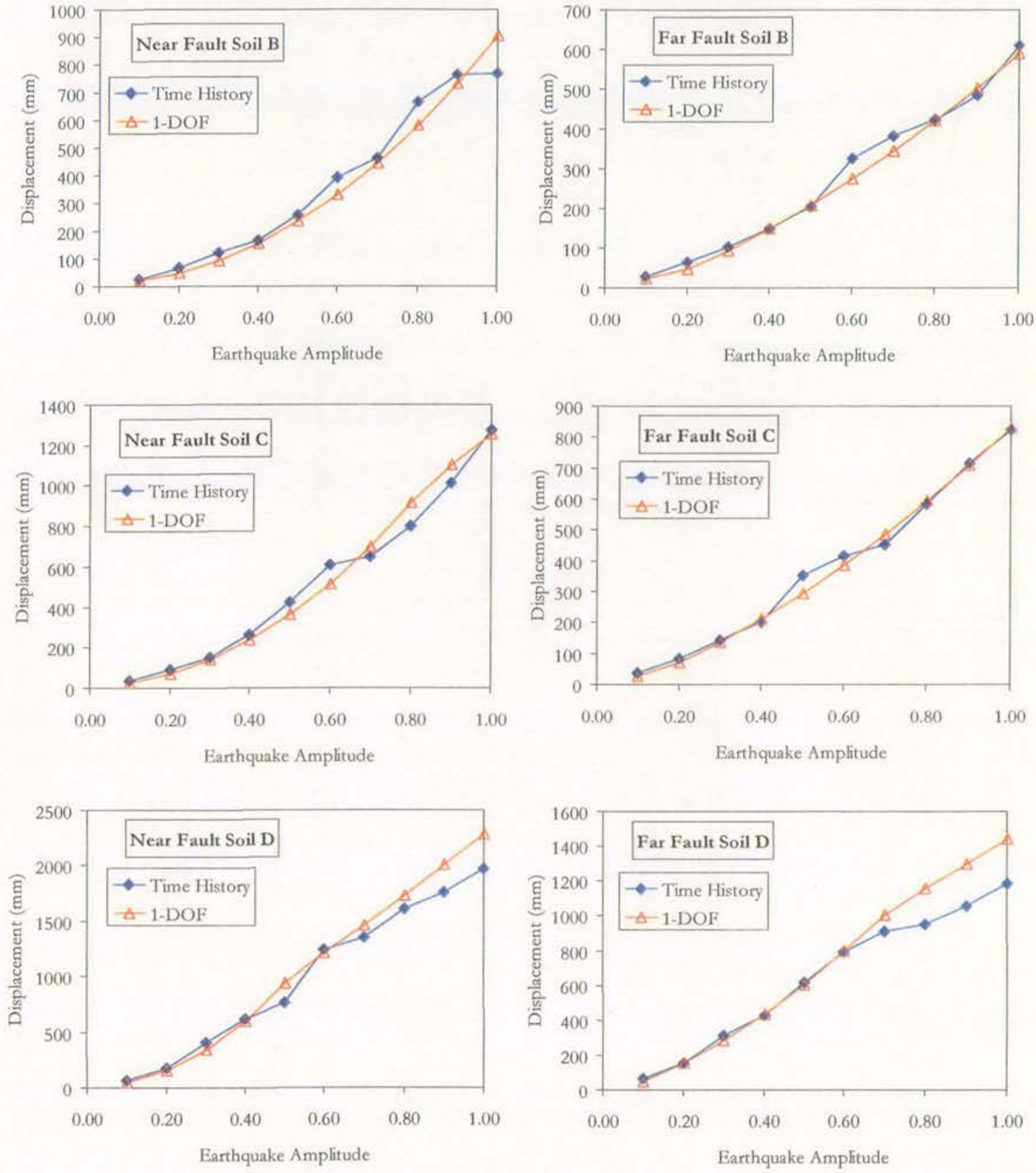

Figures A- 22 Run 2-3-G 3.600 m Wall Length 3 Story Rock

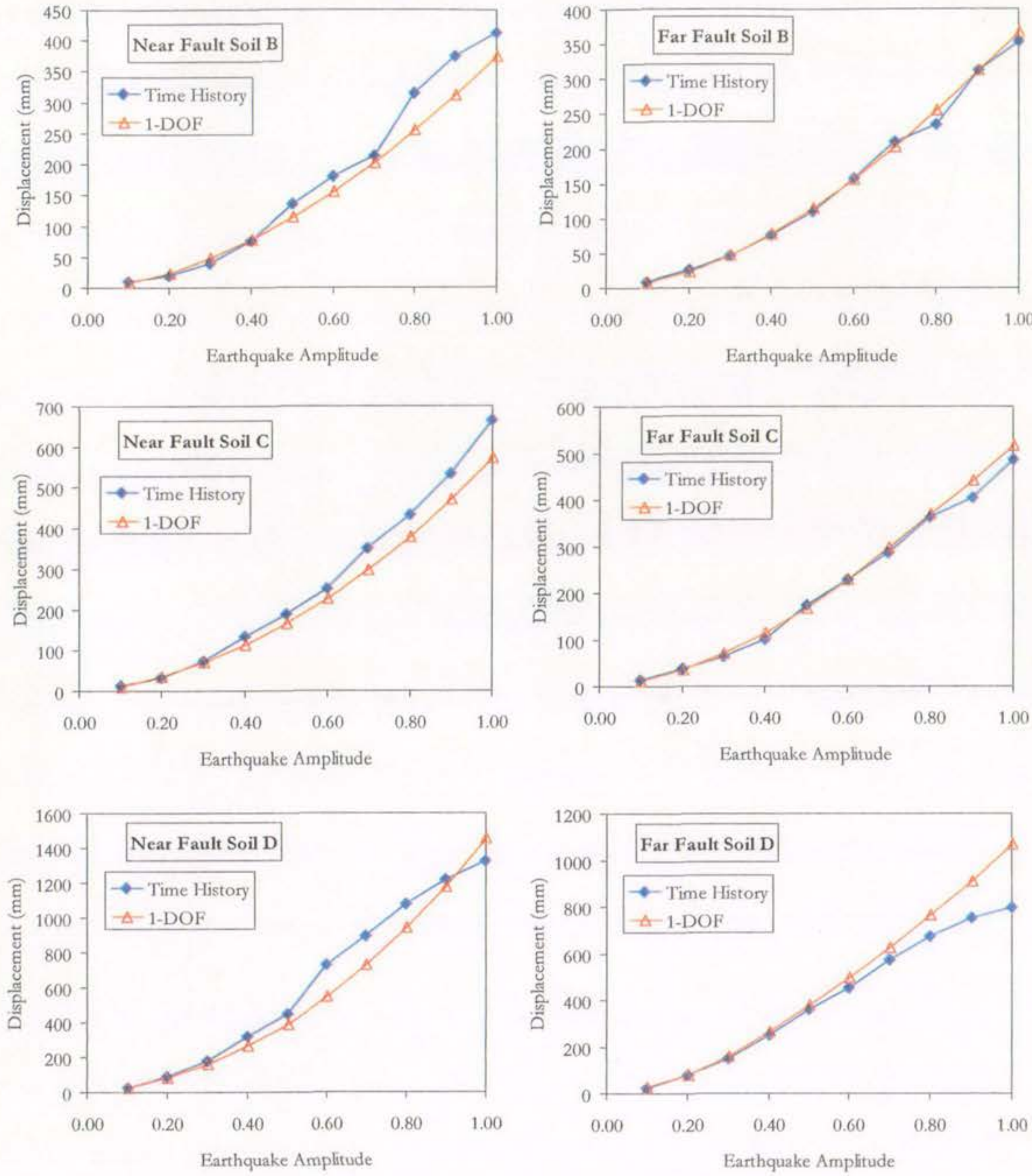

Figures A- 23 Run 2-4-B 3.600 m Wall Length 4 Story Medium Clay

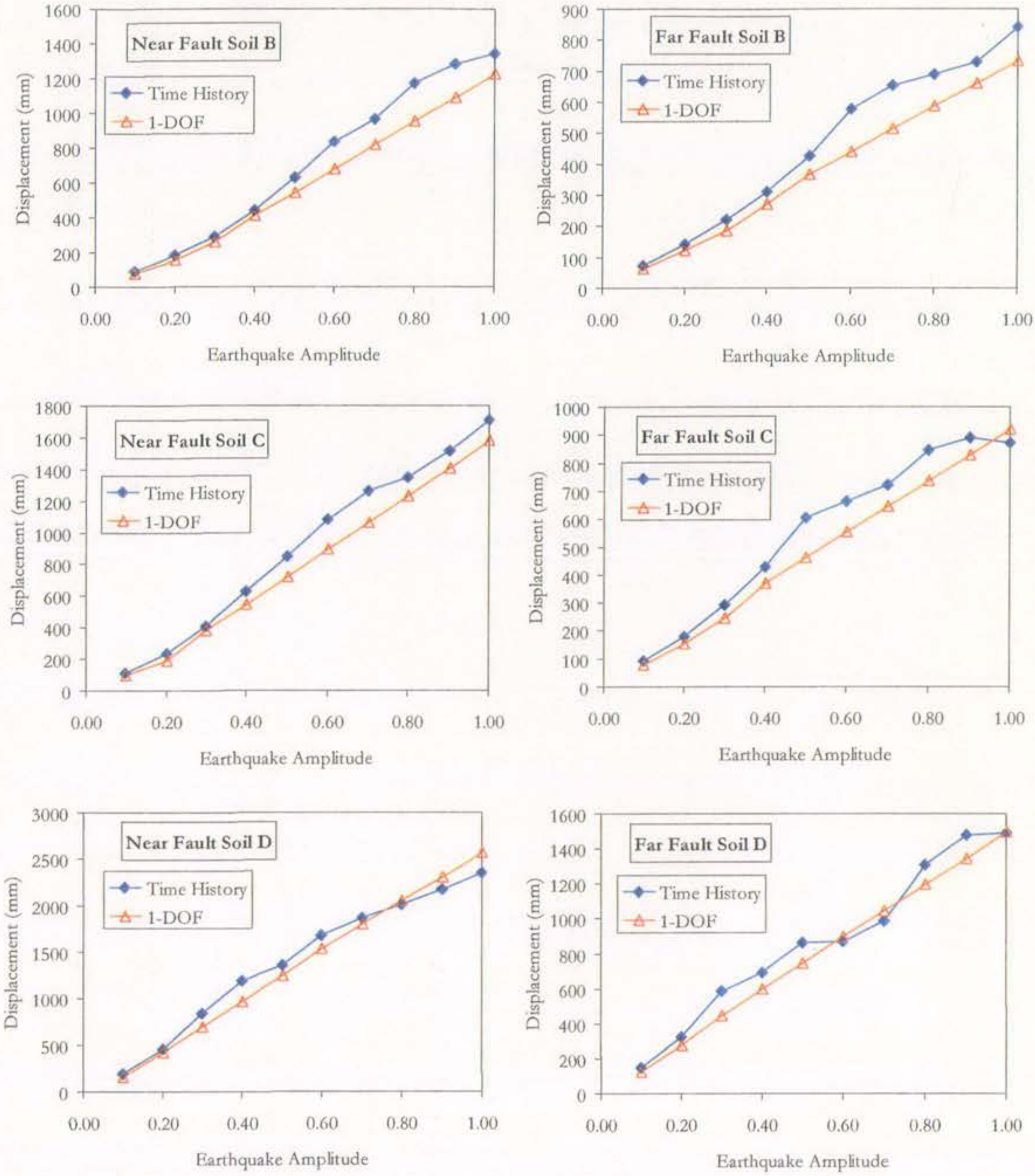

Figures A- 24 Run 2-4-B 3.600 m Wall Length 4 Story Medium Gravel

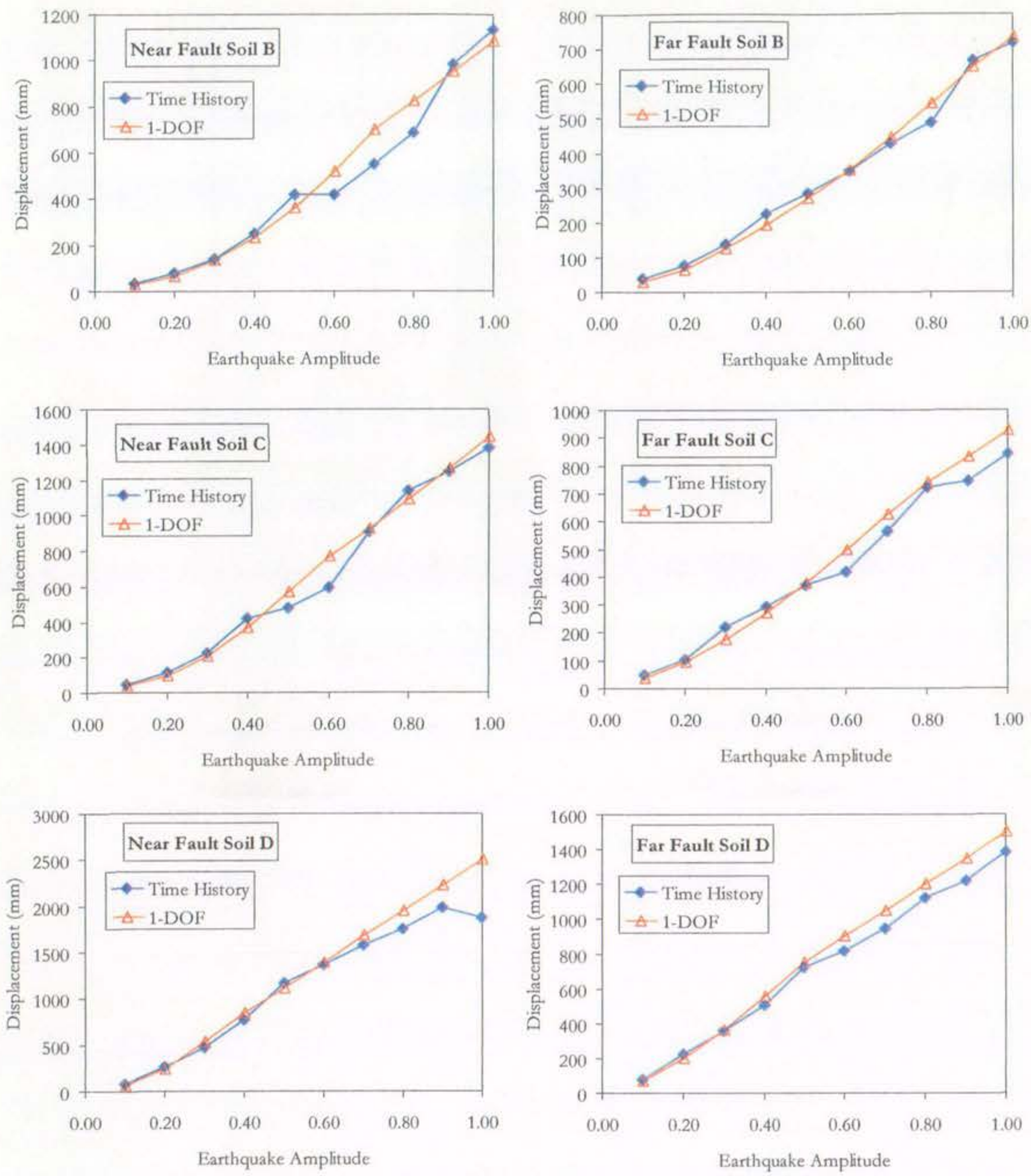

Figures A- 25 Run 2-4-B 3.600 m Wall Length 4 Story Rock

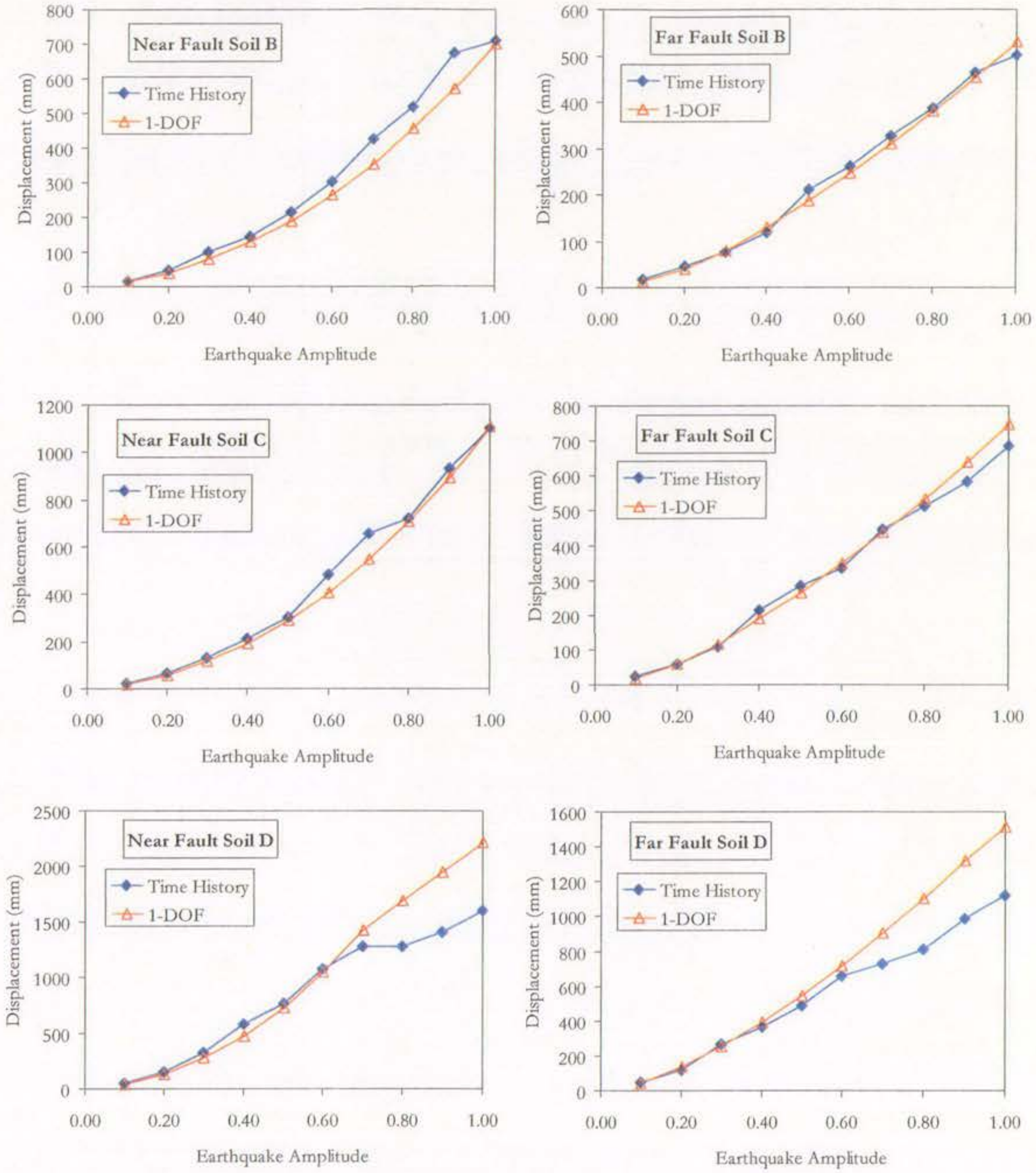

Figures A- 26 Run 2-4-B 3.600 m Wall Length 5 Story Medium Clay

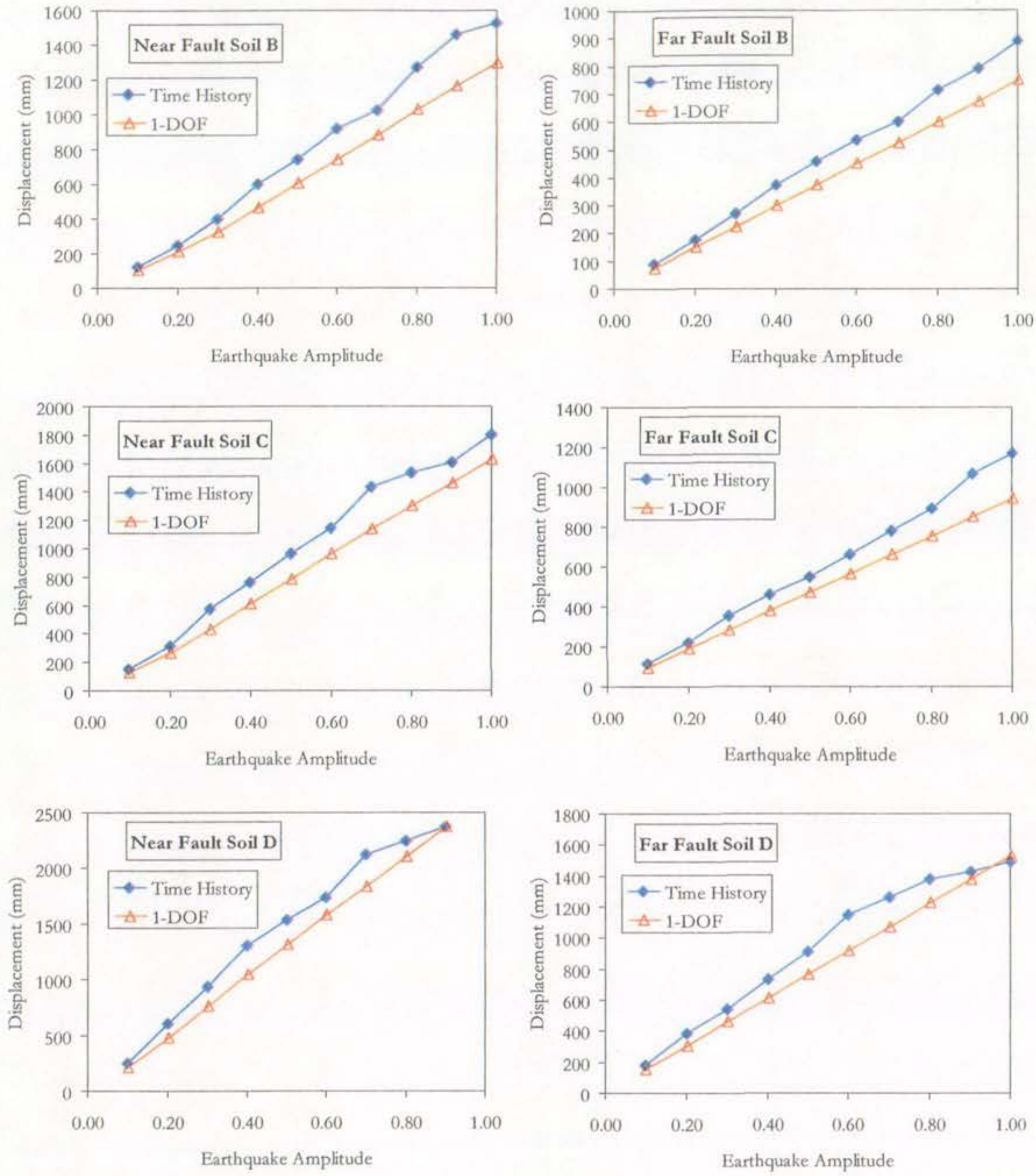

Figures A- 27 Run 2-4-B 3.600 m Wall Length 5 Story Medium Gravel

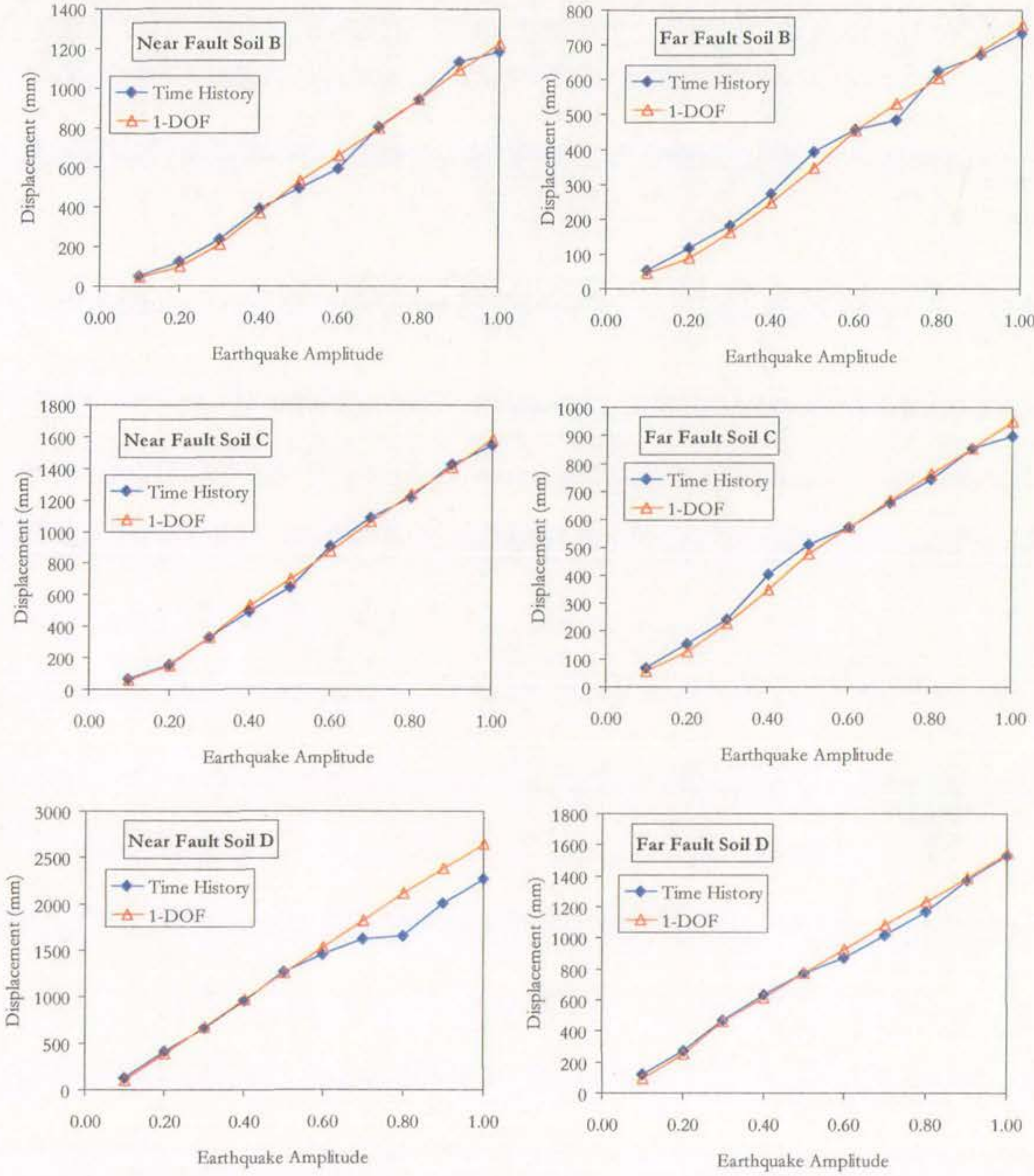

Figures A- 28 Run 2-4-B 3.600 m Wall Length 5 Story Rock

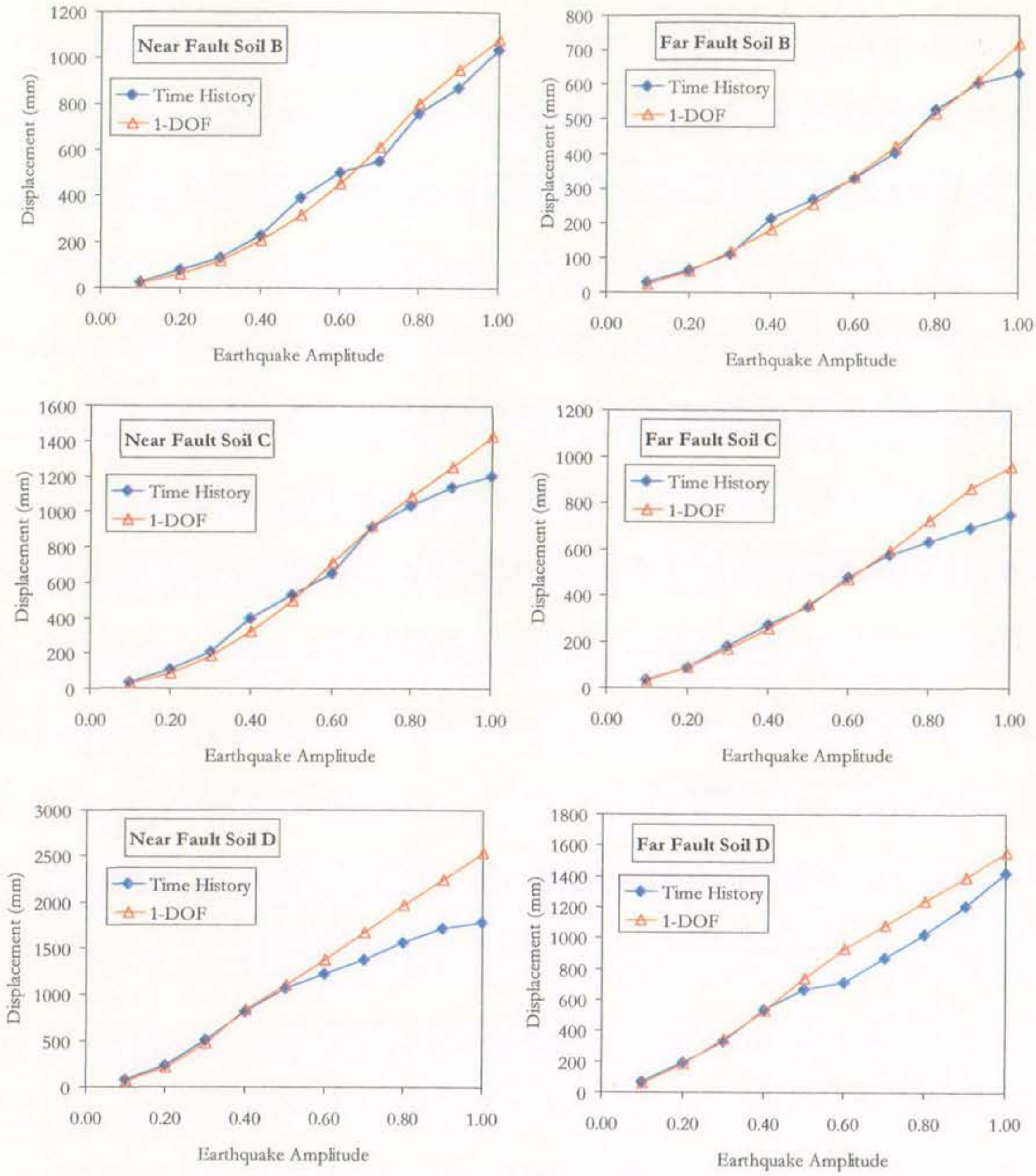

Figures A- 29 Run 2-4-B 3.600 m Wall Length 6 Story Medium Clay

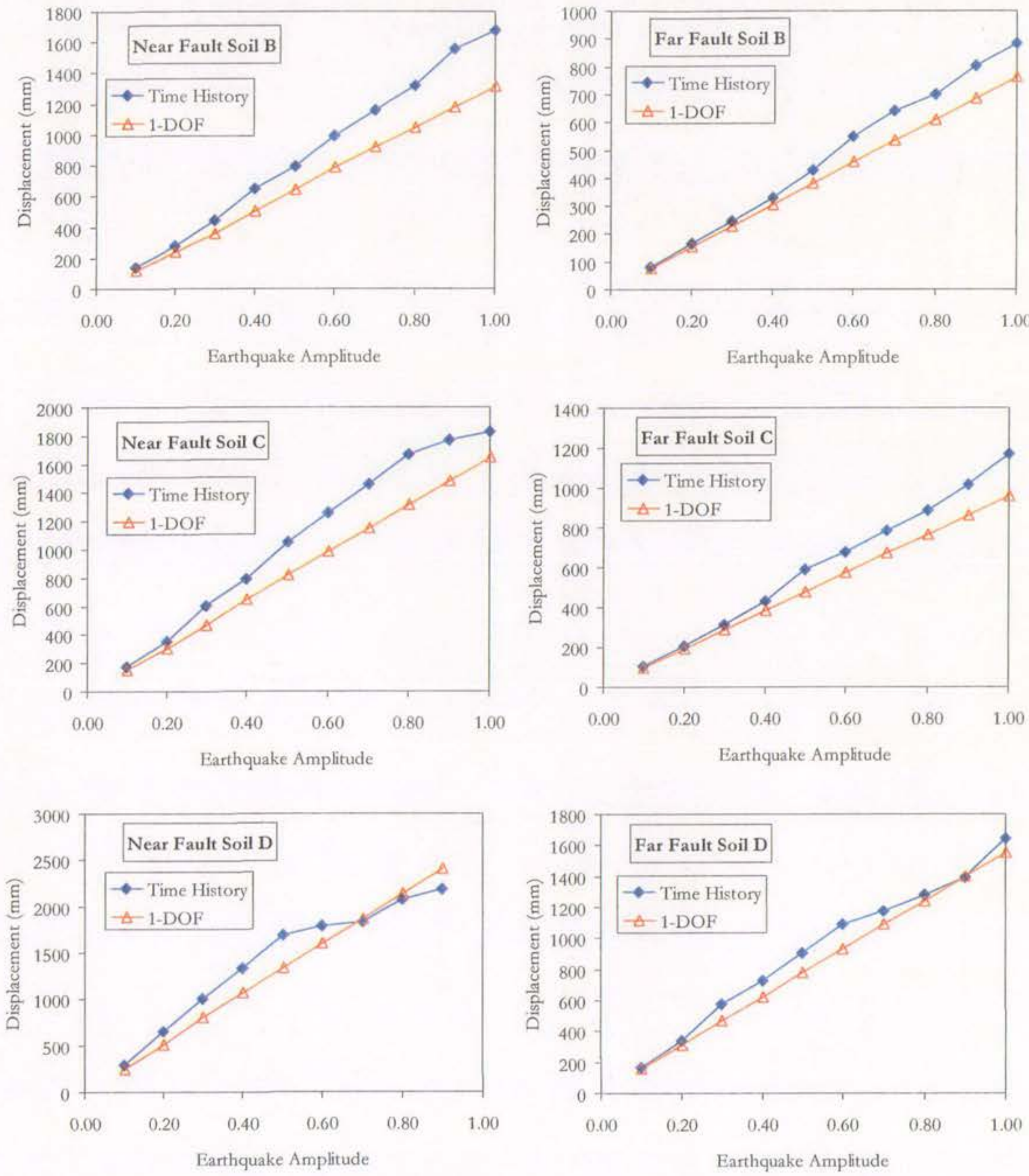

Figures A- 30 Run 2-4-B 3.600 m Wall Length 6 Story Medium Gravel

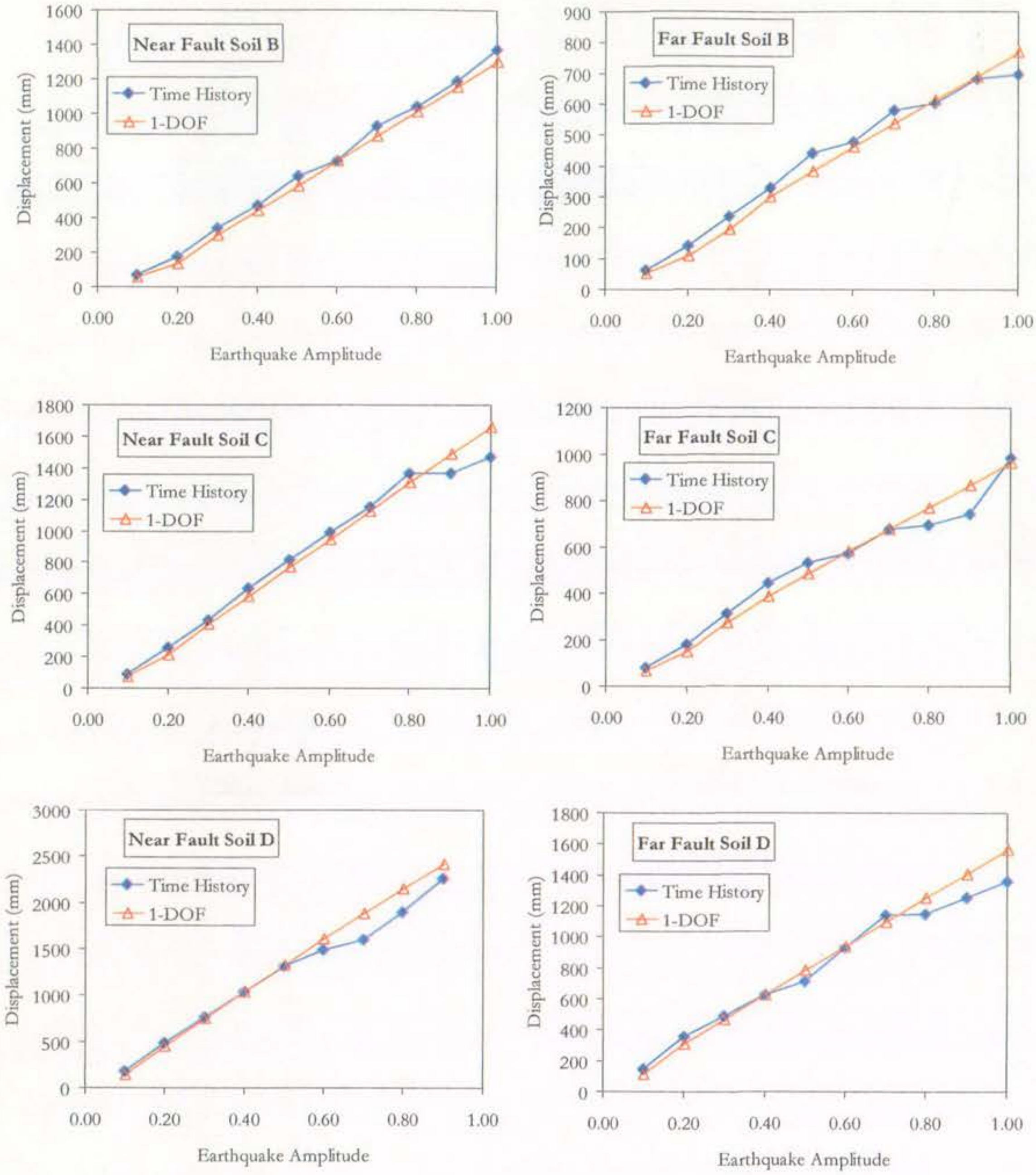

Figures A- 31 Run 2-4-B 3.600 m Wall Length 6 Story Rock

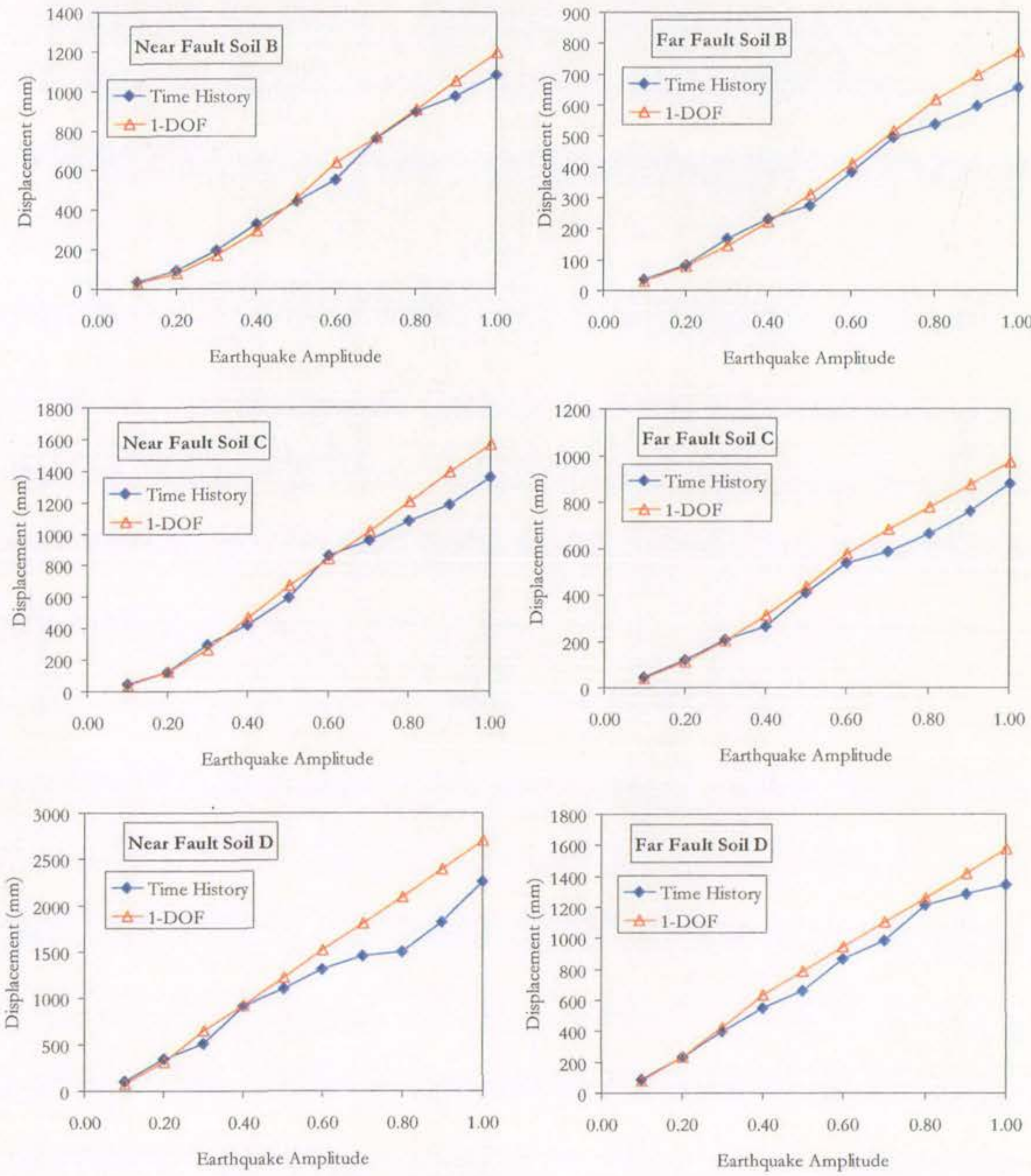

Figures A- 32 Run 3-1-B 14.400 m Wall Length 1 Story Medium Clay

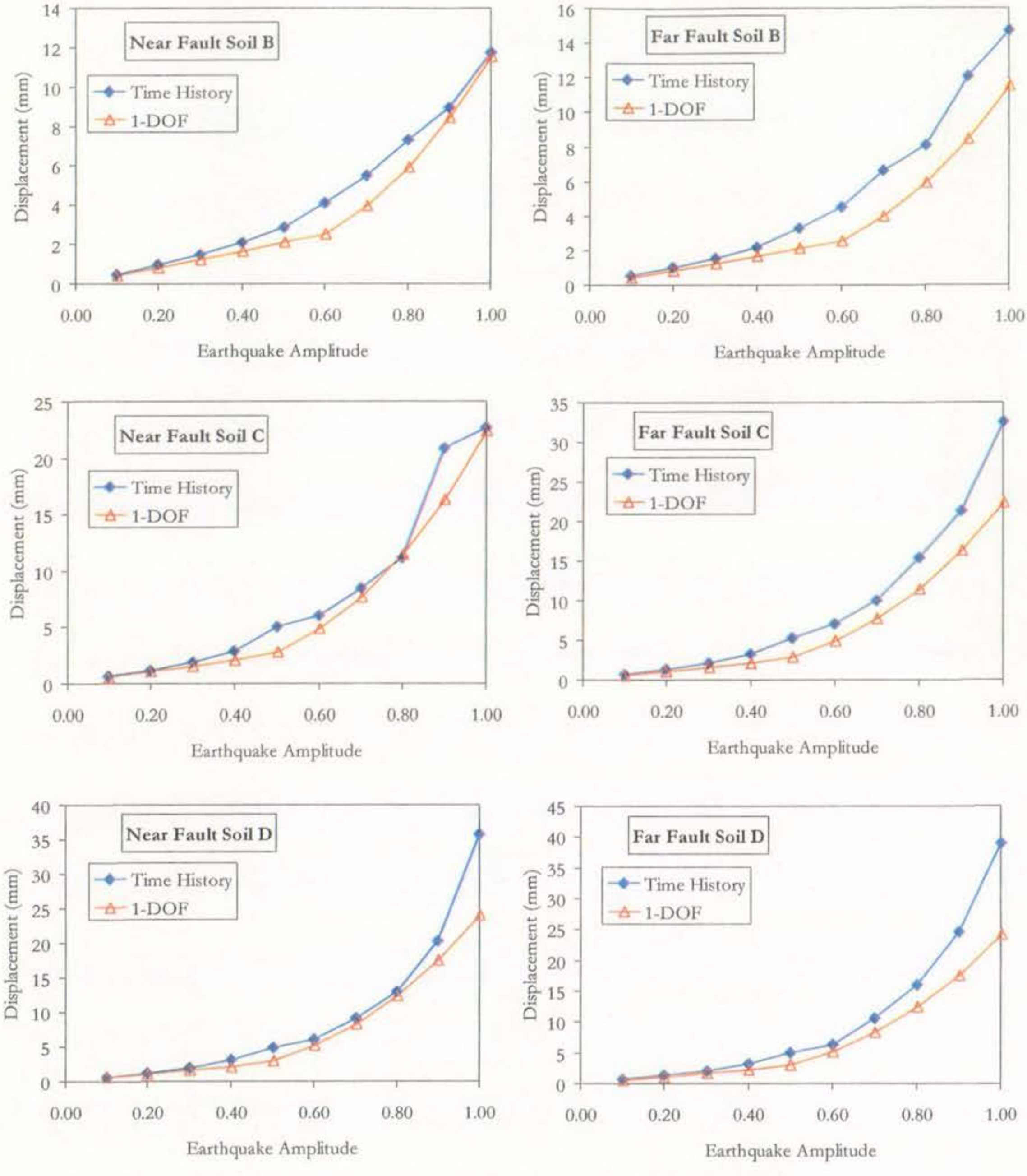

Figures A- 33 Run 3-1-E 14.400 m Wall Length 1 Story Medium Gravel

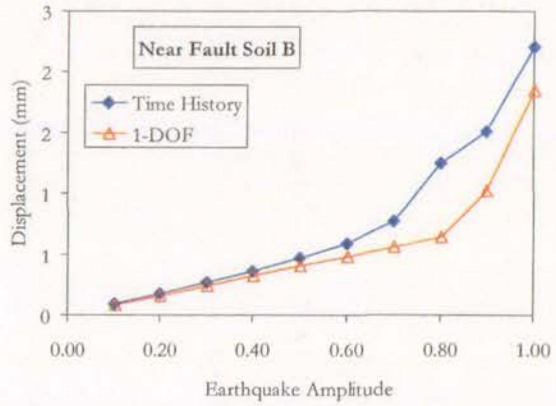

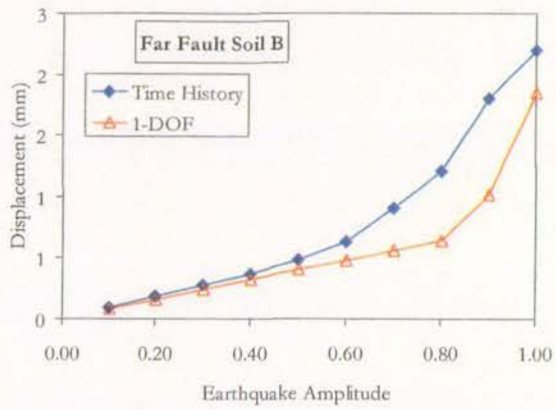

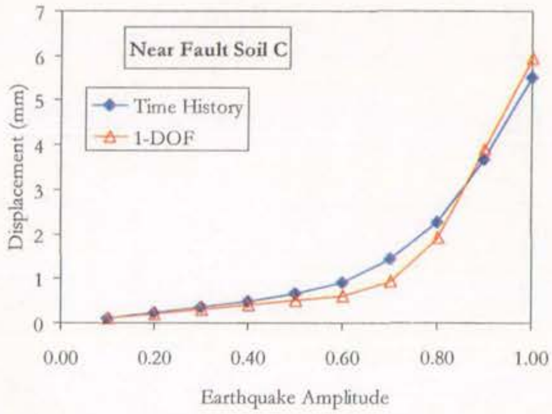

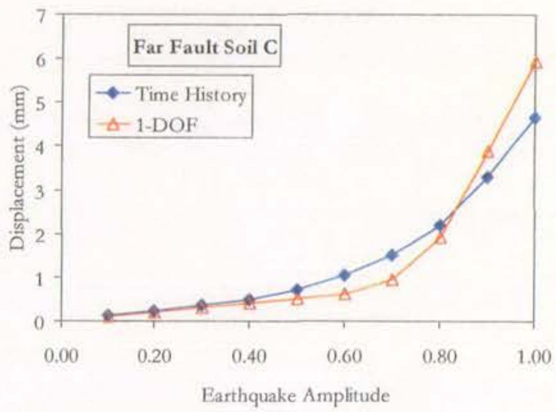

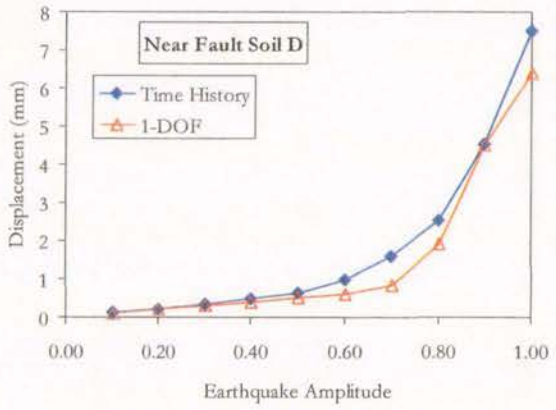

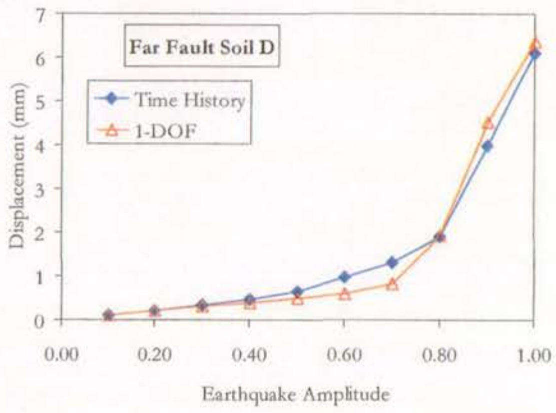

Figures A- 34 Run 3-1-G 14.400 m Wall Length 1 Story Rock

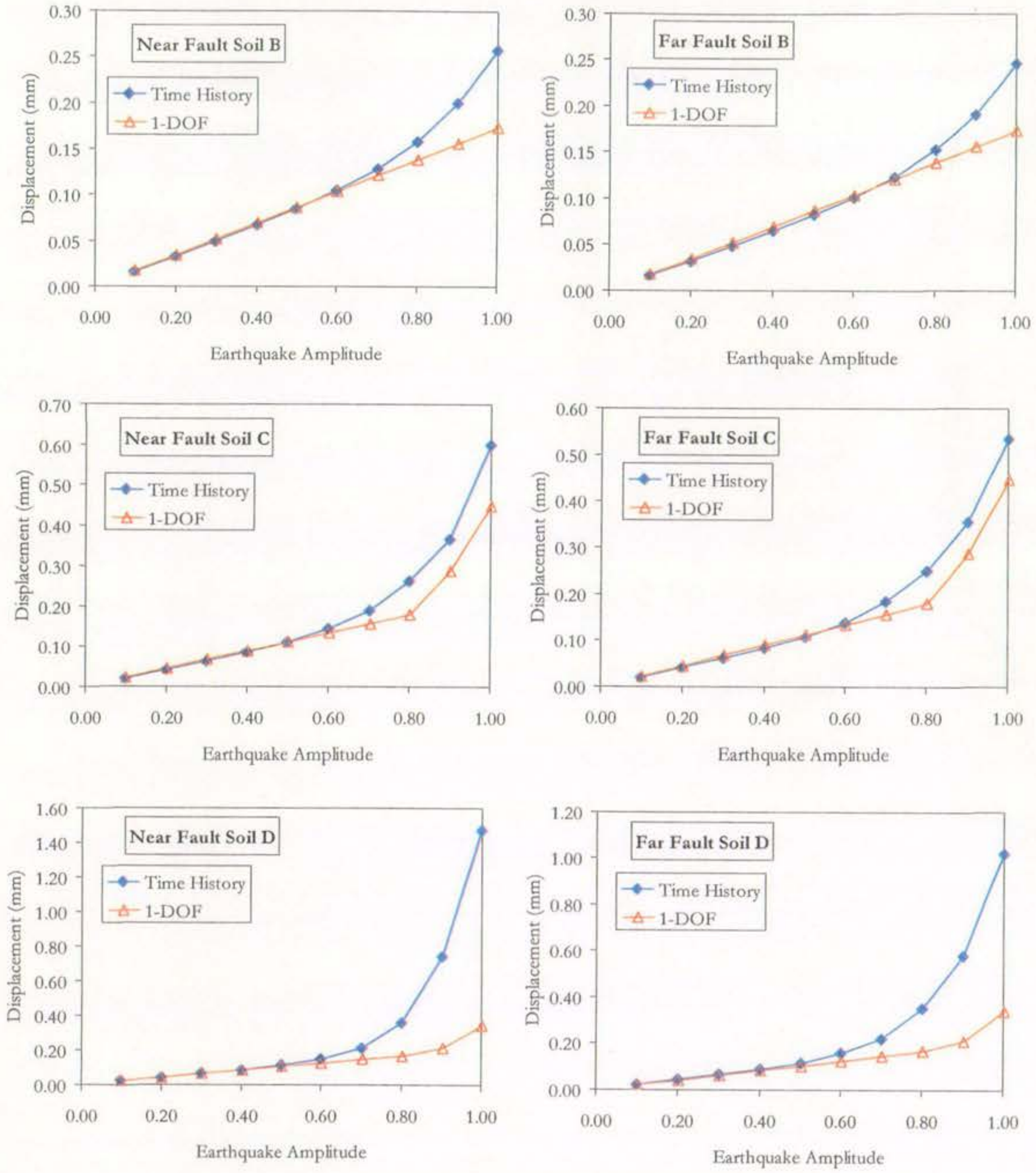

Figures A- 35 Run 3-2-B 14.400 m Wall Length 2 Story Medium Clay

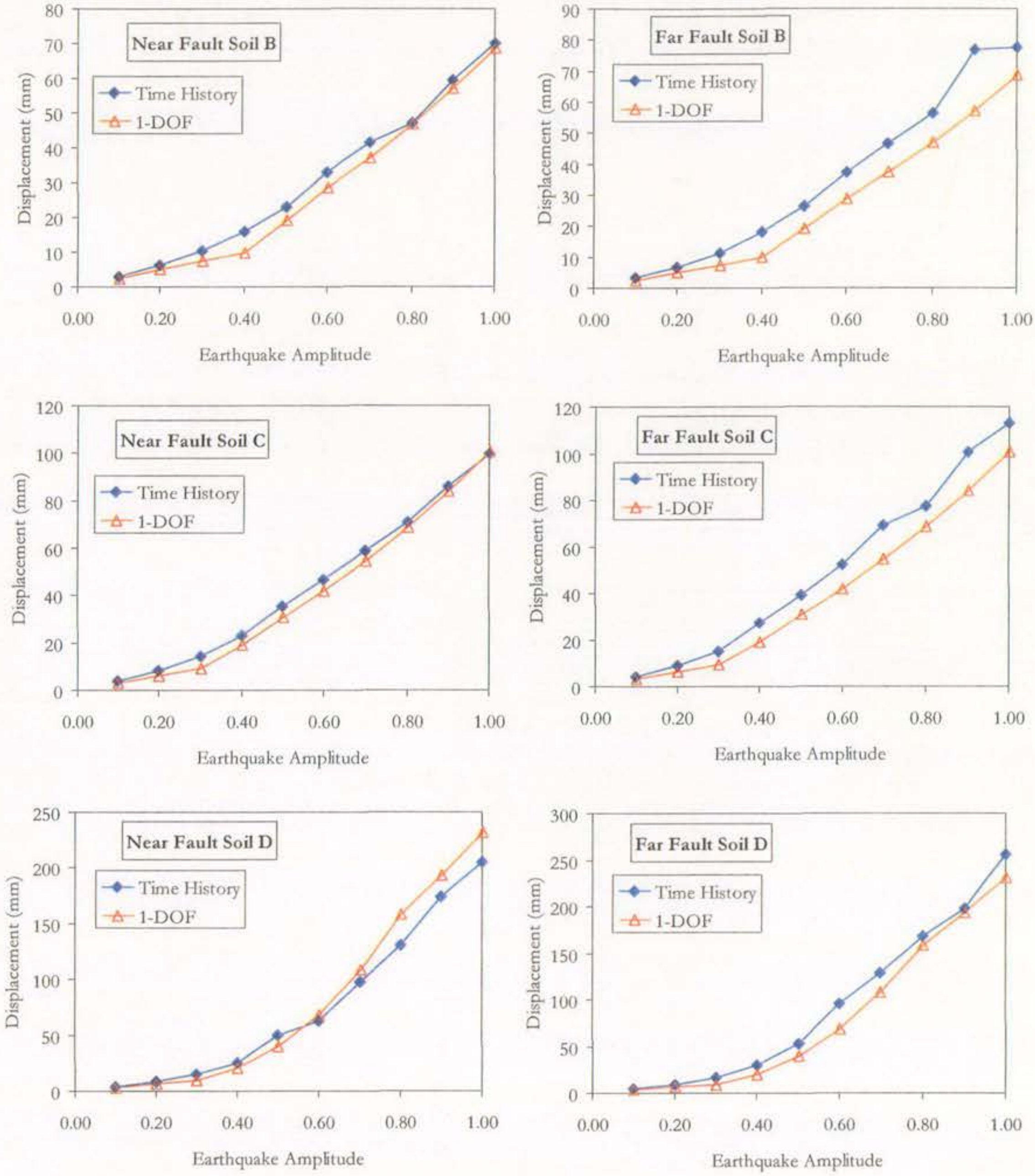

Figures A- 36 Run 3-2-E 14.400 m Wall Length 2 Story Medium Gravel

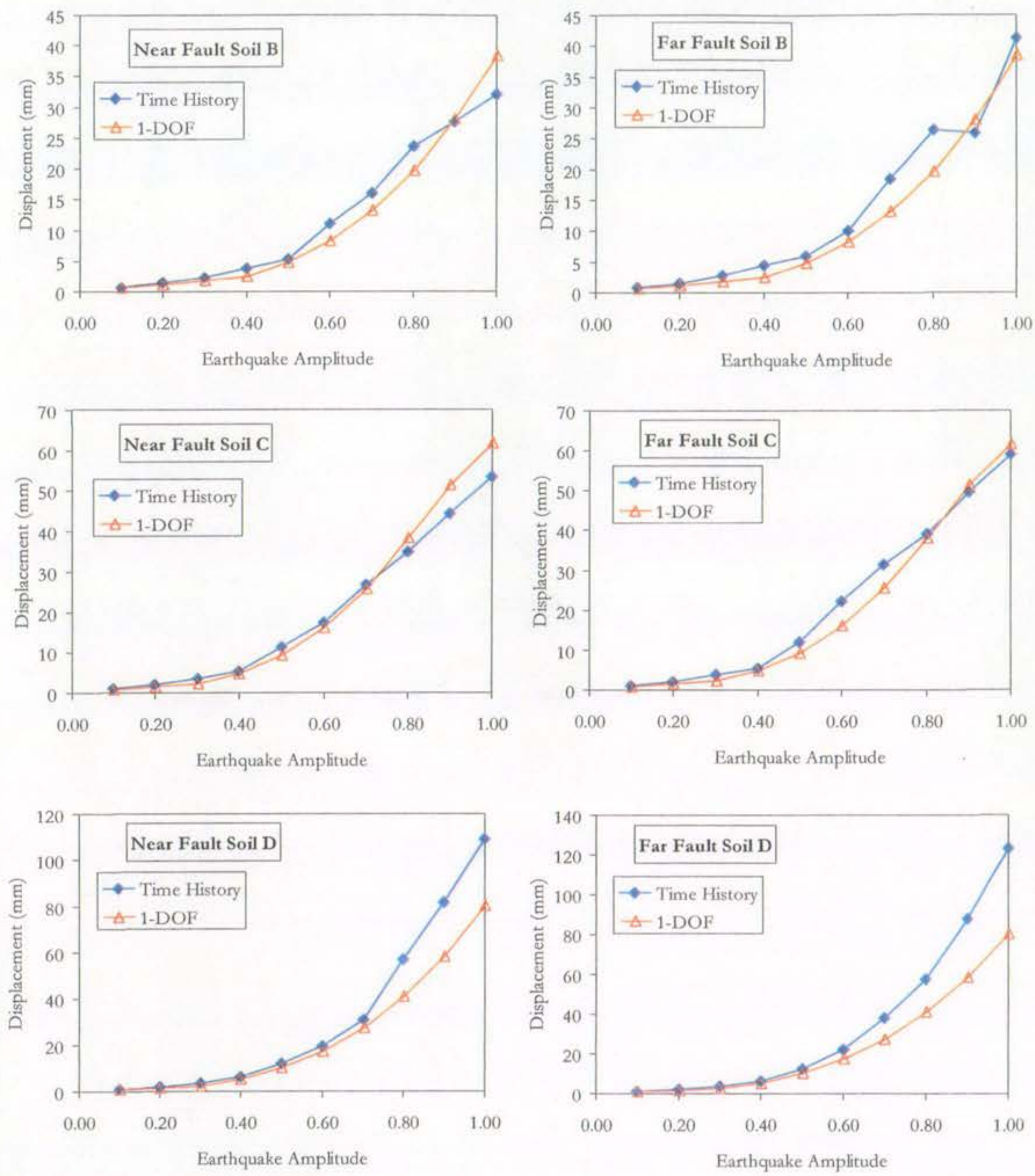

Figures A- 37 Run 3-2-G 14.400 m Wall Length 2 Story Rock

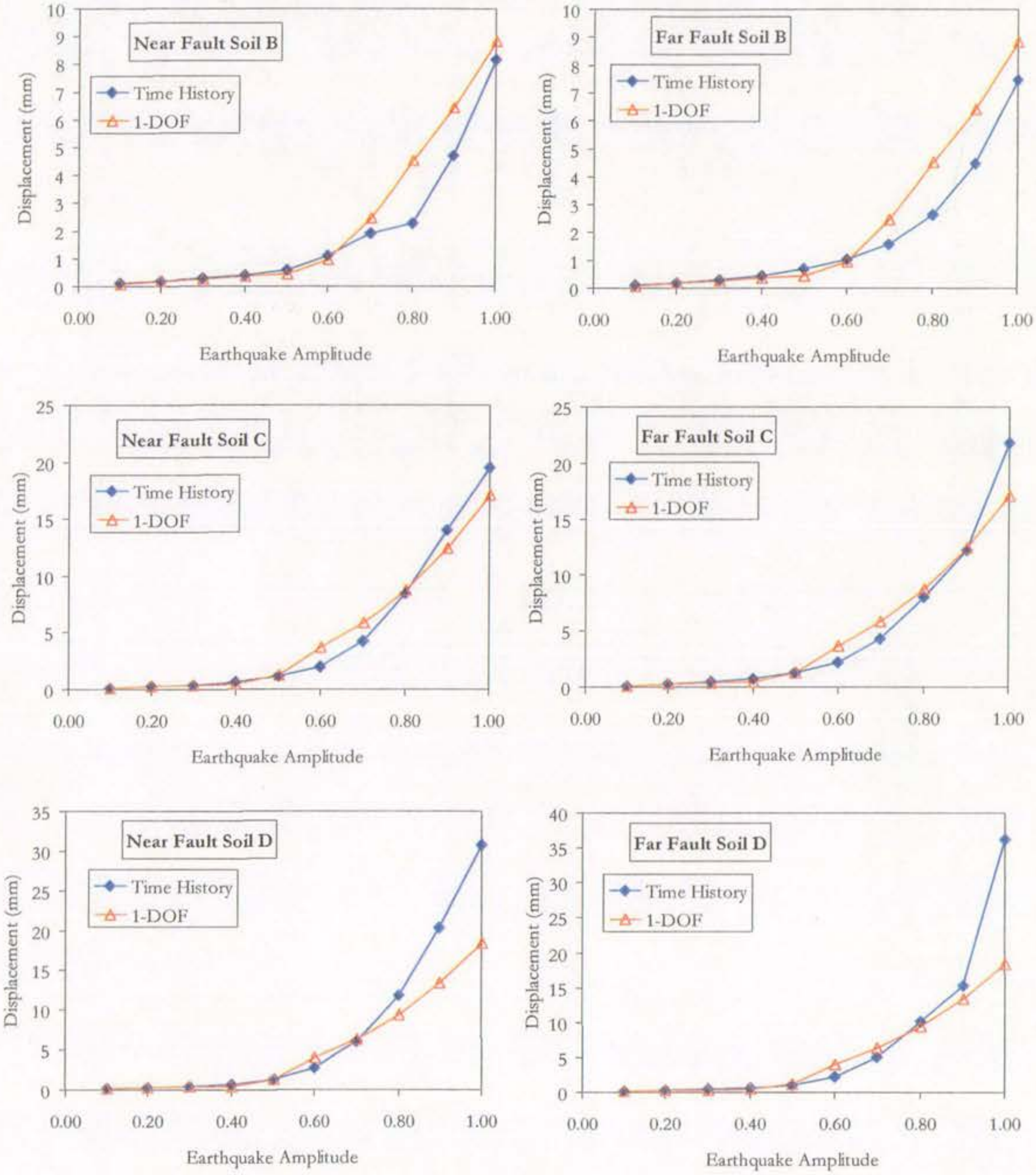

Figures A- 38 Run 3-3-B 14.400 m Wall Length 3 Story Medium Clay

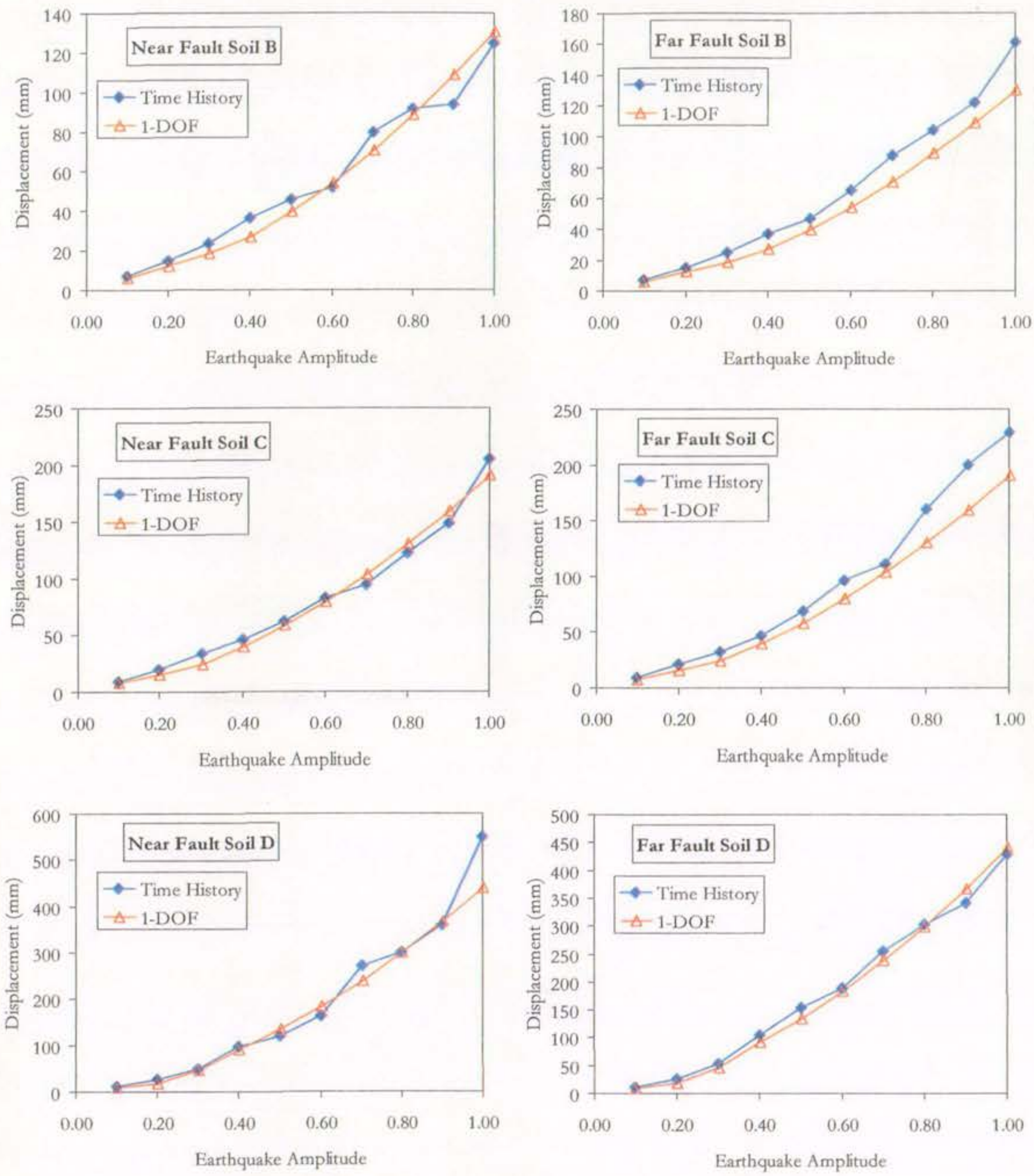

Figures A- 39 Run 3-3-E 14.400 m Wall Length 3 Story Medium Gravel

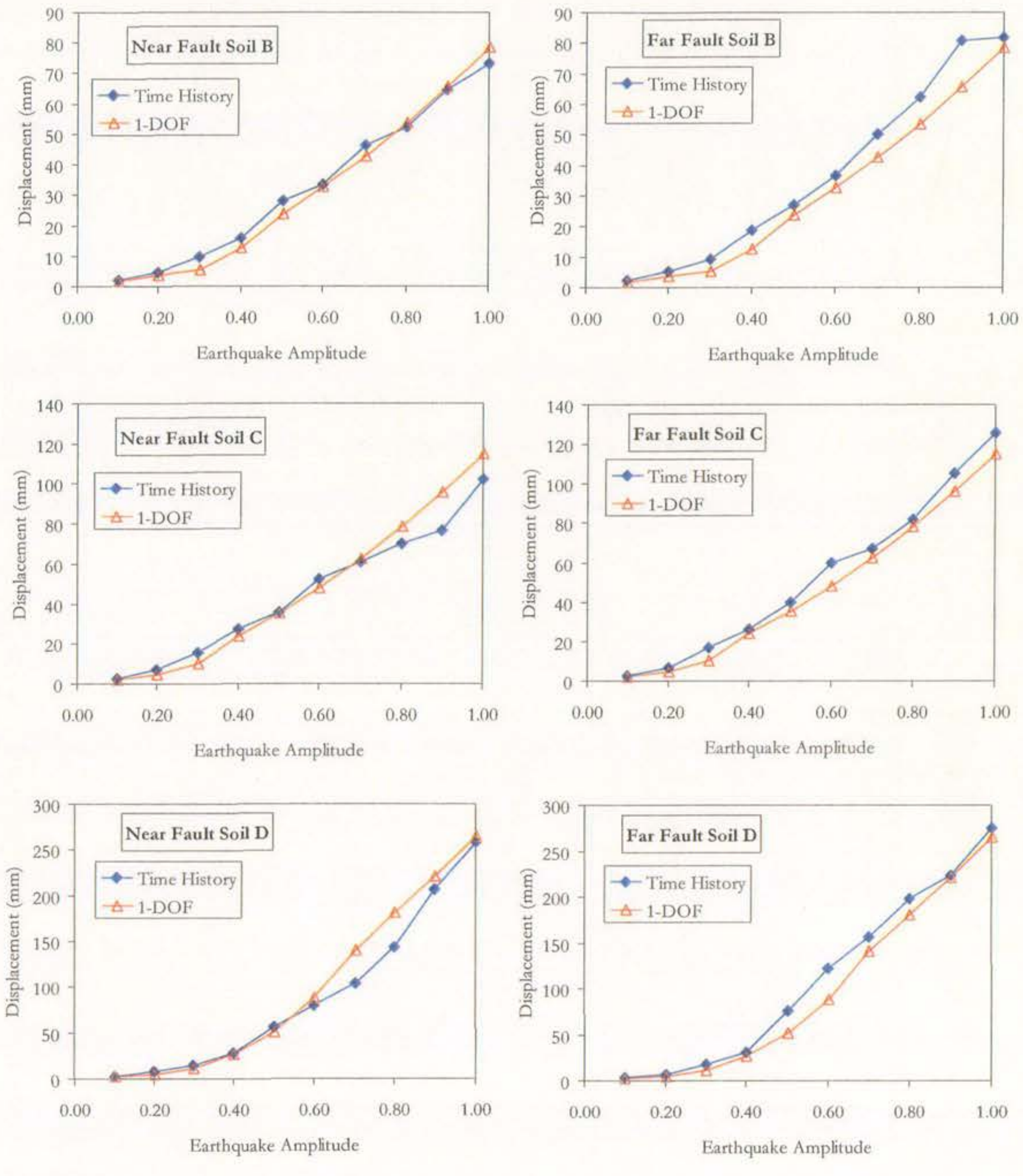

Figures A- 40 Run 3-3-G 14.400 m Wall Length 3 Story Rock

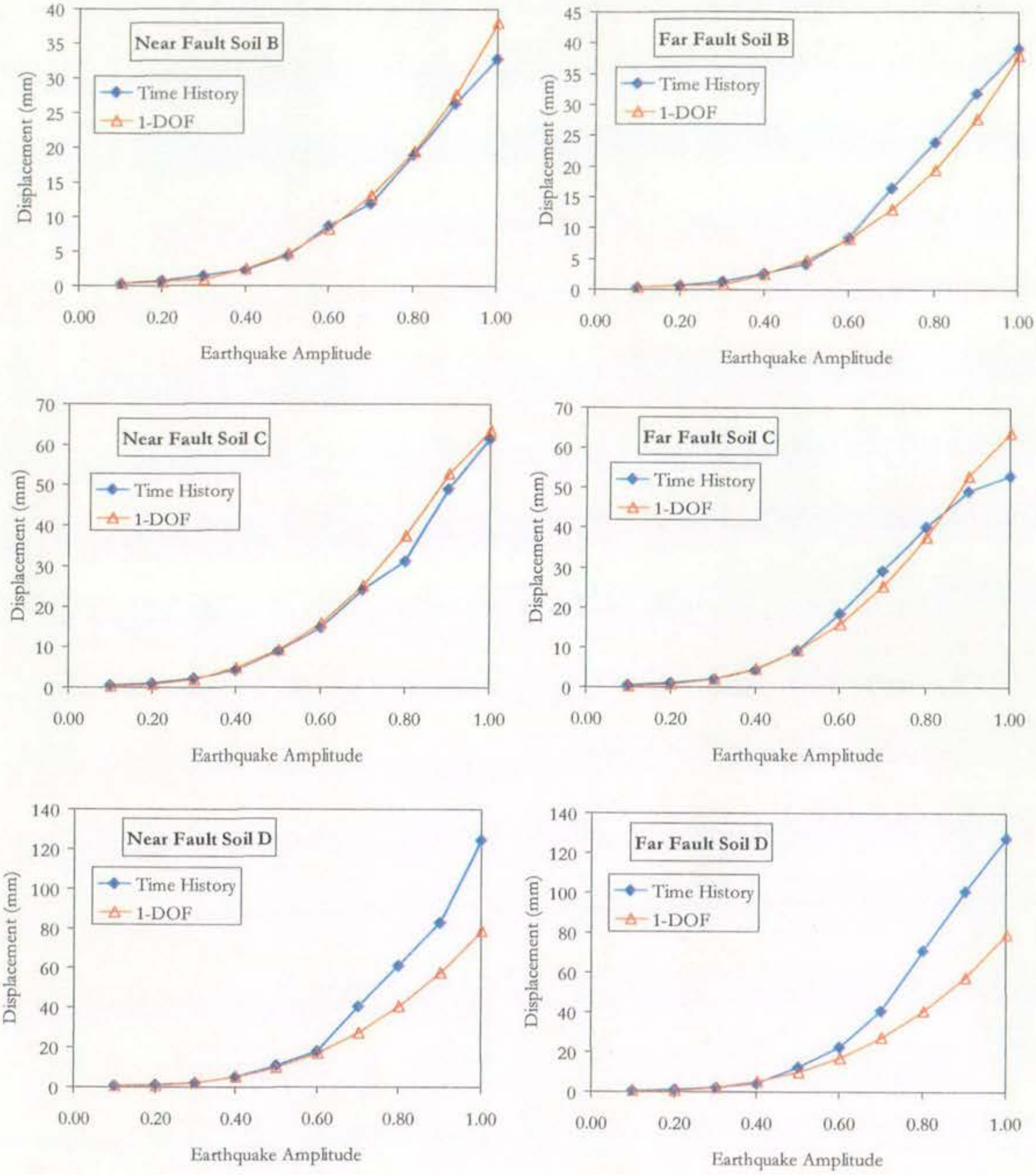

Figures A- 41 Run 12-3-B 7.200 m + 3.600 m Wall Length 3 Story Medium Clay

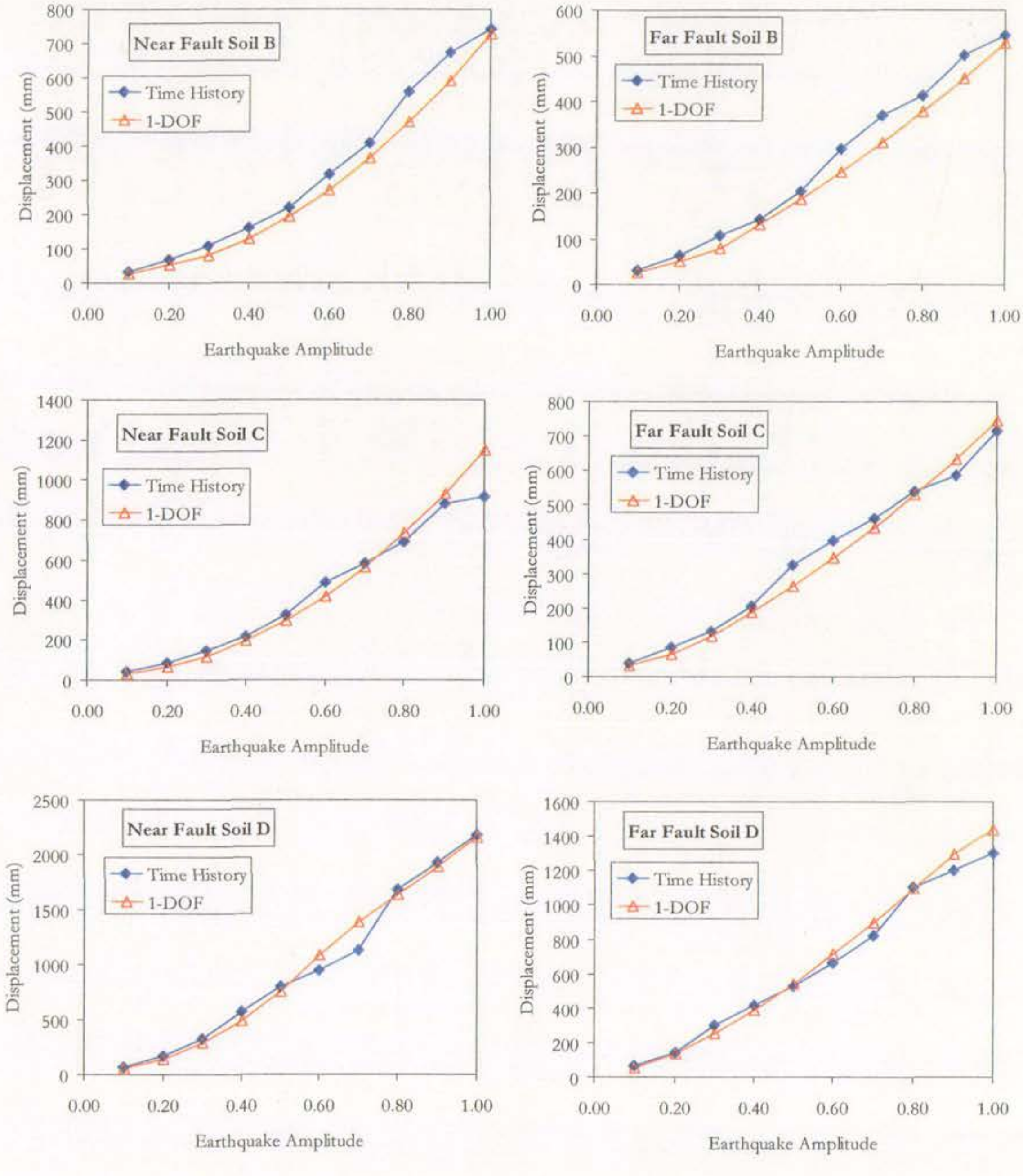

Figures A- 42 Run 12-3-E7.200 m + 3.600 m Wall Length 3 Story Medium Gravel

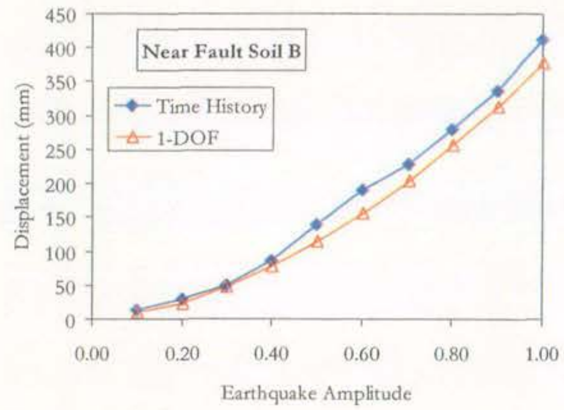

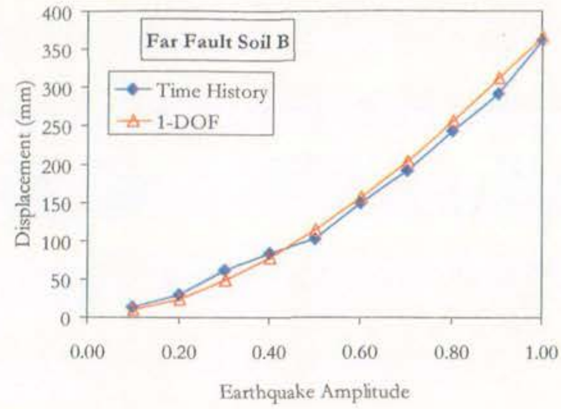

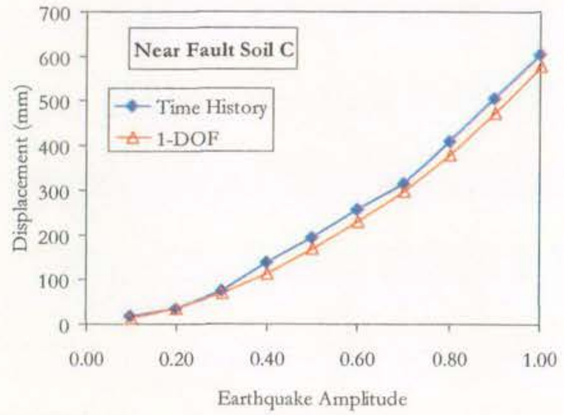

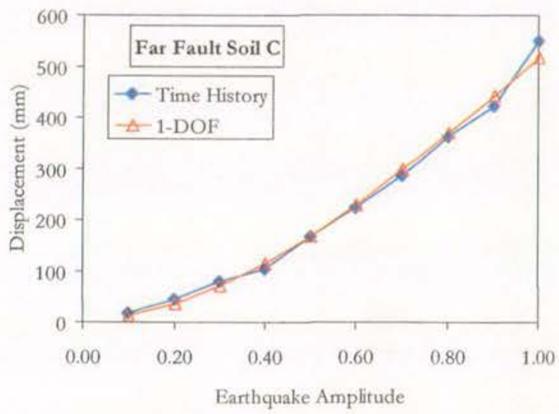

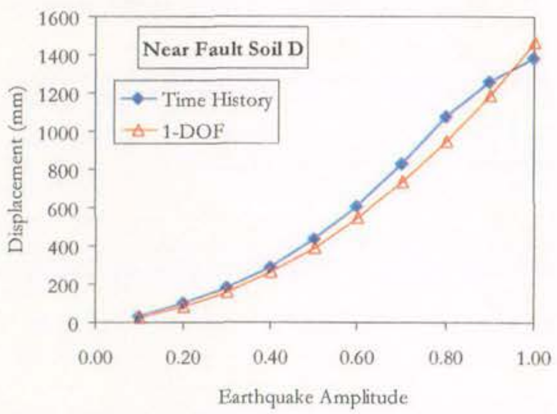

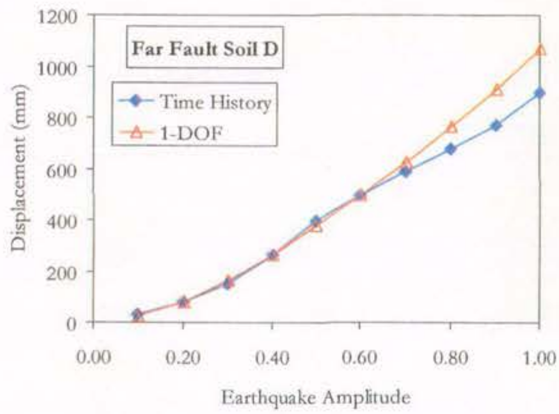

Figures A- 43 Run 12-3-G 7.200 m + 3.600 m Wall Length 3 Story Rock

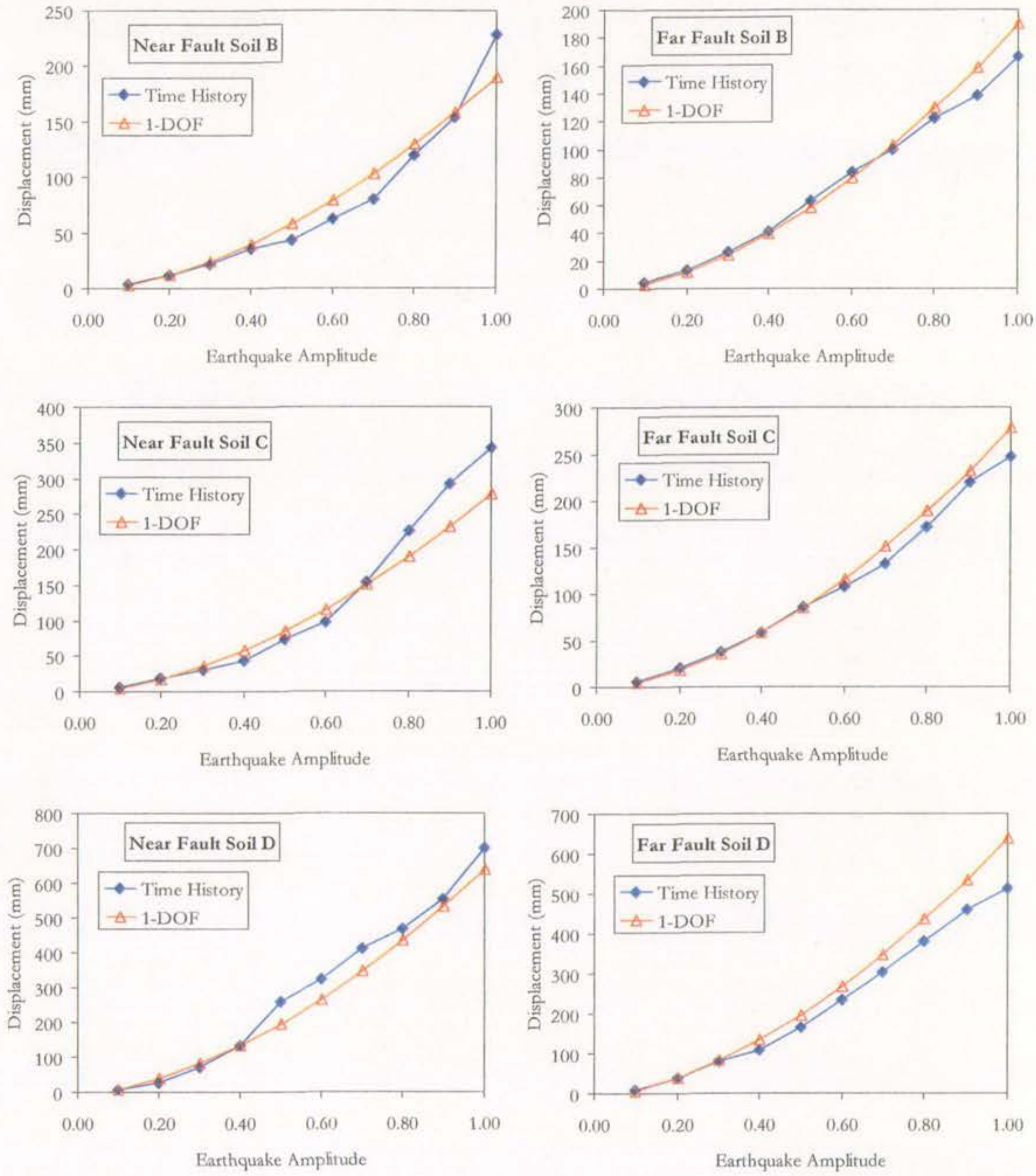

Figures A- 44 U-Shaped Wall 7.200 m x 14.400 m 3 Story Medium Clay

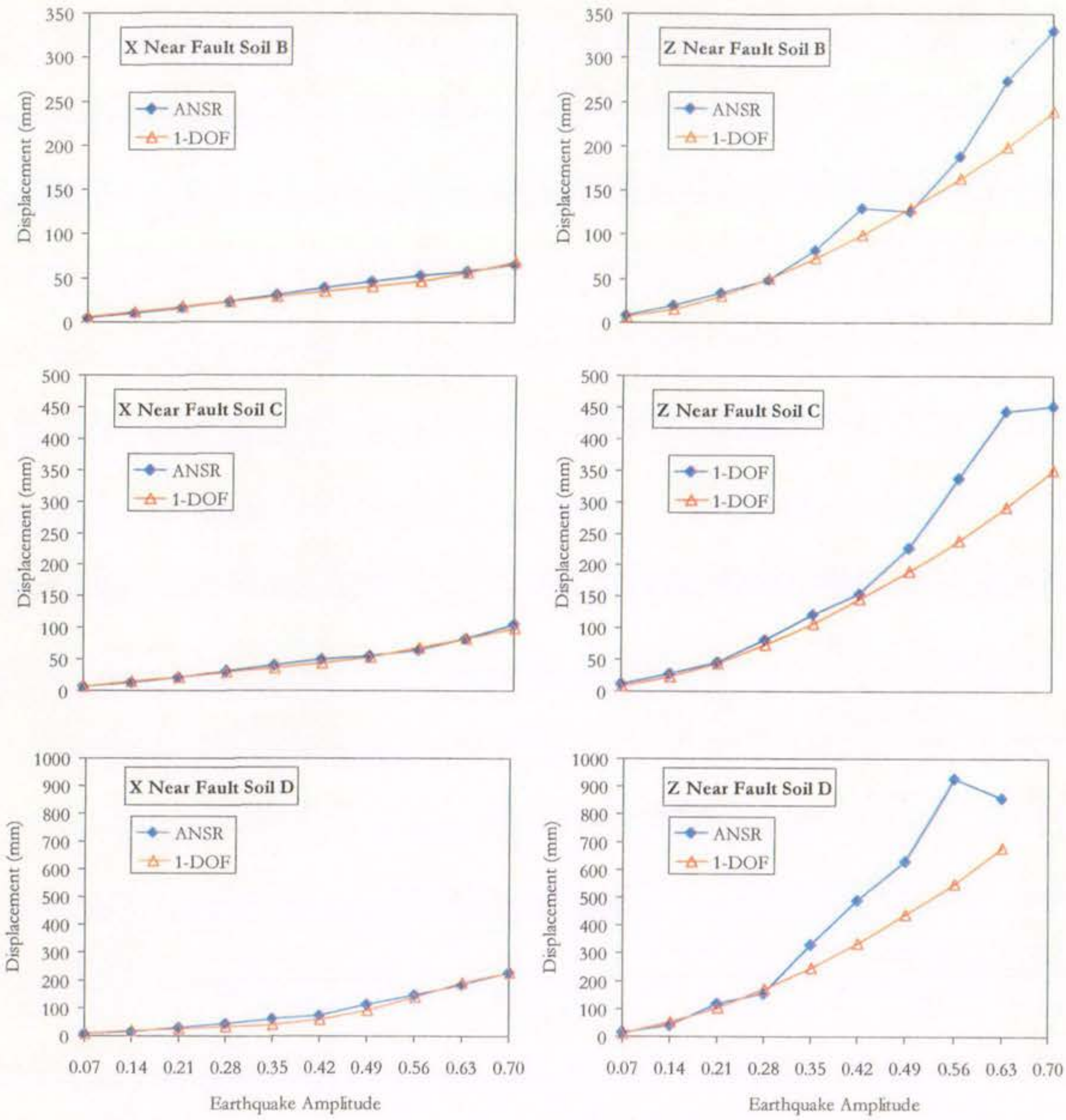

Figures A- 45 U-Shaped Wall 7.200 m x 14.400 m 3 Story Medium Gravel

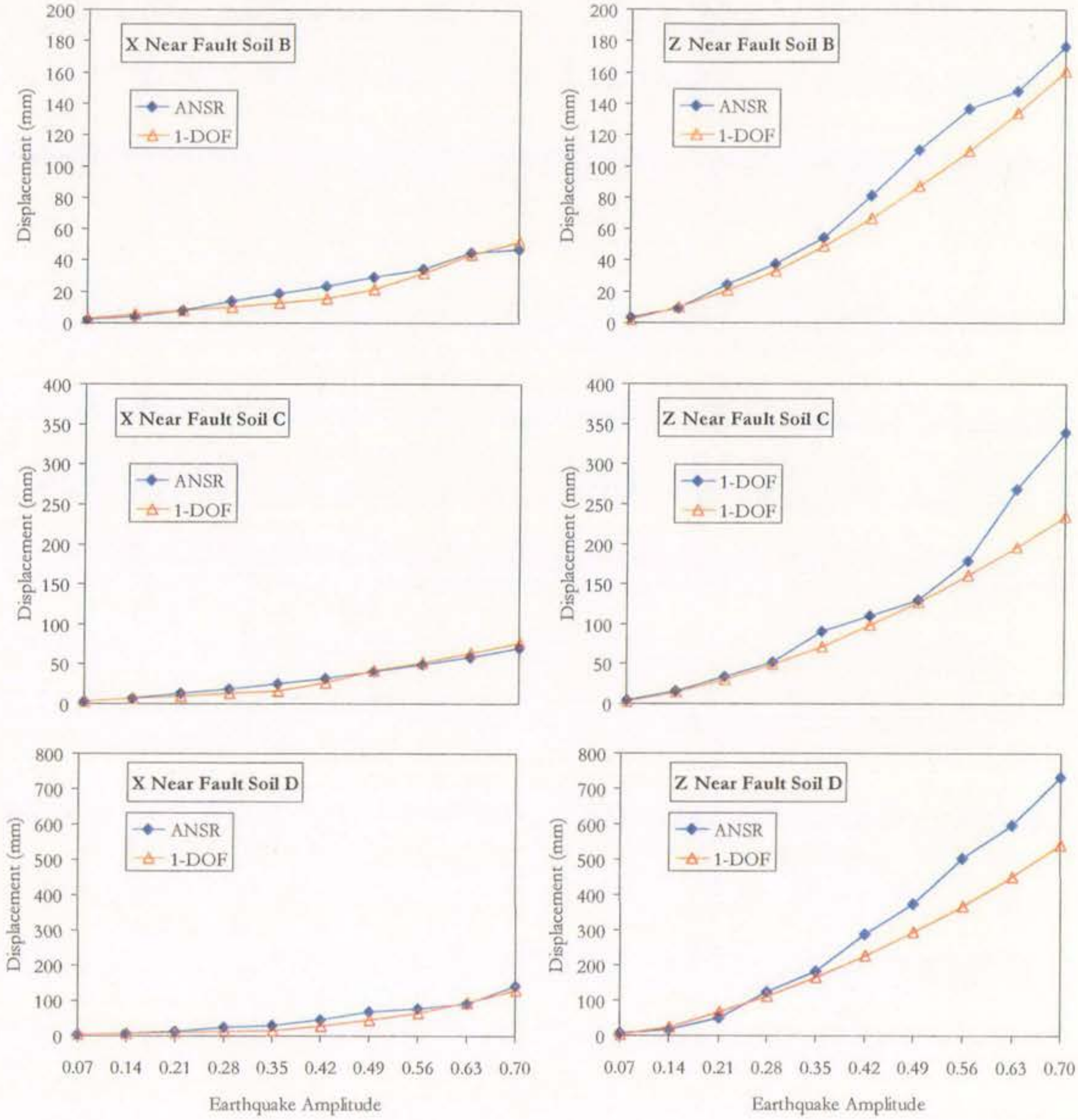

Figures A- 46 U-Shaped Wall 7.200 m x 14.400 m 3 Story Rock

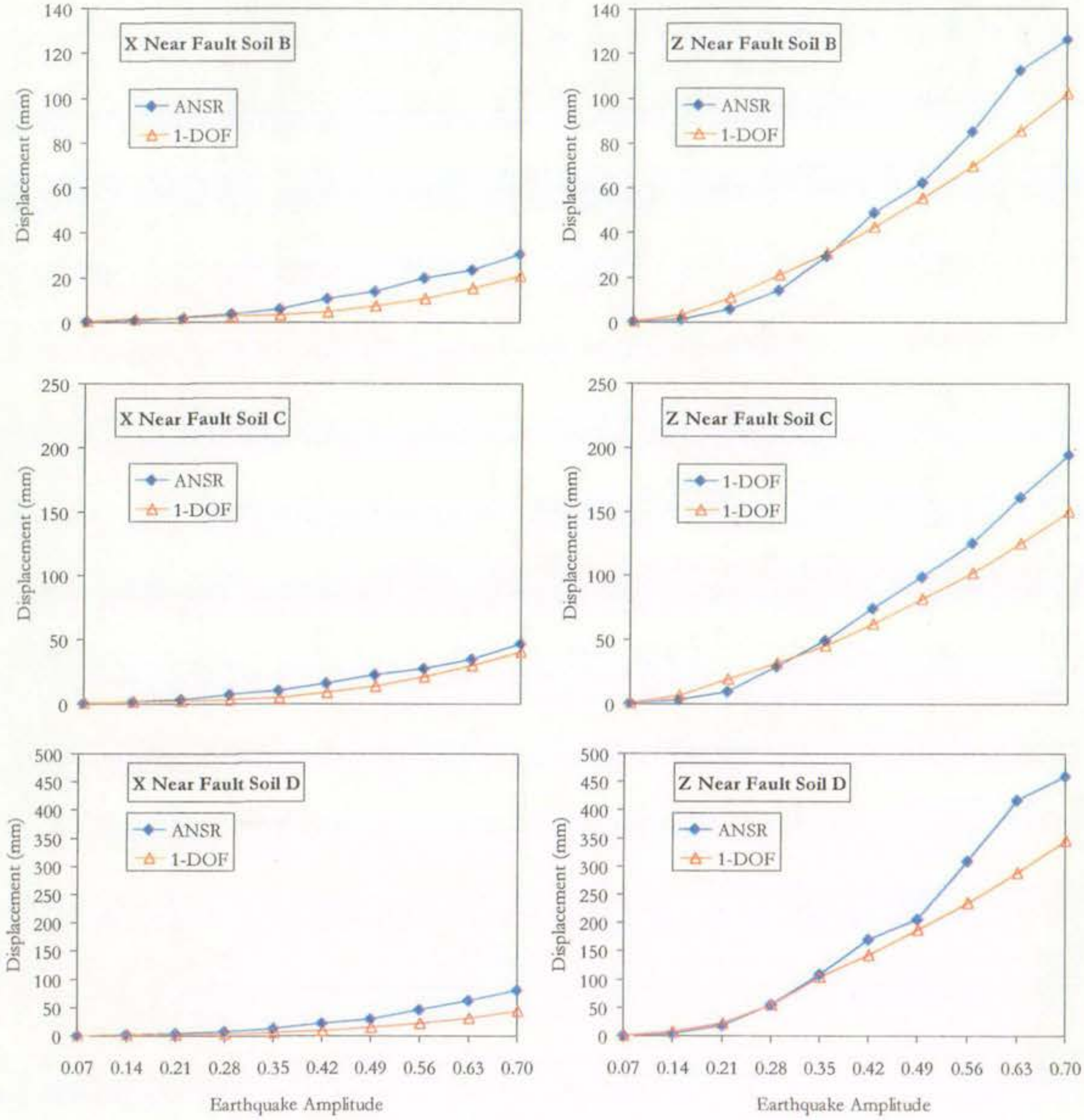

Figures A- 47 U-Shaped Wall 14.400 m x 14.400 m 2 Story Medium Clay

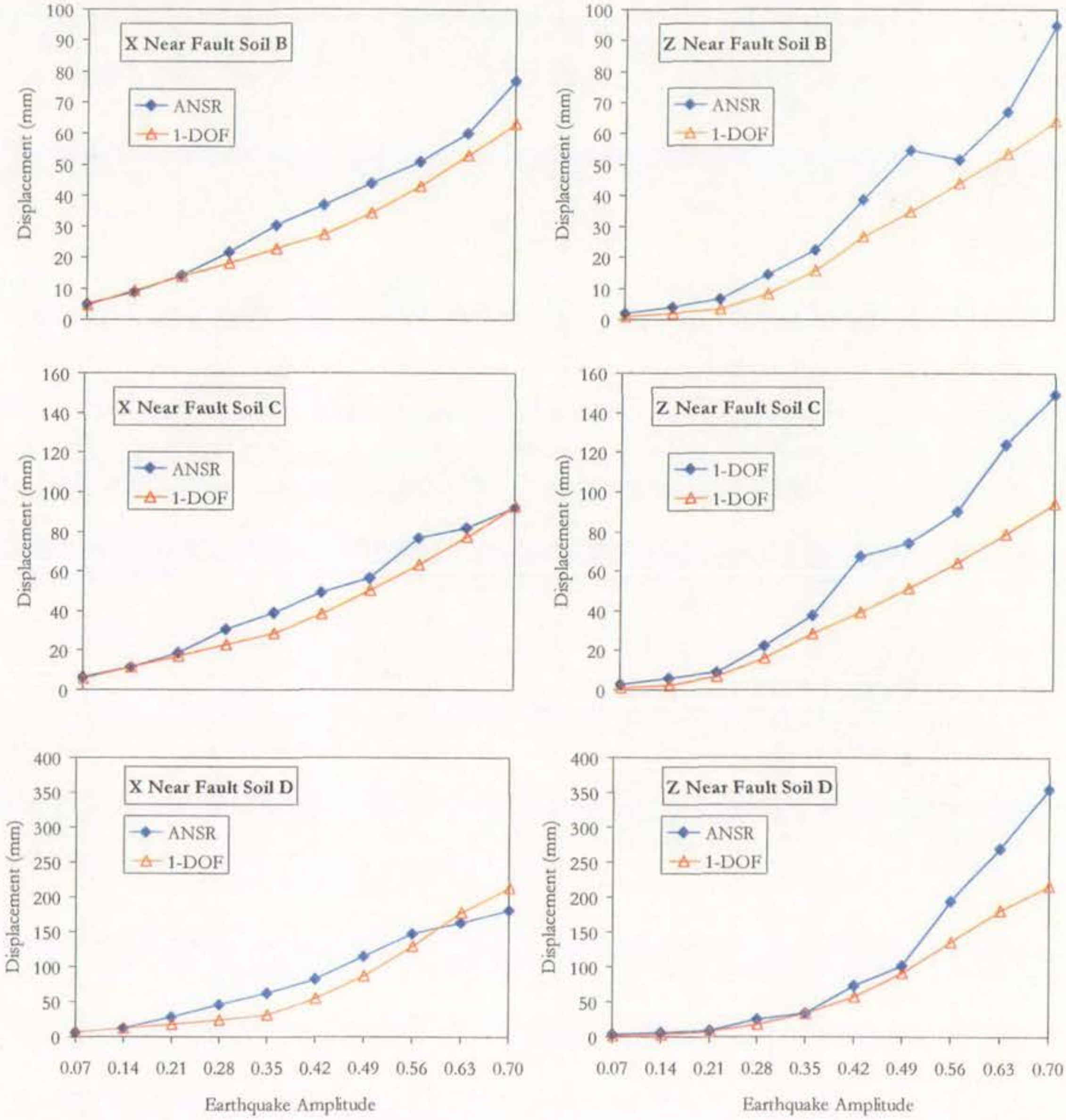

Figures A- 48 U-Shaped Wall 14.400 m x 14.400 m 2 Story Medium Gravel

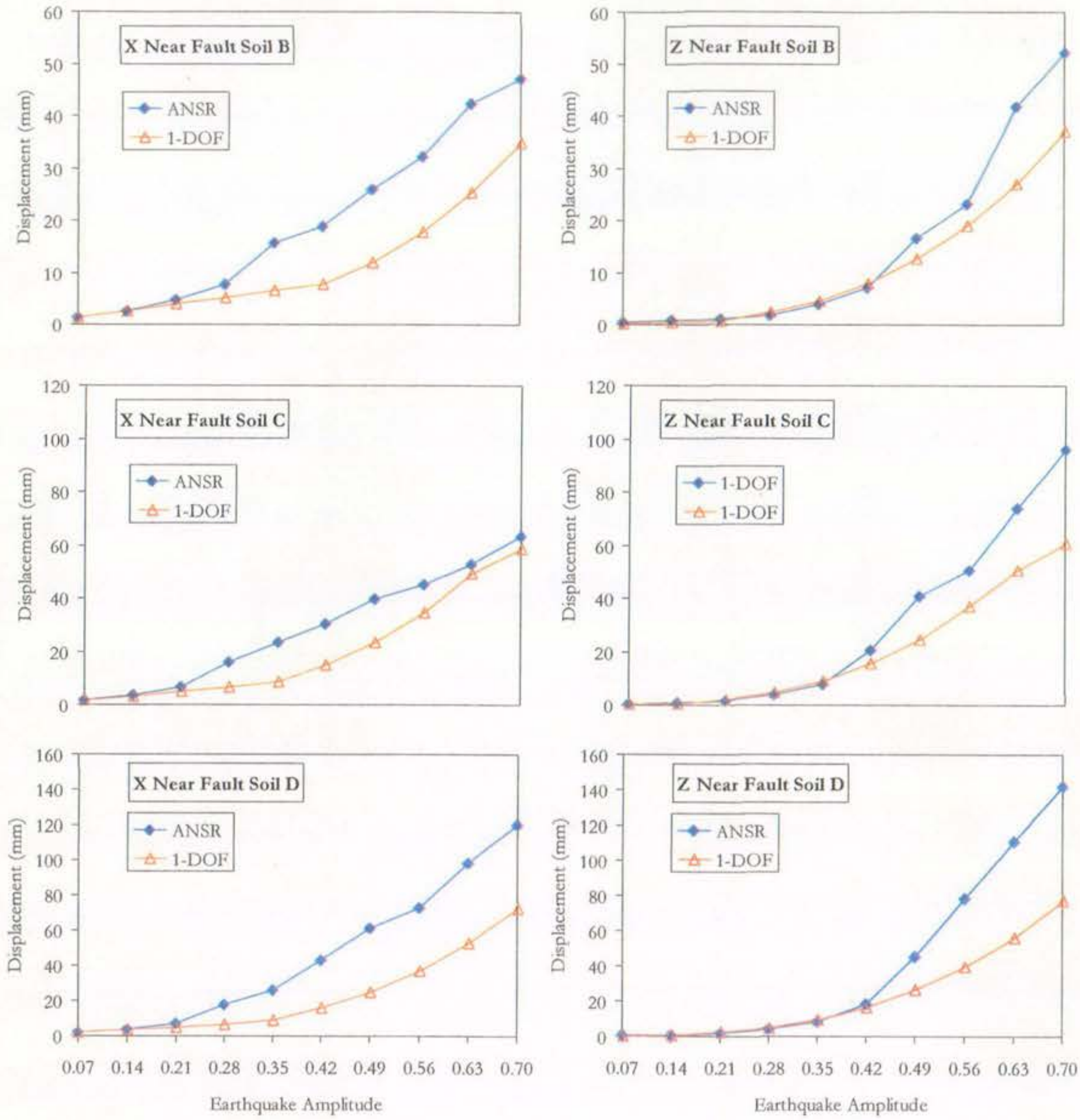

Figures A- 49 U-Shaped Wall 14.400 m x 14.400 m 2 Story Rock

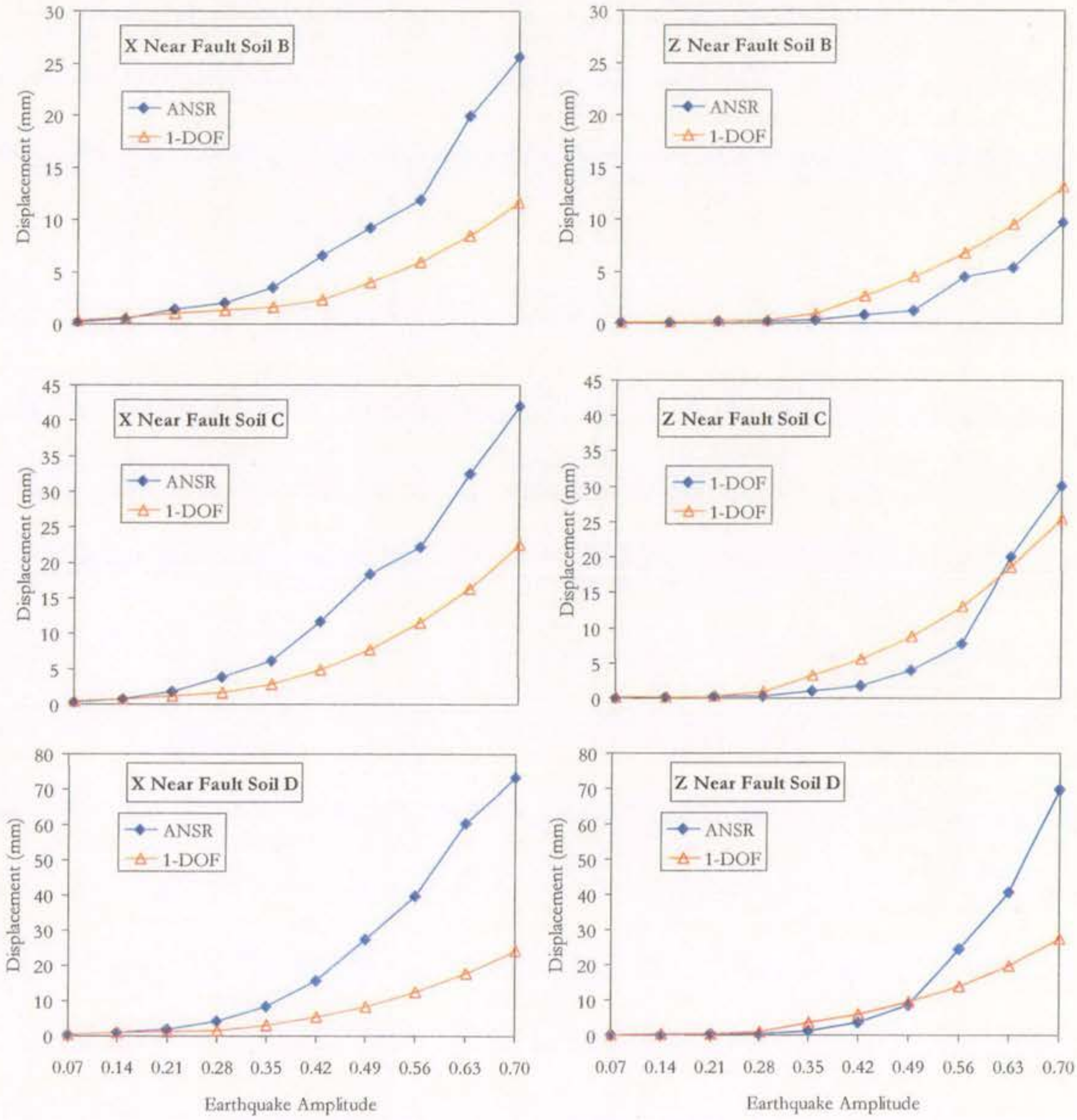

Figures A- 50 Non-Symmetrical Wall 2 Story Medium Clay

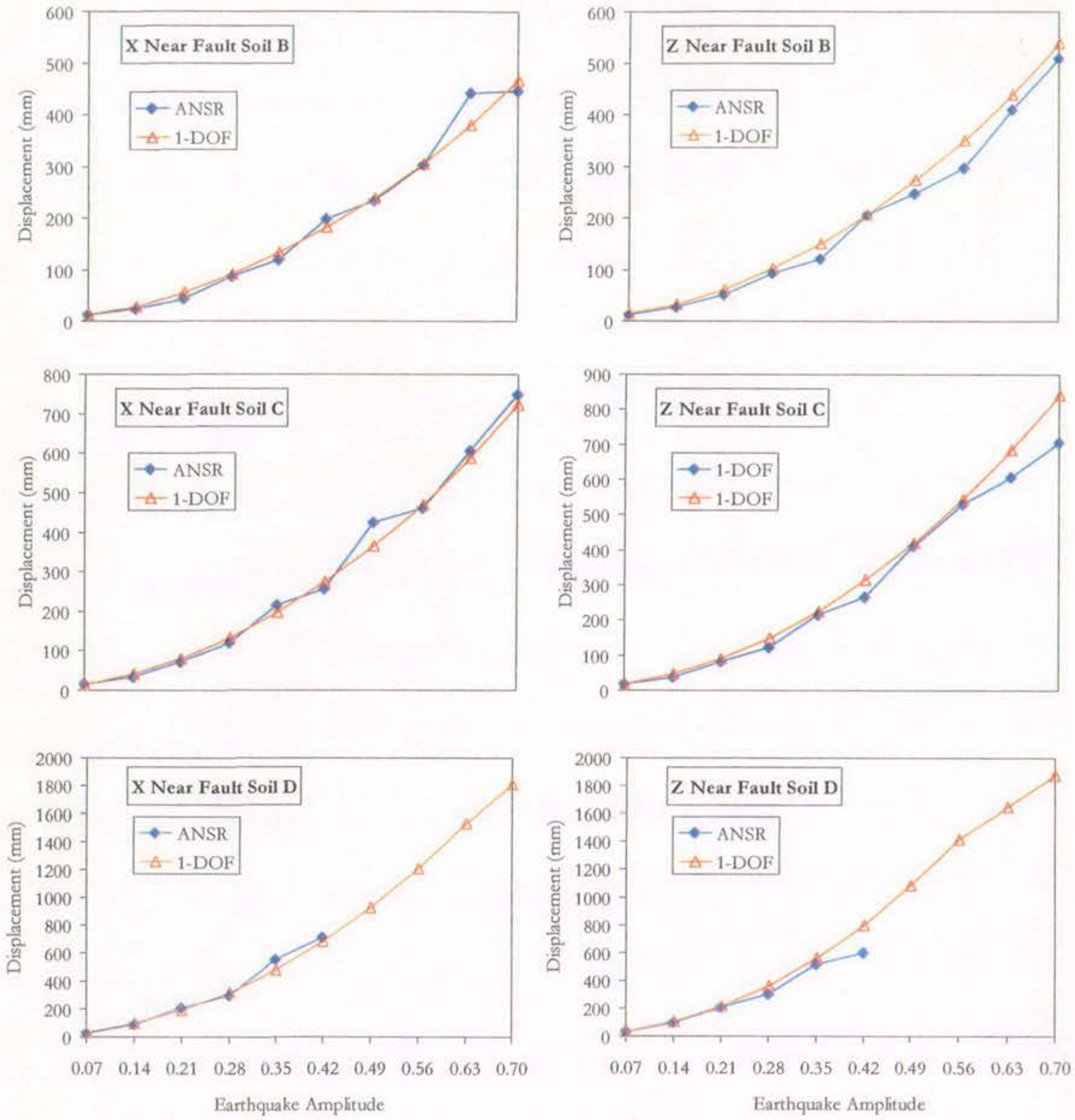

Figures A- 51 Non-Symmetrical Wall 2 Story Medium Gravel

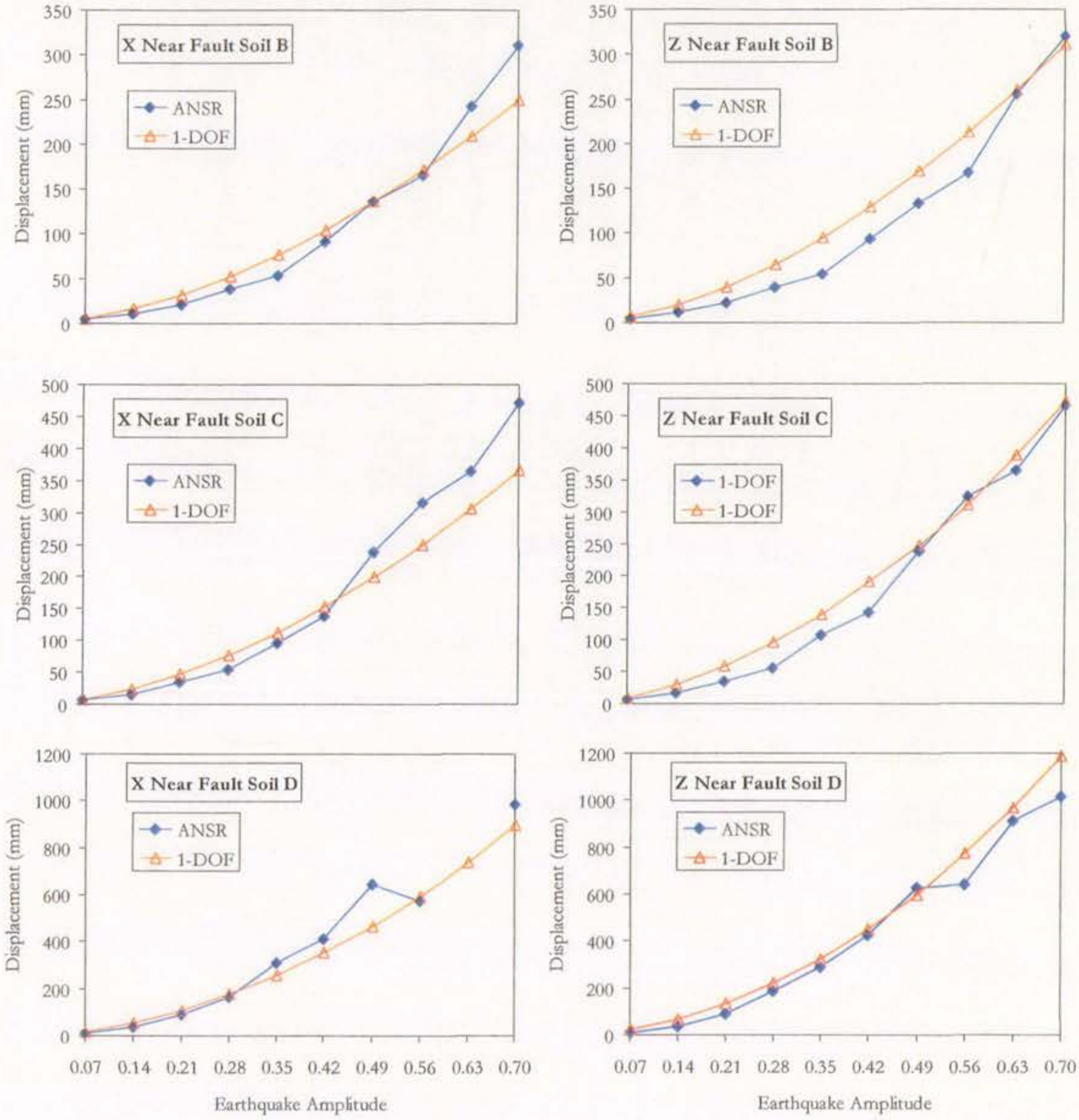

Figures A- 52 Non-Symmetrical Wall 2 Story Rock

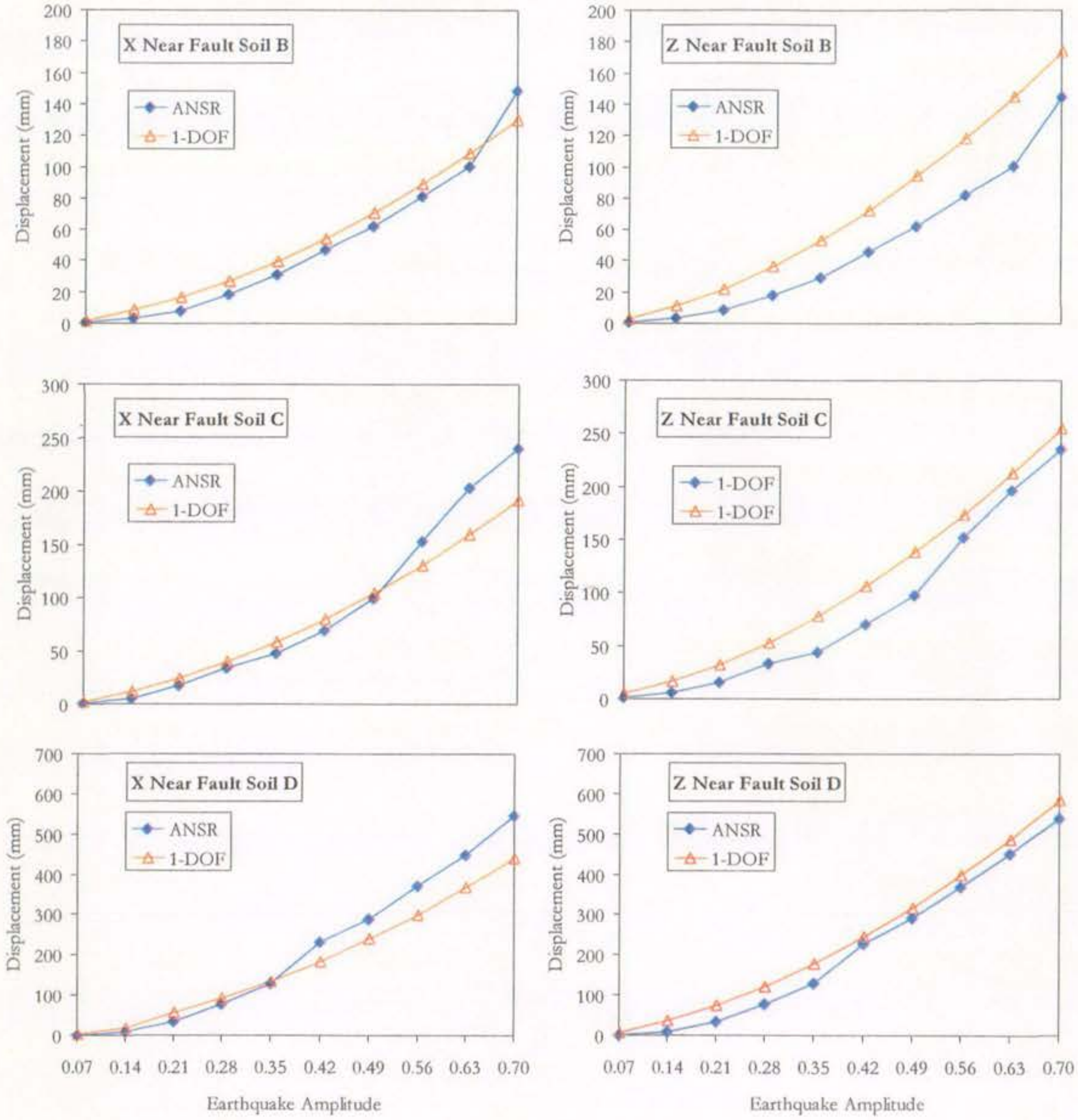

HolmesConsultingGroup

STRUCTURAL AND CIVIL ENGINEERS

Office directory and contact

Auckland

Hamilton

Tauranga

Hawkes Bay

Wellington

Christchurch

Queenstown

www.holmesgroup.com